Issue 3 2015 | Volume 11

The Journal on Advanced Studies in Theoretical and Experimental Physics, including Related Themes from Mathematics

PROGRESS IN PHYSICS

"All scientists shall have the right to present their scientific research results, in whole or in part, at relevant scientific conferences, and to publish the same in printed scientific journals, electronic archives, and any other media." — Declaration of Academic Freedom, Article 8

ISSN 1555-5534

The Journal on Advanced Studies in Theoretical and Experimental Physics, including Related Themes from Mathematics

PROGRESS IN PHYSICS

A quarterly issue scientific journal, registered with the Library of Congress (DC, USA). This journal is peer reviewed and included in the abstracting and indexing coverage of: Mathematical Reviews and MathSciNet (AMS, USA), DOAJ of Lund University (Sweden), Zentralblatt MATH (Germany), Scientific Commons of the University of St. Gallen (Switzerland), Open-J-Gate (India), Referativnyi Zhurnal VINITI (Russia), etc.

Electronic version of this journal:
http://www.ptep-online.com

Advisory Board

Dmitri Rabounski,
Editor-in-Chief, Founder

Florentin Smarandache,
Associate Editor, Founder

Larissa Borissova,
Associate Editor, Founder

Editorial Board

Pierre Millette
millette@ptep-online.com

Andreas Ries
ries@ptep-online.com

Gunn Quznetsov
quznetsov@ptep-online.com

Felix Scholkmann
scholkmann@ptep-online.com

Ebenezer Chifu
chifu@ptep-online.com

Postal Address

Department of Mathematics and Science,
University of New Mexico,
705 Gurley Ave., Gallup, NM 87301, USA

Copyright © *Progress in Physics*, 2015

All rights reserved. The authors of the articles do hereby grant *Progress in Physics* non-exclusive, worldwide, royalty-free license to publish and distribute the articles in accordance with the Budapest Open Initiative: this means that electronic copying, distribution and printing of both full-size version of the journal and the individual papers published therein for non-commercial, academic or individual use can be made by any user without permission or charge. The authors of the articles published in *Progress in Physics* retain their rights to use this journal as a whole or any part of it in any other publications and in any way they see fit. Any part of *Progress in Physics* howsoever used in other publications must include an appropriate citation of this journal.

This journal is powered by LaTeX

A variety of books can be downloaded free from the Digital Library of Science:
http://www.gallup.unm.edu/~smarandache

ISSN: 1555-5534 (print)
ISSN: 1555-5615 (online)

Standard Address Number: 297-5092
Printed in the United States of America

July 2015 **Vol. 11, Issue 3**

CONTENTS

Information for Authors and Subscribers

Progress in Physics has been created for publications on advanced studies in theoretical and experimental physics, including related themes from mathematics and astronomy. All submitted papers should be professional, in good English, containing a brief review of a problem and obtained results.

All submissions should be designed in LaTeX format using *Progress in Physics* template. This template can be downloaded from *Progress in Physics* home page http://www.ptep-online.com. Abstract and the necessary information about author(s) should be included into the papers. To submit a paper, mail the file(s) to the Editor-in-Chief.

All submitted papers should be as brief as possible. Short articles are preferable. Large papers can also be considered in exceptional cases. Letters related to the publications in the journal or to the events among the science community can be applied to the section *Letters to Progress in Physics*.

All that has been accepted for the online issue of *Progress in Physics* is printed in the paper version of the journal. To order printed issues, contact the Editors.

This journal is non-commercial, academic edition. It is printed from private donations. (Look for the current author fee in the online version of the journal.)

A New Understanding of Particles by $\overrightarrow{G}$-Flow Interpretation of Differential Equation

Linfan Mao
Chinese Academy of Mathematics and System Science, Beijing 100190, P. R. China.
E-mail: maolinfan@163.com

Applying mathematics to the understanding of particles classically with an assumption that if the variables t and x_1, x_2, x_3 hold with a system of dynamical equations (1.4), then they are a point (t, x_1, x_2, x_3) in $\mathbb{R}^4$. However, if we put off this assumption, how can we interpret the solution space of equations? And are these resultants important for understanding the world? Recently, the author extended Banach and Hilbert spaces on a topological graph to introduce $\overrightarrow{G}$-flows and showed that all such flows on a topological graph $\overrightarrow{G}$ also form a Banach or Hilbert space, which enables one to find the multiverse solution of these equations on $\overrightarrow{G}$. Applying this result, this paper discusses the $\overrightarrow{G}$-flow solutions on Schrödinger equation, Klein-Gordon equation and Dirac equation, i.e., the field equations of particles, bosons or fermions, answers previous questions by "yes", and establishes the many world interpretation of quantum mechanics of H. Everett by purely mathematics in logic, i.e., mathematical combinatorics.

1 Introduction

Matter consists of bosons with integer spin n and fermions with half-integer spin $n/2$, $n \equiv 1 \pmod 2$. The elementary particles consist of leptons and hadrons, i.e. mesons, baryons and their antiparticles, which are composed of quarks [16]. Thus, a hadron has an internal structure, which implies that all hadrons are not elementary but leptons are, viewed as point particles in elementary physics. Furthermore, there is also unmatter which is neither matter nor antimatter, but something in between [19-21]. For example, an atom of unmatter is formed either by electrons, protons, and antineutrons, or by antielectrons, antiprotons, and neutrons.

Usually, a particle is characterized by solutions of differential equation established on its wave function $\psi(t, x)$. In non-relativistic quantum mechanics, the wave function $\psi(t, x)$ of a particle of mass m obeys the Schrödinger equation

$$i\hbar \frac{\partial \psi}{\partial t} = -\frac{\hbar^2}{2m} \nabla^2 \psi + U, \tag{1.1}$$

where, $\hbar = 6.582 \times 10^{-22}$MeVs is the Planck constant, U is the potential energy of the particle in applied field and

$$\nabla = \left(\frac{\partial}{\partial x}, \frac{\partial}{\partial y}, \frac{\partial}{\partial z}\right) \text{ and } \nabla^2 = \frac{\partial^2}{\partial x^2} + \frac{\partial^2}{\partial y^2} + \frac{\partial^2}{\partial z^2}.$$

Consequently, a free boson $\psi(t, x)$ hold with the Klein-Gordon equation

$$\left(\frac{1}{c^2}\frac{\partial^2}{\partial t^2} - \nabla^2\right)\psi(x, t) + \left(\frac{mc}{\hbar}\right)^2 \psi(x, t) = 0 \tag{1.2}$$

and a free fermion $\psi(t, x)$ satisfies the Dirac equation

$$\left(i\gamma^\mu \partial_\mu - \frac{mc}{\hbar}\right)\psi(t, x) = 0 \tag{1.3}$$

in relativistic forms, where,

$$\begin{aligned} \gamma^\mu &= \left(\gamma^0, \gamma^1, \gamma^2, \gamma^3\right), \\ \partial_\mu &= \left(\frac{1}{c}\frac{\partial}{\partial t}, \frac{\partial}{\partial x_1}, \frac{\partial}{\partial x_2}, \frac{\partial}{\partial x_3}\right), \end{aligned}$$

c is the speed of light and

$$\gamma^0 = \begin{pmatrix} I_{2\times 2} & 0 \\ 0 & -I_{2\times 2} \end{pmatrix}, \ \gamma^i = \begin{pmatrix} 0 & \sigma_i \\ -\sigma_i & 0 \end{pmatrix}$$

with the usual Pauli matrices

$$\sigma_1 = \begin{pmatrix} 0 & 1 \\ 1 & 0 \end{pmatrix}, \ \sigma_2 = \begin{pmatrix} 0 & -i \\ i & 0 \end{pmatrix},$$

$$\sigma_3 = \begin{pmatrix} 1 & 0 \\ 0 & -1 \end{pmatrix}.$$

It is well known that the behavior of a particle is on superposition, i.e., in two or more possible states of being. But *how to interpret this phenomenon in accordance with (1.1)–(1.3)* ? The many worlds interpretation on wave function of (1.1) by H. Everett [2] in 1957 answered the question in machinery, i.e., viewed different worlds in different quantum mechanics and the superposition of a particle be liked those separate arms of a branching universe ([15], also see [1]). In fact, H. Everett's interpretation claimed that the state space of particle is a multiverse, or parallel universe ([23, 24]), an application of philosophical law that *the integral always consists of its parts*, or formally, the following.

Definition 1.1([6],[18]) *Let* $(\Sigma_1; \mathcal{R}_1)$, $(\Sigma_2; \mathcal{R}_2)$, $\cdots$, $(\Sigma_m; \mathcal{R}_m)$ *be m mathematical or physical systems, different two by two. A Smarandache multisystem* $\widetilde{\Sigma}$ *is a union* $\bigcup_{i=1}^{m} \Sigma_i$ *with rules* $\widetilde{\mathcal{R}} = \bigcup_{i=1}^{m} \mathcal{R}_i$ *on* $\widetilde{\Sigma}$*, denoted by* $\left(\widetilde{\Sigma}; \widetilde{\mathcal{R}}\right)$.

Furthermore, *things are inherently related, not isolated* in the world. Thus, every particle in nature is a union of elementary particles underlying a graph embedded in space, where, a graph G is said to be embeddable into a topological space $\mathscr{E}$ if there is a $1-1$ continuous mapping $f: G \to \mathscr{E}$ with $f(p) \neq f(q)$ if $p \neq q$ for $\forall p, q \in G$, i.e., edges only intersect at end vertices in $\mathscr{E}$. For example, a *planar graph* such as those shown in Fig. 1.

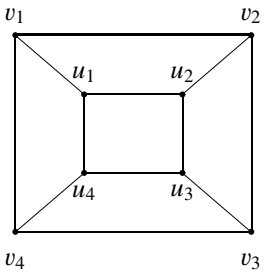

Fig. 1

Definition 1.2([6]) *For any integer $m \geq 1$, let $\left(\widetilde{\Sigma}; \widetilde{\mathcal{R}}\right)$ be a Smarandache multisystem consisting of mathematical systems $(\Sigma_1; \mathcal{R}_1), (\Sigma_2; \mathcal{R}_2), \cdots, (\Sigma_m; \mathcal{R}_m)$. An inherited topological structures $G^L\left[\widetilde{\Sigma}; \widetilde{\mathcal{R}}\right]$ on $\left(\widetilde{\Sigma}; \widetilde{\mathcal{R}}\right)$ is defined by*

$$V\left(G^L\left[\widetilde{\Sigma}; \widetilde{\mathcal{R}}\right]\right) = \{v_{\Sigma_1}, v_{\Sigma_2}, \cdots, v_{\Sigma_m}\},$$

$$E\left(G^L\left[\widetilde{\Sigma}; \widetilde{\mathcal{R}}\right]\right) = \{(v_{\Sigma_i}, v_{\Sigma_j}) | \Sigma_i \bigcap \Sigma_j \neq \emptyset,\ 1 \leq i \neq j \leq m\}$$

with a labeling $L: v_{\Sigma_i} \to L(v_{\Sigma_i}) = \Sigma_i$ and $L: (v_{\Sigma_i}, v_{\Sigma_j}) \to L(v_{\Sigma_i}, v_{\Sigma_j}) = \Sigma_i \bigcap \Sigma_j$, where $\Sigma_i \bigcap \Sigma_j$ denotes the intersection of spaces, or action between systems Σ_i with Σ_j for integers $1 \leq i \neq j \leq m$.

For example, let $\widetilde{\Sigma} = \bigcup_{i=1}^{4} \Sigma_i$ with $\Sigma_1 = \{a, b, c\}$, $\Sigma_2 = \{a, b\}$, $\Sigma_3 = \{b, c, d\}$, $\Sigma_4 = \{c, d\}$ and $\mathcal{R}_i = \emptyset$. Calculation shows that $\Sigma_1 \bigcap \Sigma_2 = \{a, b\}$, $\Sigma_1 \bigcap \Sigma_3 = \{b, c\}$, $\Sigma_1 \bigcap \Sigma_4 = \{c\}$, $\Sigma_2 \bigcap \Sigma_3 = \{b\}$, $\Sigma_2 \bigcap \Sigma_4 = \emptyset$, $\Sigma_3 \bigcap \Sigma_4 = \{c, d\}$. Such a graph $G^L\left[\widetilde{\Sigma}; \widetilde{\mathcal{R}}\right]$ is shown in Fig. 2.

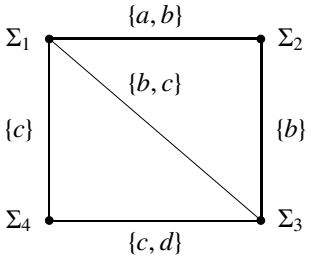

Fig. 2

Generally, a particle should be characterized by $\left(\widetilde{\Sigma}; \widetilde{\mathcal{R}}\right)$ in theory. However, we can only verify it by some of systems $(\Sigma_1; \mathcal{R}_1)$, $(\Sigma_2; \mathcal{R}_2)$, $\cdots$, $(\Sigma_m; \mathcal{R}_m)$ for the limitation of human beings because he is also a system in $\left(\widetilde{\Sigma}; \widetilde{\mathcal{R}}\right)$. Clearly, the underlying graph in H. Everett's interpretation on wave function is in fact a binary tree and there are many such traces in the developing of physics. For example, a baryon is predominantly formed from three quarks, and a meson is mainly composed of a quark and an antiquark in the models of Sakata, or Gell-Mann and Ne'eman on hadrons ([14]), such as those shown in Fig. 3, where, $q_i \in \{\mathbf{u}, \mathbf{d}, \mathbf{c}, \mathbf{s}, \mathbf{t}, \mathbf{b}\}$ denotes a quark for $i = 1, 2, 3$ and $\overline{q}_2 \in \left\{\overline{\mathbf{u}}, \overline{\mathbf{d}}, \overline{\mathbf{c}}, \overline{\mathbf{s}}, \overline{\mathbf{t}}, \overline{\mathbf{b}}\right\}$, an antiquark. Thus, the underlying graphs $\overrightarrow{G}$ of a meson, a baryon are respectively $\overrightarrow{K}_2$ and $\overrightarrow{K}_3$ with actions. In fact, a free quark was not found in experiments until today. So it is only a machinery model on hadrons. Even so, it characterizes well the known behavior of particles.

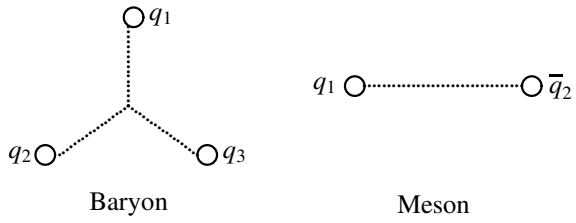

Fig. 3

It should be noted that the geometry on Definition 1.1–1.2 can be also used to characterize particles by combinatorial fields ([7]), and there is a priori assumption for discussion in physics, namely, *the dynamical equation of a subparticle of a particle is the same of that particle*. For example, the dynamical equation of quark is nothing else but the Dirac equation (1.3), a characterizing on quark from the macroscopic to the microscopic, the quantum level in physics. However, (1.3) cannot provide such a solution on the behaviors of 3 quarks. We can only interpret it similar to that of H. Everett, i.e., there are 3 parallel equations (1.3) in discussion, a seemly rational interpretation in physics, but not perfect for mathematics. Why this happens is because the interpretation of solution of equation. Usually, we identify a particle to the solution of its equation, i.e., if the variables t and x_1, x_2, x_3 hold with a system of dynamical equations

$$\mathscr{F}_i\left(t, x_1, x_2, x_3, u_t, u_{x_1}, \cdots, u_{x_1 x_2}, \cdots\right) = 0,$$

$$\text{with} \quad 1 \leq i \leq m, \tag{1.4}$$

the particle in $\mathbb{R} \times \mathbb{R}^3$ is a point (t, x_1, x_2, x_3), and if more than one points (t, x_1, x_2, x_3) hold with (1.4), the particle is nothing else but consisting of all such points. However, the solutions of (1.1)–(1.3) are all definite on time t. *Can this interpretation be used for particles in all times*? Certainly not because a particle can be always decomposed into elementary particles, and it is a little ambiguous which is a point, the particle itself or its one of elementary particles sometimes.

This speculation naturally leads to a question on mathematics, i.e., *what is the right interpretation on the solution of differential equation accompanying with particles*? Recently, the author extended Banach spaces on topological graphs $\overrightarrow{G}$ with operator actions in [13], and shown all of these extensions are also Banach space, particularly, the Hilbert space with unique correspondence in elements on linear continuous functionals, which enables one to solve linear functional equations in such extended space, particularly, solve differential equations on a topological graph, i.e., find multiverse solutions for equations. This scheme also enables us to interpret the superposition of particles in accordance with mathematics in logic.

The main purpose of this paper is to present an interpretation on superposition of particles by $\overrightarrow{G}$-flow solutions of (1.1)–(1.3) in accordance with mathematics. Certainly, the geometry on non-solvable differential equations discussed in [9]–[12] brings us another general way for holding behaviors of particles in mathematics. For terminologies and notations not mentioned here, we follow references [16] for elementary particles, [6] for geometry and topology, and [17]–[18] for Smarandache multi-spaces, and all equations are assumed to be solvable in this paper.

2 Extended Banach $\vec{G}$-flow space

2.1 Conservation laws

A conservation law, such as those on energy, mass, momentum, angular momentum and electric charge states that a particular measurable property of an isolated physical system does not change as the system evolves over time, or simply, constant of being. Usually, a local conservation law is expressed mathematically as a continuity equation, which states that the amount of conserved quantity at a point or within a volume can only change by the amount of the quantity which flows in or out of the volume. According to Definitions 1.1 and 1.2, a matter in the nature is nothing else but a Smarandache system $\left(\widetilde{\Sigma};\widetilde{\mathcal{R}}\right)$, or a topological graph $G^L\left[\left(\widetilde{\Sigma};\widetilde{\mathcal{R}}\right)\right]$ embedded in $\mathbb{R}^3$, hold with conservation laws

$$\sum_k \mathbf{F}(\mathbf{v})_k^- = \sum_l \mathbf{F}(\mathbf{v})_l^+$$

on $\forall v \in V\left(G^L\left[\left(\widetilde{\Sigma};\widetilde{\mathcal{R}}\right)\right]\right)$, where, $\mathbf{F}(\mathbf{v})_k^-$, $k \geq 1$ and $\mathbf{F}(\mathbf{v})_l^+$, $l \geq 1$ denote respectively the input or output amounts on a particle or a volume v.

2.2 $\vec{G}$-flow spaces

Classical operation systems can be easily extended on a graph $\overrightarrow{G}$ constraint on conditions for characterizing the unanimous behaviors of groups in the nature, particularly, go along with the physics. For this objective, let $\overrightarrow{G}$ be an oriented graph with vertex set $V(G)$ and arc set $X(G)$ embedded in $\mathbb{R}^3$ and let $(\mathscr{A};\circ)$ be an operation system in classical mathematics, i.e., for $\forall a, b \in \mathscr{A}$, $a \circ b \in \mathscr{A}$. Denoted by $\overrightarrow{G}^L_{\mathscr{A}}$ all of those labeled graphs $\overrightarrow{G}^L$ with labeling $L : X\left(\overrightarrow{G}\right) \to \mathscr{A}$. Then, we can extend operation $\circ$ on elements in $\overrightarrow{G}^{\mathscr{A}}$ by a ruler following:

R: *For* $\forall \overrightarrow{G}^{L_1}, \overrightarrow{G}^{L_2} \in \overrightarrow{G}^L_{\mathscr{A}}$, *define* $\overrightarrow{G}^{L_1} \circ \overrightarrow{G}^{L_2} = \overrightarrow{G}^{L_1 \circ L_2}$, *where* $L_1 \circ L_2 : e \to L_1(e) \circ L_2(e)$ *for* $\forall e \in X\left(\overrightarrow{G}\right)$.

For example, such an extension on graph $\overrightarrow{C}_4$ is shown in Fig. 4, where, $\mathbf{a_3}$=$\mathbf{a_1}\circ\mathbf{a_2}$, $\mathbf{b}_3$ =$\mathbf{b_1}\circ\mathbf{b_2}$, $\mathbf{c_3}$=$\mathbf{c_1}\circ\mathbf{c_2}$, $\mathbf{d}_3$ =$\mathbf{d_1}\circ\mathbf{d_2}$.

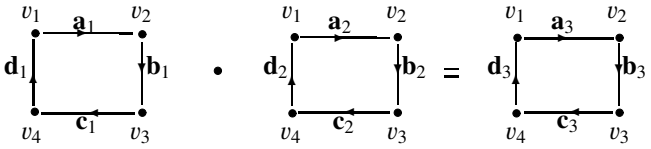

Fig. 4

Clearly, $\overrightarrow{G}^{L_1} \circ \overrightarrow{G}^{L_2} \in \overrightarrow{G}^L_{\mathscr{A}}$ by definition, i.e., $\overrightarrow{G}^L_{\mathscr{A}}$ is also an operation system under ruler **R**, and it is commutative if $(\mathscr{A},\circ)$ is commutative,

Furthermore, if $(\mathscr{A},\circ)$ is an algebraic group, $\overrightarrow{G}^L_{\mathscr{A}}$ is also an algebraic group because

(1) $\left(\overrightarrow{G}^{L_1} \circ \overrightarrow{G}^{L_2}\right) \circ \overrightarrow{G}^{L_3} = \overrightarrow{G}^{L_1} \circ \left(\overrightarrow{G}^{L_2} \circ \overrightarrow{G}^{L_3}\right)$ for $\forall \overrightarrow{G}^{L_1}, \overrightarrow{G}^{L_2}, \overrightarrow{G}^{L_3} \in \overrightarrow{G}^{\mathscr{A}}$ because

$$(L_1(e) \circ L_2(e)) \circ L_3(e) = L_1(e) \circ (L_2(e) \circ L_3(e))$$

for $e \in X\left(\overrightarrow{G}\right)$, i.e., $\overrightarrow{G}^{(L_1 \circ L_2) \circ L_3} = \overrightarrow{G}^{L_1 \circ (L_2 \circ L_3)}$.

(2) there is an identify $\overrightarrow{G}^{L_{1_{\mathscr{A}}}}$ in $\overrightarrow{G}^L_{\mathscr{A}}$, where $L_{1_{\mathscr{A}}} : e \to 1_{\mathscr{A}}$ for $\forall e \in X\left(\overrightarrow{G}\right)$;

(3) there is an uniquely element $\overrightarrow{G}^{L^{-1}}$ for $\forall \overrightarrow{G}^L \in \overrightarrow{G}^L_{\mathscr{A}}$.

However, for characterizing the unanimous behaviors of groups in the nature, the most useful one is the extension of vector space $(\mathscr{V};+,\cdot)$ over field $\mathcal{F}$ by defining the operations $+$ and $\cdot$ on elements in $\overrightarrow{G}^{\mathscr{V}}$ such as those shown in Fig. 5 on graph $\overrightarrow{C}_4$, where $\mathbf{a}$, $\mathbf{b}$, $\mathbf{c}$, $\mathbf{d}$, $\mathbf{a}_i$, $\mathbf{b}_i$, $\mathbf{c}_i$, $\mathbf{d}_i \in \mathscr{V}$ for $i = 1, 2, 3$, $\mathbf{x_3}$=$\mathbf{x_1}$+$\mathbf{x_2}$ for $\mathbf{x}$=$\mathbf{a}$, $\mathbf{b}$, $\mathbf{c}$ or $\mathbf{d}$ and $\alpha \in \mathcal{F}$.

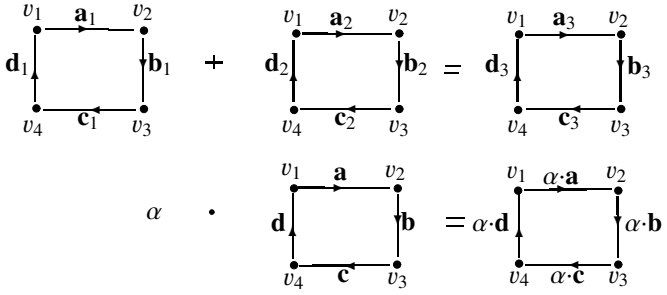

Fig. 5

A $\overrightarrow{G}$-*flow* on $\overrightarrow{G}$ is such an extension hold with $L(u,v) = -L(v,u)$ and conservation laws

$$\sum_{u\in N_G(v)} L(v,u) = \mathbf{0}$$

for $\forall v \in V\left(\overrightarrow{G}\right)$, where $\mathbf{0}$ is the zero-vector in $\mathscr{V}$. Thus, a $\overrightarrow{G}$-flow is a subfamily of $\overrightarrow{G}^L_{\mathscr{V}}$ limited by conservation laws. For example, if $\overrightarrow{G} = \overrightarrow{C}_4$, there must be $\mathbf{a}$=$\mathbf{b}$=$\mathbf{c}$=$\mathbf{d}$, $\mathbf{a}_i$=$\mathbf{b}_i$=$\mathbf{c}_i$=$\mathbf{d}_i$ for $i = 1, 2, 3$ in Fig. 5.

Clearly, all conservation $\overrightarrow{G}$-flows on $\overrightarrow{G}$ also form a vector space over $\mathcal{F}$ under operations + and $\cdot$ with zero vector $\mathbf{O} = \overrightarrow{G}^{L_{\mathbf{0}}}$, where $L_{\mathbf{0}}: e \to \mathbf{0}$ for $\forall e \in X\left(\overrightarrow{G}\right)$. Such an extended vector space on $\overrightarrow{G}$ is denoted by $\overrightarrow{G}^{\mathscr{V}}$.

Furthermore, if $(\mathscr{V}; +, \cdot)$ is a Banach or Hilbert space with inner product $\langle\cdot,\cdot\rangle$, we can also introduce the *norm* and *inner product* on $\overrightarrow{G}^{\mathscr{V}}$ by

$$\left\|\overrightarrow{G}^L\right\| = \sum_{(u,v)\in X\left(\overrightarrow{G}\right)} \|L(u,v)\|$$

or

$$\left\langle \overrightarrow{G}^{L_1}, \overrightarrow{G}^{L_2} \right\rangle = \sum_{(u,v)\in X\left(\overrightarrow{G}\right)} \langle L_1(u,v), L_2(u,v)\rangle$$

for $\forall \overrightarrow{G}^L, \overrightarrow{G}^{L_1}, \overrightarrow{G}^{L_2} \in \overrightarrow{G}^{\mathscr{V}}$, where $\|L(u,v)\|$ is the norm of $L(u,v)$ in $\mathscr{V}$. Then it can be verified that

(1) $\left\|\overrightarrow{G}^L\right\| \geq 0$ and $\left\|\overrightarrow{G}^L\right\| = 0$ if and only if $\overrightarrow{G}^L = \mathbf{O}$;

(2) $\left\|\overrightarrow{G}^{\xi L}\right\| = \xi\left\|\overrightarrow{G}^L\right\|$ for any scalar ξ;

(3) $\left\|\overrightarrow{G}^{L_1} + \overrightarrow{G}^{L_2}\right\| \leq \left\|\overrightarrow{G}^{L_1}\right\| + \left\|\overrightarrow{G}^{L_2}\right\|$;

(4) $\left\langle \overrightarrow{G}^L, \overrightarrow{G}^L \right\rangle = \sum_{(u,v)\in X\left(\overrightarrow{G}\right)} \langle L(u^v), L(u^v)\rangle \geq 0$ and $\left\langle \overrightarrow{G}^L, \overrightarrow{G}^L \right\rangle = 0$ if and only if $\overrightarrow{G}^L = \mathbf{O}$;

(5) $\left\langle \overrightarrow{G}^{L_1}, \overrightarrow{G}^{L_2} \right\rangle = \overline{\left\langle \overrightarrow{G}^{L_2}, \overrightarrow{G}^{L_1} \right\rangle}$ for $\forall \overrightarrow{G}^{L_1}, \overrightarrow{G}^{L_2} \in \overrightarrow{G}^{\mathscr{V}}$;

(6) For $\overrightarrow{G}^L, \overrightarrow{G}^{L_1}, \overrightarrow{G}^{L_2} \in \overrightarrow{G}^{\mathscr{V}}$ and $\lambda, \mu \in \mathcal{F}$,

$$\begin{aligned}&\left\langle \lambda\overrightarrow{G}^{L_1} + \mu\overrightarrow{G}^{L_2}, \overrightarrow{G}^L \right\rangle\\ &= \lambda\left\langle \overrightarrow{G}^{L_1}, \overrightarrow{G}^L \right\rangle + \mu\left\langle \overrightarrow{G}^{L_2}, \overrightarrow{G}^L \right\rangle.\end{aligned}$$

The following result is obtained by showing that Cauchy sequences in $\overrightarrow{G}^{\mathscr{V}}$ is converges hold with conservation laws.

Theorem 2.1([13]) *For any topological graph $\overrightarrow{G}$, $\overrightarrow{G}^{\mathscr{V}}$ is a Banach space, and furthermore, if $\mathscr{V}$ is a Hilbert space, $\overrightarrow{G}^{\mathscr{V}}$ is a Hilbert space also.*

According to Theorem 2.1, the operators action on Banach or Hilbert space $(\mathscr{V}; +, \cdot)$ can be extended on $\overrightarrow{G}^{\mathscr{V}}$, for example, the linear operator following.

Definition 2.2 *An operator $\mathbf{T}: \overrightarrow{G}^{\mathscr{V}} \to \overrightarrow{G}^{\mathscr{V}}$ is linear if*

$$\mathbf{T}\left(\lambda\overrightarrow{G}^{L_1} + \mu\overrightarrow{G}^{L_2}\right) = \lambda\mathbf{T}\left(\overrightarrow{G}^{L_1}\right) + \mu\mathbf{T}\left(\overrightarrow{G}^{L_2}\right)$$

for $\forall \overrightarrow{G}^{L_1}, \overrightarrow{G}^{L_2} \in \overrightarrow{G}^{\mathscr{V}}$ and $\lambda, \mu \in \mathscr{F}$, and is continuous at a $\overrightarrow{G}$-flow $\overrightarrow{G}^{L_0}$ if there always exist a number $\delta(\varepsilon)$ for $\forall \epsilon > 0$ such that

$$\left\|\mathbf{T}\left(\overrightarrow{G}^L\right) - \mathbf{T}\left(\overrightarrow{G}^{L_0}\right)\right\| < \varepsilon$$

if

$$\left\|\overrightarrow{G}^L - \overrightarrow{G}^{L_0}\right\| < \delta(\varepsilon).$$

The following interesting result generalizes the result of Fréchet and Riesz on linear continuous functionals, which opens us mind for applying $\overrightarrow{G}$-flows to hold on the nature.

Theorem 2.3([13]) *Let $\mathbf{T}: \overrightarrow{G}^{\mathscr{V}} \to \mathbb{C}$ be a linear continuous functional. Then there is a unique $\overrightarrow{G}^{\widehat{L}} \in \overrightarrow{G}^{\mathscr{V}}$ such that*

$$\mathbf{T}\left(\overrightarrow{G}^L\right) = \left\langle \overrightarrow{G}^L, \overrightarrow{G}^{\widehat{L}} \right\rangle$$

for $\forall \overrightarrow{G}^L \in \overrightarrow{G}^{\mathscr{V}}$.

Particularly, if all flows $L(u,v)$ on arcs (u,v) of $\overrightarrow{G}$ are state function, we extend the differential operator on $\overrightarrow{G}$-flows. In fact, a *differential operator* $\frac{\partial}{\partial t}$ or $\frac{\partial}{\partial x_i}: \overrightarrow{G}^{\mathscr{V}} \to \overrightarrow{G}^{\mathscr{V}}$ is defined by

$$\frac{\partial}{\partial t}: \overrightarrow{G}^L \to \overrightarrow{G}^{\frac{\partial L}{\partial t}}, \quad \frac{\partial}{\partial x_i}: \overrightarrow{G}^L \to \overrightarrow{G}^{\frac{\partial L}{\partial x_i}}$$

for integers $1 \leq i \leq 3$. Then, for $\forall \mu, \lambda \in \mathcal{F}$,

$$\begin{aligned}&\frac{\partial}{\partial t}\left(\lambda\overrightarrow{G}^{L_1} + \mu\overrightarrow{G}^{L_2}\right)\\ &= \frac{\partial}{\partial t}\left(\overrightarrow{G}^{\lambda L_1 + \mu L_2}\right) = \overrightarrow{G}^{\frac{\partial}{\partial t}(\lambda L_1 + \mu L_2)}\\ &= \overrightarrow{G}^{\frac{\partial}{\partial t}(\lambda L_1) + \frac{\partial}{\partial t}(\mu L_2)} = \overrightarrow{G}^{\frac{\partial}{\partial t}(\lambda L_1)} + \overrightarrow{G}^{\frac{\partial}{\partial t}(\mu L_2)}\\ &= \frac{\partial}{\partial t}\overrightarrow{G}^{(\lambda L_1)} + \frac{\partial}{\partial t}\overrightarrow{G}^{(\mu L_2)}\\ &= \lambda\frac{\partial}{\partial t}\overrightarrow{G}^{L_1} + \mu\frac{\partial}{\partial t}\overrightarrow{G}^{L_2},\end{aligned}$$

i.e.,

$$\frac{\partial}{\partial t}\left(\lambda\overrightarrow{G}^{L_1} + \mu\overrightarrow{G}^{L_2}\right) = \lambda\frac{\partial}{\partial t}\overrightarrow{G}^{L_1} + \mu\frac{\partial}{\partial t}\overrightarrow{G}^{L_2}.$$

Similarly, we know also that

$$\frac{\partial}{\partial x_i}\left(\lambda\overrightarrow{G}^{L_1} + \mu\overrightarrow{G}^{L_2}\right) = \lambda\frac{\partial}{\partial x_i}\overrightarrow{G}^{L_1} + \mu\frac{\partial}{\partial x_i}\overrightarrow{G}^{L_2}$$

for integers $1 \le i \le 3$. Thus, operators $\dfrac{\partial}{\partial t}$ and $\dfrac{\partial}{\partial x_i}$, $1 \le i \le 3$ are all linear on $\overrightarrow{G}^{\mathscr{V}}$.

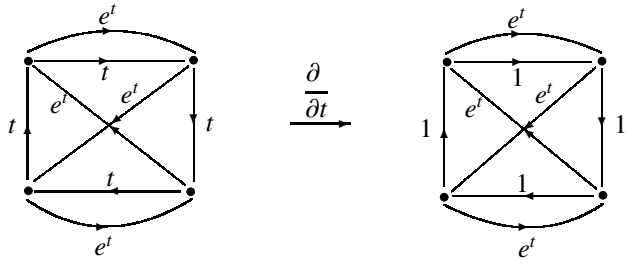

Fig. 6

Similarly, we introduce *integral operator* $\int : \overrightarrow{G}^{\mathscr{V}} \to \overrightarrow{G}^{\mathscr{V}}$ by

$$\int : \overrightarrow{G}^{L} \to \overrightarrow{G}^{\int L dt}, \quad \overrightarrow{G}^{L} \to \overrightarrow{G}^{\int L dx_i}$$

for integers $1 \le i \le 3$ and know that

$$\int \left(\mu \overrightarrow{G}^{L_1} + \lambda \overrightarrow{G}^{L_2}\right) = \mu \int \left(\overrightarrow{G}^{L_1}\right) + \lambda \int \left(\overrightarrow{G}^{L_2}\right)$$

for $\forall \mu, \lambda \in \mathcal{F}$,

$$\int \circ \left(\frac{\partial}{\partial t}\right) \text{ and } \int \circ \left(\frac{\partial}{\partial x_i}\right) : \overrightarrow{G}^{L} \to \overrightarrow{G}^{L} + \overrightarrow{G}^{L_c},$$

where L_c is such a labeling that $L_c(u, v)$ is constant for $\forall (u, v) \in X\left(\overrightarrow{G}\right)$.

3 Particle equations in $\vec{G}$-flow space

We are easily find particle equations with nonrelativistic or relativistic mechanics in $\overrightarrow{G}^{\mathscr{V}}$. Notice that

$$i\hbar \frac{\partial \psi}{\partial t} = E\psi, \qquad -i\hbar \nabla \psi = \overrightarrow{p}^2 \psi$$

and

$$E = \frac{1}{2m}\overrightarrow{p}^2 + U,$$

in classical mechanics, where ψ is the state function, $E, \overrightarrow{p}, U$ are respectively the energy, the momentum, the potential energy and m the mass of the particle. Whence,

$$\begin{aligned} \mathbf{O} &= \overrightarrow{G}^{(E - \frac{1}{2m}\overrightarrow{p}^2 - U)\psi} \\ &= \overrightarrow{G}^{E\psi} - \overrightarrow{G}^{\frac{1}{2m}\overrightarrow{p}^2 \psi} - \overrightarrow{G}^{U\psi} \\ &= \overrightarrow{G}^{i\hbar \frac{\partial \psi}{\partial t}} - \overrightarrow{G}^{-\frac{\hbar}{2m}\nabla^2 \psi} - \overrightarrow{G}^{U\psi} \\ &= i\hbar \frac{\partial \overrightarrow{G}^{L_\psi}}{\partial t} + \frac{\hbar}{2m}\nabla^2 \overrightarrow{G}^{L_\psi} - \overrightarrow{G}^{L_U}\overrightarrow{G}^{L_\psi}, \end{aligned}$$

where $L_\psi : e \to$ state function and $L_U : e \to$ potential energy on $e \in X\left(\overrightarrow{G}\right)$. According to the conservation law of energy, there must be $\overrightarrow{G}^{U} \in \overrightarrow{G}^{\mathscr{V}}$. We get the Schrödinger equation in $\overrightarrow{G}^{\mathscr{V}}$ following.

$$-i\hbar \frac{\partial \overrightarrow{G}^{L_\psi}}{\partial t} = \frac{\hbar}{2m}\nabla^2 \overrightarrow{G}^{L_\psi} - \widehat{U}\overrightarrow{G}^{L_\psi}, \tag{3.1}$$

where $\widehat{U} = \overrightarrow{G}^{L_U} \in \overrightarrow{G}^{\mathscr{V}}$. Similarly, by the relativistic energy-momentum relation

$$E^2 = c^2 \overrightarrow{p}^2 + m^2 c^4$$

for bosons and

$$E = c\alpha_k \overrightarrow{p}_k + \alpha_0 mc^2$$

for fermions, we get the Klein-Gordon equation and Dirac equation

$$\left(\frac{1}{c^2}\frac{\partial^2}{\partial t^2} - \nabla^2\right)\overrightarrow{G}^{L_\psi} + \left(\frac{cm}{\hbar}\right)\overrightarrow{G}^{L_\psi} = \mathbf{O} \tag{3.2}$$

and

$$\left(i\gamma^\mu \partial_\mu - \frac{mc}{\hbar}\right)\overrightarrow{G}^{L_\psi} = \mathbf{O}, \tag{3.3}$$

of particles in $\overrightarrow{G}^{\mathscr{V}}$ respectively. Particularly, let $\overrightarrow{G}$ be such a topological graph with one vertex but only with one arc. Then, (3.1)–(3.3) are nothing else but (1.1)–(1.3) respectively. However, (3.1)–(3.3) conclude that we can find $\overrightarrow{G}$-flow solutions on (1.1)–(1.3), which enables us to interpret mathematically the superposition of particles by multiverse.

4 $\vec{G}$-flows on particle equations

Formally, we can establish equations in $\overrightarrow{G}^{\mathscr{V}}$ by equations in Banach space $\mathscr{V}$ such as (3.1)–(3.3). However, the important thing is not just on such establishing but finding $\overrightarrow{G}$-flows on equations in $\mathscr{V}$ and then interpret the superposition of particles by $\overrightarrow{G}$-flows.

4.1 $\vec{G}$-flow solutions on equation

Theorem 2.3 concludes that there are $\overrightarrow{G}$-flow solutions for a linear equations in $\overrightarrow{G}^{\mathscr{V}}$ for Hilbert space $\mathscr{V}$ over field $\mathcal{F}$, including algebraic equations, linear differential or integral equations without considering the topological structure. For example, let $ax = b$. We are easily getting its $\overrightarrow{G}$-flow solution $x = \overrightarrow{G}^{a^{-1}L}$ if we view an element $b \in \mathscr{V}$ as $b = \overrightarrow{G}^{L}$, where $L(u, v) = b$ for $\forall (u, v) \in X\left(\overrightarrow{G}\right)$ and $0 \ne a \in \mathcal{F}$, such as those shown in Fig. 7 for $\overrightarrow{G} = \overrightarrow{C}_4$ and $a = 3$, $b = 5$.

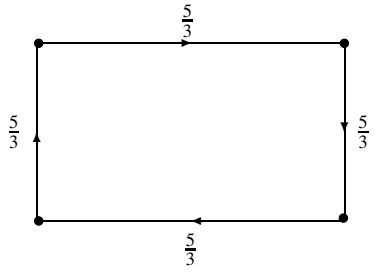

Fig. 7

Generally, we know the following result:

Theorem 4.1([13]) *A linear system of equations*

$$\begin{cases} a_{11}x_1 + a_{12}x_2 + \cdots + a_{1n}x_n = b_1 \\ a_{21}x_1 + a_{22}x_2 + \cdots + a_{2n}x_n = b_2 \\ \cdots\cdots\cdots\cdots\cdots\cdots\cdots\cdots \\ a_{m1}x_1 + a_{m2}x_2 + \cdots + a_{mn}x_n = b_m \end{cases}$$

with $a_{ij}, b_j \in \mathcal{F}$ for integers $1 \leq i \leq n, 1 \leq j \leq m$ holding with

$$\operatorname{rank}\left[a_{ij}\right]_{m\times n} = \operatorname{rank}\left[a_{ij}\right]^{+}_{m\times(n+1)}$$

has $\overrightarrow{G}$-flow solutions on infinitely many topological graphs $\overrightarrow{G}$, where

$$\left[a_{ij}\right]^{+}_{m\times(n+1)} = \begin{bmatrix} a_{11} & a_{12} & \cdots & a_{1n} & L_1 \\ a_{21} & a_{22} & \cdots & a_{2n} & L_2 \\ \cdots & \cdots & \cdots & \cdots & \cdots \\ a_{m1} & a_{m2} & \cdots & a_{mn} & L_m \end{bmatrix}.$$

We can also get $\overrightarrow{G}$-flow solutions for linear partial differential equations ([14]). For example, the Cauchy problems on differential equations

$$\frac{\partial X}{\partial t} = c^2 \sum_{i=1}^{n} \frac{\partial^2 X}{\partial x_i^2}$$

with initial value $X|_{t=t_0} = \overrightarrow{G}^{L'} \in \overrightarrow{G}^{\mathscr{V}}$ is also solvable in $\overrightarrow{G}^{\mathscr{V}}$ if $L'(u,v)$ is continuous and bou- nded in $\mathbb{R}^n$ for $\forall (u,v) \in X\left(\overrightarrow{G}\right)$ and $\forall \overrightarrow{G}^{L'} \in \overrightarrow{G}^{\mathscr{V}}$. In fact, $X = \overrightarrow{G}^{L_F}$ with $L_F : (u,v) \to F(u,v)$ for $\forall (u,c) \in X\left(\overrightarrow{G}\right)$, where

$$\begin{aligned} F(u,v) &= \frac{1}{(4\pi t)^{\frac{n}{2}}}\left(\int_{-\infty}^{+\infty} e^{-\frac{(x_1-y_1)^2+\cdots+(x_n-y_n)^2}{4t}}\right. \\ &\times \left. L'(u,v)(y_1,\cdots,y_n)dy_1\cdots dy_n\right) \end{aligned}$$

is such a solution.

Generally, if $\overrightarrow{G}$ can be decomposed into circuits $\overrightarrow{C}$, the next result concludes that we can always find $\overrightarrow{G}$-flow solutions on equations, no matter what the equation looks like, linear or non-linear ([13]).

Theorem 4.2 *If the topological graph $\overrightarrow{G}$ is strong-connected with circuit decomposition*

$$\overrightarrow{G} = \bigcup_{i=1}^{l} \overrightarrow{C}_i$$

such that $L(u,v) = L_i(\boldsymbol{x})$ for $\forall (u,v) \in X\left(\overrightarrow{C}_i\right)$, $1 \leq i \leq l$ and the Cauchy problem

$$\begin{cases} \mathscr{F}_i(\boldsymbol{x}, u, u_{x_1}, \cdots, u_{x_n}, u_{x_1x_2}, \cdots) = 0 \\ u|_{\boldsymbol{x}_0} = L_i(\boldsymbol{x}) \end{cases}$$

is solvable in a Hilbert space $\mathscr{V}$ on domain $\Delta \subset \mathbb{R}^n$ for integers $1 \leq i \leq l$, then the Cauchy problem

$$\begin{cases} \mathscr{F}_i(\boldsymbol{x}, X, X_{x_1}, \cdots, X_{x_n}, X_{x_1x_2}, \cdots) = 0 \\ X|_{\boldsymbol{x}_0} = \overrightarrow{G}^{L} \end{cases}$$

such that $L(u,v) = L_i(\boldsymbol{x})$ for $\forall (u,v) \in X\left(\overrightarrow{C}_i\right)$ is solvable for $X \in \overrightarrow{G}^{\mathscr{V}}$.

In fact, such a solution is constructed by $X = \overrightarrow{G}^{L_{u(\mathbf{x})}}$ with $L_{u(\mathbf{x})}(u,v) = u(\mathbf{x})$ for $(u,v) \in X\left(\overrightarrow{G}\right)$ by applying the input and the output at vertex v all being $u(\mathbf{x})$ on $\overrightarrow{C}$, which implies that all flows at vertex $v \in V\left(\overrightarrow{G}\right)$ is conserved.

4.2 $\vec{G}$-flows on particle equation

The existence of $\overrightarrow{G}$-flow solutions on particle equations (1.1)–(1.3) is clearly concluded by Theorem 4.2, also implied by (3.1)–(3.3) for any $\overrightarrow{G}$. However, the superposition of a particle P shows that there are $N \geq 2$ states of being associated with a particle P. Considering this fact, a convenient $\overrightarrow{G}$-flow model for elementary particle fermions, the lepton or quark P is by a bouquet $\overrightarrow{B}_N^{L_\psi}$, and an antiparticle $\overline{P}$ of P presented by $\overrightarrow{B}_N^{L_{\psi^{-1}}}$ with all inverse states on its loops, such as those shown in Fig. 8.

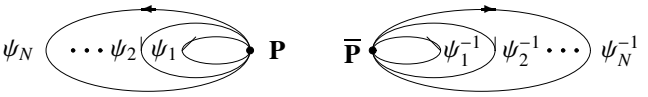

Particle Antiparticle

Fig. 8

An elementary unparticle is an intermediate form between an elementary particle and its antiparticle, which can be presented by $\overrightarrow{B}_N^{L_\psi^C}$, where $L_\psi^C : e \to L_{\psi^{-1}}(e)$ if $e \in C$ but $L_\psi^C : e \to L_\psi(e)$ if $e \in X\left(\overrightarrow{B}_N\right) \setminus C$ for a subset $C \subset X\left(\overrightarrow{B}_N\right)$, such as those shown in Fig. 9,

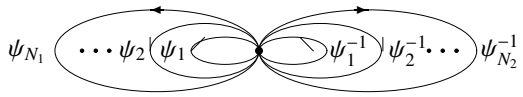

Fig. 9 Unparticle

where $N_1, N_2 \geq 1$ are integers. Thus, an elementary particle with its antiparticles maybe annihilate or appears in pair at a time, which consists in an elementary unparticle by combinations of these state functions with their inverses.

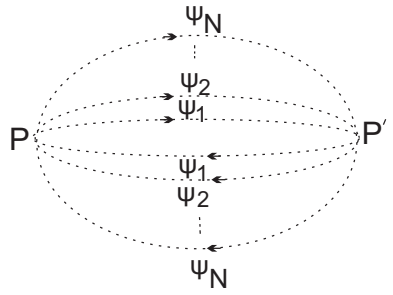

Fig. 10 $\overrightarrow{D^{\perp}}^{L_\psi}_{0,2N,0}$

For those of mediate interaction particle quanta, i.e., boson, which reflects interaction between particles. Thus, they are conveniently presented by dipole $\overrightarrow{D^{\perp}}^{L_\psi}_{0,2N,0}$ but with dotted lines, such as those in Fig. 10, in which the vertex P, P' denotes particles, and arcs with state functions $\psi_1, \psi_2, \cdots, \psi_N$ are the N states of P. Notice that $\overrightarrow{B}^{L_\psi}_N$ and $\overrightarrow{D^{\perp}}^{L_\psi}_{0,2N,0}$ both are a union of N circuits.

According to Theorem 4.2, we consequently get the following conclusion.

Theorem 4.3 *For an integer $N \geq 1$, there are indeed $\overrightarrow{D^{\perp}}^{L_\psi}_{0,2N,0}$ -flow solution on Klein-Gordon equation (*1.2*), and $\overrightarrow{B}^{L_\psi}_N$ -flow solution on Dirac equation (*1.3*).*

Generally, this model enables us to know that the $\overrightarrow{G}$-flow constituents of a particle also.

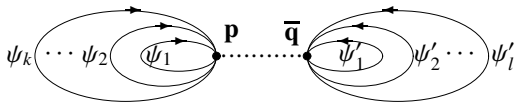

Fig. 11 Meson

Thus, if a particle $\widetilde{P}$ is consisted of l elementary particles $P_1, P_1, \cdots, P_l$ underlying a graph $\overrightarrow{G}\left[\widetilde{P}\right]$, its $\overrightarrow{G}$-flow is obtained by replace each vertex v by $\overrightarrow{B}^{L_{\psi v}}_{N_v}$ and each arc e by $\overrightarrow{D^{\perp}}^{L_{\psi e}}_{0,2N_e,0}$ in $\overrightarrow{G}\left[\widetilde{P}\right]$, denoted by $\overrightarrow{G}^{L_\psi}\left[\overrightarrow{B}_v, \overrightarrow{D}_e\right]$. For example, the model of Sakata, or Gell-Mann and Ne'eman on hadrons claims that the meson and the baryon are respectively the dipole $\overrightarrow{D^{\perp}}^{L_{\psi e}}_{k,2N,l}$-flow shown in Fig. 11 and the triplet $\overrightarrow{G}$-flow $\overrightarrow{C^{\perp}}^{L_\psi}_{k,l,s}$ shown in Fig. 12,

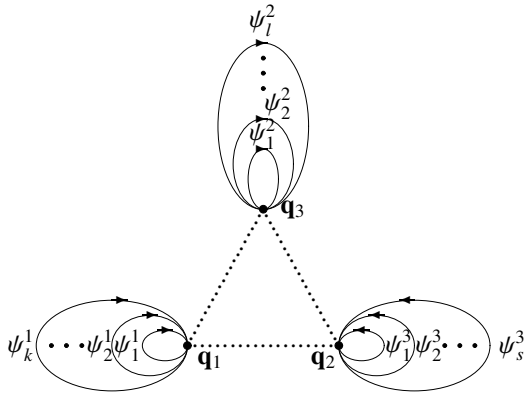

Fig. 12 Baryon

Theorem 4.4 *If $\widetilde{P}$ is a particle consisted of elementary particles $P_1, P_1, \cdots, P_l$ for an integer $l \geq 1$, then $\overrightarrow{G}^{L_\psi}\left[\overrightarrow{B}_v, \overrightarrow{D}_e\right]$ is a $\overrightarrow{G}$-flow solution on the Schrödinger equation (*1.1*) whenever λ_G is finite or infinite.*

Proof If λ_G is finite, the conclusion follows Theorem 4.2 immediately. We only consider the case of $\lambda_G \to \infty$. In fact, if $\lambda_G \to \infty$, calculation shows that

$$\begin{aligned} & i\hbar \lim_{\lambda_G\to\infty}\left(\frac{\partial}{\partial t}\left(\overrightarrow{G}^{L_\psi}\left[\overrightarrow{B}_v, \overrightarrow{D}_e\right]\right)\right) \\ &= \lim_{\lambda_G\to\infty}\left(i\hbar\frac{\partial}{\partial t}\left(\overrightarrow{G}^{L_\psi}\left[\overrightarrow{B}_v, \overrightarrow{D}_e\right]\right)\right) \\ &= \lim_{\lambda_G\to\infty}\left(-\frac{\hbar^2}{2m}\nabla^2\overrightarrow{G}^{L_\psi}\left[\overrightarrow{B}_v, \overrightarrow{D}_e\right] + \overrightarrow{G}^{L_U}\right) \\ &= -\frac{\hbar^2}{2m}\nabla^2 \lim_{\lambda_G\to\infty}\overrightarrow{G}^{L_\psi}\left[\overrightarrow{B}_v, \overrightarrow{D}_e\right] + \overrightarrow{G}^{L_U}, \end{aligned}$$

i.e.,

$$\begin{aligned} & i\hbar \lim_{\lambda_G\to\infty}\left(\frac{\partial}{\partial t}\left(\overrightarrow{G}^{L_\psi}\left[\overrightarrow{B}_v, \overrightarrow{D}_e\right]\right)\right) \\ &= -\frac{\hbar^2}{2m}\nabla^2 \lim_{\lambda_G\to\infty}\overrightarrow{G}^{L_\psi}\left[\overrightarrow{B}_v, \overrightarrow{D}_e\right] + \overrightarrow{G}^{L_U}. \end{aligned}$$

In particular,

$$i\hbar \lim_{N\to\infty}\left(\frac{\partial \overrightarrow{B}^{L_\psi}_N}{\partial t}\right) = -\frac{\hbar^2}{2m}\nabla^2 \lim_{N\to\infty}\overrightarrow{B}^{L_\psi}_N + \overrightarrow{G}^{L_U},$$

$$i\hbar \lim_{N\to\infty}\frac{\partial}{\partial t}\left(\overrightarrow{D^{\perp}}^{L_\psi}_{0,2N,0}\right) = -\frac{\hbar^2}{2m}\nabla^2 \lim_{N\to\infty}\overrightarrow{D^{\perp}}^{L_\psi}_{0,2N,0} + \overrightarrow{G}^{L_U}$$

for bouquets and dipoles. □

5 $\vec{G}$-flow interpretation on particle superposition

The superposition of a particle P is depicted by a Hilbert space $\mathscr{V}$ over complex field $\mathbb{C}$ with orthogonal basis $|1\rangle, |2\rangle, \cdots, |n\rangle, \cdots$ in quantum mechanics. In fact, the linearity of Schrödinger equation concludes that all states of particle P are in such a space. However, an observer can grasp only one state, which promoted H. Everett devised a multiverse consisting of states in splitting process, i.e., the quantum effects spawn countless branches of the universe with different events occurring in each, not influence one another, such as those shown in Fig. 13, and the observer selects by randomness, where the multiverse is $\bigcup\limits_{i\geq 1}\mathscr{V}_i$ with $\mathscr{V}_{kl}=\mathscr{V}$ for integers $k\geq 1,\ 1\leq l\leq 2^k$ but in different positions.

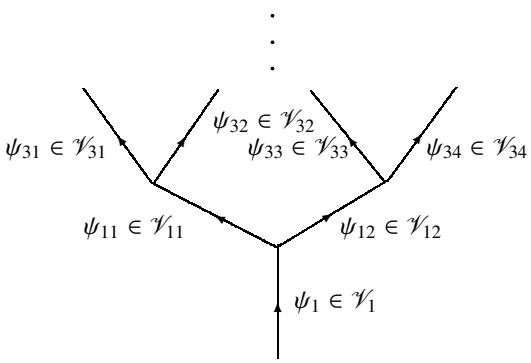

Fig. 13

Why it needs an interpretation on particle superposition in physics lies in that we characterize the behavior of particle by dynamic equation on state function and interpret it to be the solutions, and different quantum state holds with different solution of that equation. However, we can only get one solution by solving the equation with given initial datum once, and hold one state of the particle P, i.e., the solution correspondent only to one position but the particle is in superposition, which brought the H. Everett interpretation on superposition. It is only a biological mechanism by infinite parallel spaces $\mathscr{V}$ but loses of conservations on energy or matter in the nature, whose independently runs also overlook the existence of universal connection in things, a philosophical law.

Even so, it can not blot out the ideological contribution of H. Everett to sciences a shred because all of these mentions are produced by the interpretation on mathematical solutions with the reality of things, i.e., scanning on local, not the global. However, if we extend the Hilbert space $\mathscr{V}$ to $\overrightarrow{B}_N^{L_\psi}$, $\overrightarrow{D^{\perp}}_{0,2N,0}^{L_\psi}$ or $\overrightarrow{G}^{L_\psi}\left[\overrightarrow{B}_v,\overrightarrow{D}_e\right]$ in general, i.e., $\overrightarrow{G}$-flow space $\overrightarrow{G}^{\mathscr{V}}$, where $\overrightarrow{G}$ is the underling topological graph of P, the situation has been greatly changed because $\overrightarrow{G}^{\mathscr{V}}$ is itself a Hilbert space, and we can identify the $\overrightarrow{G}$-flow on $\overrightarrow{G}$ to particle P, i.e.,

$$P=\overrightarrow{G}^{L_\psi}\left[\overrightarrow{B}_v,\overrightarrow{D}_e\right] \tag{5.1}$$

for a globally understanding the behaviors of particle P whatever $\lambda_G\to\infty$ or not by Theorem 4.4. For example, let $P=\overrightarrow{B}_N^{L_\psi}$, i.e., a free particle such as those of electron e^-, muon μ^-, tauon τ^-, or their neutrinos ν_e,ν_μ,ν_τ. Then the superposition of P is displayed by state functions ψ on N loops in $\overrightarrow{B}_N$ hold on its each loop with

$$\text{input } \psi_i=\text{ ouput } \psi_i \text{ at vertex } P$$

for integers $1\leq i\leq N$. Consequently,

$$\text{input } \sum_{i\in I}\psi_i=\text{ ouput } \sum_{i\in I}\psi_i \text{ at vertex } P$$

for $\forall I\subset\{1,2,\cdots,N\}$, the conservation law on vertex P. Furthermore, such a $\overrightarrow{B}_N^{L_\psi}$ is not only a disguise on P in form but also a really mathematical element in Hilbert space $\overrightarrow{B}^{\mathscr{V}}$, and can be also used to characterize the behavior of particles such as those of the decays or collisions of particles by graph operations. For example, the β-decay $n\to p+e^-+\mu_e^-$ is transferred to a decomposition formula

$$\overrightarrow{C^{\perp}}_{k,l,s}^{L_{\psi_n}}=\overrightarrow{C^{\perp}}_{k_1,l_1,s_1}^{L_{\psi_p}}\bigcup\overrightarrow{B}_{N_1}^{L_{\psi_e}}\bigcup\overrightarrow{B}_{N_2}^{L_{\psi_\mu}},$$

on graph, where, $\overrightarrow{C^{\perp}}_{k_1,l_1,s_1}^{L_{\psi_p}}$, $\overrightarrow{B}_{N_1}^{L_{\psi_e}}$, $\overrightarrow{B}_{N_2}^{L_{\psi_\mu}}$ are all subgraphs of $\overrightarrow{C^{\perp}}_{k,l,s}^{L_{\psi_n}}$. Similarly, the β- collision $\nu_e+p\to n+e^+$ is transferred to an equality

$$\overrightarrow{B}_{N_1}^{L_{\psi_{\nu_e}}}\bigcup\overrightarrow{C^{\perp}}_{k_1,l_1,s_1}^{L_{\psi_p}}=\overrightarrow{C^{\perp}}_{k_2,l_2,s_2}^{L_{\psi_n}}\bigcup\overrightarrow{B}_{N_2}^{L_{\psi_e}}.$$

Even through the relation (5.1) is established on the linearity, it is in fact truly for the linear and non-liner cases because the underlying graph of $\overrightarrow{G}^{L_\psi}\left[\overrightarrow{B}_v,\overrightarrow{D}_e\right]$-flow can be decomposed into bouquets and dipoles, hold with conditions of Theorem 4.2. Thus, even if the dynamical equation of a particle P is non-linear, we can also adopt the presentation (5.1) to characterize the superposition and hold on the global behavior of P. Whence, it is a presentation on superposition of particles, both on linear and non-linear.

6 Further discussions

Usually, a dynamic equation on a particle characterizes its behaviors. But *is its solution the same as the particle*? Certainly not! Classically, a dynamic equation is established on characters of particles, and different characters result in different equations. Thus the superposition of a particle should be characterized by at least 2 differential equations. However, for a particle P, all these equations are the same one by

chance, i.e., one of the Schrödinger equation, Klein-Gordon equation or Dirac equation, which lead to the many world interpretation of H. Everett, i.e., put a same equation or Hilbert space on different place for different solutions in Fig. 12. As it is shown in Theorems 4.1 – 4.4, we can interpret the solution of (1.1)–(1.3) to be a $\overrightarrow{G}^{L_\psi}\left[\overrightarrow{B}_v, \overrightarrow{D}_e\right]$-flow, which properly characterizes the superposition behavior of particles by purely mathematics.

The $\overrightarrow{G}$-flow interpretation on differential equation opens a new way for understanding the behavior of nature, particularly on superposition of particles. Generally, the dynamic equations on different characters maybe different, which will brings about contradicts equations, i.e., non-solvable equations. For example, we characterize the behavior of meson or baryon by Dirac equation (1.3). However, we never know the dynamic equation on quark. Although we can say it obeying the Dirac equation but it is not a complete picture on quark. If we find its equation some day, they must be contradicts because it appear in different positions in space for a meson or a baryon at least. As a result, the $\overrightarrow{G}$-solutions on non-solvable differential equations discussed in [9]–[12] are valuable for understanding the reality of the nature with $\overrightarrow{G}$-flow solutions a special one on particles.

As it is well known for scientific community, any science possess the falsifiability but which depends on known scientific knowledge and technical means at that times. Accordingly, it is very difficult to claim a subject or topic with logical consistency is truth or false on the nature sometimes, for instance the multiverse or parallel universes because of the limitation of knowing things in the nature for human beings. In that case, a more appreciated approach is not denied or ignored but tolerant, extends classical sciences and developing those of well known technical means, and then get a better understanding on the nature because the pointless argument would not essentially promote the understanding of nature for human beings ([3,4,22]).

Submitted on April 8, 2015 / Accepted on April 15, 2015

References

1. Bousso R. and Susskind L. Multiverse interpretation of quantum mechanics. *Physical Review*, 2012, D85 (4), DOI:10.1103; *Phys. Rev.* D.85.045007.
2. Everett H. Relative state formulation of quantum mechanics. *Rev. Mod. Phys.*, 1957, v. 29, 454–462.
3. George E. Does the multiverse really exist? *Scientific American*, 2011, v. 305 (2), 38–43.
4. Kragh H. Contemporary history of cosmology and controversy over the multiverse. *Annals of Science*, 2009, v. 66 (4), 529.
5. Tian Ma. View Physics by Mathematics – Elementary Particles and Unified Field Theory (in Chinese). Science Press, Beijing, 2014.
6. Linfan Mao. Combinatorial Geometry with Applications to Field Theory. The Education Publisher, USA, 2011.
7. Linfan Mao. Combinatorial fields – an introduction. *International J. Math. Combin.*, 2009, v. 3, 1–22.
8. Linfan Mao. Relativity in combinatorial gravitational fields. *Progress in Physics*, 2010, v. 6 (3), 39–50.
9. Linfan Mao. Global stability of non-solvable ordinary differential equations with applications. *International J. Math. Combin.*, 2013, v. 1, 1–37.
10. Linfan Mao. Geometry on G^L-systems of homogenous polynomials. *International J. Contemp. Math. Sciences*, 2014, v. 9 (6), 287–308.
11. Linfan Mao. Non-solvable equation systems with graphs embedded in $\mathbf{R}^n$. in Proceedings of the First International Conference on Smarandache Multispace and Multistructure, The Education Publisher, July 2013.
12. Linfan Mao. Cauchy problem on non-solvable system of first order partial differential equations with applications. *Methods and Applications of Analysis*, (Accepted for publication).
13. Linfan Mao. Extended Banach $\overrightarrow{G}$-flow spaces on differential equations with applications. *Electronic J. Mathematical Analysis and Applications*, 2015, v. 3 (2), 59–91.
14. Nambu Y. Quarks: Frontiers in Elementary Particle Physics. World Scientific Publishing, 1985.
15. Byrne Peter The many worlds of Hugh Everett III. *Scientific American*, December 2007, 98–105.
16. Quang Ho-Kim and Pham Xuan Yem. Elementary Particles and Their Interactions. Springer-Verlag, Berlin-Heidelberg, 1998.
17. Smarandache F. *Paradoxist Geometry*, State Archives from Valcea, Rm. Valcea, Romania, 1969, and in Paradoxist Mathematics, Collected Papers (Vol. II), Kishinev University Press, Kishinev, 1997, 5–28.
18. Smarandache F. Multi-space and multi-structure, in Neutrosophy – Neutrosophic Logic, Set, Probability and Statistics, American Research Press, 1998.
19. Smarandache F. A new form of matter – unmatter, composed of particles and anti-particles. *Progress in Physics*, 2005, v. 1 (1), 9–11.
20. Smarandache F. Verifying unmatter by experiments, more types of unmatter. *Progress in Physics*, 2005, v. 1 (2), 113–116.
21. Smarandache F. and Rabounski D. Unmatter entities inside nuclei, predicted by the Brightsen nucleon cluster model. *Progress in Physics*, 2006, v. 2 (1), 14–18.
22. Steinhardt P. Theories of anything. http://www.edge.org/response-detail/25405, 2014.
23. Tegmark M. Parallel universes in Science and Ultimate Reality: From Quantum to Cosmos. in Barrow J. D., Davies P. C. W. and Harper C. L. (eds), Cambridge University Press, 2003.
24. Tegmark M. Our mathematical universe: My quest for the ultimate nature of reality. Knopf Doubleday Publishing Group, 2014.

Question of Planckian "Action" in Gravitational Wave Detection Experiments

Joseph F. Messina
Topical Group in Gravitation, American Physical Society, P.O. Box 130520,
The Woodlands, TX 77393, USA. E-mail: jfmessina77@yahoo.com

It is shown that in the absence of a *purely* gravitational measurement of Planck's constant one *cannot* at present rule out the possibility that the ripples in the curvature of the *fabric* of spacetime may be *scaled* by a more diminutive "action" whose detection requires sensitivities beyond the standard quantum limit. An experiment that could unequivocally test this possibility is suggested.

1 Introduction

The search for gravitational waves, one of the centerpieces of general relativity, has been a work in progress for over five decades. Two main forms of detectors are currently in use worldwide. The first, pioneered by Weber [1] in the 1960s, is based on the expectation that a passing gravitational wave will induce a mechanical oscillation in a cryogenically cooled cylindrical bar whose resonance can then be amplified and recorded. The second method, using lasers, is designed to measure spacetime geometry variations between mirrors suspended in vacuum using interferometry in a Michelson configuration.

Despite the ever increasing sensitivity of these detectors these ripples in the curvature of the fabric of spacetime have yet to be detected. After these many years of experimentation one may therefore be justified in questioning whether the failure to detect these perturbations is symptomatic of yet to be discovered physics beyond the standard quantum limit.

It should be observed that if we examine this question from a quantum mechanical perspective we are inevitably struck by the fact that the role of Planck's constant in gravitational wave phenomena has always been taken for granted without questions regarding the possible limits of its applicability being asked, which is somewhat perplexing since no *purely* gravitational measurement of Planck's constant exists. As will be shown in this paper, if pursued, this element of uncertainty gives rise to the possibility that gravitational quanta may not be *scaled* by Planck's constant.

2 Scaling of gravitational quanta

It should be emphasized from the outset that any discussion of this possibility has as its foundation the irrefutable fact that nature has made available *two* immutable elementary "actions" in the context of the framework of quantum mechanics. That is, Planck's familiar constant, h, which has been shown experimentally to play an indispensable role in the microphysical realm, and a second, more diminutive "action" formed from two of the fundamental constants of quantum mechanics, namely, e^2/c – the ratio of the square of the elementary charge to the velocity of light, which has the value 7.6957×10^{-37} J s.

In what follows I shall put forward an experimentally verifiable hypothesis in favor of a dynamical interpretation of the fabric of spacetime. That is, we shall allow for the possibility that this more diminutive "action" is an *intrinsic* property of the fabric of spacetime; the *size* of the gravitational quanta being always *scaled* in terms of e^2/c. Implicit in this conceptualization is the widely held expectation that spacetime should play a dynamic role in its own right, rather than being a passive observer.

3 Possible experimental test

Clearly, the most direct way of verifying if this hypothesis corresponds to reality is to measure the *vibrational* displacement induced in a resonant detector by a passing gravitational wave. To give an illustration, let us assume, using the "action" constant e^2/c, that a gravitational quantum of *angular* frequency ω has an energy

$$E = \left(\frac{e^2}{2\pi c}\right)\omega\,. \tag{1}$$

We can then profit from the fact that the *vibrational* energy induced in a *resonant* detector, by a gravitational wave, can be converted to the fractional change in *vibrational* displacement by making use of the relation between amplitude x_0, energy E and the total mass M for a harmonic oscillator, in the familiar form

$$E = \frac{1}{2}M\omega^2 x_0^2\,. \tag{2}$$

If we now take as an example Weber's seminal experiment, which used as an antenna a 1400 kg cylindrical aluminum bar that had a natural *resonance* frequency ν_0 of 1660 Hz, we can readily compute the *vibrational* displacement, x, caused by a *single* quantum of gravitational radiation of *angular* frequency $\omega = 2\pi\nu_0$, and energy $(e^2/2\pi c)\,\omega$. Combining Eqs. (1) and (2) and then substituting these values, we obtain

$$\begin{aligned} x &= \sqrt{\frac{2}{M\omega}\frac{e^2}{2\pi c}} \\ &\approx 1.3 \times 10^{-22}\ \text{m}. \end{aligned} \tag{3}$$

Needless to say, such extraordinarily small displacements could not be measured with the technology available in Weber's day. Indeed, even today such a feat remains out of reach since there are no resonant-mass antennas in operation that have the required sensitivity.

Fortunately, since Weber's pioneering work in the 1960s numerous projects have been undertaken in an effort to enhance detector sensitivity. One of the more innovative of these efforts has been the development of the Schenberg *spherical* resonant-mass telescope in Brazil [2], which has the advantage of being omnidirectional. When fully operational it will provide information regarding a wave's amplitude, polarization, and direction of source. The detector program, which we shall presently exploit, uses an 1150 kg spherical resonant-mass made of a copper-aluminum alloy, and has a *resonance* frequency ν_0 of 3200 Hz. The *vibrational* displacement caused by a *single* quantum of gravitational radiation of *angular* frequency $\omega = 2\pi\nu_0$ can easily be computed by direct substitution of these values in Eq. (3). We thus obtain

$$x \approx 1.0 \times 10^{-22} \text{ m}. \tag{4}$$

Verification of this result is contingent on the Schenberg surpassing the standard quantum limit by *squeezing* the signal, which should result in a ten-fold increase in sensitivity. Clearly, in the absence of a physical law that prohibits an elementary "action" smaller than Planck's this result must be taken seriously.

4 Summary

The possibility was raised that gravitational quanta may not be scaled by Planck's constant. It was shown that in the absence of a *purely* gravitational measurement of Planck's constant one *cannot* at present rule out the possibility that gravitational quanta may be *scaled* by the more diminutive of nature's two *elementary* "actions", namely, e^2/c, which was conjectured to be an *intrinsic* property of the fabric of spacetime. A possible experiment requiring sensitivities beyond the standard quantum limit was suggested.

Acknowledgments

I would like to thank Dr. Odylio Aguiar for his update on the status of the Schenberg detector, and his assessment of its potential. I also wish to thank Dr. Alexander Khalaidovski for his assessment of the potential of the squeezed light technique for reducing quantum noise.

Submitted on April 11, 2015 / Accepted on April 15, 2015

References

1. Weber J. Evidence for Discovery of Gravitational Radiation. *Phys. Rev. Lett.*, 1969, v. 22, 1320–1324.
2. Aguiar O. D. The Brazilian Spherical Detector: Progress and Plans. *Class. Quantum Grav.*, 2004, v. 21, 457–463.

Appendix

The recognition of the "action" e^2/c as an intrinsic property of the fabric of spacetime inevitably leads to quantum uncertainty at a more fundamental level than Planck's constant, in the analogous form

$$(\Delta x)(\Delta p) \approx \frac{e^2}{c} \tag{1}$$

where, as usual, x is uncertainty of position, and p the uncertainty in momentum. Its implication for the *temporal* events that make up the big bang can be simply illustrated in terms of the *sub-Planckian* unit of time, T_0, analogous to the Planck time $T_P = \sqrt{\hbar G/c^5}$, in the form

$$T_0 = \sqrt{\frac{e^2}{2\pi c}\frac{G}{c^5}} = 1.837 \times 10^{-45} \text{ s} \tag{2}$$

where $(e^2/2\pi c)$ is the reduced *sub-Planckian* "action" constant, G is the Newtonian gravitational constant, and c is the velocity of light. Unfortunately, because of the *sub-Planckian* uncertainty principle, Eq. (1), we are prevented from speculating on times shorter than 10^{-44} seconds after the big bang, which is an order of magnitude prior to the Planck era (10^{-43} seconds). The disparity in this temporal sequence of events is, needless to say, cosmologically significant since it implies that a *sub-Planckian* era *preceded* the Planck era in the nascent universe, which should be discernible from its gravitational signature.

Dynamical 3-Space: Anisotropic Brownian Motion Experiment

Reginald T. Cahill

School of Chemical and Physical Sciences, Flinders University, South Australia. E-mail: reg.cahill@flinders.edu.au

In 2014 Jiapei Dai reported evidence of anisotropic Brownian motion of a toluidine blue colloid solution in water. In 2015 Felix Scholkmann analysed the Dai data and detected a sidereal time dependence, indicative of a process driving the preferred Brownian motion diffusion direction to a star-based preferred direction. Here we further analyse the Dai data and extract the RA and Dec of that preferred direction, and relate the data to previous determinations from NASA Spacecraft Earth-flyby Doppler shift data, and other determinations.

1 Introduction

In 2014 Jiapei Dai [1] reported evidence of anisotropic Brownian motion, and in 2015 Felix Scholkmann [3] detected a sidereal time dependence, indicative of a process driving the preferred Brownian motion diffusion direction to a star-based preferred direction. Here we further analyse the Dai data and extract the RA and Dec of that preferred direction, and relate the data to previous determinations from NASA spacecraft Earth-flyby Doppler shift data, and other determinations [5]. It is shown that the anisotropic Brownian motion is an anisotropic "heating" generated by the dynamical 3-space [4].

2 Anisotropic Brownian motion

Dai in Wuhan City detected anisotropic Brownian motion by loading a small drop of toluidine blue solution into a container of water. The diffusion pattern was photographed starting within 30 sec of loading the water cell and then once every ten minutes until the end of observations [1]. The images were analysed using image analysis software. The observations were performed 24 times per day, and repeated from December 22, 2011 to March 23, 2013.

The image of the diffusion anisotropy is illustrated in Figure 1, with directions measured from East in a clockwise direction. Dai reported the preferred direction of diffusion from 15 days, plotted against Wuhan Solar Time. In Fig. 2 that data has been replotted against Local Sidereal Time for Wuhan City. We now analyse that data from the point of view of a preferred 3-space velocity, where the Right Ascension, RA, is defined by when the preferred diffusion direction is from S to N. The Declination is to be determined by the dynamic range of the diffusion direction over one day, as in Fig. 4. We report herein that the anisotropic Brownian motion data confirms various properties of the 3-space flow previously reported [5].

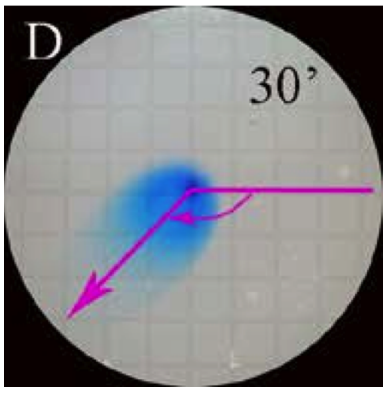

Fig. 1: Illustration of anisotropic diffusion of the toluidine blue solution in water, 30 min after inserting drop. The preferred direction is measured clockwise in degrees from East. Reproduced from [1].

3 Dynamical 3-space

The Schrödinger equation must be extended to include the dynamical space [6]

$$i\hbar\frac{\partial\psi(\mathbf{r},t)}{\partial t} = -\frac{\hbar^2}{2m}\nabla^2\psi(\mathbf{r},t) + V(\mathbf{r},t)\psi(\mathbf{r},t) - \\ -i\hbar\left(\mathbf{v}(\mathbf{r},t)\cdot\nabla + \frac{\mathbf{1}}{\mathbf{2}}\nabla\cdot\mathbf{v}(\mathbf{r},\mathbf{t})\right)\psi(\mathbf{r},t). \quad (1)$$

Here $\mathbf{v}(\mathbf{r},t)$ is the velocity field describing the dynamical space at a classical field level, [4], and the coordinates $\mathbf{r}$ give the relative location of $\psi(\mathbf{r},t)$ and $\mathbf{v}(\mathbf{r},t)$, relative to a Euclidean embedding space, and also used by an observer to locate structures. This is not an aether embedded in a non-dynamical space, but a dynamical space which induces an embedding space or coordinate system. This minimal generalisation of the original Schrödinger equation arises from the replacement $\partial/\partial t \to \partial/\partial t + \mathbf{v}.\nabla$, the Euler derivative, which ensures that the quantum system properties are determined by the dynamical space, and not by the embedding coordinate system. The extra $\nabla\cdot\mathbf{v}$ term in (1) is required to make the hamiltonian in (1) hermitian.

4 Analysing Brownian motion data

For a plane wave $\psi = e^{i\mathbf{k}\cdot\mathbf{r}-i\omega t}$, for water molecules, this results in an energy shift $E = \hbar\omega \to E + \hbar\mathbf{k}\cdot\mathbf{v}$. The Dai data in Fig. 2 reveals a complex behaviour, with not all data revealing a RA for the preferred flow. However this is explainable by two key observations. First the fluctuations in the 3-space

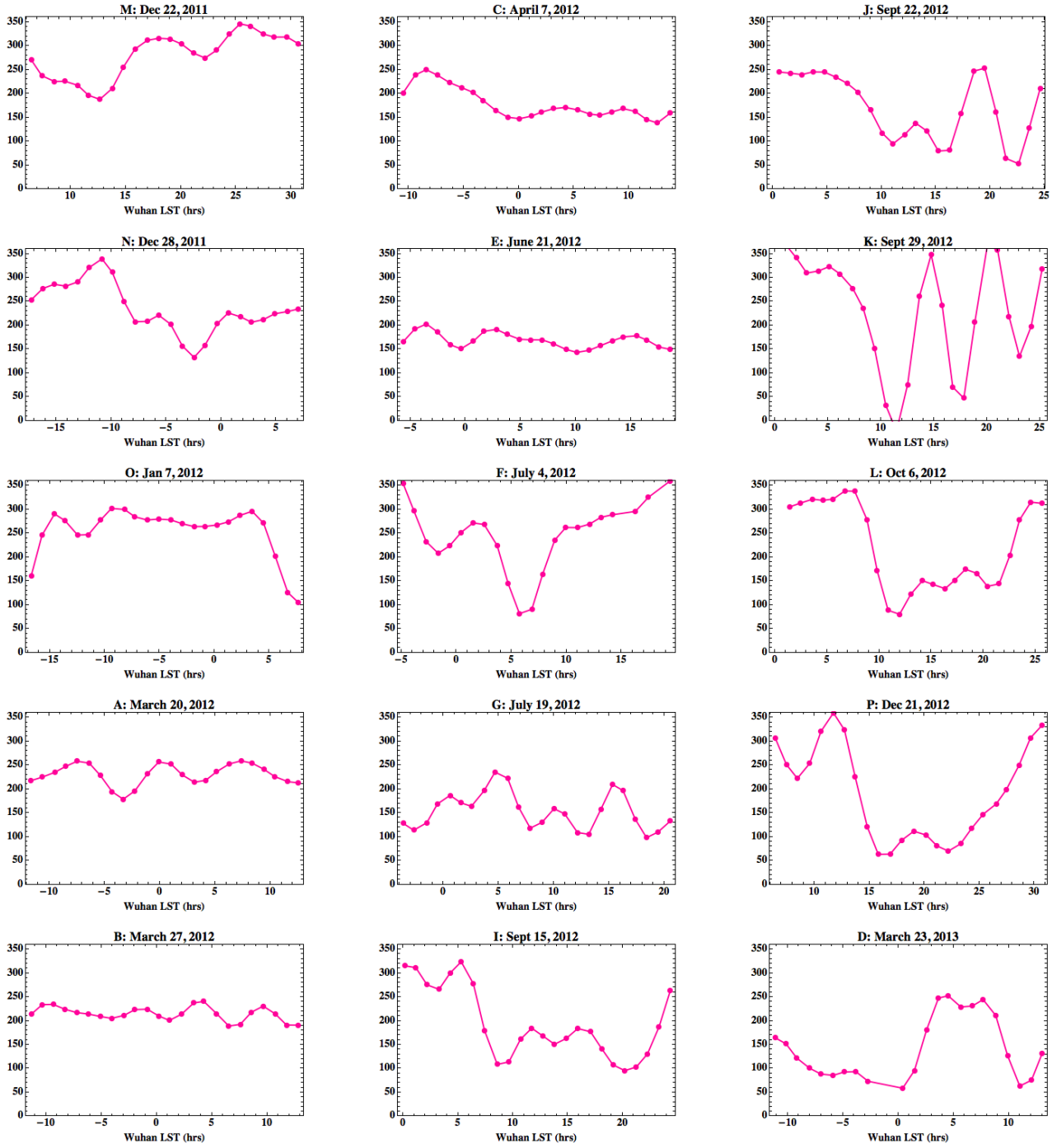

Fig. 2: Dai data [1], showing preferred direction of colloidal diffusion, plotted against Wuhan Local Sidereal Time (LST), for the various indicated days. The coding M, N, ... refers to the labelling in [1], which reported the data against Wuhan local solar time. The preferred direction of diffusion is measured as indicated in Fig. 1.

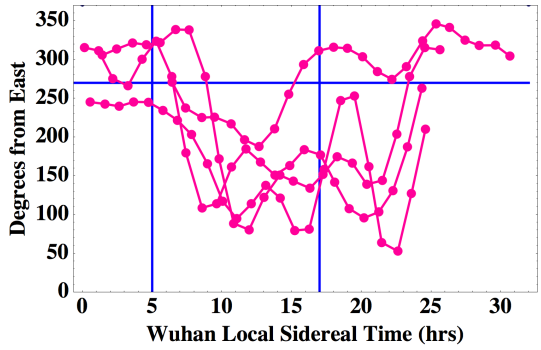

Fig. 3: Plot of the better data from Fig. 2: M, I, J, L. These days show trend of preferred direction to be from South to North (270°) at ~5 hrs LST. A similar trend might be expected for 17hrs LST, but is not seen in all days shown. This is because at this approximate LST the space flow passes more deeply through the Earth, see Fig. 5, which results in considerable increase in turbulence.

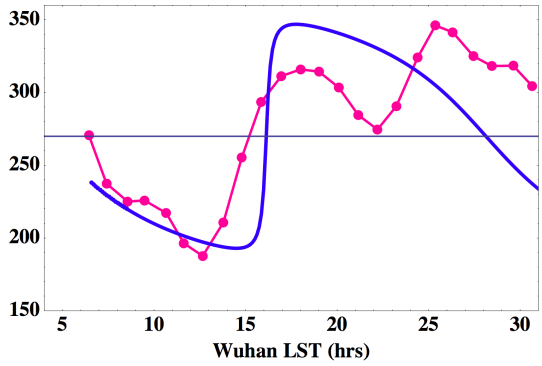

Fig. 4: Plot of Dai data vs Wuhan LST for Dec 22, 2011 (plot M in Fig. 2). Smooth curve (blue) is predicted form for RA=5hrs, Dec=60°S. The RA is defined by when dynamical 3-space flow direction is from S to N, here RA 5hrs and 17hrs. The Dec determines the variation in direction, here 270° ± 40°. Note the increased turbulence, manifesting as fluctuations in direction of the flow, when the flow is more deeply through the Earth. For Dec 8, 1992, the NASA Doppler shift data gave RA=5.23hrs, Dec=80°S, [5].

flow manifest as changes in both speed and direction. When the data for the better days is plotted, as in Fig. 3, we see that the RA cluster around 5hrs Local Sidereal Time. However we would also expect to see the data crossing the due N direction (270°) some 12 hours later. However the data in Fig. 3 shows much noisier variations. This second key observation is that this is also expected as during these times the 3-space flow has passed deeply into the earth, as shown in Fig. 5, and this results in increased turbulence in both speed and direction. One consequence of this is that future studies of anisotropic Brownian motion should be performed well into the southern hemisphere. Finally, from the 3-space turbulence, we expect the best quality data, being least affected by 3-space turbulence, would be for day M. That data is shown in Fig. 4, which gives an approximate RA=5hrs, Dec=60°S. This is consistent with the RA and Dec for December from the NASA Doppler shift data [5].

5 Conclusion

That the known characteristics of the 3-space flow agree with results from the anisotropy of the Brownian motion data suggests a simple mechanism, namely that the 3-space flow generates an energy shift in the water molecules; $E \to E + \hbar\mathbf{k}\cdot\mathbf{v}$, where $\mathbf{k}$ is the wavenumber vector for water molecules, and that this is largest for water molecules moving in the direction of $\mathbf{v}$. This results in water molecules moving in the direction of $\mathbf{v}$ having a greater kinetic energy, and imparting more momentum to the toluidine colloidal particles than water molecules moving in the opposite direction. So the $-i\hbar\mathbf{v}\cdot\nabla$ term gives rise to an enhanced Brownian diffusion in the direction of $\mathbf{v}$.

A similar effect was observed by Shnoll [7] in which the α decay rate of ^{239}Pu is directional dependent. This is also explained by the $-i\hbar\mathbf{v}\cdot\nabla$ term, as it causes the α kinetic energy to be different in different directions related to $\mathbf{v}$, and so affects the quantum tunnelling process, with more α emerging in the direction of $\mathbf{v}$.

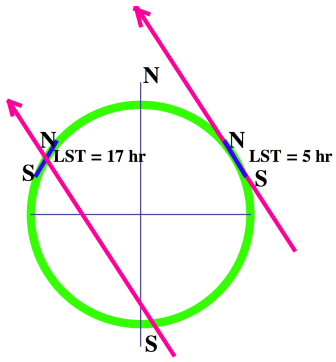

Fig. 5: Cross section of Earth showing Wuhan horizontal planes and the local N and S directions at Local Sidereal Times of 5 hr and 17 hr. Also shown is dynamical 3-space flow direction, with a Declination of -60°. At LST of ~17hr the flow passes most deeply into the Earth, resulting in significant turbulence, as revealed by the Brownian motion data in Figs. 3 and 4.

Submitted on April 2, 2015 / Revised on April 17, 2015
/ Accepted on April 20, 2015

References

1. Dai J. Macroscopic Anisotropic Brownian Motion is Related to the Directional Movement of a "Universe Field". *Natural Science*, 2014, v. 6 (2), 54–58.
2. Scholkmann F. Indications for a Diurnal and Annual Variation in the Anisotropy of Diffusion Patterns – A Reanalysis of Data Presented by J. Dai (2014, Nat. Sci.). *Progress in Physics*, 2014, v. 10 (4), 232–235.
3. Scholkmann F. Solar-Time or Sidereal-Time Dependent? The Diurnal Variation in the Anisotropy of Diffusion Patterns Observed by J. Dai (2014, Nat. Sci.). *Progress in Physics*, 2015, v. 11 (2), 137–138.

4. Cahill R. T. Discovery of Dynamical 3-Space: Theory, Experiments and Observations – A Review. *American Journal of Space Science*, 2013, v. 1 (2), 77–93.
5. Cahill R. T. Combining NASA/JPL One-Way Optical-Fiber Light-Speed Data with Spacecraft Earth-Flyby Doppler-Shift Data to Characterise 3-Space Flow. *Progress in Physics*, 2009, v. 5 (4), 50–64.
6. Cahill R. T. Dynamical Fractal 3-Space and the Generalised Schrödinger Equation: Equivalence Principle and Vorticity Effects. *Progress in Physics*, 2006, v. 2 (1), 27–34.
7. Shnoll S. E. Cosmophysical Factors in Stochastic Processes. American Research Press, Rehoboth, New Mexico, USA, 2012. http://www.ptep-online.com.

Beyond Quantum Fields: A Classical Fields Approach to QED

Clifford Chafin

Department of Physics, North Carolina State University, Raleigh, NC 27695. E-mail: cechafin@ncsu.edu

A classical field theory is introduced that is defined on a tower of dimensionally increasing spaces and is argued to be equivalent to QED. The domain of dependence is discussed to show how an equal times picture of the many coordinate space gives QED results as part of a well posed initial value formalism. Identical particle symmetries are not, a priori, required but when introduced are clearly propagated. This construction uses only classical fields to provide some explanation for why quantum fields and canonical commutation results have been successful. Some old and essential questions regarding causality of propagators are resolved. The problem of resummation, generally forbidden for conditionally convergent series, is discussed from the standpoint of particular truncations of the infinite tower of functions and a two step adiabatic turn on for scattering. As a result of this approach it is shown that the photon inherits its quantization $\hbar\omega$ from the free lagrangian of the Dirac electrons despite the fact that the free electromagnetic lagrangian has no $\hbar$ in it. This provides a possible explanation for the canonical commutation relations for quantum operators, $[\hat{P}, \hat{Q}] = i\hbar$, without ever needing to invoke such a quantum postulate. The form of the equal times conservation laws in this many particle field theory suggests a simplification of the radiation reaction process for fields that allows QED to arise from a sum of path integrals in the various particle time coordinates. A novel method of unifying this theory with gravity, but that has no obvious quantum field theoretic computational scheme, is introduced.

1 Introduction

Quantum field theory, in some ways, marks the ultimate state of our understanding of physics. In its computational exactness, it can be thrilling yet its conceptual grounding is very unsatisfactory. Field theory has its origins in the 1920's and 1930's when attempts to include particle creation and the quantization of the photon necessitated a larger mathematical structure [13, 17]. Fock space seemed to have sufficient features to encompass the intrinsic quantum and particle number variable features. The ladder operators of the harmonic oscillator could be formally modified to give an algebra that allowed these various particle number spaces to interact. Different attempts to generate an equation of motion and find transition rates led to various formal procedures. Classical lagrangians were varied in a formal manner with "second quantized" operators in approaches by Schwinger and Tomanaga and systematic procedures to handle the divergent terms were introduced [15, 17]. Feynman gave a very intuitive approach using path integrals that was put into a formal structure by Dyson. This approach has gained prominence due to its ease of organizing the terms of the expansion.

Quantum mechanics is the quantum theory of fixed particle number systems. Certain quasi-classical approaches made the treatment of radiative decay possible without QED at low energies. Nevertheless, even in this low energy domain, the theory had lingering conceptural problems. Measurement and the "collapse of the wavefunction" led to paradoxes that have spawned an enormous literature [7]. Decoherence is a popular "explanation" of these effects but these tend to rely on assumptions that are just pushed off to other parts of the analysis [16]. The Born interpretation, due to its simplicity and historical inertia, still dominates most treatments of classical-quantum interactions. Some may object that there are now ways to treat measurements independently of the Born interpretation to handle to new sorts of quantum nondemolition measurements [11] but these ultimately involve other ad hoc statistical assumptions. Quantum statistical mechanics has never found any solid conceptual footing despite the frequent success of its formalism in describing thermodynamic behavior and providing numerical results. This problem is often given a short comment in books on the subject and little progress has been made. Ultimately, an initial data formulation approach must resolve all of these issues in terms of the dynamical equations and provide evidence for the kinds of initial data that is physically relevant.

The quantum field theory approach to quantum mechanics is on a solid footing. Even though operators may change the particle number, it is always changed back at every order in the expansion. One may show [15] that this gives an exact isomorphism with the Schrödinger, Heisenberg and interaction picture versions of QM. This leads to the Feynman path integral approach to quantum mechanics which, while equivalent, generally gives absurdly difficult derivations of results compared to other means. In contrast, regularization of the path integral has never had a very solid mathematical foundation but applying the theory in a "standard" fashion gives correct results. The main uses of QFT is in relativistic physics, quasiparticle motions in condensed matter and in the "Wick rotated" form which converts temporal evolution

to a high temperature expansion of the thermodynamic potentials. The correspondence of QFT in the case of quasiparticle evolution to that of Schrödinger evolution is itself challenging [2]. Fundamentally, one must give a description of the many-body wavefunction's excited states to give such a correspondence. This has led to the popularity of Green's function methods in condensed matter physics since it sidesteps this difficult work and leads directly to calculations. The validity of the derivation of the Kubo formula [8] has been extensively criticized [9] but it has, nevertheless, proved to be of great use over a broader range of phenomena than should be expected.

Given that no true classical-quantum correspondence of objects is known, it is unclear when one should impose classical structures (like hydrodynamics) on the system and when to extract certain properties (like viscosity) by quantum means. This is of particular interest in the study of ultracold gas dynamics [5] and superfluid Helium. There are popular and sometimes successful approaches for doing this but it is never clear that they must follow from the true many body dynamical theory or that we have simply made enough assumptions to stumble on to the tail of a correct derivation, the first, and correct part of which is a mystery to us. The general vagueness and nonspecificity of the subject allows theorists great freedom to generate calculations that then can be compared with experimental or Monte-Carlo data for affirmation of which ones to keep. This very freedom should undermine our reasons for faith in our theory and intuition. Instead it, together with professional publication demands, seems to create a selective pressure in favor of optimism and credulity on the part of practitioners and an air of mystical prophecy of our physics fathers and those who derive experimentally matching results.

In relativistic field theory, where particle creation is important, there are additional problems. Renormalization is necessary because of the local interactions of particles and fields. Classical physics certainly has such a problem and the radiation reaction problem of classical electrodynamics still has unanswered questions [14]. The series derived from QFT in the relativistic and quasiparticle cases tend to be asymptotic series and conditionally converging. Nonetheless, it seems very important to resum these series over subsets of diagrams to get desired approximations and Green's functions that are analytically continued to give the propagator pole structure corresponding to masses and lifetimes of resonances. The path integral itself has too large a measure to give a rigorous derivation. Regularization procedures, like putting the integrals on a Euclidean lattice for computation, length scale cutoffs, Wilson momentum cutoffs, dimensional regularization and others, are introduced to get finite results [13]. Of the conceptual problems facing quantum theory, renormalization will be shown to be a rather modest one. Justifying the use of resummation will be much more serious.

The Schrödinger approach to quantum mechanics has a special place. Questions of causality and geometric intuition are most naturally discussed in a real space picture. The diffusive nature of this equation is problematic but vanishes in the relativistic limit of the Dirac equation. Unfortunately, this is exactly where particle creation effects become important. In relativistic classical field theory, all causality questions are resolvable systematically. The structure of the equations ensures that it is valid. Other advantages of classical fields are that they are deterministic, propagate constraints exactly, give clearly obeyed conservation laws and introduce a specificity that allows all philosophical questions and thought experiments to be resolved through examination of their own mathematically consistent structure. In some cases, like relativity, our intuition may need to be updated but how this is to be done is made clear through such examples. QFT clearly works at the level of computation for many problems. This makes one believe that maybe our precursory arguments and descriptions leading to those calculations are fine and merely need elaboration. Given the success of so many calculations, it comes as a great disappointment that almost any interacting field theory is inconsistent [6].

Beyond these problems, the use of one particle lagrangians and couplings that get promoted to many body interacting theory through canonical quantization or propagator methods lead to a kind of conceptual disconnect that makes the solid implications of classical field theory, e.g. Noether's theorem and conservation laws, unclear. These conservation laws can be formally defined by a correspondence of operators and checked but are no longer strict implications of the symmetries of a lagrangian. The symmetries of one-particle systems themselves require a more explicit definition in the many body case where multiple coordinate labels of the wavefunction Ψ can describe independent motions but the current state of theory does not present a solid enough foundation to show how and when to make this manifest as an important symmetry. The meaning of a "propagator" in classical theory is simple yet it is often not appreciated that the full reality described by a Klein-Gordon (KG) field is not necessarily contained in the support of ϕ in a given constant time slice due to its second order nature. This is often lost in confusing discussions in terms of positive and negative energy components. This will be resolved for both KG and Dirac equations in the classical and quantum cases and clear up any apparently acausal effects without reference to commutation relations and formal measurement.

It is an emotionally identical state to feel that something is wrong but unclear, lacking sufficient specificity, or that we simply don't understand. The formal character of quantum field theory has produced a useful computational tool but left enough vague and ill-defined that there is plenty to improve. It is interesting that it has been proved that no interacting quantum field theory is consistent [6]. People typically shrug this off as with the other conceptual troubles in quantum theory. At some point people have to generate work or do some-

thing else but eventually formal approaches are destined to lose productivity. Beyond that is the lack of satisfaction that one really understands what one is doing. It is very common in physics to find clever solutions or long derivations that turn out to be flawed. Classical systems exist as well posed initial value problems so that they can be tackled from many angles: perturbation theory, conservation laws, idealized systems, ... A well posed such problem that describes field theory would doubtlessly open some new doors.

The foregoing was to show that some new approach to the reality described by QFT is justified. In doing so, QFT's successes are the best guide to start. In the following we will seek a well-posed classical relativistic theory over a tower of spaces of increasing dimension that will have some loose correspondence with Fock space. This will not be guided by the computational convenience it affords but logical and mathematical consistency and specificity. Since we are taking the point of view that the fields are valid at all time (so implicitly have an "emergent measurement theory" at work) we don't need to think of "particles" as something more than a label for some axes in our higher dimensional space. It will turn out that we will need a larger encompassing structure than field theory on Fock space to describe the phenomenology of QFT adequately. From this we can derive QFT phenomenology in a suitable limit and use its rigid structure to answer conceptual questions in a more convincing fashion. Since this will strictly be a deterministic covering to QFT we consider for it a new name, *deterministic wave mechanics* (DWM). Its purpose is to elucidate an explanation of why quantum field theory works and give a framework for modifications, like the inclusion of gravity, that may have a well posed structure but not exist in the framework of QFT itself. In the following we will use QED as a particular case but the generalizations will be evident.

2 Overview

The goal here is to introduce set of many particle number spaces where energy, mass, charge, probability, stress, ... can travel between the spaces at two-body diagonals. This will necessitate we make sense of multiple time labels and have a well defined set of initial data and regions where interacting fields can consistently evolve in this high dimensional many-time structure. Because there will be no "field operators" there will be no need for a translationally invariant vacuum to build particles from. If we start with N electrons, the number of photons may increase and electron-positron pairs can appear but the net charge is the same in every space where nonzero amplitude exists. This eliminates the basis of Haag's theorem and its contradiction.

Firstly, we will introduce separate equations of motion and particle labels for electrons and positrons. The amplitude of each of these will be positive locally and interactions will not change this. Negative norm states exist but are never utilized by the system. This is due to a symmetry of the dynamical equations not a constraint akin to the Gupta-Bueler formalism. The photon fields will be described by both A and $\dot{A}$ labels so that, each "photon" will now have $4 \to 2 \times 4$ coordinate labels. An important distinction here with QFT is that there will be nonzero functions in the "tower" of fields that have zero norm. For example, in a one-electron zero-photon system, $\psi(x)$ has full norm while the function in the one-electron and Φ_{em} sector is nonzero. The norm of electromagnetic fields will not be a simple square of the function amplitude but a function of its amplitude and derivatives in such a way that only if there are imaginary parts will it contribute to the "norm." Thus our tower of functions will involve many nonzero ones that have no norm and the electromagnetic field can pick up some complex components. This suggests that our theory may have a larger configuration space than QFT. A explanation of QFT may arise from this by thinking of QFT tracking the flow of norm and other conserved quantities through the system while ignoring these higher nonzero functions and, in some gauges, treating them as constraints.

Once we have a suitable configuration space, equations of motion and reasonable sense of "future" we seek a mapping of QED into the space. The tools used to treat scattering in QFT involve "adiabatic turn on/off" of the interactions, regularization and renormalization. Typically we sum over special subsets of diagrams and adjust the "bare" parameters to get the right free behavior for these modifications. The regularization can be easily dealt with as in classical theory by assuming finite size effects. This is essential for the radiation reaction. It is still unclear how QFT can treat the radiation reaction adequately so this alone may introduce new physics. The sort of initial data with interactions already "on" requires we work with a truncated set of the total space on interactions. Implicit here is that the bare parameters be chosen to give the right momenta and other observable for the "free" particles (in the sense that they are ballistic not that interactions are turned off). The structure of the theory allows us to adjust couplings and interactions with far more freedom than QFT for perturbative purposes. Resummation has always been the most dubious aspect of QFT. Conditionally convergent series should not be rearranged so having a limiting method to make sense of this is an important improvement. In this paper we will not prove an isomorphism with QED, and, given the inconsistencies in the theory, this may be for the best. A foundation is laid with some arguments for its ability to generate QED results, but given the scope of the subject, much more work remains than can be done in this one paper.

Finally we will discuss a method of combining this with gravity by promoting the γ matrices themselves. This will require some extension of most fields to allow dual pairs so that the quadratic lagrangians become bilinear. Such a method is distinct from vierbein approaches and works on a flat background. Some important extensions of the notion of gauge freedom arise here and the "reality" of the particles can be

shown to move causally yet not be definable in any obvious fashion in terms of the fields.

3 The configuration space

3.1 Dirac fields

In the early days of the Dirac equation, interpretations have evolved from a proposed theory of electrons and protons to that of electrons and positrons with positrons as "holes" in an infinitely full electron"sea" to that of electrons with positrons as electrons moving "backwards in time." The first interpretation failed because the masses of the positive and negative parts are forced to be equal. The second was introduced out of fear that the negative energy solutions of the Dirac equations would allow a particle to fall to endlessly lower energies. The last was introduced as a computational tool. The negative mass solutions were to be reinterpreted as positive mass with negative charge. Necessary fixes to this idea are subtly introduced through the anticommutation relations and the algebraic properties of the vacuum ground state used in the field theory approach.* If we are going to seek a classical field theory approach to this problem we need another mechanism.

In a universe containing only electrons and positrons we require the fields Ψ_e, Ψ_p, Ψ_{ee}, $\Psi_{ep}\ldots$ where the number of spinor and coordinate labels is given by the number of particle type labels as in $\Psi_{ee} = \Psi^{ab}_{ee}(x^\mu, y^\nu)$. The lagrangian density must distinguish electrons and positron by their charge only. Since we have not included any photons yet and we have asserted that positive norm will be enforced on the initial data (and suggested it will be propagated even in the interacting case) these will have equations of motion that follow from the related one particle lagrangians

$$\begin{aligned}\mathcal{L}_e &= i\hbar\bar{\psi}_e\gamma^\mu\nabla_\mu\psi_e - m\bar{\psi}_e\psi_e\\ \mathcal{L}_p &= i\hbar\bar{\psi}_p\gamma^\mu\nabla_\mu\psi_p + m\bar{\psi}_p\psi_p.\end{aligned} \tag{1}$$

The sign of the charge will be discussed when the electromagnetic field is added but, at this point, could be chosen either $\pm q$. We confine ourselves to the Dirac representation and the positron lagrangian is chosen so that its rest positive energy contribution is in the v component of the spinor $\binom{u}{v}$ unlike the the electron case. We will only be interested in initial data with positive energy. Later we will see that this is consistent with the kinds of creation and annihilation operator couplings in QED that allows positrons to have positive energy. We still need a lagrangian for our many particle wavefunctions. In this noninteracting case, we consider this to be built of a sum of the one particle ones so that the lagrangian of the two electron field $\Psi_{ab}(x^\mu, y^\nu)$ is

$$\begin{aligned}\mathcal{L}_{ee} = {}& i\hbar\Psi^*_{af}\gamma^0_{ab}\gamma^\mu_{bc}\nabla_\mu\Psi_{cf} - m\Psi^*_{ab}\gamma^0_{ac}\Psi_{cb} +\\ &+ i\hbar\Psi^*_{fa}\gamma^0_{ab}\gamma^\nu_{bc}\nabla_\nu\Psi_{fc} - m\Psi^*_{ab}\gamma^0_{ac}\Psi_{cb}\end{aligned} \tag{2}$$

where we have explicitly written out the indices associated with spinor labels and coordinates and the summation convention is assumed for all repeated indices. The action is to be computed by integrating over a region in the 2-fold Lorentz space $\mathbb{R}^4\times\mathbb{R}^4$. Variation of the function can be done holding it constant along y and x respectively leading to the usual equations of motion along the separate time coordinates t^x, t^y for a product function $\Psi = \psi_1(x^\mu)\,\psi_2(y^\nu)$.

From a dynamical point of view, we are mostly interested in the cases where the fields are all evaluated at equal times. However we should ask what it even means to evaluate a function at two different times. When is this even meaningful? If we specify $\Psi(x^\mu_1, x^\nu_2)$ at $t_1 = t_2$ we desire to know into what region of this many-time future we should expect a solution. Further explanation of the equal time evolution is discussed in Sec. 3.4.

Considering free propagators we can evolve the data from (x_1, x_2) in the t_1 direction indefinitely and similarly for t_2. The domain of dependence is then the union of the two backwards light-cones $|x'_1 - x_1| < c\,(t_{1'} - t_1)$ and $|x'_2 - x_2| < c\,(t_{2'} - t_2)$. Interactions will allow free evolution for such a function except on 2-body diagonals $x^\mu = y^\nu$. When these cones intersect these regions sources and sinks with other particle number functions will arise. When these produce a net change in amplitude versus simply a potential force remains to be seen. Furthermore, it is still unclear that we can derive the static electromagnetic force effects from such a restricted local interaction. This will be explained later but first we investigate the case of free photons.

3.2 Photons

The classical electromagnetic field is a real vector field A^μ. For our many body generalization as $\Psi^\mu_a \sim \psi_a(x)\,A^\mu(y)$ we will have, generally nonseparable, combinations of electromagnetic and electron fields so making the assignment of which is "real" is ambiguous. We will find that phase differences between these fields on the many body diagonals give sources and sinks of amplitude from one particle number space to another. Firstly, let us consider the classical electromagnetic field which we can, loosely, think of as a single particle field.† The lagrangian of the electromagnetic field is

$$\mathcal{L}_A = -\frac{1}{4}F^{\mu\nu}F_{\mu\nu} \tag{3}$$

where $F_{\mu\nu} = \partial_{[\mu}A_{\nu]} = \partial_\mu A_\nu - \partial_\nu A_\mu$. For now consider only the "classical" field theory case where we have one field of each type on $\mathbb{R}^4$. The complex Klein-Gordon field has a norm conservation law induced by the global phase change $\phi \to \phi e^{i\gamma}$. In this case of a noninteracting electromagnetic field we have equations of motion $\Box A^\mu = 0$ and, allowing complex values, we have four independent global phase changes allowed in

*It is interesting to note that it is precisely the properties of this ground state that lead to the inconsistencies shown by Haag's theorem.

†Generally classical electromagnetic fields are considered as combinations of photon fields of all photon number.

addition to the usual $A_\mu \to A_\mu + \nabla\xi$ gauge freedom. We will revisit this shortly and reveal how photon quantization arises naturally from the lagrangian once coupling is introduced.

One important distinction of the electromagnetic fields versus the Dirac fields is that the equations are second order. These can be rendered into first order equations by introducing an auxiliary field $C^\mu = \dot{A}^\mu$ so that the equations of motion become

$$\begin{aligned} \partial_t A^\mu &= C^\mu \\ \partial_t C^\mu &= \partial_i \partial^i A^\mu. \end{aligned} \tag{4}$$

The extension to the many particle case leads to a proliferation of functions akin to the rapid number of increasing spin states for multiple Dirac fields. In each time direction of a two photon state $A^{\mu\nu}(x^\alpha, y^\beta)$ we need first and second order time derivatives. A complete set of first order initial data is then A, $C_x = \partial_{t^x} A$, $C_y = \partial_{t^y} A$, and $C_{x,y} = \partial_{t^x,t^y} A$ with equations of motion

$$\begin{aligned} \partial_{t^x} A^{\mu\nu} &= C_x^{\mu\nu} \\ \partial_{t^y} A^{\mu\nu} &= C_y^{\mu\nu} \\ \partial_{t^x} C_x^{\mu\nu} &= \partial_i \partial^i A^{\mu\nu} \\ \partial_{t^y} C_y^{\mu\nu} &= \partial_j \partial^j A^{\mu\nu} \\ \partial_{t^x} C_y^{\mu\nu} &= \partial_{t^y} C_x^{\mu\nu} = C_{x,y}^{\mu\nu} = C_{y,x}^{\mu\nu} \\ \partial_{t^x} C_{x,y}^{\mu\nu} &= \partial_i \partial^i C_y^{\mu\nu} \\ \partial_{t^y} C_{x,y}^{\mu\nu} &= \partial_j \partial^j C_x^{\mu\nu} \end{aligned} \tag{5}$$

where the roman indices are spatial indices related to the corresponding spacetime indices as $(t^x, x^i) = x^\mu, (t^y, y^j) = y^\nu$, etc. We can see that the number of first order fields for a source free N-photon system is $4 \cdot 2^N$ analogous to the number of spin subspaces for an N-electron system. A convenient notation for this is (P, Q) where P, Q can be 0 or 1 and the pair indicates how many derivatives of A with respect to x and y are taken. This notation gives (suppressing spacetime indices)

$$\begin{aligned} A &= C_{00} \\ C_x &= C_{10} \\ C_y &= C_{01} \\ C_{x,y} &= C_{11} \end{aligned} \tag{6}$$

which will be convenient for later generalization.

3.3 Interactions

The presence of interactions is what makes dynamics interesting. The mixing of gauge freedom means that any notion of "reality" of an electron now involves a photon field as is illustrated through the Aharonov-Bohm (A-B) effect. This is seen in the definition of a gauge invariant electron current in its explicit use of A. In the many body case we need a set of interaction terms tailored for our, now distinct, equations of motion for electrons and positrons. It also radically constrains our domain of dependence in this many time coordinate space.

Let us begin with the classical or "one body" case. The interaction terms tailored for electrons and positrons are respectively:

$$\begin{aligned} \Lambda_{eA} &= -q\bar{\psi}_a^{(e)} \gamma_{ab}^\mu A_\mu \psi_b^{(e)} \\ \Lambda_{pA} &= -q\bar{\psi}_a^{(p)} \gamma_{ab}^\mu A_\mu \psi_b^{(p)}. \end{aligned} \tag{7}$$

The free Dirac equation does not require such extra terms but we will include them from now on to make the interaction terms nicer. The sign stays the same here because of the sign flip in the charge induced by the γ^0 factor in the Dirac representation where we assume the amplitude for the resting positron is chosen in the "v" component of the spinor $\psi = \binom{u}{v}$. We previously changed the sign of the mass term in $\mathcal{L}_p$ so that the energy of this field is positive.

Including the interaction term $\mathcal{L}_e$, variation of the action yields the equations of motion

$$\begin{aligned} \tfrac{\partial F_{\mu\nu}}{\partial x^\nu} &= q j_\mu = q\bar{\psi}\gamma\psi \\ i\hbar\gamma\psi + qA^\mu\gamma_\mu\psi - m\psi &= 0. \end{aligned} \tag{8}$$

These are not all dynamic. Since the first is a second order equation of motion, the equations of motion must have two time derivatives. In this case we have the constraint $\nabla \cdot E = q\rho = q j_0$ which is propagated by the equations of motion. This is induced by the conservation law we derive from the sources, $\partial_\mu j^\mu = 0$ which shows that only three of these equations are now dynamical. We can rewrite this as a set of first order equations by the definition $C_\mu = \partial_t A_\mu$. Choosing the Lorentz gauge, $\partial_\mu A^\mu = -C_t + \partial_i A^i = 0$, we obtain $\Box A^\mu = q j^\mu$ in a form that automatically generates compatibility with the conservation of charge and is propagated for all time.

Interactions for the many body case, QED, involves two ways of coupling electrons and positrons to the electromagnetic field: a lone electron can couple to a lone electron and a photon or a photon can couple to an electron and a positron. We are not interested in any of the common "backwards in time" mnemonics or procedures here since this is an initial value approach. Firstly we should give a picture of the "tower" of states that need to be coupled.

$$\begin{aligned} &\alpha \\ &\Psi^\mu_{(A),Q}(x), \Psi^{\mu\nu}_{(AA),QR}(x,y)\dots \\ &\Psi_{(e),a}(x), \Psi^\mu_{(eA),aQ}(x,y), \Psi^{\mu\nu}_{(eAA),aQR}(x,y,z)\dots \\ &\Psi_{(p),a}(x), \Psi^\mu_{(pA),aQ}(x,y), \Psi^{\mu\nu}_{(pAA),aQR}(x,y,z)\dots \\ &\Psi_{(ep),ab}(x,y), \Psi^\mu_{(epA),abQ}(x,y,z), \\ &\qquad\qquad , \Psi^{\mu\nu}_{(epAA),abQR}(x,y,z,w)\dots \\ &\dots \end{aligned} \tag{9}$$

The first line holds a complex value α that indicates occupancy of the "vacuum" state. The next line gives the pure photon states. The N photon state has $4 \cdot 2^N$ degrees of freedom (dof) in the free case if we have not imposed any gauge constraints. Below this are the one electron states with the 1, 2, ... photon states to the right. Below are the one positron states with the various photon number states then the electron and positron states with corresponding photon number cases. The action to describe these as free fields is given by a collection of independent actions

$$\begin{aligned} S_{(e)} &= \int \left(i\hbar \Psi^*_a \gamma^\mu_{ab} \partial_\mu \Psi_b - m \Psi^*_a \Psi_a \right) dx \\ S_{(ee),1} &= \iint \left(i\hbar \Psi^*_{ba} \gamma^0_{bc} \gamma^\mu_{cd} \partial_\mu \Psi_{da} - m \Psi^*_{ba} \gamma^0_{bc} \Psi_{ca} \right) dxdy \\ S_{(ee),2} &= \iint \left(i\hbar \Psi^*_{ab} \gamma^0_{bc} \gamma^\nu_{cd} \partial_\nu \Psi_{ad} - m \Psi^*_{ab} \gamma^0_{bc} \Psi_{ac} \right) dxdy \\ &\dots \end{aligned} \tag{10}$$

The action for a single particle photon field is

$$\begin{aligned} S_{(A)} &= -\int \tfrac{1}{4} F^{\mu\nu} F_{\mu\nu} \, dx \\ &= -\tfrac{1}{4} \int \left(\partial^{[\mu} \Psi^{*\nu]}_{(A)} \right) \left(\partial_{[\mu} \Psi^{(A)}_{\nu]} \right) dx \end{aligned} \tag{11}$$

where we have included a complex conjugation. This seems unnecessary since we generally consider the electromagnetic field to be real. When we consider the functions that correlate electron and photon fields we will see that we cannot neglect it. The two photon actions are*

$$\begin{aligned} S_{(AA),1} =& -\tfrac{1}{4} \int \left(\partial^{[\mu}_{(x)} \Psi^{*\nu]\alpha}_{(AA)}(x^{\cdot}, y^{\cdot}) \right) \\ & \left(\partial^{(x)}_{[\mu} \Psi^{(AA)}_{\nu]\alpha}(x^{\cdot}, y^{\cdot}) \right) dxdy \\ S_{(AA),2} =& -\tfrac{1}{4} \int \left(\partial^{[\mu}_{(y)} \Psi^{*\nu\alpha]}_{(AA)}(x^{\cdot}, y^{\cdot}) \right) \\ & \left(\partial^{(y)}_{[\mu} \Psi^{(AA)}_{\nu\alpha]}(x^{\cdot}, y^{\cdot}) \right) dxdy \\ S_{(AC),1} =& -\tfrac{1}{4} \int \left(\partial^{[\mu}_{(x)} \Psi^{*\nu]\alpha}_{(AC)}(x^{\cdot}, y^{\cdot}) \right) \\ & \left(\partial^{(x)}_{[\mu} \Psi^{(AC)}_{\nu]\alpha}(x^{\cdot}, y^{\cdot}) \right) dxdy \\ S_{(CA),2} =& -\tfrac{1}{4} \int \left(\partial^{[\mu}_{(y)} \Psi^{*\nu\alpha]}_{(CA)}(x^{\cdot}, y^{\cdot}) \right) \\ & \left(\partial^{(y)}_{[\mu} \Psi^{(CA)}_{\nu\alpha]}(x^{\cdot}, y^{\cdot}) \right) dxdy \end{aligned} \tag{12}$$

where the $1, 2, \dots$ subscripts on the actions indicate the respective coordinate label $x^{\cdot}, y^{\cdot} \dots$ where the derivatives are being taken. The previous notation we used to distinguish coordinate order for the Dirac fields is not available here because of the more complicated index structure and we replace A and C as field labels with $\Psi_{(A)}$ and $\Psi_{(C)}$ for the sake of a uniform notation when both electrons and photons are present. Here we explicitly include the coordinates and label the first coordinate, $x^{\cdot}$, in the derivative operator $\partial^\mu_{(x)}$ and order the indices in $\Psi^{\mu\nu}$ to correspond to $x^{\cdot}$ and $y^{\cdot}$ respectively. The square backets, [ ], indicate antisymmetry over the two indices immediately to their open sides. The first order time derivative data from the "inactive" coordinates, those not being dynamically evolved by the particular lagrangian, are included with the C labels to get a full set of first order initial data. Variation of these lagrangians, through a combination of explicit and implicit expressions, gives the four functions $\Psi^{\mu\nu}_{(C_{PQ})}$ and eight linear Equations of Motion (EoM) for each function in each of the two time directions t^x, t^y.

The (noninteracting) mixed one-electron one-photon actions on $\Psi(x^{\cdot}, y^{\cdot})$ to generate EoM in each time label are

$$\begin{aligned} S_{(eA),1} =& \int \left(i\hbar \Psi^{*,\nu}_{(eA),a} \gamma^\mu_{ab} \partial^{(x)}_\mu \Psi_{(eA),b\nu} - \right. \\ & \left. - m \Psi^{*\nu}_{(eA),a} \Psi^{(eA)}_{a\nu} \right) dx \\ S_{(eA),2} =& -\tfrac{1}{4} \int \left(\partial^{[\mu}_{(y)} \Psi^{*\nu]}_{(eA),a} \right) \left(\partial^{(y)}_{[\mu} \Psi^{(eA)}_{a\nu]} \right) dx. \end{aligned} \tag{13}$$

Generalizations to higher particle numbers from here are evident but rapidly become onerous. Symmetries among identical particle types are not required by these actions but it is not hard to see that imposing them as initial data lets them be propagated.

To give an interesting theory there must be interactions. The vacuum u is strictly formal and does not couple to anything. We know that electrons and positrons can annihilate and electrons/positrons can scatter and produce a photon. The couplings must be "local" in some sense that we enforce, with inspiration from QED, as

$$\begin{aligned} S_{(e)} =& \int \left(i\hbar \bar{\Psi}^*_a \gamma^\mu_{ab} \partial_\mu \Psi_b - m \bar{\Psi}^*_a \Psi_a \right) dx \\ & + \Lambda_{(e-eA)} \\ S_{(eA),1} =& \int \left(i\hbar \bar{\Psi}^{*,\nu}_{(eA),a} \gamma^\mu_{ab} \partial^{(x)}_\mu \Psi_{(eA),b\nu} - \right. \\ & \left. - m \bar{\Psi}^{*\nu}_{(eA),a} \Psi^{(eA)}_{a\nu} \right) dx + \Lambda_{(eA-eAA)} \\ S_{(eA),2} =& -\tfrac{1}{4} \int \left(\partial^{[\mu}_{(y)} \Psi^{*\nu]}_{(eA),a} \right) \left(\partial^{(y)}_{[\mu} \Psi^{(eA)}_{a\nu]} \right) dx + \\ & + \Lambda_{(e-eA)} + \Lambda_{(eep-eA)} \\ &\dots \end{aligned} \tag{14}$$

where the "bar" action over the Ψ is hiding a γ^0 considered to be contracted on the active spinor indices. Here we see that the one-electron field $\psi = \Psi_{(e)}$ feels the electromagnetic field from $\Psi_{(eA)}$ as we evolve in its time coordinate direction $t^{(e)}$. The notion of locality for this interaction is chosen so that ψ feels the field of $\Psi_{(eA)}$ when all three spacetime coordinates agree. In this case, this gives only a self energy contribution but will give the usual two body static interaction for two charges. Conversely, the field $\Psi_{(eA)}$ feels the influence of ψ as a source where all three coordinates agree when we evolve in the time direction $t^{(eA)}_2$, the second time label corresponding

*The "upper" or "lower" state of the particle type labels (AA), (AC), (eA) etc. have no meaning but are chosen to make the expression as uncluttered as possible. Summation conventions are in effect for spacetime and spinor indices.

to A. For an electron-positron pair production or annihilation amplitude we give a similar definition of locality.

Explicitly, the couplings are

$$\begin{aligned}\Lambda_{e-eA} &= -q\int \bar{\Psi}^{(e)}_{a}(x^{\cdot})\gamma^{\mu}_{ab}\Psi^{(eA)}_{\mu,b}(y^{\cdot},z^{\cdot})\delta(x^{\cdot}-y^{\cdot})\\ &\quad \delta(x^{\cdot}-z^{\cdot})\,dxdydz\\ \Lambda_{p-pA} &= -q\int \bar{\Psi}^{(p)}_{a}(x^{\cdot})\gamma^{\mu}_{ab}\Psi^{(pA)}_{\mu,b}(y^{\cdot},z^{\cdot})\delta(x^{\cdot}-y^{\cdot})\\ &\quad \delta(x^{\cdot}-z^{\cdot})\,dxdydz\\ \Lambda_{ep-A} &= \pm q\int \Psi^{(ep)*}_{ab}(x^{\cdot},y^{\cdot})\gamma^{0}_{ac}\gamma^{\mu}_{cb}\Psi^{(A)}_{\mu}(z^{\cdot})\delta(x^{\cdot}-y^{\cdot})\\ &\quad \delta(x^{\cdot}-z^{\cdot})\,dxdydz.\end{aligned} \tag{15}$$

The sign of the pair production term is not clearly constrained here and neither is our choice of where to place the complex conjugations. Comparison with QED suggests that the sign be chosen negative and these be the correct choices of conjugation and contraction with γ^0 factors. The evolution of the free equations ensures conservation of the stress-energy, charge and particle number. These coupling terms can introduce relative phase differences at these many-body diagonals so can act as source and sink terms for amplitude. The complexity of the quantum version of the photon is important in generating these sources and in creating a norm conservation law that governs the flow of "norm-flux" between these spaces. Interestingly the conservation of charge and norm arise from the same global phase symmetry. The electron-positron field has no net charge yet will have a well defined norm from the phase symmetry $\Psi_{ab}\rightarrow e^{i\theta}\Psi_{ab}$ in the free lagrangians

$$\begin{aligned}S_{(ep),1} &= \iint\left(i\hbar\Psi^{*}_{ba}\gamma^{0}_{bc}\gamma^{\mu}_{cd}\partial^{(x)}_{\mu}\Psi_{da}-\right.\\ &\quad \left.-m\Psi^{*}_{ba}\gamma^{0}_{bc}\Psi_{ca}\right)dxdy\\ S_{(ep),2} &= \iint\left(i\hbar\Psi^{*}_{ab}\gamma^{0}_{bc}\gamma^{\nu}_{cd}\partial^{(y)}_{\nu}\Psi_{ad}+\right.\\ &\quad \left.+m\Psi^{*}_{ab}\gamma^{0}_{bc}\Psi_{ac}\right)dxdy.\end{aligned} \tag{16}$$

There is an obvious extension of these interactions to the tower of fields. We need to discuss why the equal times slice of the evolution* here is most related to what we see and experience. Before we do this let us consider the electrostatic interaction between two electrons. It has always seemed a little ad hoc that we impose the two point interaction $\frac{q}{4\pi}|x_1^2-x_2^2|^{-1}$ for a function $\Psi(x,y)$ in quantum mechanics. Certainly we can write down a one body wavefunction $\psi(x)$ and vector potential A^{μ} and impose a classical 4D lagrangian. We find an electrostatically driven self spreading distribution where the density of the norm gives the charge density. This is not at all what we see for the two charge quantum system. No such self-force is manifested beyond the usual quantum pressure.

*Specifically, for any many body point of any function of the tower, we choose all the times corresponding to the spatial coordinates equal: $t^1=t^2=t^3\ldots$.

Given the fields $\Psi^{(ee)}_{ab}(x^{\cdot},y^{\cdot})$ and $\Psi^{(eeA),\mu}_{ab}(x^{\cdot},y^{\cdot},z^{\cdot})$, we see that when we impose the Coulomb gauge that

$$\Psi^{(eeA),t}_{ab}=\Psi^{(ee)}_{ab}(x,y)\,\frac{q}{4\pi}\left(|\vec{x}^{\,2}-\vec{z}^{\,2}|^{-1}+|\vec{y}^{\,2}-\vec{z}^{\,2}|^{-1}\right). \tag{17}$$

The nature of the self-energy for such a theory seems more opaque than in the classical case where we can consider it in terms of finitely sized objects [14]. Locality and causality here are not so forgiving with such a construction and a constituent based approach would likely require an infinite number of fields of vanishing mass and charge that bind to a state of finite extent with the center-of-mass coordinates appearing as the x^{μ},y^{ν} coordinates in our $\Psi^{(ee)}_{ab}$. We will not discuss this point further but should be aware of the complication in managing self field contributions that affect both the energy and momenta of particles. Shortly we will see that even though $\Psi^{(eeA),t}_{ab}$ is nonzero it contains zero norm and that there is an infinite tower of such nonzero fields above it. This is not so evident in QFT which we may think of as tracking the nonzero norm of the fields through the tower. Now would be a good time to emphasize that these are all classical fields in a tower of spaces of growing dimensionality. There are no Grassmann variables, q-numbers or field operators and their associated commutation relations. These have always been conceptually dubious or ad hoc constructions on which field theory is built and the goal of our construction is to show why (and when) they work.

3.4 Diagonal time evolution

The relationship between the quantum and classical worlds is an enduring problem. It is not just explaining quantum measurement that is troublesome. Encoding the classical world in a quantum description is a challenge to do correctly. Naive approaches have led to such useful results as band theory and the Kubo relations but ultimately lead to inconsistencies. One approach is to assume the classical world is a very restricted subset of localized many body wavefunctions that are sparsely distributed in the total Fock space. The usual quantum statistics then follow trivially along with an arrow of time [1, 3]. The new problem is justifying such initial data. In this many time description we have the further challenge of justifying why we, as observers, seem to observe the universe of "equal times" and not the vast regions of unequal space and time locations where the many body quality of the description is more evident.

Possible explanations for this is that interactions occur at many body diagonals. Since our observations require interactions this is the part of the universe we see. In general, many body wavefunctions do not act in a form similar to discrete state machines which seem to underlie our notions of memory and consciousness. The special cases do seem to define our classical world. We will show that the equal times evolution defines the motion everywhere so all the other regions are

defined by them and so give no other possible observations of the world.

As an example, consider the evolution of the two photon field $A^{\mu\nu}(x^\alpha, y^\beta)$ along the $t^x = t^y$ axis with respect to $t = t^x + t^y$

$$\begin{aligned}
\partial_t A^{\mu\nu} &= C_x^{\mu\nu} + C_y^{\mu\nu} \\
\partial_t C_x^{\mu\nu} &= \partial_i \partial^i A^{\mu\nu} + C_{x,y}^{\mu\nu} \\
\partial_t C_y^{\mu\nu} &= \partial_j \partial^j A^{\mu\nu} + C_{x,y}^{\mu\nu} \\
\partial_t C_{x,y}^{\mu\nu} &= \partial_i \partial^i C_y^{\mu\nu} + \partial_j \partial^j C_x^{\mu\nu}.
\end{aligned} \tag{18}$$

It is unclear if this is particularly useful but it does illustrate how the evolution along the equal times axis is locally determined in the equal time coordinate t. However, we still need to evolve spatially in a neighborhood of this diagonal so the many body and many time propagator approach seems hard to avoid.

3.5 Quantization of the photon

Here we show that the quantization of the photon inherits its norm from the purely electron part of the lagrangians. This is the photon analog to the way that the "reality" of the Schrödinger electron picks up a contribution from A in the current $j^k = \frac{\hbar}{m}\nabla^k\phi - eA^k$.* This explains how the photon quantization condition can be a function of $\hbar$ despite having no such factor in its own lagrangian. It is quantized in the sense that if all the amplitude (normalized to 1) is initially in the lepton fields then it is all converted to a photon then the factor $\hbar\omega$ gives the magnitude of the photon norm. Up to this point we have been using units where $c = \mu_0 = \epsilon_0 = 1$ but left $\hbar$ general. In this section, we revert to full SI units to emphasize this connection more clearly.

In the free field cases, the usual definitions of momentum, energy... follow from the stress tensors for the classical Dirac and electromagnetic fields regardless of whether they are real or complex. The one additional conserved quantity that Dirac fields have is "norm" associated with the complex global phase freedom. The fields in the tower possess a U(1) symmetry in the sense that $\Psi \to \Psi e^{i\theta}$ and similar transformations for every function in the tower leaves the set of lagrangians invariant. When a fermion and photon field interact the coupling terms act as complex source terms resulting in, for example, a complex $\Psi^{(eA)}$ functions as the amplitude of $\Psi^{(e)}$ decreases. Since this is not generally a separable function, we cannot say whether the photon or electron part is complex individually but can predict the phase difference between the function pair and derive a many body conserved norm.

Firstly, we can modify the photon lagragian to allow complex fields as

$$\mathcal{L}_A = \frac{1}{4\mu_0}\left(\partial_\mu A^*_\nu \partial^\mu A^\nu + \partial_\mu A_\nu \partial^\mu A^{\nu^*}\right) \tag{19}$$

*We have neglected the "spin current" fraction here for simplicity.

This is essentially the massless Klein-Gordon field. The conserved current is

$$j_\mu = \frac{i}{4\mu_0}\left(\partial_\mu A_\nu \cdot A^{*\nu} - A_\nu \cdot \partial_\mu A^{*\nu}\right) \tag{20}$$

Consider the case of a complex plane wave solution $A_y(x,t) = \mathcal{A}e^{i(kx-\omega t)}$. If this was a real (classical) field there would be no current and norm would equal zero. For the complex case, $\rho = j_0 = \mathcal{A}^2\omega/2\mu_0$ and $j_x = -\mathcal{A}^2 k/2\mu_0$. In computing the norm for $\Psi^{(eA)}$ we need to use this $j^0_{(A)}$ and evaluate

$$\begin{aligned}
\hat{\mathcal{N}}(\Psi_{(eA)}) = \tfrac{i}{2\mu_0}\iint \Big(&\partial_t^{(A)}\Psi^{(eA)}_{a\nu}\Psi^{*\nu}_{(eA),a} - \\
&-\Psi^{(eA)}_{a\nu}\partial_t^{(A)}\Psi^{*\nu}_{(eA),a}\Big)\,dx^3dy^3 \\
= \tfrac{i}{2\mu_0}\iint \Big(&\Psi^{(eC)}_{a\nu}\Psi^{*\nu}_{(eA),a} - \\
&-\Psi^{(eA)}_{a\nu}\Psi^{*\nu}_{(eC),a}\Big)\,dx^3dy^3
\end{aligned} \tag{21}$$

where $\hat{\mathcal{N}}$ is the norm operator defined by j^0 for the argument function. A Dirac field gives a conserved $\int \psi^*\psi$ so this clearly gives the correct electron-photon conserved current in the noninteracting case so this is the quantity that is conserved along the equal times diagonal. Let the volume of the space be $V = 1$. Now let us investigate the implications of simultaneous conservation of energy and norm in a radiative decay process.

Suppose we start with an excited positronium state $\Psi^*_{(ep)}$ that radiates with frequency ω into the state $\{\Psi_{(epA)}, \Psi_{(epC)}\}^\dagger$ and possibly higher photon number ones. The resulting photon must have the same frequency ω since this is the frequency at which the source term oscillates. The initial norm for the states is $\hat{\mathcal{N}}\Psi_{(ep)} = 1$ and $\hat{\mathcal{N}}\Psi_{(epA)} = 0$. Our goal is to find the resulting norms after the transfer is completed, in these units. This will tell us the ratio of energy to norm transferred, which we construe as the meaning of photon quantization.

Assume the resulting function is $\Psi_{(epx)} = \Psi'_{(ep)}\mathcal{A}e^{i(kx-\omega t)}$ where $\hat{\mathcal{N}}(\Psi'_{(ep)}) = 1$. Since these lagrangians are coupled the coefficients they define a relative size for them which are respectively $\hbar$ at $t = 0$ (from the factor in the kinetic term in the electron and positron lagrangians) and

$$\hat{\mathcal{N}}\Psi_{(epA)} = \hat{\mathcal{N}}\Psi_{(A)} = \mathcal{A}^2\omega/2\mu_0 \tag{22}$$

at $t = t_f$. Since these must be equal we obtain the amplitude of the wave as $\mathcal{A} = (2\mu_0\hbar/\omega)^{1/2}$. The final energy of the system must be the same with the electron and positron in a new state with $\Delta E_{(ep)} = \Delta E_{(epA)}$. The photon contribution is given by $E_{(A)} = \int \frac{1}{2\mu_0}C^2 dx = \frac{1}{2\mu_0}\mathcal{A}^2\omega^2 = \hbar\omega$. This shows that to radiate any more energy an additional photon would need to be generated.

†Note that the notation $\{,\}$ does not denote anticommutation here. These are functions and the braces here just indicate a set.

In quantum mechanics and quantum field theory this is one of the assumptions that is hidden in the formalism. Since we are constructing an explicit classical field theory we do not have such a liberty. It was not, a priori, necessary that a transfer of energy, $\hbar\omega$, from a decay between two eigenstates give a unit norm transfer. We might have had a partial occupancy of the $\Psi_{(epA)}$ state and not completely emptied the $\Psi_{(ep)}$ one or had to resort to higher $\Psi_{(epAA\ldots)}$ states to contain all the norm that was generated by the event. This is the first actual derivation of the "quantization" of the photon. In this model, the statement of photon quantization is more precisely stated that the ratio of energy flux to norm flux between different photon number states is $j_E/j_n = \hbar\omega$, at least for the case where the frequency of the radiation is monochromatic. It is interesting that the photon "norm" depends on $\hbar$ even though the only lagrangian with such a factor is that of the fermions. The coupling has done several things. It introduces a constraint on one of the components of the electromagnetic field from the current conservation of the charges. It mixes the "reality" of the A and ψ fields to give the electron current. Here we see that it also induces the proportionality constant in the norm flux of the photon between different particle number spaces. This relationship between norm and energy flux may be what underlies the success of the formal commutation relations for field operators $[\hat{P}, \hat{Q}] = i\hbar$ [4].

4 Dynamics

We have not firmly established an isomorphism with QED for a precise subset of initial data. Ideally, imposing the usual particle symmetries on such data and evolving will match the usual scattering amplitudes. We have several barriers to doing this. Firstly is renormalization and the singularity of the coupling terms. The dimensionality of the space is so enormous and the number of nonzero yet norm free subspaces is infinitely large so finding an economical and compact manner to even start the problem is unclear if possible at all. Even finding the suitable "dressed" particles to scatter is not yet accomplished. The largest hurdle to overcome is probably the fact that no interacting field theory is well defined by Haag's theorem. This has been solved here so it might be unfair to even ask for an isomorphism between the theories. However, QED has a record of impressive calculations and the most reasonable notion of "isomorphism" may be to reproduce these. The foundational aspects of QED were designed after the fact on the tail of a process of refining procedures to obtain useful calculations so the inconsistency of these foundations may not be so important. Let us begin with a process of restricting the subspaces in a fashion that gives observable particles with enough of the interactions necessary for good approximations. Given the expanse of QED we cannot do all the work necessary to make a convincing case for this theory in a single paper. Some of this section is meant to be suggestive of more essential work ahead, not an exhaustive argument or thorough calculation to this end.

4.1 Scattering and adiabatic coupling changes

One of the most frustrating aspects of QFT is that the interim state of the system is clouded in the language of "virtual particles" and it seems to be not well defined at every time. Our measurements are confined to in and out states once the interactions are over. This is a formulaic extension to bound states where the interaction persists but this does not solve this problem. The current formulation shows that there is a well defined state at every time. Ironically, the in and out state picture has more problems at $t = \pm\infty$! This is because the interactions have been "turned off" here so the "virtual cloud" of many particle states that must always accompany a particle are no longer there. By adjusting the bare mass parameter slowly we can make an association with such states of the same net mass and momentum.

This is already formally discussed in many books. Here we will make some small changes that don't affect the results but make the process a bit more logical. Firstly, notice that the equations of motion above have been selected to give the usual propagators in the single time coordinate functions and the couplings to model those of QED. The role of the many photon coordinate spaces has been suppressed by the QED formalism and we see that there are many more spaces to consider than in the usual treatment. Once we impose the Coulomb gauge, we see that many of the constraints described by the "longitudinal photons" are just nonzero zero-norm functions in the tower.

If we consider the case of scattering of two particles, say an electron and a positron, we should properly "dress" them first. This suggests we partition our tower into a set of higher photon and electron-positron pair spaces that only couple to these particles separately. By turning on the interaction parameters slowly enough we can force the net mass and momentum of these waves to be the same without inducing any unwanted reflection. Since we typically work with plane waves of infinite extent instead of wave packets, we don't have a natural way to let spatial separation of packets prevent them from interacting but we can now use a second adiabatic turn on that lets these towers now interact and couple to the set of higher photon and electron-positron pair spaces that include both of these in more interesting ways. The more flowery aspects of QED such as "the positron is an electron moving backwards in time" is removed by our positive mass independent equation for the positron and superluminal virtual particles are now to be understood as a feature of evolving propagators in separate time spaces to arrive at the equal times result. We will now show that the apparent superluminal contributions to the Feynman propagator is actually a constraint on consistent initial data not faster than light effects that are cancelled by a measurement ansatz.

4.2 Causality considerations

The divergences we see in field theory with interactions are directly related to the singular nature of the δ-function coupling in the lagrangian. This is usually phrased in the loose semi-classical language of quantum theory as the "particles are point-like". We already expressed that our opinion was that finer nonsingular structure existed at a level we cannot yet probe. The oldest method of handling such a situation is with "cutoffs". Naively done, these are intrinsically nonrelativistic for reasons of their small nonlocality. We can make them as mild a problem as possible by choosing them in the local frame defined by the two body currents at the interaction diagonal. Specifically, it is here we need to couple two fields such as $\Psi_{(e)}$ and $\Psi_{(eA)}$ so that the electron field of $\Psi_{(e)}$ generates the electromagnetic field in $\Psi_{(eA)}$ as a source at the $x_e = x_A$ diagonal. The current $j^\mu(\Psi_{(e)})$ defines a velocity $v = j/\rho$. This specifies a local frame to construct a spherical region of radius r_0. We can then modify the electromagnetic source interaction term as $\bar{\Psi}_{(e)}\gamma^\mu\Psi_{(eA);a\mu}\delta(x_{(e),1} - x_{(e),2})\delta(x_{(e)} - x_{(A)}) \to \bar{\Psi}_{(e)}\gamma^\mu\Psi_{(eA);a\mu}\delta(x_{(e),1} - x_{(e),2})f(v, x_{(e)}, \Theta(r_0 - |x_{(e)} - x_{(A)}|))$ where f gives a boost distortion to the r_0 sphere in the rest frame defined by the current. As long as the oscillations we consider are much longer than r_0 this has little contribution to nonlocal and nonrelativistic errors for a long time. It does create a recursive (hence nonlinear) definition. We only expect cutoffs to be useful when the details of the cutoff are not important in the result. It is expected that this extension of the usual cutoff procedure will give new radiation reaction contributions not present in QED although it is possible that other regularization procedures to cut off integrals may effectively do this implicitly. The small range of the boost dependent shape of the cutoff has effects only for field gradients that can probe it, however, this is exactly the case in the radiation reaction problem. There is considerable belief that the radiation reaction force and rate of particle creation is not captured by standard QED and that all such approaches are plagued with the pre-acceleration problems standard in the classical case [14] but some useful limits have been derived [10].

The perturbative schemes generally built on the interaction representation yields a time ordered exponential [13, 17] of terms ordered by the number of discrete interactions in the terms. The details of this construction allow S_F to be pieced together from forwards and backwards propagators in a spacelike slice. This results in a propagator that lives outside the light cone. Usual arguments [13] tell us that the vanishing of the commutator of the field operators outside the light cone is sufficient for causality, an explanation that sounds excessively hopeful and reaching but all too familiar to students of QFT. For our initial data formalism there is no such analog. Firstly let us argue that this unconfined behavior of $S(x - y)$ at $t^x = t^y = 0$ is not an expression of acausal behavior just a statement that the "reality" the initial data has not been localized to start with. How can this be? We could start with a classical delta function source and evolve with this and arrive at a true solution that evolves past the light cone. The usual answer to this is obscured by the usual cloudy use of positive and negative energy states in QFT. Here we have distinct equations of motion or electrons and positrons so the "negative energy" components are a reality to contend with and not to be "reinterpreted" through some measurement ansatz.

To address this consider the case of the classical (massive) KG equation

$$\nabla^2\phi - \partial_t^2\phi = \frac{m^2}{\hbar^2}\phi \tag{23}$$

where the propagator has the same problem. Here the initial data is ϕ and $\dot{\phi}$. Localizing ϕ as a delta function gives

$$\begin{aligned} \phi &= \sum e^{i(px-\omega t)} \\ \dot{\phi} &= -i\sum E_p e^{i(px-\omega t)} \end{aligned} \tag{24}$$

where $E_p = \omega(p) = \sqrt{p^2 + m^2/\hbar^2}$. This shows that whatever reality is associated with the KG field ϕ is not localized even though ϕ itself is. Interestingly, if we force localization of $\dot{\phi}$ then $\phi = i(2\pi)^3\sum E_p^{-1}e^{i(px-\omega t)} = i(2\pi)^3 G_p(x)$ so it embodies the delocalized initial data we complain about in the propagator. We can produce a localization of ϕ and $\dot{\phi}$ by setting $\phi(x) = \delta(x)$ and $\dot{\phi} = 0$ as the particular linear combination

$$\phi(x, t = 0) = \frac{1}{2\pi}\int_0^\infty dk\left(ae^{ikx+i\omega(k)t} + be^{-ikx-i\omega(k)t}\right)|_{t=0} \tag{25}$$

with $a + b = 1$ and $a - b = 0$ so $a = b = \frac{1}{4}$ but this will turn out not to be the interesting solution for coupling of KG to a positive energy Dirac field.

Our inability to constrain the total reality (charge, energy, mass, ...) of the particle to a point indicates that we have a constraint on our physical initial data not a measure of the incompleteness of our basis or a causality problem with our propagators. It should now not be surprising that a similar situation arises for the Dirac fields. For a spin up, positive energy state, localization of all components is inconsistent with the equations of motion. In coupling the Dirac field to the KG (or electromagnetic) field we cannot couple a delocalized Dirac packet to a localized one and the use of the propagator G_p to build the interaction now is more reasonable that the solution given by (25) since it follows directly from the Fourier transforms of the couplings Λ_{e-eA}, Λ_{ee-eeA}, etc.

4.3 Subspace restrictions and resummation

The problems of finding initial data and evolving in an infinite tower of spaces is daunting. The perturbative solutions embodied in the path integral approach are a way of working around this without stating it in these terms. The problems of field theory are often such that a finite perturbative approach is inadequate. Superconductivity is a canonical example of

this where this "nonperturbative" behavior delayed an explanation for half a century. Summing over the same diagrammatic sequence such as with "ladder diagrams" lets us capture some small slice of the infinite character of the space and derive new effective propagators where effective mass terms arise. The number of terms in the total perturbative expansion grow exponentially so it is unclear if such a sum actually has any meaning to which we are attempting convergence. We now know that such series are generally asymptotic so that there is no meaning to them in this limit. However, these particularly abbreviated series have been very valuable and are often capturing essential parts of the physics.

In this article, we are seeking a higher standard of conceptual justification for such sums. Even though we cannot hope to complete this task in a single article, let us seek a foundation for such calculations based on the data set and coupling provided. The self energies have been addressed through a relativistically valid, if slightly nonlocal, approach through cutoffs. Consider a single particle of mass parameter m and momentum p. This should be thought of as including $\Psi_{(e)}, \Psi_{(eA)}, \Psi_{(eAA)}, \ldots$ (and associated C_{PQ} fields) with all amplitude in the bottom state but constraints holding in the upper level functions but no other space couplings. This can be exactly and easily solved with the Coulomb gauge imposed at each level. Turning up the other interactions through the pair creation states $\Psi_{(eep)}, \Psi_{(eepA)}, \ldots$ can be done independently since the couplings between all function pairs, labelled by q, can be controlled separately. These states acquire little contribution in dressing a lone charge because they add so much energy to the system although the effects can be larger during deep scattering events with other charges.

In order to evolve such a system with a gradually changing interaction term while preserving the net norm, mass, and charge (observed from a distance) we can control the m and q parameters and an overall multiplicative constant, β, of the system. The final observed mass is the net energy of the system in the rest frame. We assert that the observed charge is determined by the electric flux that we can observe through large spheres in the A-coordinate subspaces in $\Psi_{(eA)}, \Psi_{(epA)}, \Psi_{(eAA)}, \ldots$. When a large "classical" body interacts with such a particle we assume it is broadly and uniformly distributed through a large variation in photon number spaces. This may seem ad hoc but for such a body to affect a lone dressed charge it must act in all the photon number spaces available or it leads to spectroscopic filtering of charge subspace components as they move in its field. Since this is not observed and we don't have a clear understanding of how classical bodies are represented with a quantum description, this seems like a reasonable supposition. These ideas lead to a prescription to modify the m, q, and β as we turn up the interaction. We need to be careful here as we now implicitly have multiple q's! This has been obscured by our choice of labeling them the same in our tower of interactions. There is the value q_{eA} that gives the self energy coupling in the towers of strictly photon number increasing states e.g. $\Psi_{(eA)}, \Psi_{(eAA)}, \Psi_{(eAAA)}, \ldots$ and the value q_{eep} that gives the couplings to the towers of electron positron pair increase $\Psi_{(e)}$, $\Psi_{(eep)}$, $\Psi_{(eeepp)}, \ldots$. Ultimately we want these parameters to be both the same. This seems to be a nontrivial process and it is somewhat impressive that the usual QED adiabatic turn on gets this to work by starting with a completely undressed charge and a single parameter.

Once we have dressed up lone charges on a subset of the towers deemed to be sufficiently rich to describe the dynamics of the process of interest, the interactions between them must be turned up. Given the states Ψ_{e_1A} and Ψ_{e_2A} we expect an antisymmetrized product of the two to give a first approximation to $\Psi_{e_1e_2A}$ and evolve these new "crossing" interaction parameters $q_{1,2}$ gradually and then hold it steady for a much longer period of time followed by a turn off of the interactions. If these adiabatic processes can be done in a way that leaves momenta of scattered waves unchanged then we can infer the actual scattering rates and angles for dressed particles. To this author, this is the simplest possible way to arrive at the scattering results from a well-posed initial value formalism. Ultimately, we must try other less restrictive subspace restrictions to show that our assumption that they made a small contribution was valid. There is reason to believe this actually works and gives the usual QED results and will be a subject of a followup work.

5 Conclusions

The need for establishing a well-defined space and set of dynamical equations for the reality described by QED, and QFT in general, has been discussed and presented in the form of a tower of spaces of continuum functions. Subsets of the dimensional labels of these spaces give meaning to the notion of "particle" and symmetries in the couplings and initial data define "identicality" of them. There have been a number of subtle issues to confront. Not the least of these is how to give meaning to the many time labels that arise in such a construction and why we, as observers built from the fields, should observe only one time. Such a construction has a number of advantages. It removes the ad hoc character of the construction and the need for the notion of "quantum fields." The inconsistencies described by Haag's theorem are resolved by a partitioning of the tower space into subsets of fixed lepton number that never couple to the ground state. Most importantly we have given an explanation for the quantization of the photon and an indication of the origin of the quantization conditions for quantum operators and the appearance of $\hbar$ in them.

The biggest downside of this construction is that of computability. QED was built from computations and arose out of many ad hoc attempts to make sense of observed dynamics on the part of many stellar physicists. The actual foundations of the subject are almost a necessary afterthought. Of course, no

class is taught this way and the foundations must come first regardless of how flimsy they are. A cynic might worry that field theory courses are filtering students based on their levels of credulity or lack of concern with consistency, a possible advantage in a field driven by extreme publication pressures.

The work here is still hardly complete and it is still to be shown that such construction can validate the successful results of QED for scattering. The subject of bound state corrections has been untouched here and an important topic that needs attention. There is good reason to believe that, ultimately, this theory will have corrections that are not found in QED and therefore be inequivalent at some level of accuracy. The subject of the radiation reaction and QED is still disputed. Given that the classical radiation reaction is resolved by keeping track of the self fields that traverse the extent of a finite body, one might worry that the renormalization procedure to handle self energy might be too simplistic and miss the asymmetric forces that must arise to give the back reaction. A primary motivation for this construction is the incorporation of gravity in a consistent fashion with the quantum world and other fundamental forces. A recent construction by the author in a classical direction relies on a greatly expanded gauge group and a flat background construction. Here couplings mock up the "geometric" effects of general relativity to observers and provides a new avenue for this problem as discussed briefly in the appendix.

A Gravity

Recently the author has presented a treatment of classical GR, electromagnetism and the Dirac field on a flat background that retains the apparently geometric features of GR and yet puts the fields on a similar footing [3]. The motivation for this is in promoting the Dirac γ^μ matrices to dynamic fields without imposing the vierbein approach. This has a number of consistency challenges to work out that will not be reproduced here. One of the essential features is that the γ^0 that is hidden in the $\bar{\Psi}$ has to go. We must replace all the $\bar{\Psi}$'s with new independent fields Φ's that implicitly do the work of them. The quadratic nature of the equations then become bilinear and, while the fields may not evolve causally, it can be shown that the gauge invariant reality of them do. Promoting the γ^μ_{ab} matrices to dynamical fields necessitates that we reinterpret them as vectors in the μ index and scalars in the a, b indices. This seems at odds with the usual SU(2) representation theory. This can be resolved by keeping track of the gauge invariant quantities and allowing new rules to actively boost fields in the space. The various details surrounding this are discussed in Chafin [1].

The metric and its inverse can be defined in terms of these fields as

$$\begin{aligned} g^{\mu\nu} &= -4^{-1}\mathrm{Tr}_{ac}\gamma^{(\mu}_{ab}\gamma^{\nu)}_{bc} \\ g_{\mu\nu} &= \mathrm{Inv}(-4^{-1}\mathrm{Tr}_{ac}\gamma^{(\mu}_{ab}\gamma^{\nu)}_{bc}), \end{aligned} \tag{26}$$

however the complexity of the inverse definition makes it more convenient to define an auxiliary field λ^μ and define the γ matrix with its index down

$$\begin{aligned} g^{\mu\nu}\delta_{ac} &= -2^{-1}\{\lambda^\mu, \lambda^\nu\} = -\lambda^{(\mu}, \lambda^{\nu)} \\ g_{\mu\nu}\delta_{ac} &= -2^{-1}\{\gamma_\mu, \gamma_\nu\} = -\gamma_{(\mu}, \gamma_{\nu)}. \end{aligned} \tag{27}$$

Some dynamic interaction terms will then lead to these forcing of the inverse matrix relation for the trace of these at low enough energy e.g. through the "Higgs-ish" coupling in the action

$$S_c = M\,|g_{\mu\nu}(\gamma)g^{\nu\rho}(\lambda) - \delta^\rho_\mu|^2 \tag{28}$$

for a large "mass" parameter M.

In our many body tower of functions we need to ask how the couplings with such a gravity field γ^μ_{ab} would work. Modeling it on the electromagnetic field by introducing γ and λ labels to Ψ as in $\Psi^\nu_{(eA\gamma),\mu,abc}(x, y, z)$ has some appeal in thinking of gravitons as correlated with other particles but is problematic in the details. When we look at the modified Dirac lagrangian we find that there is always an extra μ index to accommodate:

$$\mathcal{L} = i(\phi_a\gamma^\mu_{ab}\partial_\mu\psi_b - \partial_\mu\phi_a\gamma^\mu_{ab}\psi_b) - 2m\phi_a\psi_a \tag{29}$$

Furthermore the γ function will need to span the full coordinate set of the function it is evolving. For example, when we wish to evolve $\Psi_{(eA)}(x, y)$ in the t^e direction we must multiply by a function $\gamma^\mu_{ab}(x, y)$ so that the $x^{(A)} = y$ coordinate must still be present even if it is only in a passive role. For these reasons it seems important to include not just a dual field $\Phi_{(eA)}$ to go with $\Psi_{(eA)}$ but an independent $\gamma^\mu_{(eA)}(x, y)$ field to contract with the derivative operator $\partial^{(e)}_x$. Note that we have labeled the gravity function γ^μ_{ab} with the electron and photon coordinate labels not some new graviton coordinate and it has only one μ and two a, b indices. This will persist regardless of how many coordinate functions are embedded in it. Thus the tower of functions of electron, positron and photon fields (and their Φ associated fields) has an associated tower

$$\begin{aligned} &\gamma^\mu_{(A),Q}(x), \gamma^\mu_{(AA),abQR}(x, y)\ldots \\ &\gamma^\mu_{(e),ab}(x), \gamma^\mu_{(eA),abQ}(x, y), \gamma^\mu_{(eAA),abQR}(x, y, z)\ldots \\ &\gamma^\mu_{(p),ab}(x), \gamma^\mu_{(pA),abQ}(x, y), \gamma^\mu_{(pAA),abQR}(x, y, z)\ldots \\ &\gamma^\mu_{(ep),ab}(x, y), \gamma^\mu_{(epA),abQ}(x, y, z), \\ &\qquad\qquad , \gamma^\mu_{(epAA),abQR}(x, y, z, w)\ldots \\ &\ldots \end{aligned} \tag{30}$$

This allows these functions to be straightforwardly coupled into the electron, positron and photon lagrangians using the mapping $g^{\mu\nu} = -8^{-1}\mathrm{Tr}\{\lambda^\mu, \lambda^\nu\}$.

The problem now is reduced to giving an evolution equation for these various γ^μ_{ab} functions in each of the implicit time directions. The Einstein-Hilbert action $S_{EH} = \int R\sqrt{g_{..}}$

suggests a start. The measure can be extracted from $g_{\mu\nu} = -8^{-1}\mathrm{Tr}\{\gamma^\mu, \gamma^\nu\}$. The geometric meaning of these terms is not clear but it is not necessarily required. We know that we want GR to arise in some, probably uncorrelated classical limit of particles over the energy scales we currently observe but beyond that we only require that we have a well defined set of evolution equations. Define the Riemann operator $\hat{R}_{(e)_i}$ to be the Riemann function of the connections $\Gamma(\lambda, \gamma)$ in terms of the two associated gravity fields where all the derivatives are taken with respect to the $x^{(e)_i}$ coordinate label, ith electron label, in the $\gamma_{(eee...ppp...AAA...)}$ function. The interactions are provided by the remaining classical lagrangians that now needs no delta function to localize the interaction.

The global gauge freedom we associate with norm $\Psi \rightarrow \Psi e^{i\theta}$ and $\Phi \rightarrow \Phi e^{-i\theta}$ does not involve the γ functions so it seems to not acquire or lose amplitude in the fashion of particle creation so exists as a new kind of field entity that makes gravity seem fundamentally different than the other fields even though the geometric nature of the theory is subverted in favor of a flat background formalism. It seems that any generalization of this theory needs three fields (with various particle label sets). It would be interesting to see if there is some high energy unification which treats them in a more symmetric fashion.

Submitted on April 17, 2015 / Accepted on April 23, 2015

References

1. Chafin C. The Quantum State of Classical Matter I: Solids and Measurements. arXiv: quant-ph/1308.2305.
2. Chafin C. The Quantum State of Classical Matter II: Thermodynamic Equilibrium and Hydrodynamics. arXiv: quant-ph/1309.1111.
3. Chafin C. The Slicing Theory of Quantum Measurement: Derivation of Transient Many Worlds Behavior, *Progress in Physics*, v. 11 (3), 221–230. arXiv: quant-ph/1410.8238.
4. Dirac P. A. M. The Principles of Quantum Mechanics, 4$^{\text{th}}$ed. Oxford University Press, New York, 1986.
5. Dalfovo F., Giorgini S., Pitaevskii L. P., Stringari S. Theory of Bose-Einstein condensation in trapped gases. *Rev. Mod. Phys.*, 1999, v. 71 (3), 463.
6. Haag R. On quantum field theories. *Kong. Dan. Vidensk. Sels., Mat. Fys. Medd.*, 1955, v. 29 (12), 1–37.
7. Jammer M. The Philosophy of Quantum Mechanics; the Interpretations of Quantum Mechanics in Historical Perspective. Wiley, New York, 1974.
8. Kubo R. Statistical-Mechanical Theory of Irreversible Processes I. *J. Phys. Soc. Japan*, 1957, v. 12, 570–586.
9. van Kampen N. The Case Against Linear Response Theory. *Phys. Norv.*, 1971, v. 5, 279–284.
10. Ilderton A., Torgrimsson G. Radiation reaction in strong field QED. *Phys Lett. B*, 2013, v. 725, 481–486.
11. Louisell W. H. Quantum Statistical Properties of Radiation. Wiley, New York, 1973.
12. Misner C. W., Thorne K. S., Wheeler J. A. Gravitation. W. H. Freeman and Company, San Francisco, 1973.
13. Peskin M. E., Schroeder D. V. An Introduction to Quantum Field Theory. Westview Press, Boulder, 1995.
14. Rohrlich F. Classical Charged Particles. World Scientific, Reading, MA, 2007.
15. Schweber S. S. An Introduction to Relativistic Quantum Field Theory. Harper and Row, New York, 1962.
16. Schlosshauer M. Decoherence, the measurement problem, and interpretations of quantum mechanics. *Rev. Mod. Phys.*, 2004, v. 76, 1267–1305.
17. Weinberg S. The Quantum Theory of Fields, Vol. I & II. Cambridge University Press, Cambridge, 1995.

The Slicing Theory of Quantum Measurement: Derivation of Transient Many Worlds Behavior

Clifford Chafin

Department of Physics, North Carolina State University, Raleigh, NC 27695. E-mail: cechafin@ncsu.edu

An emergent theory of quantum measurement arises directly by considering the particular subset of many body wavefunctions that can be associated with classical condensed matter and its interaction with delocalized wavefunctions. This transfers questions of the "strangeness" of quantum mechanics from the wavefunction to the macroscopic material itself. An effectively many-worlds picture of measurement results for long times and induces a natural arrow of time. The challenging part is then justifying why our macroscopic world is dominated by such far-from-eigenstate matter. Condensing cold mesoscopic clusters provide a pathway to a partitioning of a highly correlated many body wavefunction to long lasting islands composed of classical-like bodies widely separated in Fock space. Low mass rapidly delocalizing matter that recombines with the solids "slice" the system into a set of nearby yet very weakly interacting subsystems weighted according to the Born statistics and yields a kind of many worlds picture but with the possibility of revived phase interference on iterative particle desorption, delocalization and readsorption. A proliferation of low energy photons competes with such a possibility. Causality problems associated with correlated quantum measurement are resolved and conserved quantities are preserved for the overall many body function despite their failure in each observer's bifurcating "slice-path". The necessity of such a state for a two state logic and reliable discrete state machine suggests that later stages of the universe's evolution will destroy the physical underpinnings required for consciousness and the arrow of time even without heat-death or atomic destruction. Some exotic possibilities outside the domain of usual quantum measurement are considered such as measurement with delocalized devices and revival of information from past measurements.

1 Introduction

The interpretation of quantum measurement has been a confounding topic since the early days of quantum mechanics. Approaches have ranged from very formulaic as in the Copenhagen interpretation to the many worlds view and decoherence [7, 9, 15, 16]. The statistics derived from these are typically excellent. Their accuracy for some systems that have some mix of classical and quantum character is still debated. Questions about locality and causality regularly arise in the case of correlations [1]. The purpose of this article is to show that a unification of classical and quantum worlds under the same description is easy given the right set of questions and that quantum statistics arise naturally from the dynamical equations of motion (and conservation laws). Specifically, the sorts of states that lead to observed classical matter arise in a natural way from a primordial delocalized and nonclassical gas due to contraction and the relative cheapness of creating low energy photons. The photon induced interactions of the induced clusters and massive proliferation of photons, hence increasing dimensionality of the space, will then lead to a kind of "slicing" of the space into many classical subspaces in the overall Fock space. The independence of these are long lasting when their particle numbers are modestly large and slow delocalization is "resliced" regularly by the interactions of delocalizing particles with the condensed matter portions of the system. The small particles that are capable of delocalizing on small time scales are mediators for further partitioning of the space with the probabilities given the square of the amplitude of its wavefunction*.

Any emergent discussion of measurement invariably runs into the need for the many body wavefunction. This is a high dimensional object and we typically have small particles with delocalization to measure that then interact and produce "collapse". This implies some separability in the net wavefunction. Any such explanation of quantum measurement must explain the following

1. The kinds of wavefunctions that correspond to classical matter and their origin;
2. The separability of the classical world from the isolated evolving quantum one;
3. The statistics of the interaction of the two.

One point often overlooked is that measurements occur at particular times and this is measurable. A delocalized packet of

*Here we are referring to the one body wavefunction, $\psi(x)$, that arises from ejection of a localized particle from classical-like matter which will produce a near product function $\Psi_N \approx \Psi_{N-1}\psi(x)$ up to symmetrizations. The framework here will help us extend measurement theory for the collapse of correlated delocalized particles in a causal manner.

an atom incident on a surface will give both a location and a time. Invariably this leads to some vague discussion involving the uncertainty relations, $\Delta x \Delta p \geq \hbar/2$ and $\Delta E \Delta t \geq \hbar/2$, however our concern is how the duration of a position measurement relates to the localization in any one slice. Our goal here is to produce a theory that has no operators or such relations as fundamentals to it. Rather we seek initial data and an evolution that deterministically arrives at the statistics and evolution we see and, ultimately, gives an explanation for the rather special subsets of wavefunctions that correspond to classical objects and the classical world.

This article will unfold as follows. First we discuss a delocalized cooling gas with proliferating photons and how these influence condensing clusters to produce islands of classical behavior for the condensed matter in the many body wavefunction. These are long lived and promote an arrow of time until the system recontracts and becomes relatively photon poor. To achieve this we need a description of matter with photon fields of varying number. Recently it has become possible to subsume the dynamics of QED in a many coordinate and many time classical field theory formalism where the observers perceive a world with *equal times* only [5]. This formalism and its associated many body conservation laws will be utilized to provide qualitative wavefunction descriptions of measurement as well as quantitative statistics. Next we discuss how the usual measurement statistics follow for such a system through "slicing" over delocalized particle coordinates with such condensed matter states. A nonlinearity, hidden while using the usual operator formalism, arises in the generation of radiation fields that removes some of the paradoxes in equilibration for purely linear operators on a Hilbert space. Finally, we use these structures to investigate some paradoxes in quantum mechanics, place some bounds on violation of Born statistics and suggest experiments to reveal such behavior.

2 Classical genesis: a first look

The primordial state of the universe is expected to be a gas that cools and condenses into stars and dust. If the photon number is zero and there are N particles, we expect a single wavefunction Ψ to describe this state*. It is clear, that a general such function is not describable by some mapping to hydrodynamics as a commutative mapping of $\Psi(X) \rightarrow (\rho(x), v(x))$ where the left hand side is governed by the Schrödinger equation and the right by Navier-Stokes. The states on the left are just too large. Instead of making an argument that the system should settle down to such a state we accept that this may never arise. It is the author's opinion that classical behavior arises from condensed matter and the proliferation of photons and that it is then induced on gases so we continue our story with nucleation.

*We ignore the role of virtual particles to this approximation.

Nucleation theory is still in a theoretically very unsatisfactory state and errors in nucleation rates are measured in orders of magnitude. However, this is fortunately not a complication to the relevant parts of our discussion. When the atoms of a gas condense into a cluster, a large number of photons are released. This means that we have now both increased the mean photon number and occupied a large region of Fock space. The ground state of a cluster of N-particles is nearly spherical (through some polygonal approximation) and rotationally invariant. This seems initially paradoxical. No discrete crystal has rotational invariance. The resolution follows from the fact that these are $3N$ dimensional wavefunctions. The translation is given by three of these and the rotational freedom by two more. Rotation always requires radial excitation, as we see from the case of the Hydrogen atom. In the case of a large cluster, this radial excitation is a centrifugal distortion. The rotationally invariant ground state has no well defined atom location, even if the structure is crystalline in that we cannot find peaks at locations r_i so that $\Psi \sim \prod_S (x_i - r_j)$. The states where such arises, as in the physical states we observe, must then be manifested by the cluster being in a mixture of high rotational eigenstates (even if having net angular momentum zero).

A surprising complication is that any classical body is in such a mixture of states so, even at "$T = 0$" it is far from its own ground state. The kinds of condensed matter we encounter have well defined shape, orientation, etc. They define a "classicality" that is very specific, three dimensional and Newtonian, and far-from-eigenstates. A solid can be specifically described and phonons given as excitations of the localized cores along particular many body diagonals and are eigenstate-like despite the ultimately transient nature of the classicality on which their description depends [4]. We now are compelled to ask how such apparently omnipresent states can arise.

Consider a pair of irregularly shaped bodies, A and B, that are spatially separated, but suffering delocalization about their centers of mass, and are bathed in a sea of photons. Let these be in their ground states initially. A photon that travels from far away and casts a shadow from body B onto A gets absorbed and produces a localized excitation on them. In the case of absorption by A the surface builds up a history through local heating or chemical changes. After many such photon events the body A has a record of the shape of body B in this shadow. Of course, some fraction of the amplitude of each photon gets absorbed by B or flies past without interaction. If the bodies A and B had localized atomic constituents, then their boundaries would be well defined and the shadows sharp. Since this is not the case we have to ask what happens. We can consider each to be a superposition of states that are in various angular orientations. This is reasonable since the centrifugal forces of these many angular states are small and make little deformation of the bodies. Each such case produces shadows that are well defined so we have a

macroscopic superposition of all the configurations with well defined orientations and atomic locations. The crucial part is how this then evolves.

Given a superposition of nearly overlapping macroscopic bodies in a space with no photons the energy change is huge. Atoms cannot sit on top of each other without inducing large repulsive forces from their electronic structure. However, for a system with a huge variation in the photon number states, such slight changes can easily have different photon numbers so be, ostensibly, at the same location but in different photon number spaces. This allows an apparent overlap with no energy cost. Specific details of this rely on an initial value (rather than operator based) description of low energy QED described in [5] and summarized below. Since the delocalization rate of large N objects is very small, such states can then evolve for long periods of time with essentially no interaction between them. Ultimately, we are such objects. Our very consciousness and memory depends on our being reliable discrete state machines. Once the expanding and cooling universe is so partitioned we have a set of "many worlds" that are sufficiently separated in Fock space to be insulated from each other. Of course, this is not expected to persist. In a gravitational contraction or long term stagnation, these worlds will come back together and the "information" made up by these separated worlds will be lost. This is an appealing way for the arrow of time to arise naturally despite the time reversal symmetry of the equations of motion. To be fair, this is a very vague and qualitative discussion. Now let us try for a more specific, but less general case in an attempt to justify this partitioning of the many body wavefunction.

3 Classical genesis: cluster collisions and photons

Here we give a justification for the "sparse worlds" state that we claim is a set of many-body wavefunctions that correspond to classical condensed matter objects (plus gas and a few delocalized particles). By this we mean that the solid and liquid objects have well defined boundaries, shapes and orientations as 3D objects but encoded in the N-body space of atoms where these atoms have well defined locations to within some localization distance determined by the electronic bonds between them. Of course, such a state is not an eigenstate. Each body will tend to delocalize both radially and in location. Such a state is an unfathomably complicated mix of eigenstates of the true system yet it makes some sense to think of the excitations of the bodies in terms of collective phonon modes as eigenstates in such clumps of matter.

Matter begins in the universe as a gas that collapses into stars and explodes to create the clusters that condense into dust that eventually coalesces into planets and other rocky objects. The gas undoubtably begins as delocalized and "correlated" in the sense that the particles have no well defined 3D locations so the many body Ψ cannot be represented as some symmetrized N-fold product. The implications of this are rarely considered. How does classical hydrodynamics arise in such a system and lead to stars of well defined location much less the larger scale density structures we observe? Is this classical localization a result of some product of our consciousness in creating a "measurement". This is pretty unpalatable to most scientists. The alternative is that such condensing occurs but the resulting stars have no well defined location, particle number, boundary and orientation relative to one another. Such a universe is a truly many body object and how it would "look" to an observer injected into it is not clear. Later we will see that the consciousness required for observation may be incompatible with such a universe.

The resolution we suggest is that this is the true state of the early universe and it is the presence of condensed matter that "slices" the space into a well defined collection of stars of well defined locations and velocities. The collapse picture implies that only one such state is selected and exists. In this picture, the the coordinates of the observer contain copies of the "observer $\otimes$ system" that cease to be the same for all values of the system coordinates. This divides the wavefunction of the many body space into a collection of independently evolving states of well defined 3D structure with long lasting independence and duration. We can then think of quantum measurement as the "auto-fibration" of the macroscopic world over the coordinates of the measured particle.

Consider a classical-like block of matter floating in space. A superposition of a star at two locations shining on such a block creates a superposition of the block in the star's coordinates. If we view the block as a measurement device that is recording observations in the changes in its surface under the influence of photons from the star, then it "observes" its own history to have the star at one continuously connected path of locations. It now has a double life as two blocks with different histories even though the number of coordinates has not changed. Its classicality has been compromised (albeit in a very minimal way) by the influence of the delocalized star even though the star and the block are widely separated and the net mass and energy transferred by the photons is typically miniscule. The "measurement device" has not forced a change in the larger system. Rather, the larger system has induced a change in the measurement device so it now follow separate paths in the many body space. This is possible, in part, due to the massive size of the many body space and its capacity to hold many classical world alternatives as distinct for long times. Note that the size of the block compared to the superimposed object is irrelevant in producing this effect.

The problem then amounts to the creation of such a set of classical-like bodies distributed in a set of sparse worlds embedded in the many body space. As a prototype world consider a collection of dust of different sizes, shapes, orientations, internal excitation, positions and velocities. These begin as a highly correlated system that has no classical meaning despite having formed solid matter. Let us start with an idealized simple system to discuss the mechanism. Consider

two solid balls of radius r but nonspecific location and velocity in many body space described by a cube of length L. Ignoring internal degrees of freedom, we can consider the system to be a 6D wavefunction in an L^6 cube with excluded volume given by the 2 body cylindrical projection of the interior of the sphere. At higher energies the wavefunction will tend to have oscillations much smaller than the radius $\lambda \ll r$. The state of the system in terms of eigenstates is assumed to be of a broad energy distribution $\Delta E \gtrsim <E>$ and have random phases or have evolved for a long but random length of time. Such a condition is necessary to have fluctuations in the many body current $\mathcal{J}$. The energy density and fluctuations then tend to uniformly fill the box and we have a soup of high frequency and highly varied oscillations bound by the excluded volume.

So far we have said nothing about photons. Let us assume there are none to start with. Currents induced by the fluctuations in the wavefunction produce flux on the boundaries of the excluded volume. Classically this corresponds to the collision of two spheres with velocities given by the two velocities

$$v_1, v_2 = \frac{\mathcal{J}}{\mathcal{P}}$$

given by the 6D current $\mathcal{J}$ and density $\mathcal{P}$ at the coordinate $X = (x_1, x_2)$. Depending on the angle and relative speed of the collision, a certain number of photons are created in the event. Photons are exceedingly inexpensive at low energies. This has led to the infrared divergence problem in QED where an unbounded number of low energy photons get created. Our finite box regularizes this to some degree but for short enough collision times no such problem arises since they cannot traverse the box during their creation.

A small change in the location of the collision creates a different number and set of photons. Thus one location can generate a large occupancy in the tower of spaces Ψ_{bb}, Ψ_{bbA}, Ψ_{bbAA}, Ψ_{bbAAA}, Ψ_{bbAAAA} ... where b indicates the coordinates of each ball and A are the photon coordinate labels. In a short time, the current flux at that location can be very different and generate a very different occupancy the the ball-photon wavefunction tower (Fock space). Once each small current fluctuation is completed, the higher photons spaces have acquired an occupancy of localized spatial position in the b-coordinates (defined by the length of time of the local fluctuation in current) and a broad number of photon waves moving away from it in the A-coordinates. The long time limit we argue is of a sum of such states distributed among the tower with almost all the amplitude having left the Ψ_{bb} state. These can now evolve with no quantum interference of other states (since all b and A coordinates would have to match up in one of the towers for this to happen). By "long time" we mean long enough for the currents in the Ψ_{bb} state to have had time to have all reached the excluded volume surface and hence pushed amplitude up the photon tower, $\tau \gtrsim L/\mathrm{Min}(v_1, v_2)$, but not so long as to cause delocalization of the amplitude in each n-photon space so these begin to interact and interfere.

The actual process "in vivo" of the universe is of course more organic and occurs while the dust is forming. It must create the orientation of the dust as well as select these subslices to have well defined atom number in each. It seems that the cheap and plentiful photon along with dust formation is what drives the formation of these "classical worlds" as isolated long lasting packets in the many body space. Quantum mechanics then arises for each of these universes by the action of condensed matter as discrete state machines. Clearly this process cannot persist forever. The universes will delocalize, meet, possibly gravitationally collapse and get driven to a density where the full correlated structure of the universe matters.

4 Measurement

Part of the formalism of quantum mechanics has been to use Hilbert space and eigenfunctions of operators to give measurement results.

These Hamiltonians are often effective Hamiltonians of subspaces created by the kinds of localized "classical" states described above. This introduces a kind of metastable feature to the evolution that is connected with the duration of the classical nature of the external world. One has to wonder what the role of the eigenstates are in arriving at measurements, specifically how one collection of matter indicates one particular operator and spectrum. In the case of position measurements, we see from above that the system has partitioned itself so that measurement of particle location is inherited by the special independently evolving nature of the classical states. In this case we say the system has been "sliced" in a manner that gives it its classical character but not into a subset of eigenstates of the net or any obvious subset of the Hamiltonian. We assert that momentum, energy and other measurements are universally inferred from position data e.g. a local color change in a material or spatial measurements at different times. It has already been long debated how general a measurement can be made from an arbitrary linear self adjoint operator (LCAO) and it is this author's opinion that position and time measurements are the fundamental sort that arise and all others are derivative.

Note that our "measurement" process has nothing to do with consciousness of an observer but of a specific property of condensed matter in a photon rich environment. In fact, photon production at low energies is so cheap that it is hard to conceive of a measurement that didn't produce copious numbers of them. Let us now consider temporal effects and measurements. It is inevitable that temporal effects arise. Wavepackets can be delocalized and measurement devices can move. This makes it clear that the measurement operator $\hat{x}$ is going to have some insufficiencies. Furthermore, measurement devices have finite spatial extent. Screens are essentially 2D so they are typically only picking up a tiny

fraction of a wavefunction's motion at any time.

To illustrate these points consider a narrow single particle packet incident on a screen with a couple of adsorption sites as in Fig. 1. We can simplify this by breaking it up into a set of disjoint regions of support as in Fig. 2. The duration of an adsorption event is not related to the length of a packet but the radiation time for the electronic decay that produces binding. For simplicity let the binding action be mediated by the release of a single photon of energy E so the radiative process has a time scale $\tau \sim \hbar/\Delta E$. Let the parcels be roughly monochromatic so they have a well defined velocity $v = j/\rho$ and the parcel widths $w \approx v\tau$. A parcel separation of nw lets the adsorption events be well separated.

When a subparcel reaches the site at x_0 it adsorbs and creates a photon so that some amplitude flows from $\psi(x)\Psi_N$, the photon free wavefunction of the system, to $\Psi_{N+1,A}$, the single photon and N+1 particle wavefunction with a radiation field flowing away from it. The operator formalism obscures some features of this problem so we invoke an equivalent formalization of low energy QED by using a many time approach where one body equations of motion hold for each time coordinate in the many body tower [5]:

$$\begin{array}{l} \vdots \\ \Psi_{N,AAA} \\ \Psi_{N,AA} \\ \Psi_{N,A} \\ \Psi_N \end{array} \tag{1}$$

We call this theory "deterministic wave mechanics" (DWM) in contrast with the formal operator and path integral formulation of the theory. A basis of states in each photon number space is given by $\Psi^{(m)}_N \mathcal{A}_m$ where $\mathcal{A}_m$ is a stationary state in the space spanned by $A^{i_1} \otimes A^{i_2} \otimes \ldots \otimes A^{i_m}$ of complex 3-vectors fields for photons*. The net norm and energy are conserved in such approach when they are defined as

$$\begin{aligned} \hat{\mathcal{N}}(\Psi_{N,n}) = & \int dx_s^{i_1} \ldots dx_s^{i_N} \bar{\Psi}_N \Psi_N \\ & + \tfrac{1}{4\mu_0} \int dx_s^{i_1} \ldots dx_s^{i_N} \int dx_A^{i_1} \ldots dx_A^{i_n} \\ & \textstyle\sum_{k=1}^{n} \left(\bar{\Psi}^{i_1 \ldots i_n} \partial_{t_A^{i_k}} \Psi_{i_1 \ldots i_n} - \partial_{t_A^{i_k}} \bar{\Psi}^{i_1 \ldots i_n} \Psi_{i_1 \ldots i_n} \right) \\ = & \int dx_s^{i_1} \ldots dx_s^{i_N} \bar{\Psi}_N \Psi_N \\ & + \tfrac{1}{4\mu_0} \int dx_s^{i_1} \ldots dx_s^{i_N} \int dx_A^{i_1} \ldots dx_A^{i_n} \\ & \textstyle\sum_{k=1}^{n} \left(\bar{\Psi}^{i_1 \ldots i_n} \hat{\mathcal{N}}^A_k \Psi_{i_1 \ldots i_n} \right). \end{aligned} \tag{2}$$

$$\begin{aligned} E_{N,k} = \bar{\Psi}_{N,k} \Big(& \textstyle\sum_{i=1}^{N} \hat{E}_{s_i} \hat{\mathcal{N}}_{1 \ldots \hat{i} \ldots N} \hat{\mathcal{N}}^A_{1 \ldots k} + \\ & + \textstyle\sum_{j=1}^{k} \hat{E}_{A_j} \hat{\mathcal{N}}_{1 \ldots N} \hat{\mathcal{N}}^A_{1 \ldots \hat{j} \ldots k} \Big) \Psi_{N,k} \end{aligned} \tag{3}$$

and we evaluate on the equal time slices $t \doteq t_{net} = t_s^{i_1} = t_s^{i_2} = \ldots = t_A^{i_1} = t_A^{i_2} = \ldots$. The operators $\hat{\mathcal{N}}_s$ and $\hat{\mathcal{N}}_A$ are the one body norm operators for massive and photon fields respectively. The operators $\hat{E}_s$ and $\hat{E}_A$ are similarly the one body energy operators. The many body versions are simply concatenations of these where the "hatted" indices are excluded. The definition of $\bar{\Psi}$ for Dirac fields is to apply γ^0's to all the spinor indices of Ψ (which have been suppressed here). Here we are interested in atomic center-of-mass wavefunctions. For these we simply require the transpose conjugate.

Using this picture we can derive the long time states of the system. The radiative decay occurs at frequency ω with an envelope of duration τ as in Fig. 6. The atom binds a location x_0 with a mean width of d so that it may be represented by a peaked function $\delta_d(x - x_0)$ akin to a delta function of finite width d. Assume the first peak arrives as time $t = 0$ and that there are only two equal pulses that contain all the amplitude of ψ. Initial data at $t \lesssim 0$ is

$$\begin{aligned} \Psi_{N+1} &= \Psi_N \psi(x, 0) \\ &= \tfrac{1}{\sqrt{2}} \Psi_N (\delta_w(x - x_0) + \delta_w(x - x_0 - wn)) \\ \Psi_{N+1,A} &= 0 \\ &\vdots \end{aligned} \tag{4}$$

The final wavefunction for $t > t' = 2\tau + n\tau$ is

$$\begin{aligned} \Psi_{N+1} &= 0 \\ \Psi_{N+1,A} &\approx \tfrac{1}{\sqrt{2}} \Psi_N \delta_d(x - x_0) \Big(\tfrac{1}{r} e^{i(kr - \omega t)} h(r - ct) \\ &\quad + \tfrac{1}{r} e^{i(kr - \omega(t - t'))} h(r - c(t - t')) \Big) e^{i\phi(t)} \hat{\epsilon}_\kappa \\ \Psi_{N,AA} &= 0 \\ \Psi_{N,AAA} &= 0 \\ &\vdots \end{aligned} \tag{5}$$

We have implicity assumed the block is essentially transparent and the radiation flies unobstructed into infinite space. (The orientation of the radiation field $\hat{\epsilon}_\kappa$ is determined by the direction of the dipole produced by the radiation. This may be a superposition of such solutions and a function of the local geometry of the solid. For now we neglect its details.) The meaning of this solution is that the wavefuction support has exactly partitioned into two parts. The "reality" of a classical field can have some surprising subtleties† [3]. In this

*Coulomb gauge is assumed for every coordinate label so that the $\Psi^{\mu=0}_{N,1}$, $\Psi^{\nu,\mu=0}_{N,2}$, etc. components are fixed by constraint.

†We can consider this as the "Schrödinger" and "first quantized" analog to usual QFT formalism in terms of field operators.

case the support and its values there contain all the meaning there is to the system. We see that we have two bound states that occurred at times $t = 0$ and $t = t'$. The packet is flying away from the location $X \approx x_0 \otimes X(0)$ at c in the x direction when viewed in the equal times coordinate t. The motion in the material coordinates is essentially static unless some other dynamics were present to start with. If we consider the block to contain a discrete state machine as in Fig. 3 that has internal dynamics that makes a record of when the event occurs, then each one exists in a kind of parallel universe with a record of a different time. Unless these photon coordinate portions of the packet are reflected or forced to interfere, this situation continues in perpetuity and each evolves according to their own record of their particular past. Should they generate their own delocalized particles and repeat this experiment they will find the Born-like $\psi^*\psi$ probabilities for when the measurement occurs. This is a direct consequence of the above norm conservation law. Ultimately the delocalization can only go on so long before the "classicality" of the system fails. The consequences of this we will soon consider.

Let us now consider a broad packet that intercepts the screen at the same time as in Fig. 4. Analogously to above, let us consider this to be broken into two parts with the width of the measurement centers and less than $w = v\tau$ as in Fig. 5. Here a similar analysis yields a resulting pair of packets radiating outwards from the two centers at the same time. Our system now seems to be split into two spatially distinct parts as indicated by the outer product in Fig. 7 where the radiative field shells have been suppressed. These shells are no longer disjoint but contain a finite volume fraction of overlap. For farther apart centers this is of order $w/R(t)$ where $R(t) = ct$. To the extent this overlap remains negligible, these solutions remain disjoint and evolve as separate worlds.

This is a good point to pause and reflect on what overlap of these systems means for evolution. The emphasis on linear operators and Hamiltonians leads one to believe that any superimposed world is equivalent to each world evolving separately. As such, when one decomposition evolves it is hard to see how anything interesting can really happen. However, there is a hidden nonlinearity in our problem. The classical radiation reaction problem holds a nonlinearly due to current acceleration which is best thought of in terms of finite sizes of radiators and crossing times [11]. Our radiation fields can be thought of in a similar fashion with a small unknown structure involving many hidden internal coordinates. The "radiation reaction" now must transfer both four momentum *and* particle norm at the interacting two-body diagonals that connect the states in the Fock space tower. The implications of this is that overlapping of states in the Fock space do not simply superimpose so there are no true eigenstates when photon interactions are included. This is to be expected. If we superimpose the eigenstates ψ_{2p} and ψ_{1s} of the Hydrogen atom then it is the presence of the current that drives amplitude from ψ_H to $\psi_{H,A}$. In the low energy limit the Hydrogenic states are stationary but the overlap drives the transition to higher photon levels. This is an intrinsic nonlinearity that is obscured by the formal operator description of quantum field theory. It is unclear if this is adequately accounted for in quantum field theory through its operator calculus.

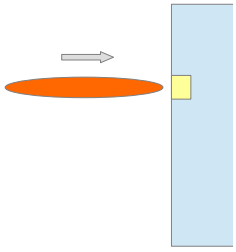

Fig. 1: A long narrow packet illustrates the measurement of event time at a particular location and how these can lead to a persistent slicing of the space (up to the delocalization time of the device) in an infinite space.

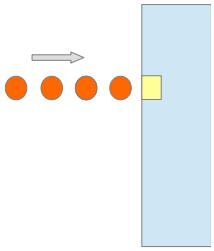

Fig. 2: An idealized sequence of packets of a *single* incident particle.

5 Slice memory and revival of measurement history

One of the unpleasant features of the many worlds interpretation is that the size of the universe seems to grow. In this and all "interpretations" of quantum mechanics, the role of the measurement device and how and when it acts lacks specificity. The action of the "observable" associated with each such device is not clearly determined by the microstructure of the device. The DWM theory here addresses each of these and lets us ask some new questions that may take us outside the bounds of traditional quantum theoretical problems. One of the obvious questions is to what extent is the measurement a complete destructive event (at least from the perspective of the observers). Can we somehow undo measurement and recover some of the delocalization and phase information from before? Now that we can nanoengineer systems and create extremely cold ones, highly decoupled from the external world, other quantum domains can be probed. A molecular two-slit experiment was recently realized [10]. In the measurement direction what happens when a measurement device itself has a mass comparable to the delocalized system it measures? Is there a measurable "back reaction" to

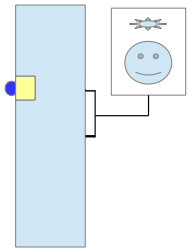

Fig. 3: A measurement device with a coupled observer or programmable device to respond to observations.

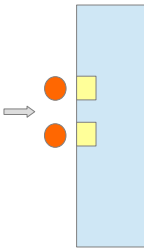

Fig. 5: An idealization of the narrow one-particle packet into localized subparcels.

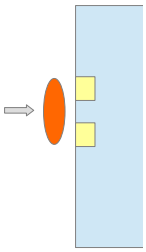

Fig. 4: A narrow one-particle packet incident on a detector surface.

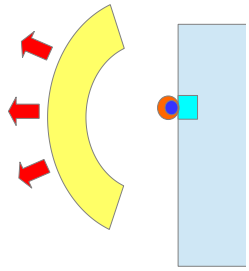

Fig. 6: The absorption of a particle at a site is correlated with radiation field moving away from the selected location.

the measurement event? If a measurement device is partially delocalized itself how does this affect the measurement once we then slice the measurement device so it is back in the fully classical domain of our experience?

5.1 Wavefunction revival: inverse measurement

On the topic of slicing of the space into independently evolving subspaces we have introduced the restriction on the form of macroscopic matter that gives a classical limit for dynamics. This was far more restrictive than the rather naive Ehrenfest-limit defined by large mass and moving packets [12]. The continuing lack of overlap given by large mass induced slow spreading and the rapid motion of light speed packets in the A-coordinate directions into an empty space help preserve this "many-worlds" picture for long times. Constraints on the space that photons can move about in leads to greater overlap possibilities and opportunities for such slices to interact through radiation absorption and production however, since low energy photons are so prolific this kind of interference may be difficult to engineer in practice. Nevertheless, we should investigate the possible bounds on slice independence.

Consider the example system given in Fig. 5. Generally, there are going to be internal motions and radiation fields that exist in any such large body. Let the incident atom be distinct from those of the device so that it is unconstrained by symmetry and the binding to the surface can be much less than that of the device particles to each other. We can imagine a situation where we heat the block and the atom ejects and delocalizes then is pulled back to the surface by an external field such that this process is iterated. The CM of the device gradually delocalizes (at a much increased rate) from this process. If this system is closed then the photon number will gradually increase as the battery driving the process loses energy. This tells us that the system is undergoing important changes and so reejecting the particles may not create a system that interferes with previous slice histories. On the other hand, if the system is in a finite volume, the radiation fields can all be contained in this finite space so that past slices eventually can interfere if the photon number does not grow much faster than the number of iterations.

It is simpler to consider the case of a photon that is absorbed at a pair of sites and then ejected as in the process $\Psi_{N,1} \rightarrow \Psi_{N,0} \rightarrow \Psi_{N,1}$. The release times for the two slices may vary over a large range but, if we restrict ourselves to looking at the fraction of amplitude that occur at the same time (e.g. by use of a beam chopper on the input and ejected flux), then the phases of the resulting two components of the single photon may be compared. After absorption, the system is a photon free wavefunction consisting of a superposition of two different internally excited states that evolves according to the net mass-energy in it. The relative phase of each space is fixed by the phase difference of the original photon at the time it was absorbed by the two sites $\Delta\phi = \phi(x_1, t = 0) - \phi(x_2, t = 0)$. Restricting our measurements to the case where the frequency of the emitted photons are the same, this phase difference should be preserved in the $T = 0$ limit. Thermal fluctuations in phase between the two points will produce

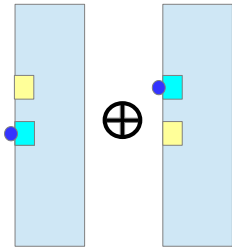

Fig. 7: The two possible configurations of a broad packet measurement (with suppressed radiative fields) exist as a kind of direct sum indexed by the coordinate label of the original incident particle.

a shift in this value. This procedure gives a measure of the regional phase fluctuations and isolation of the system.

5.2 Measurement back reaction

The subject of back reaction has been around for some time [8]. If one believes in a collapse picture then one can readily see that center of mass motion is not conserved in a position measurement. This means either it is truly not conserved or there is an unspecified back reaction on the system. In DWM we see that conservation laws only hold for the totality of slices not for individual "observer-paths". Therefore no back reaction is expected. We can utilize a pair of ultracold traps to give a specific test of this. Given a delocalized large mass molecule in a pair of widely separated traps we can send an atom through two paths to make contact with each of these. If a collapse produces a net conservation of all the usual conserved quantities then the center of mass shift will be proportional to the separation of the traps so can be made as large as desired and easily detected by florescent behavior of the molecule.

5.3 Nested and fuzzy measurement

The meaning of superposition of macroscopic objects has been debated at least as long as the famous Schrödinger's cat paradox [2, 13]. By our judicious selection of initial data we see that this is resolvable. The overlap of such states is explained by the proper consideration of correlations of photon fields in partitioning the system under such a slicing event as above. The nature of macroscopic superposition does however beg some interesting questions when the measuring device is also delocalized. For example, if the incident ψ has positive and negative regions that are shared equally over the same site due to delocalization then the net norm of ψ at that site may be zero. Does this mean there is no probability of adsorption at the site and the amplitude there is reflected? Furthermore, we can ask if the order of a meta-observer's action on the system in measuring the measurement device before it acts on the ψ or after makes any difference in the resulting statistics. These two scenarios can be classified as "fuzzy measurements" and "nested measurements".

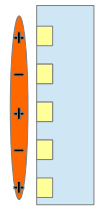

Fig. 8: A broad narrow packet incident on a screen. There is a relatively slow phase oscillation component parallel to the surface that matches the possible adsorption sites.

Firstly, consider a "device" that is a pair of separated, localized and slowly spreading heavy atoms or molecules in a trap. This allows for the possibility of the larger bodies capturing a small atom then moving the bound bodies around before ejecting the light atom from them. If the atoms are initially well localized and remain so for the duration of the experiment then the resulting phases on revival will be determined by the amplitude emission time and rate from each source atom. Note that this situation depends on the particles and what is moving them. If they are isolated like a gas then this is certainly true. If, however, the particles are being localized and moved by macroscopic classical matter or radiation that then is absorbed by it then the interactions with the external world may produce a slicing of the system. There may be no "meta-observer" or other unsliced mechanism to eject the light atoms and produce a spreading in its coordinate direction that causes the system to be seen as a wavefunction with some stored phase history and an external world. We can apply a radiation field to eject the light atom but have no way to know that our counterparts in the other slices have chosen to do the same.

Let us now extend the above case of the heavy atoms to the case of a measurement device i.e. a screen, as in Fig. 4. Here let us utilized a nearly monochromatic (wavelength λ) packet moving towards the screen but with a slow additional phase oscillation ($\lambda_{\|} \ll \lambda$) parallel to the screen surface. Let the screen have five adsorption sites and have separation equal to half this long wavelength oscillation $D = \lambda_{\|}/2$ as in Fig. 8. Now let the measurement device be delocalized in the vertical direction by a vertical shift D. We consider this to be in the form of two narrow packets of equal amplitude akin to the case of the incident wave in Fig. 5. The resulting initial state is described by the sum of configurations in Fig. 9.

Upon interaction the sites on the screen now feel both a positive and negative amplitude component of the wave. This is our first case of a correlated two body system. The system slices into a set of $4 + 5 = 9$ cases where the first four correspond to a screen that is upwardly displaced by D and the other five do not. For an "observer" living in the screen body itself, one of these cases appears to represent his initial data for the evolving future for all the initial data he has available to him. If somehow these slices are brought together in his future and the photon fields radiated from the adsorption

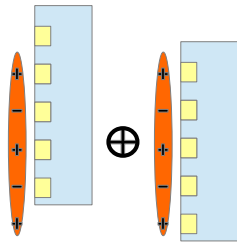

Fig. 9: A superimposed case of a measurement device with vertical delocalization and an incident wave packet.

events are confined with the system, the neighboring slices can interfere and this would seem to be a statistical aberration that flows from an unknown source. Now let us consider the situation from the "meta-observer" outside the system. This person can interact with the screen before or after the screen interacts with the packet. The bifurcation of amplitude gives the same results in both cases so there is nothing "fuzzy" about the measurement from the delocalized device and the measurement operations commute.

6 Conclusions

One alternate title to this article could have been: "The Cheap Photon and the Classical Limit: The Origin of Discrete State Machines, the Apparently 3D World, Quantum Measurement, the Arrow of Time and Why You Have Any Memory at All". It is impressive that such disparate topics should all be connected to mapping the classical world properly into quantum mechanics. A sister document on the dynamic process of thermalization and time dependent fluctuations has also been recently completed by this author [4]. The many body wavefunction of a system is a complicated high dimensional object. By including the photons a large number of degrees of freedom appear that allows condensing matter to sparsely occupy subdomains corresponding to very similar objects that retain independent existence for long periods of time. This provides a subset of wavefunctions that correspond to classical bodies that can withstand many quantum slicing events without producing significant overlap. The release of low mass particles from a condensed matter "classical" body leads to a product function state where the low mass component spreads rapidly and, when reabsorbed, creates a bifurcated class of such classical states with probabilities given by the Copenhagen interpretation defining a set of measurement events. These are locations and times specified by the atomic granularity scale of our condensed matter and a temporal granularity scale by the photon decay process associated with binding times. This resolves the paradoxes of quantum measurement and introduces an arrow of time in a rather simple fashion. We have argued that the genesis of such a state follows naturally from early universe conditions assuming condensation of small clusters of very low internal energy have time to interact and produce the localized classicality that partition the wavefunction into Newtonian-like parts.

One of the more unclear features yet to be resolved here is in the behavior of gases. Gases are made of light particles that have rapid delocalization so the persistent localization property we have argued for solids is not applicable. Collisions with solids surfaces of a container produce some localization by the slicing process but low diffusion rates suggest that this does not propagate well into the bulk of the gas. Hydrodynamic and thermodynamic behavior either requires some regular interaction with condensed matter by collision or possibly by photons or by some other process. We know that such gases have the power of producing quantum like measurement paths in cloud chambers (though clouds by definition involve condensed droplets). These are not pointlike but linelike events. This introduces an interesting direction to further investigate this model. Ultracold gas dynamics has become a very popular probe of quantum limits on viscosity [6, 14]. It is not clear that at such low temperatures for gases bound by fields and so not in contact with condensed matter, that hydrodynamics and thermodynamics are valid limiting behaviors on any timescale. These macroscopic formal models are often justified by vague scaling arguments. It is hard to argue against them because we have lacked a proper quantum description of gases in its "classical" limit. If this can be found, we may have a framework to see how well such a description can hold in the ultracold case and if such parameters like temperature and viscosity can have any relevant meaning for them.

Submitted on April 17, 2015 / Accepted on April 23, 2015

References

1. Bell J. S. On the problem of hidden variables in quantum mechanics. *Rev. Mod. Phys.*, 1966, v. 38, 447–452.
2. Carpenter R. H. S., Anderson A. J. The death of Schrödinger's cat and of consciousness-based wave-function collapse. *Annales de la Fondation Louis de Broglie*, 2006, v. 31 (1), 45–52.
3. Chafin C. Gauge freedom and relativity: A unified treatment of electromagnetism, gravity and the Dirac field. *Prog. in Phys.*, 2015, v. 11 (1), 25–37. arXiv: quant-ph/1410.8238.
4. Chafin C. Thermalization in quantum systems: an emergent approach. arXiv: quant-ph/1412.1347.
5. Chafin C. Beyond quantum fields: a classical fields approach to QED. *Progress in Physics*, 2015, v. 11 (3), 208–220.
6. Dalfovo F., Giorgini S., Pitaevskii L. P., Stringari S. Theory of Bose-Einstein condensation in trapped gases. *Rev. Mod. Phys.*, 1999, v. 71 (3), 463.
7. Everett H. "Relative state" formulation of quantum mechanics. *Rev. Mod. Phys.*, 1957, v. 29, 454–462.
8. Holland P. Hamiltonian theory of wave and particle in quantum mechanics II: Hamilton-Jacobi theory and particle back-reaction. *Nuovo Cimento B*, 2001, v. 116, 1143-1172.
9. Jammer Max. The Philosophy of Quantum Mechanics; the Interpretations of Quantum Mechanics in Historical Perspective. Wiley, New York, 1974.
10. Kreidi K et al. Interference in the collective electron momentum in double photoionization of H_2. *Phys. Rev. Lett.*, 2008, v. 100 (13), 133005.

11. Rohrlich F. Classical Charged Particles. World Scientific, Reading, MA, 2007.
12. Sakurai J. J. Modern Quantum Mechanics, 2nd ed. Addison Wesley, New York, 1993.
13. Schrödinger E. Die gegenwärtige Situation in der Quantenmechanik. *Naturwissenschaften*, 1935, v. 23, 49.
14. Son D. T. and Starinets A. O. Viscosity, black holes, and quantum field theory. *Ann. Rev. Nucl. Part. Sci.*, 2007, v. 57 (95), 95–118. arXiv: hep-th/0704.0240.
15. Schlosshauer M. Decoherence, the measurement problem, and interpretations of quantum mechanics. *Rev. Mod. Phys.*, 2004, v. 76, 1267–1305.
16. von Neumann J. Mathematical Foundations of Quantum Mechanics. Princeton University Press, Princeton, 1955.

Synchronous Changes of the Shape of Histograms Constructed from the Results of Measurements of ^{90}Sr β-Decay and ^{239}Pu α-Decay Observed in More than 3000 km Distant Laboratories

E. Y. Filin, A. V. Repkov, V. V. Voronov, A. A. Tolokonnikova[1], S. E. Shnoll[1,2]

[1]Institute of Theoretical and Experimental Biophysics, Russian Academy of Sciences.
[2]Department of Physics, Moscow State University, Russia.
E-mail: shnoll@mail.ru

It was discovered many years ago that histograms constructed from the results of measurements of various natural processes are not random. The histogram shape was demonstrated to be determined by the diurnal rotation and circumsolar movement of the Earth and to be independent of the nature of the process considered [1-17]. The results of those works change our basic views about stochasticity of natural processes. When the time series of physical measurements, which are traditionally considered stochastic, are transformed into the series of histograms constructed for an *optimally small number* of the results (i.e., *optimally short segment* of the time series), one can see regular changes in the histogram shape. The paper illustrates the main manifestations of this phenomenon by comparing the results of ^{90}Sr β-radioactivity and ^{239}Pu α-decay measurements, with the distance between the laboratories in which the data were collected being about 3000 km.

1 Introduction

The material for our research were results of long-term measurements of ^{239}Pu α-radioactivity in Pushchino (at the latitude of 54° north and longitude of 37°38' east) and ^{90}Sr β-radioactivity in Novosibirsk (at the latitude of 55°02'13" north and longitude of 82°54'05" east). The data were collected with a 1-second interval for many days. With the aid of Edwin Pozharsky's computer program GM [3], non-overlapping 60-point segments of 1-second time series were transformed into series of 1-minute histograms. The same program was used for a visual comparison of the histograms – after the procedures of smoothing, stretching, squeezing and mirror transformation, necessary to achieve the maximal similarity (for details, see [1]).

2 Experimental details

α-Radioactivity of a ^{239}Pu preparation was measured using low-voltage semiconductor detectors with collimators [10]. β-Radioactivity was measured using CTC-6 Geiger counters fixed in a metal case in a horizontal position, with their longitudinal axis directed along the azimuth of NN-SSW NNW-SSO (~320°). The source of β-radiation (^{90}Sr–^{90}Y, a flat disk of 20 mm diameter) was fixed 10 cm above the counter, with its radiating surface directed downwards to the counter.

3 Results

Fig. 1 shows a time series: the results of ^{90}Sr β-activity measurements. According to all fitting criteria, it is a purely stochastic process obeying the Poisson statistics.

As seen from Fig. 2, the results of measurements shown in Fig. 1 ideally correspond to the Poisson-Gauss statistics. That is why radioactive decay is considered an ideal example of the stochastic process. In Fig. 3, however, the same material of Fig. 1 is shown without smoothing, in the form of cumulative layers, where every next layer adds 3000 measurement points to the previous layer.

This figure demonstrates that contrary to the law of large numbers (the total number of measurements is 259200), the fine structure of the layered lines is not smoothed when the number of measurements is increased – it becomes even sharper. This paradox has a general character and can be observed in the measurements of any "stochastic" physical

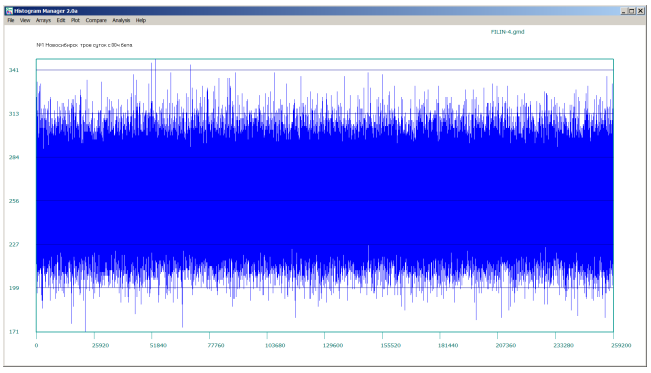

Fig. 1: A time series – the results of 1-second ^{90}Sr β-activity measurements for a period of 3 days (from 00:00 of June 19, 2013 to 23:59 of June 21, 2013). Novosibirsk local time (UTC + 7). X-axis: time, seconds. Y-axis: number of β-decays per second.

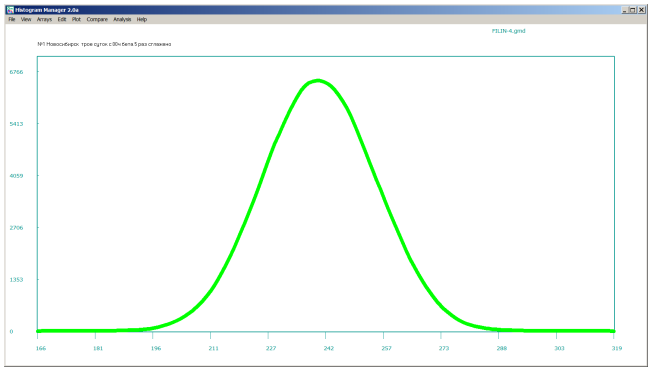

Fig. 2: Distribution of the results of measurements shown in Fig. 1. An ideal Poisson-Gauss distribution. X-axis: radioactivity, counts per second. Y-axis: number of results with the corresponding radioactivity value.

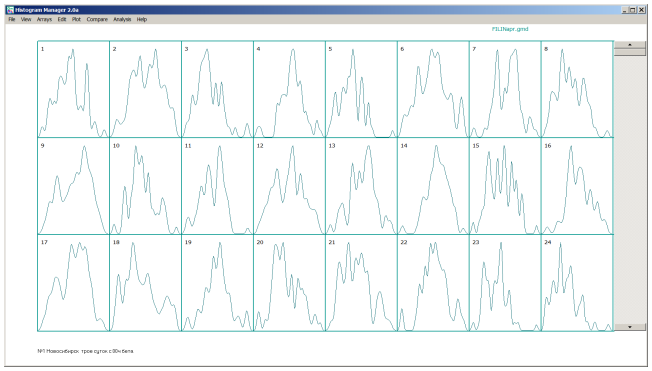

Fig. 4: Measurements of ^{90}Sr β-radioactivity. Transformation of a time series (Fig. 1) into a sequence of 60-point histograms smoothed 5 times. The figure shows the first 24 histograms from the total set of 4320 histograms.

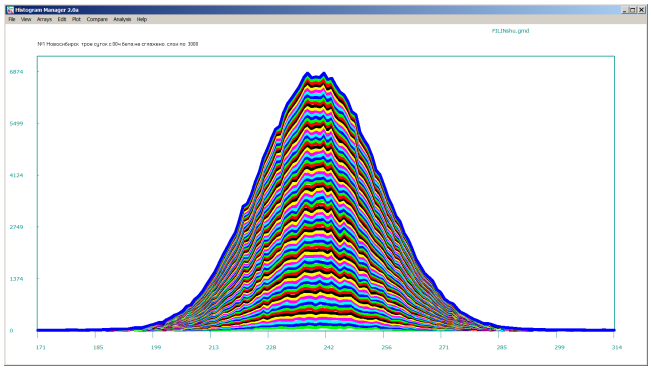

Fig. 3: Non-smoothed layered distribution of the results shown in Fig. 1. Every layer adds 3000 measurement points to the neighbor layer below. The axes are as in Fig. 2.

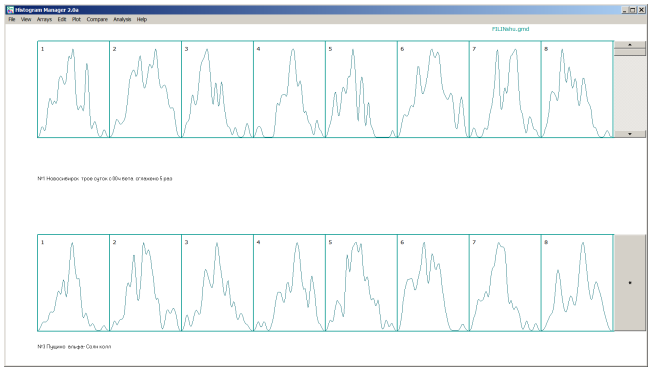

Fig. 5: A screenshot demonstrating comparison of two histogram sequences. Top band: measurements of ^{90}Sr β-radioactivity; bottom band: measurements of ^{239}Pu α-radioactivity. For each step, both bands shift forward by one number, and the new histograms, appearing at the right, are compared: the new top with all the bottom ones and the new bottom with all the top ones – this being repeated 360 times to build a distribution of the number of similar histogram pairs over the interval between these histograms (see Fig. 7 and hereinafter).

process [1].

In the paper, though, we consider histograms constructed for an *optimally small* number of measurements. It is transformation of time series into sequences of such *inconsistent* histograms, revealing well-reproducible cosmo-physical regularities, indicating nonrandomness of "stochastic" physical processes [1]. In the paper, this is demonstrated through synchronous measurements of ^{90}Sr β-radioactivity in Novosibirsk and ^{239}Pu α-radioactivity in Pushchino; the distance between these laboratories is about 3000 km.

The subject of this paper – as that of our previous works [1-17] – is the demonstration of regularities in the change of the shape of histograms constructed from an optimally small (30–60) number of results. Such a transformation of time series of the results of measurements into the sequences of histograms reveals the nonrandom character of these time series.

Fig. 4 shows some histograms constructed for the segments of the time series represented in Fig. 1. Each segment contains 60 ^{90}Sr β-radioactivity measurement points; the histograms were smoothed 5 times.

The fact that changes of the shape of such histograms in time are not random follows from a number of regularities found in our previous studies [1-17]. Even a careful examination of Fig. 4 would indicate this nonrandomness. It can, however, be estimated quantitatively. A quantitative measure of nonrandomness of the shape of inconsistent histograms is the results of their thorough comparison. The histograms can be compared either by a human expert, with the aid of Edwin Pozharsky's program, or by application of completely automated algorithms written by V. Gruzdev [19] and V.V. Strelkov et al. [18, 20–22].

Fig. 5 illustrates the procedure of pairwise histogram comparison, showing histograms constructed from the results of synchronous measurements of ^{90}Sr β-radioactivity in No-

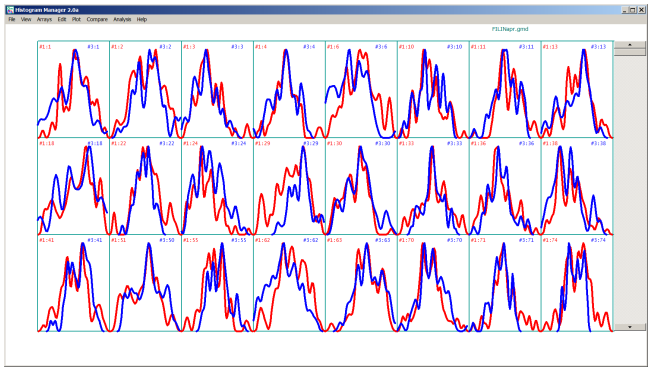

Fig. 6: A fragment of the computer journal (archive). Pairs of histograms considered similar by an expert.

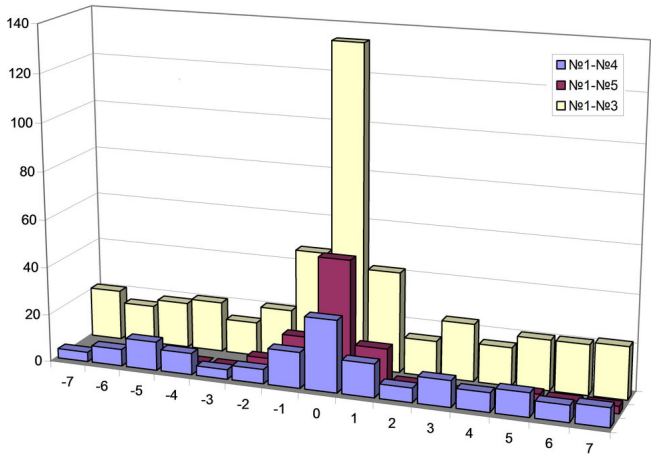

Fig. 7: Distribution of the number of pairs of similar histograms over the interval between them. Measurements of ^{90}Sr β-radioactivity in Novosibirsk and ^{239}Pu α-radioactivity in Pushchino with the collimators directed to the Sun (no. 3), Polar star (no. 4) or west (no. 5). Pairs no. 1-3; 1-4; 1-5. X-axis: intervals between similar histograms (min). Y-axis: number of similar histograms per 360 compared pairs.

vosibirsk (top band) and ^{239}Pu α-radioactivity in Pushchino (bottom band). Each band contained 360 numbers. In total, about 20,000 histogram pairs were compared, and the results are given in Figs. 6 and 7.

Fig. 6 shows an example of the histogram pairs that an expert deemed similar upon visual comparison.

Fig. 7 demonstrates the results of histogram comparison in the synchronous measurements of ^{90}Sr β-radioactivity in Novosibirsk and ^{239}Pu α-radioactivity in Pushchino in 3 variants of experimental setup: with the collimator aimed at the Polar star (no. 4); with the collimator constantly aimed at the Sun (no. 3) (on a rotating platform compensating for the diurnal rotation of the Earth); with the collimator directed west (no. 5). These results are represented as a dependence of the number of similar histogram pairs on the interval between the histograms.

As seen in Fig. 7, when the collimator in Pushchino is aimed at the Polar star, there is no synchronism in the change of histogram shape in Novosibirsk and Pushchino. When the collimator in Pushchino is directed west, synchronism is not very apparent but statistically significant ($P < 10^{-3}$). When the collimator is aimed at the Sun, synchronism is evident ($P < 10^{-7}$).

We shall not discuss now why the extent of synchronism depends on the direction of collimators in Pushchino (for details, see [1]). What is important is that with other conditions being equal, these differences in the experimental setup make the effects observed statistically significant. Therefore, the shape of histograms constructed from the results of measurements of β- and α-radioactivity at the distance between the laboratories ~3000 km does not depend on the nature of the process measured and the method of measurement. This agrees with the conclusion that the shape of histograms and its changes are determined by the orbital movement and diurnal rotation of the Earth and other cosmo-physical factors [1, 10–17].

This conclusion is confirmed by demonstration of the effects that are traditional for our works. The first effect is the

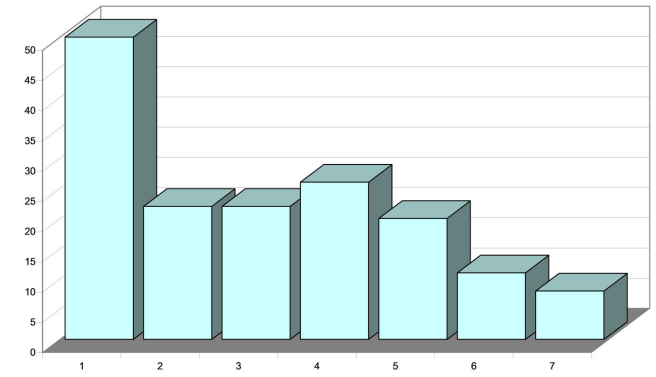

Fig. 8: Measurements of ^{90}Sr β-activity. The "effect of near zone", a higher probability of neighbor histograms (interval = 1) to be similar comparatively to the histograms separated by larger intervals. X-axis is time interval in minutes, Y-axis is number of similar histograms per 360 compared pairs.

"effect of near zone". It means that the neighbour histograms are much more probable to be similar, and Fig. 8 shows how it looks for the β-activity measurements.

Since histograms are constructed for non-overlapping segments of time series, the effect of near zone is the first sign of histogram shape to be determined by an external factor [1]. The second traditional effect, indicating cosmo-physical conditionality of the shape of histograms, is the existence of two clearly resolvable near-daily periods: sidereal and solar [1]. Fig. 9 shows these near-daily periods revealed in the measurements of ^{90}Sr β-activity in Novosibirsk (no. 1) and ^{239}Pu α-activity in Pushchino (no. 3–5)

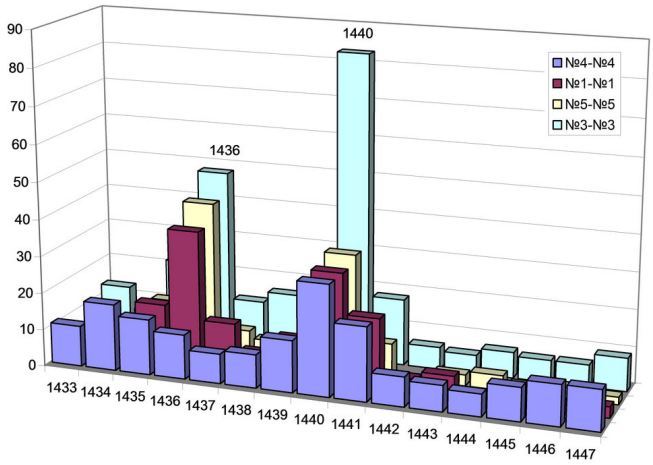

Fig. 9: Sidereal (1436 min) and solar (1440 min) daily periods in the appearance of similar histograms in the measurements of ^{90}Sr β-activity in Novosibirsk (no. 1) and ^{239}Pu α-activity in Pushchino (no. 3, 4, 5). Collimator is aimed at the Sun – no. 3; collimator is aimed at the Polar star – no. 4; collimator is directed west – no. 5. X-axis is time interval in minutes, Y-axis is number of similar histograms per 360 compared pairs.

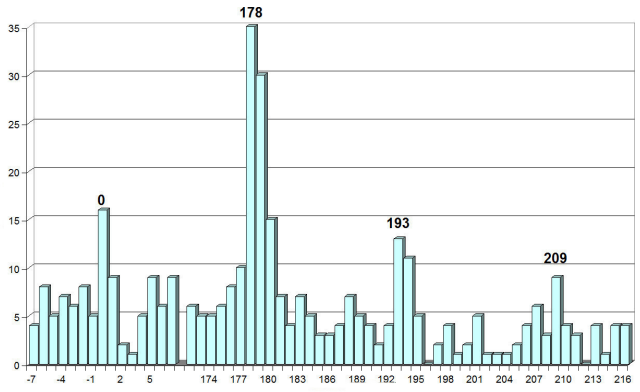

Fig. 10: Effect of synchronism by local time revealed upon comparison of the histograms constructed for the measurements of ^{90}Sr β-activity in Novosibirsk and ^{239}Pu α-activity in Pushchino with a collimator directed west. X-axis is time interval in minutes, Y-axis is number of similar histograms per 360 compared pairs.

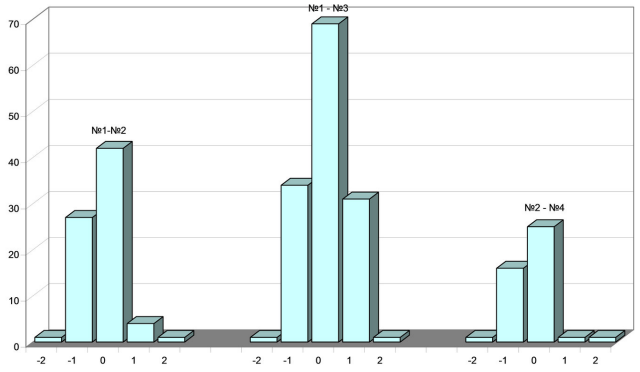

Fig. 11: Measurements of ^{90}Sr β-activity. The "palindrome effect" revealed upon comparison of a daytime histogram sequence (no. 1; from 6:00 to 18:00 by accurate local time) to the non-inverse (no. 2) and inverse (no. 3) nighttime sequences (from 18:00 to 6:00 of the next day) and the next daytime sequence (no. 4). X-axis is time interval in minutes, Y-axis is number of similar histograms per 360 compared pairs.

The existence of well-resolvable sidereal and solar daily periods means a sharp anisotropy of the effects observed. The difference between the direction at the immobile stars (sidereal daily period) and the Sun (solar daily period) is about 1 degree. As seen in Fig. 9, these periods are 4 minutes apart, i.e., they are resolved with the accuracy of 15 angular minutes. We also observe spatial anisotropy in the effects of synchronism by the absolute and local time [1, 11].

One can see the effect of spatial anisotropy in Fig. 10, which demonstrates local-time synchronism in the change of the shape of histograms constructed for the measurements of ^{90}Sr β-activity in Novosibirsk (no. 1) and ^{239}Pu α-activity in Pushchino with a west-directed collimator. The calculated difference in local time is equal to 179–180 min. As seen in Fig. 10, there is a sharp extremum – evidence of the effect – at 178^{th} minute (peak height, 134 similar pairs). Other extrema, corresponding to the moments of absolute-time synchronism (at 0^{th}, 193^{rd} and 209^{th} minutes), are substantially lower (peak height, 16 similar pairs and less).

Thus, the measurements of ^{90}Sr β-activity performed in Novosibirsk give us another confirmation of universality of the effects described earlier.

As the last illustration, we shall consider the "effect of palindrome", which indicates a dependence of the histogram shape on the spatial relation between the directions of the Earth diurnal rotation and its movement along the circumsolar orbit [8, 9]. The effect consists in the reverse change of the histogram sequences at the moments when the relation between the directions alternates its sign. According to the previously published works, it occurs at 6:00 and 18:00 by accurate (longitudinal) local time. In the course of its diurnal rotation, the Earth starts moving against its orbital translocation at 6:00. At 18:00, the directions of both movements become the same. The effect manifests itself in a dramatic difference in the similarity of consecutive histograms when a "daytime" histogram sequence (from 6:00 to 18:00) is compared to either inverse or non-inverse "nighttime" sequence (from 18:00 to 6:00 of the next day). This effect is illustrated in Fig. 11.

The effect of palindrome is clearly seen in Fig. 11. After inversion of one half of a day (in the points of palindrome), the number of similar histogram pairs doubles.

4 Discussion

The objective of this paper was to check if the results of ^{90}Sr β-activity measurements conducted by E.Y. Filin can be compared with the results of other measurements obtained within the research on "cosmo-physical fluctuations". As follows from the presented data, all the expected effects were reproduced with these experiments. Since β-particles run a distance of a few meters in the air (in contrast to α-particles, which run only a few centimeters), these measurements can be a valuable tool for a study of the spatial anisotropy of the observed effects.

Acknowledgements

The authors are grateful to M.E. Astashev and V.A. Kolombet for their help in measuring α-activity and data processing, as well as for participation in the discussion of the results.

Submitted on March 31, 2015 / Accepted on April 29, 2015

References

1. Shnoll S.E. Cosmo-physical factors in stochastic processes. Svenska Fysikarkivet, Stockholm, 2009.
2. Shnoll S.E., Kolombet V.A., Pozharsky E.V., Zenchenko T.A., Zvereva I.M., Konradov A.A. Realization of discrete states in the course of fluctuations of macroscopic processes. *Uspekhi Fiz. Nauk*, 1998, v. 168(10), 1129–1140 (in Russian).
3. Shnoll S.E., Kolombet V.A., Pozharsky E.V., Zenchenko T.A., Zvereva I.M., Kondradov A.A. Cosmo-physical causation of "macroscopic fluctuations". *Biofizika*, 1998, v. 43(5), 909–915 (in Russian).
4. Shnoll S.E., Zenchenko T.A., Zenchenko K.I., Pozharsky E.V., Kolombet V.A., Konradov A.A. Regular changes in the fine structure of statistical distributions as a consequence of cosmo-physical causes. *Uspekhi Fiz. Nauk*, 2000, v. 170(2), 214–218 (in Russian).
5. Shnoll S.E. Changes in fine structure of stochastic distributions as a consequence of space-time fluctuations. *Progress in Physics*, 2006, v. 2, 39–45.
6. Shnoll S.E. Fine structure of statistical distributions as a reflection of spatial and gravitational anisotropy of our world. *Russian Chem. J.* (Journal of D.I. Mendeleev's Russian Chemical Society), 2007, v. 51(1), 150–157 (in Russian).
7. Shnoll S.E. A cosmo-physical nature of the "idea of shape" of histograms constructed from the results of measurements of processes of diverse nature. In "Metaphysics. XXI Century", 2007, issue 2 (Y.S. Vladimirov, ed.) Binomial C Press, 284–319 (in Russian).
8. Shnoll S.E., Panchelyuga V.A., Shnoll S.E. The palindrome effect. *Progress in Physics*, 2008, v. 2, 151–153.
9. Shnoll S.E. The "scattering of the results of measurements" of processes of diverse nature is determined by the Earth's motion in the inhomogeneous space-time continuum. The effect of "half-year palindromes". *Progress in Physics*, 2009, v. 1, 3–7.
10. Shnoll S.E. and Rubinstein I.A. Regular changes in the fine structure of histograms revealed in the experiments with collimators which isolate beams of alpha-particles flying at certain directions. *Progress in Physics*, 2009, v. 2, 83–95.
11. Shnoll S.E., Rubinstein I.A., Vedenkin N.N. "The arrow of time" in the experiments in which alpha-activity was measured using collimators directed east and west. *Progress in Physics*, 2010, v. 1, 26–29.
12. Kaminsky A.V. and Shnoll S.E. Cosmophysical factors in the fluctuation amplitude spectrum of Brownian motion. *Progress in Physics*, 2010, v. 3, 25–30.
13. Shnoll S.E., Astahev M.E., Rubinshtein I.A., Kolombet V.A., Shapovalov S.N., Bokalenko B.I., Andreeva A.A., Kharakoz D.P., Melnikov I.A. Synchronous measurements of alpha-decay of ^{239}Pu carried out at North pole, Antarctic, and in Pushchino confirm that the shapes of the respective histograms depend on the diurnal rotation of the Earth and on the direction of the alpha-particle beam. *Progress in Physics*, 2012, v. 3, 11–16.
14. Rubinshtein I.A., Shnoll S.E., Kaminsky A.V., Kolombet V.A., Astashev M.E., Shapovalov S.N., Bokalenko B.I., Andreeva A.A., Kharakoz D.P. Dependence of changes of histogram shapes from time and space direction is the same when intensities of fluctuations of both of light-diode provided light flux and ^{239}Pu alpha-activity are measured. *Progress in Physics*, 2012, v. 3, 17–24.
15. Shnoll S.E., Kaminsky A.V., Rubinstein I.A., Shapovalov S.N., Kharakoz D.P. Fine structure of the fluctuation-amplitude spectra constructed for the results of measurements of processes of diverse nature as a characteristic of inhomogeneities (anisotropy) of space-time. In "Metaphysics. XXI Century", 2012, issue 3 (Y.S. Vladimirov, ed.), Binomial C Press, 36–66 (in Russian).
16. Shnoll S.E. Fractality, "coastline of the Universe", movement of the Earth and macroscopic fluctuations. *Biofizika*, 2013, v. 58(2), 357–376 (in Russian).
17. Rubinstein I.A., Kaminsky A.V., Tolokonnikova A.A., Kolombet V.A., Shnoll S.E. Basic phenomena of "macroscopic fluctuations" are repeated on light beams generated by lasers or light-emitting diodes. *Biophysics* (transl. from *Biofizika*, in Russian), 2014, v. 59, issue 3, 492–502.
18. Kaminsky A.V., Rubinstein I.A., Shapovalov S.N., Tolokonnikova A.A., Kolombet V.A. and Shnoll S.E. "Macroscopic fluctuations" of light beams as a novel tool for astrophysical studies. *Astrophys. Space Sci.*, 2015, v. 355, 9–21.
19. Strelkov V.V. A new measure for histogram comparison in time series analysis. *Pattern Recognition Letters*, 2008, v. 29, 1768–1774.
20. Gruzdev A. Algorithmization of histogram comparing process. Calculation of correlations after deduction of normal distribution curves. *Progress in Physics*, 2012, v. 3, 25–28.
21. Khmaladze E.V. Martingal limit theorems for separate statistics. *Probability Theory and Its Applications*, 1983, v. 28(3), 504 (in Russian).
22. Udaltsova N.V., Urinov I.K. Estimation of the probability of observed extrema in the histograms constructed from small samples. In the Proceedings of the 3rd All-Union Conference "Perspective Methods of Planning and Analysis" (Grodno), 1988, p. 155–156 (in Russian).
23. Bodrova N.B. Udaltsova N.V., Ivanov P.S., Shnoll S.E. On the non-randomness of the shape of inconsistent histograms. SCBR Preprint, Pushchino, 1989.

Polarized Light from the Sun: Unification of the Corona and Analysis of the Second Solar Spectrum – Further Implications of a Liquid Metallic Hydrogen Solar Model

Pierre-Marie Robitaille[1] and Dmitri Rabounski[2]

[1]Department of Radiology, The Ohio State University, 395 W. 12th Ave, Columbus, Ohio 43210, USA
E-mails: robitaille.1@osu.edu[1], rabounski@ptep-online.com[2]

In order to account for the slight polarization of the continuum towards the limb, proponents of the Standard Solar Model (SSM) must have recourse to electron or hydrogen-based scattering of light, as no other mechanism is possible in a gaseous Sun. Conversely, acceptance that the solar body is comprised of condensed matter opens up new avenues in the analysis of this problem, even if the photospheric surface itself is viewed as incapable of emitting polarized light. Thus, the increased disk polarization, from the center to the limb, can be explained by invoking the scattering of light by the atmosphere above the photosphere. The former is reminiscent of mechanisms which are known to account for the polarization of sunlight in the atmosphere of the Earth. Within the context of the Liquid Metallic Hydrogen Solar Model (LMHSM), molecules and small particles, not electrons or hydrogen atoms as required by the SSM, would primarily act as scattering agents in regions also partially comprised of condensed hydrogen structures (CHS). In addition, the well-known polarization which characterizes the K-corona would become a sign of emission polarization from an anisotropic source, without the need for scattering. In the LMHSM, the K, F, and T-coronas can be viewed as emissive and reflective manifestations of a single coronal entity adopting a radially anisotropic structure, while slowly cooling with altitude above the photosphere. The presence of "dust particles", advanced by proponents of the SSM, would no longer be required to explain the F and T-corona, as a single cooling structure would account for the properties of the K, F, and T coronas. At the same time, the polarized "Second Solar Spectrum", characterized by the dominance of certain elemental or ionic spectral lines and an abundance of molecular lines, could be explained in the LMHSM, by first invoking interface polarization and coordination of these species with condensed matter in the chromosphere. The prevalence of polarized signals from the Rare Earth metals, a chemically unique group of the periodic table, provides powerful evidence, based on the "Second Solar Spectrum", that chemical reactions and coordination are taking place in the atmosphere of the Sun. This concept is also supported by the polarized signal from lithium, an element previously hypothesized to assist in stabilizing metallic hydrogen structures. The possibility that some atoms are coordinated with CHS implies that the relative abundance of elements cannot be simply ascertained through the analysis of emission or absorption lines in the solar atmosphere.

... it follows that a body, which absorbs more rays from one plane of polarization than from another, sends out in the same ratio more rays from the first plane of polarization than from the second.

Gustav Kirchhoff, 1860 [1]

1 Introduction

Recently, considerable doubt has been raised [2–4] relative to Kirchhoff's formulation of his law of thermal emission [1]. In this regard, the equivalence between emitted and absorbed radiation under conditions of thermal equilibrium, properly known as Stewart's law [5], has not been questioned. However, the German scientist's claim that the radiation within an arbitrary cavity will always be independent of the nature of the walls, while subject only to the temperature and the frequency of observation, has never been demonstrated experimentally and is unsupported by mathematical derivation [2–4]. Regrettably, even the proof of Kirchhoff's law of thermal emission, as advanced by Max Planck, has been found to be physically unsound [2].* As such, beyond the restatement of Stewart's law [5], it would appear that little can be preserved from Kirchhoff's classic paper [1].

Yet, there is an experimental aspect of Kirchhoff's work which can never be discounted, namely that a tourmaline plate can absorb radiation more favorably in one plane than in the other [1, § 16]:

*Since mathematics is the language of physics, this is a serious problem for all those who adhere to the validity of Kirchhoff's claims [2].

> *"A tourmaline plate, cut parallel to the optic axis, absorbs, at ordinary temperatures, more of the rays which strike it normally, if the plane of polarization of these is parallel to the axis than when it is perpendicular to it. Assuming that the tourmaline plate retains this property when it is at a glowing heat, it must give out rays in a direction normal to it, which are partially polarized in the plane passing through the optic axis and which is the plane perpendicular to that which is called the plane of polarization of tourmaline. I have proved this striking deduction from theory by experiment and it confirmed the same."*

With this observation, Kirchhoff was emphasizing that certain objects, especially when highly anisotropic in their crystal structure, could emit polarized light [6, p. 604]. Kirchhoff's finding, that the light emitted by a heated tourmaline plate was polarized in the same plane as that which preferentially absorbed light, had also been noted by Balfour Stewart [7, § 68]. P. P. Feofilov addressed this aspect of nature in his classic text on *The Physical Basis of Polarized Emission* [8, p. 33–34]:

> *"... in order that the polarization should appear in the radiation due to a macroscopic system, it is necessary that the mutual orientation of the elementary radiating systems should not be random. A random aggregate of anisotropic elementary radiators, gives, clearly, a completely unpolarized radiation. A regular orientation of the separate elements of a macroscopic system may be due to the properties of the system itself, and this is the case, for example, in anisotropic crystals, or it may be induced from outside by electric and magnetic fields, by mechanical action, or finally, by light incident from outside the system, since a light ray, because of its nature, is always anisotropic ... In the case of regular crystals, the orientation of the emitting centers may be complete, and the emitted light may be practically totally polarized ... "*

In the case of tourmaline, the degree of polarization can approach 40% [9, p. 112].

Beyond crystals, it is not generally known that incandescent metals can often be a source of strongly polarized light [9, p. 110 & 138]. This effect does not occur when observing metals perpendicular to the surface, but polarization can approach 90% when the angle of observation departs substantially from the normal, in studying a clean metal [9, p. 110 & 138]. Thin metal wires exhibit polarized emission [10, 11] and the heat radiation, from small but long cylindrical objects, can also be highly polarized [12]. More recently, polarized light emission has been noted from individual carbon nanotubes, their fibers, bundles, and arrays (see [13, 14] and references therein). Importantly, within these carbon-based bundles, the light emission maintained a blackbody spectral appearance [13].

Fig. 1: An anisotropic tourmaline crystal (National Mining Hall of Fame and Museum — Leadville, CO; 3/18/2015; Photo by PMR).

Still, Kirchhoff's observation relative to tourmaline [1], these others [6–14], and many more, which highlight the importance of anisotropy relative to the emission of polarized light, have been discounted by astronomy. Clearly, since the Standard Solar Model (SSM) advocates that the Sun is gaseous in nature, there is little room in modern astrophysics for condensed matter.* The stars are thought to be devoid of solids and liquids. Rather, most astronomers believe that these objects are composed either of gaseous plasmas or highly degenerate matter, in accordance with the stellar type involved and the dictates of mathematical models. Nonetheless, ample evidence exists that the Sun itself is comprised of condensed matter or, more specifically, of metallic hydrogen [15]. Thus, it is fitting to reconsider the lessons of the tourmaline plate [1] in order to obtain a new perspective with respect to the emission of polarized light by the Sun and the stars.

2 Polarized light in the corona

Knowledge that the solar corona emitted polarized light was first gained at the eclipse of 1868 [16, p. 44]. Schuster provided a mathematical treatment of the problem as early as 1879 [17]. But it was not until R. K. Young analyzed photographic plates of the eclipses of 1901, 1905, and 1908 with a Hartmann microphotometer, that the extent of polarization could be properly quantified [18]. Young discovered that polarization increased gradually, with increasing elevation above the photosphere, to a value of ~37% before slowly starting to decrease. He also noted [18] that the corona was

*With the exception perhaps of some planets, meteors, asteroids, etc.

> *"...formed from matter which has been projected from the Sun"* and that *"The distribution of matter in the corona is dependent on high inverse powers of the distance from the Sun's center, probably the sixth or eighth or a combination of the two."*

Young also believed that the polarization was due to the scattering of photospheric light by small particles. As a consequence of such early studies, it was established that the light arising from the K-corona was radially polarized [18].

With the advent of the Lyot coronograph in 1930, the study of the solar corona outside of total eclipses became possible [19]. That same year, Minnaert published his work on the nature of the continuous coronal light and its polarization [20]. Minnaert considered the idea that the corona was self-luminous [20]. Sixty years earlier, William Harkness had viewed a total eclipse from Iowa and had also concluded that the corona was *"...a highly rarefied self-luminous atmosphere surrounding the Sun"* [21, p. 199].

However, the concept that the corona could be self-luminous has been largely abandoned by astronomy. In part, this dates back to the days of Schuster and his analysis of the polarization question. The British scientist had treated a luminous sphere surrounded by small particles which could scatter the light, thereby producing the desired polarization [17]. Schuster noted that [17]:

> *"In reality the polarisation rapidly diminishes and very soon a point is reached at which no polarisation can be observed; the corona must therefore contain some matter which is either self-luminous or too large to polarise the light while scattering it ...The rapid decrease of polarisation with increasing distances from the Sun, as well as the comparatively small amount of observed polarization, shows that a large part of the light is not due to scattering particles. This light may either be produced by incandescence, or by particles which are too large to polarise the light in the act of scattering it."*

Like Schuster, Minnaert also left open the possibility that the corona was capable of both scattering photospheric light and self-emission [20]. For his presentation, Minnaert considered that the scattering, leading to polarization, was taking place through the action of free electrons.

Within the context of the SSM, K-coronal polarization is thought to be produced by relativistic electrons which scatter photospheric light such that most Fraunhofer lines can no longer be observed [16, p. 4-5 & 135].

At the same time, streamers are known to constitute the most polarized portion of the corona, with values ranging from 30-60% [16, p. 136–138]. Such findings, along with Young's discovery that the degree of polarization could first increase and then decrease with elevation above the photosphere [18], provide strong evidence that the cause of polarization must involve structure and not simply the presence of relativistic free electrons.

In this respect, given the degree of ionized atoms in the E-corona [16, p. 4–5 & 135], it is doubtful that the determinations of electron density from polarization measurements could be accurate [16]. Furthermore, such calculations discount the notion that condensed matter may well be present in this region of the Sun [22]. It has been proposed that the metallic hydrogen which makes up the corona is electron starved and this, in turn, not MK temperatures, leads to the presence of the highly ionized atoms which characterize the E-corona [23, 24]. The Liquid Metallic Hydrogen Solar Model (LMHSM) [15, 22–24] leaves little possibility for the presence of substantial numbers of free electrons, in the upper coronal atmosphere of the Sun. In order that a star can remain stable, it must work to salvage both its hydrogen [25–27] and its electrons [22–24]. Such an idea has only been advanced within the context of the LMHSM [15, 22–27].*

3 Unifying the K-, F-, and T-coronas in the LMHSM

Throughout much of the solar atmosphere, K-coronal polarized light is mixed with F-coronal radiation. The F-corona is characterized by the presence of Fraunhofer lines and, in the SSM, is believed to be produced by dust particles which act to scatter photospheric light without polarization [16, p. 4–5 & 135]. Indeed, polarization has been utilized as a basis of discriminating between the K- and F-coronas, as F-coronal light was initially thought to be unpolarized [32–34]. However, it soon became clear that the polarization of the F-corona beyond $5R_\odot$ could not be ignored [35].† Using the degree of polarization, attempts to excise a K-coronal signal has been

*One of the authors (PMR) recently became aware that Professor J.E. Hirsch proposed, in 1989, that sunspots might be composed of metallic hydrogen based on the presence of strong magnetic fields in these regions: *"Sunspots are characterized by having a lower temperature than their environment, and very strong magnetic fields. It is natural to conclude that metallic hydrogen develops large spin polarization in these regions"* [28]. Since no lattice structure was specified to account for the emission of sunspots, Professor Hirsch appears to have adopted the accepted view from the SSM that the lower emissivities from these structures are associated with decreased temperatures [28] and not due to changes in emissivity as a result of increased metallic character [15]. Unlike Robitaille, who has promoted the idea that sunspots reflect slightly higher densities relative to the photosphere [15], Professor Hirsch speaks of a lower density inside sunspots [28]. At the same time, Hirsch makes a compelling case for the importance of metallic hydrogen throughout astronomy, as a universal cause of magnetism. On a related question, based on solar densities of $\sim 150 g/cm^3$ associated with the SSM, Professor Setsuo Ichimaru has advanced that the solar core might be comprised of metallic hydrogen [29–31]. Conversely, while Robitaille recognizes the presence of a solar core, he has advocated that the Sun possesses a nearly uniform density of $\sim 1 g/cm^3$ (see [15] and references cited therein). This is because a density of $150 g/cm^3$ in the core, as proposed by Ichimaru [29–31], would leave little material to build condensed structures on the photosphere. Further, Robitaille's position is in keeping with the idea that liquids are essentially incompressible.

†Coronal polarization has been measured out to an amazing 10 solar radii [36, p. 187].

used to compute electron densities in this region [32–35]. The problem rests in that electron densities calculated in this manner are dictated by the very mechanism proposed for the polarization, without any independent confirmation that polarization was in fact produced by electrons. In addition, it is evident that there should be a strong decrease in free electron density as a function of distance from the Sun (e.g. [36, p. 188]). It is difficult to justify distant polarization with relativistic electrons.

Relative to the nature of the "dust" which is believed to constitute F-coronal matter in the SSM, Mukai et al. [37] advocated, in 1974, that graphite grains were the most likely candidate. They envisioned that the grains would sublime, as the distance to the solar surface was decreased, hence accounting for the known reduction in the F-coronal contribution in this direction [37]. A T-corona has also been hypothesized to exist, in order to account for the increased reddening of coronal light with increasing altitude above the photosphere [16, p. 4–5 & 135]. This reddening had been noted long ago by Allen [38]:

> *"microphotograms for solar distances varying from $R = 1.2\,s$ to $R = 2.6\,s$ show that the coronal radiation reddens slightly as the distance from the Sun is increased."*

Pondering on all of these fragmented pieces of information, there is a need to arrive at a unifying principle relative to the corona of the Sun.*

Rather than speak of the K-, F-, and T- coronas as separate entities [16, p. 4–5 & 135], the idea should be entertained that the corona is composed of condensed matter which is manifesting spatially variable emissive, reflective, and structural properties. It is logical to postulate that condensed coronal matter is based on photospheric Type-1 metallic hydrogen which has been ejected from the solar surface [22–24]. Since photospheric matter produces unpolarized radiation, it is reasonable that, in the lower solar atmosphere, coronal material will also lack the ability to significantly polarize light. Nonetheless, it will remain capable of self-emission. With elevation above the solar surface, the ejected photosheric material, which now constitutes the corona, begins to adopt a radially anisotropic structure, as manifested by streamers, for instance. Such structural anisotropy thereby enables the emission of polarized light from incandescent radially aligned coronal material [8]. This explains the presence of the K-coronal signals. No Fraunhofer lines are present, because the coronal matter is self-luminous and positioned above the elevation where intense absorption by free atoms or ions is possible. With increased elevation above the photosphere, coronal material begins to cool, loosing incandescence. In response to decreased temperatures, emissivity decreases and reflectivity increases, much like the iron rod placed in a forge. With increased reflectivity, coronal material becomes less able to emit polarized light in the visible range. Rather, it now increasingly reflects photospheric light. That is why the Fraunhofer lines become visible in the F-coronal spectrum. At the same time, since coronal material is cooling, it begins to emit its light, not in the visible, but in the infrared. Hence, the production of the T-coronal spectrum.

With this new proposal, the K-, F-, and T- coronas simply become manifestations of the same coronal material. A streamer can be viewed as a real structure whose emissive and reflective behavior is characterized by both temperature and structural changes within the *same* entity. A streamer is unlikely to be comprised of an assembly of isolated gaseous ions or atoms, as currently held by the SSM, as the simplest explanation for such structure rests upon condensed matter.

As for the E-corona [39], it is being produced, not by the presence of MK temperatures in the corona, but rather through the removal of atomic and ionic electrons by condensed coronal material [15,22–24]. With increased elevation above the photoshere, the coronal metallic hydrogen, which acts to channel electrons back onto the solar surface, can be viewed as becoming increasingly electron starved. As a result, any ion or atom which comes into contact with such material will be likely to be stripped of electrons, since the Sun is working to maintain neutrality [22–24]. Electron affinities, not extreme temperatures, govern the production of highly ionized elements in the corona.

4 Polarization at the solar limb

In 1946, Chandrashekhar, through mathematical consideration of Thomson scattering by electrons [40, p. 249], first advanced that the body of the stars could emit a continuous spectrum, characterized by polarization, concluding that [41]

> *"the degree of polarization must vary from zero at the center of the disk to 11 per cent at the limb"*

Using similar approaches, Sobolev confirmed Chandrashekhar's finding [42] and the problem has been extensively reviewed [43, p. 119–203].

According to Dolginov, Gnedin and Silant'ev [43, p. 120], stellar polarization can be attributed to three major factors:

> *"a) nonsphericity of stellar shape, b) the eclipses of a hot star within a binary system, c) scattering in a nonspherical circumstellar envelope by gas flux."*

They argue that even a spherical star can have mechanisms for changes in luminosity across its surface, the most important of which might be temperature variations [43, p. 121]. The scattering of light by electrons has continued to play an

*The idea that the F-corona was produced by interplanetary dust particles was initially adopted in accounting for the behavior of the corona, even within the context of the LMHSM [22–24]. However, upon further reflection, it is clear that the SSM explanation for the presence of the F-corona should not be salvaged.

important role, relative to accounting for the production of polarized light in the context of gaseous stars and the SSM.

In the final analysis, the need to account for the production of polarized light in a gaseous object requires a suspension of objective reality. For instance, Chandrashekhar's analysis depends on the generation of polarized light from a gaseous star [41]. Yet, at the same time, the SSM views the Sun and the stars as a nearly ideal blackbody emitters [44–46]. It is well-known that blackbodies are incapable of emitting polarized light, by definition (see [47, p. 450], and [48, §5 &107]). Hence, it should have been difficult for proponents of the SSM to accept Chandrashekhar's claim that a gaseous star could emit up to 11.7% polarized light at the limb, a number which was actually very large [41]. In order to reconcile Chandrashekhar's findings with the SSM and blackbody behavior, a gaseous Sun must be divided into that opacity region which produces the thermal spectrum and an upper layer responsible for polarization [49,50]. The reality remains that, since the Sun sustains convection currents and conduction, it makes for a very poor example of a blackbody [15], as highlighted by Max Planck himself [48, § 51]. Moreover, because Thomson scattering by an electron is frequency independent [51, p. 69] and the polarization of the continuous solar spectrum is frequency dependent, Rayleigh scattering by neutral hydrogen had to be introduced to reconcile theory [40–43] with solar observations [49, 50].

In order to account for the slight degree of frequency-dependent polarization in the continuous spectrum towards the solar limb, it is more prudent to postulate that the body of the Sun emits unpolarized light. A single photon can be considered which leaves the photosphere at the center of the solar disk. That photon, if it escapes at an angle far from the normal, could then travel in the direction of the limb. Along its path, it will encounter molecules and small particles which could cause scattering in the direction of the Earth. In this manner, photons experiencing a 90° scatter towards the Earth could then be polarized.* It does not depend on the electron and does not necessitate that the body of the Sun itself emit polarized light, as theoreticians have proposed [41–43]. The only requirement rests in acceptance that both polarizing molecules and various forms of condensed matter† exist above the photosphere of the Sun, a concept supported by ample evidence, including both spectroscopy and coronal seismology [15].

5 Polarization and second solar spectrum

Beyond the frequency dependent polarization of the continuous solar spectrum [49, 50], the Sun also emits polarized light from numerous individual spectral lines. In combination, these two findings lead to the "Second Solar Spectrum" [49,50,56–67]. Brief historical accounts of this problem have been presented [58, 61] and the major features of the Second Solar Spectrum are as follows:

1. Relative to the Fraunhofer spectrum, these signals are extremely weak, rarely exceeding a Q/I level of 10^{-3} in the visible range [57, 58].

2. The most important atomic lines in the Second Solar Spectrum are produced from Ti I and Cr I [58]. These two elements possess ground state electronic configurations of $[Ar]3d^24s^2$ and $[Ar]3d^54s^1$, respectively.‡

3. The phase of the emission lines relative to the continuum can be highly variable [61]. Therefore, spectroscopic lines are said to either add to (i.e. polarize [61]) or subtract from (i.e. depolarize [62]) the continuum polarization. It is also said that the lines appear, either in emission or absorption, for the same reason [50], but that the strongest lines tend to be depolarizing [57].

4. The strongest polarizing lines include the following: H I , Na I, Mg I, Ca I, Ca II (6.11 eV), Ti I, Ti II (6.83 eV), V I, V II (6.75 eV), Cr I, Mn I, Fe I, Co I, Ni I, Cu I, Sr I, Sr II (5.69 eV), Zr I, Zr II (6.63 eV), Nb II (6.76 eV), Ru I, Pb I, Ba I, and Ba II (5.21 eV) [61].§

5. The spectrum is particularly rich in molecular lines, including, most notably, lines from MgH, C_2, and CN [56,57, 63–65]. The intensity of this polarization increases towards the solar limb.

6. The spectrum contains an amazing array of lines from the Rare Earth elements: Sc II (6.56 eV), Y I, Y II (6.22 eV), La II (5.58 eV), Ce II (5.54 eV), Nd II (5.53 eV), Sm II (5.64 eV), Eu II (5.67 eV), Gd II (6.15 eV), Dy II (5.94 eV), and Yb I [61].

7. Lithium, Li, is barely detectable in the regular solar spectrum of the photosphere [70], but its doublet at 6708 Å appears at the $\sim 10^{-4}$ level in the polarized spectrum [57, 67]. This constitutes a tremendous increase in relative detectability for this element.

5.1 The second solar spectrum and the standard solar model

Adherence to the SSM brings many difficulties when studying the Second Solar Spectrum. A means must first be found to excite these atoms or molecules, such that they can later emit the required line spectrum. The only reasonable mechanism available, in the context of a gaseous Sun, involves

*The phenomenon parallels that which occurs daily with sunlight in the atmosphere of the Earth [9, 47, 52–54].

†Atomic clusters are known to be polarizable [55, p. 64–85]. Thus, it might be appropriate to consider that small hydrogen based atomic clusters might also be present in the solar chromosphere and corona.

‡The calculated, or experimentally determined, static electric dipole polarizabilities, α_D, of neutral atoms in their ground state are readily available (see e.g. [68, p. 11] and [69, § 10; 188–189]). However, these values are of limited interest for this problem, as the polarizability of the excited atoms or ions may be more appropriate to consider, but are not easily ascertained.

§The elements followed by a Roman numeral I are neutral and said to be in spectroscopic state I. Elements in the +1 oxidation state are in the second spectroscopic state (i.e. state II). The ionization energy for each element involved in producing its state II ion is provided in brackets [69, § 10;197–198].

direct excitation through photon absorption and subsequent re-emission. Thus, a random process is invoked. Chemical reactions are never considered, despite the fact that the chemically similar Rare Earth elements produce prominent signals. Furthermore, all ionic strongly polarizing lines present were produced by the removal of a single electron from atoms, requiring ~6 eV of energy, as can be ascertained by examining the ionization potentials listed in 4 and 6 above.

In the SSM, a polarization mechanism must also be advanced, namely anisotropic radiation. Thus, in order to polarize the emitting species, proponents of the SSM must also have recourse to anisotropic light as follows [57]:

> *"The polarization arises because the incident radiation, being anisotropic, induces a net dipole moment in the scattering particle. If the particle does not suffer a collision before it re-radiates, the phase relations between the vector components of the dipole moment ... are preserved and become imprinted on the scattered radiation."*

Such arguments bring further complications, as a cause for anisotropic radiation in the atmosphere of a fully gaseous Sun must now also be advanced. In the end, the center-to-limb variation (CLV) in solar intensity is adopted, to account for the anisotropic light [49, 50, 57]. However, at the level where these lines are being produced, such a mechanism is unlikely to be valid. Thus, it is also advanced that *"... local inhomogeneities on the Sun will produce scattering polarization all over the solar disk ..."* [57]. But, in the SSM, there can be no local cause of inhomogeneities. The magnetic fields, so often advanced to explain such inhomogeneities, cannot be reasonably generated in the context of a gaseous Sun [15].

Finally, since many of the lines appear to *depolarize* the continuum polarization, some means of accounting for this effect must be brought forward. In this regards, three mechanisms have been hypothesized [61]: 1) Hanle depolarization produced by random magnetic fields [57, 71], 2) collisional depolarizations produced by hydrogen atoms (see [72] and references cited therein) and 3) radiation transfer effects (see [72] and references cited therein). Consequently, magnetic fields must be applied in the SSM, both to produce the anisotropic light required for polarization and as a means of depolarization. At the same time, collisional depolarization using the hydrogen atom contradicts one of the tenets of the gaseous Sun, namely that collisional processes are not significant in the gaseous solar atmosphere associated with the SSM: *"Collisional processes of excitation and de-excitation occur so seldom that they are of no importance"* [73, p. 10]. This is because, within this model, the chromosphere and corona exist as tremendous vacuums, essentially devoid of material and with inferred densities of less than 10^{-12} g/cm^3 (see references within [15]). While computations of collisional and radiation transfer effects might be reasonably applied to a few lines, the problem becomes daunting, when considering an entire spectrum, especially given that *"... our knowledge of the collisional rates is still very limited"* and *"... there are many physical processes that are involved in the generation and modification of the polarization"* [61].

The dilemmas faced in the context of the SSM relative to accounting for the Second Solar Spectrum has been outlined [61]:

> *"... probably one of the most important questions concerning the whole Second Solar Spectrum, that still waits for an answer, is why only particular lines, of certain elements, produce strong polarizing signals. For instance, one can wonder why some elements are particularly present with their lines in the Second Solar Spectrum, whereas other elements of comparable abundance are totally absent."*

5.2 The second solar spectrum and the LMHSM

Novel insight can be gained, with respect to the Second Solar Spectrum, if the findings are interpreted within the context of a model wherein condensed matter participates in the generation of spectroscopic lines.

5.2.1 Excitation and relaxation in the LMHSM

Contrary to the SSM which advocates that emitting species must first be excited through the interaction with light, followed by re-emission disconnected from chemical processes, the LMHSM proposes that all emission lines are inherently linked to chemical or electrical processes in the Sun [23–27]. In the corona, the interaction between free atoms or ions with condensed matter results in the production of highly ionized species, like FeXXV [23, 24], since condensed matter has the ability to maintain a higher electron affinity than a free atom. It is this affinity, not the presence of extreme temperatures, which is hypothesized to be responsible for the production of such highly ionized atoms in the corona [23, 24]. In this manner, the body of the Sun can recapture lost electrons, by stripping coronal atoms or ions and channeling the resulting harvest back down to the photosphere. Consequently, the emission lines observed in the corona are associated with the capture of electrons from free atoms or ions by condensed matter. Such processes should be exothermic in nature, hence their association with light emission [23, 24]. Electron capture is thus associated with the activation of a highly ionized species which then emits the well known coronal lines. Unlike the SSM, light need not be invoked to excite these highly ionized species. Collisional relaxation processes are not important in this region of the Sun. Any excited ion achieves the ground state through the emission of light.

As for the chromosphere, it has been viewed as the site of proton and hydrogen recapture [25–27]. The hypothesized condensation reactions take advantage of hydrogen's tremen-

dous ability to form hydrides. These are then used to deposit hydrogen atoms onto condensed hydrogen structures, CHS [25–27]. Such a model can account for the presence of both He I and He II emission lines in the chromospheric spectrum [27]. In this case, line emission becomes associated with exothermic hydrogen based condensation reactions [25–27]. Collisional processes of excited atoms or ions back to the ground state is not necessary either for further excitation or relaxation back to the ground state.

In combination, the mechanisms advanced in the corona and chromosphere act to reclaim both protons and electrons in the outer solar atmosphere and, thereby, help to maintain mass and charge balance in the LMHSM. Such means of preserving the integrity of the Sun are absent in the SSM.

As mentioned above, in order to account for the behavior of several ions in the Second Solar Spectrum, collisional depolarization mechanisms have been invoked (see [72] and references cited therein). Yet, such random processes are unlikely to be of true significance in governing the behavior of emission lines in this spectrum, as definite lineshapes must depend on repeatable processes, not chance occurrence. Moreover, the densities for the chromosphere proposed in the SSM of 10^{-12} g/cm^3 (see references within [15]), leave little room for such processes. Lineshapes are inherently linked to the environment in the vicinity of the emitter itself. It is this microenvironment which must be considered, not the presence of macroscopic phenomena, as will be addressed in the next section.

In the LMHSM, the presence of condensed matter and elevated chromospheric densities, well-beyond the densities of the Earth's atmosphere, are entirely compatible with a condensed solar photosphere. Unlike the setting proposed by the SSM, collisional processes can be invoked in the LMHSM. Such processes do not need to play any role in understanding the emission lines of the chromosphere and corona. But they can provide an important relaxation mechanism for the Fraunhofer lines, as the atoms involved in photon absorption, must relax again prior to repeating the process. It is here that collisional relaxation mechanisms can play an important function, beyond simple scattering, in the context of the LMHSM. This is because, the LMHSM does not insist that the chromosphere of the Sun possesses a density which is vacuum-like and greatly inferior to that in the Earth's atmosphere. This is another important advantage of the LMHSM over the SSM.

5.2.2 Chemical reactions and the second solar spectrum

Rather than speak of polarizing (or emission) and depolarizing (or absorption) signals, it is best to consider all the lines in the Second Solar Spectrum as inherently polarized, but with an emission phase which can either add to or subtract from the polarized continuum. Thus, lineshape becomes a question of phase, as with any other spectroscopic process.

If a species is to have a net phase, then it must be relative to a common framework. In nuclear magnetic resonance (NMR), phase is determined relative to receiver channels placed in quadrature, with respect to one another, as dictated by a master oscillator. In NMR, lineshapes reflect specific nuclear environments and populations at the local level. These same principles can guide lineshape analysis in the Sun, with phase being determined by electronic orbital orientation relative to a polarizing interface. Since emission lines are being observed, then chemical activation of the emitting species can once again be invoked, but this time within the context of coordination of the emitting species.

As noted in introduction to section 5, the Second Solar Spectrum is characterized by many powerful lines from molecules and the Rare Earth elements [74]. Rare Earth metals are actually relatively abundant in the Earth's crust [74] and they are likely to be similarly abundant in the Sun with respect to the other metals, as polarization studies suggest. These elements share a common outer electron configuration often with a single electron in an outer d-shell and two electrons in the immediately inferior s-shell. In this regard, the Lanthanide series is slowly filling the 4f-shell, while maintaining a ($6s^25d^1$) outer configuration. The latter is similar to the Group IIIB elements of scandium (Sc), Yttrium (Y), and Lanthanum (La), which have outer electronic configurations of $4s^23d^1$, $5s^24d^1$, and $6s^25d^1$, respectively. Generally speaking, atoms with a single unpaired electron are easiest to polarize.

The presence of the Rare Earth elements in the Second Solar Spectrum strongly suggests that *a similar chemical reaction is responsible for all of these lines*. It is likely that these reactions involve the condensation of hydrogen onto CHS, a process which has been inherently tied to the function of the chromosphere in the LMHSM [25–27].

Consequently, Rare Earth metal hydrides could interact with CHS in the chromosphere. Upon release of their hydrogen atom, the resulting activated Rare Earth metal would be interface polarized by the adjacent CHS with which it would remain at least partially interacting. In this way, atomic orbitals always maintain the same orientation, relative to the surface and relative to all other ions or atoms involved in similar interactions with CHS, while maintaining coordination. As a result, the relative phase of all atoms involved in such processes would be dictated by coordination with the charged interface. Upon relaxation through emission, these atoms would then be released in association with the delivery of hydrogen.

The ability to deliver hydrogen and the exact strength and nature of the associated coordination would depend on the atomic species involved. Some atoms, like He for instance, may well participate in condensation reactions [27], but given their nobel gas electronic configurations, might be difficult to polarize and might remain uncoordinated during emission. Others, like the nobel gases below helium in group VIIIA of

the periodic table, would not be expected to interact at all with hydrogen. Hence, given their inability to participate in condensation reactions, they should be devoid of neutral atom chromospheric emission lines.

Thus, within the context of the LMHSM, it is reasonable to conceive that structures comprised of condensed matter exist in the chromosphere. Such condensed hydrogen structures, CHS, could possess a surface electric charge polarizing any atom brought in its proximity through interface polarization mechanisms. Each atomic species involved in condensation reactions would have a preferred means of being coordinated with the surface, in a manner dependent on their atomic orbitals. In such a way, it is possible to explain why a given line would adopt a consistent and at times complex appearance in the Second Solar Spectrum.

Support for the idea that chemical reactions are involved can be gained by appreciating not only the prevalence of the chemically similar Rare Earth metals, but also from the fact that all of the most polarizing lines from ions arise from elements with a first ionization potential of ~ 6 eV [61]. This cannot be coincidental, but strongly supports the contention that chemistry, and not random processes, are involved.

The same is true for the presence of molecular lines. Note that the three most important molecular species observed, namely CN, MgH, and C2, all have the potential of delivering hydrogen to CHS structures, through species such as HCN, MgH_2, HC_2, and HCCH.

Note also that, at first glance, none of the elements from Group IVA, VA, VIA, and VIIA (with the exception of Pb at the bottom of group IVA), appear to participate in generating the Second Solar Spectrum. Since these atoms are increasingly electronegative towards the upper right of the periodic table, they may share a lack of ability to enter into condensation reactions that involve the delivery of a hydrogen atom.

Finally, the presence of a doublet signal from Li in the polarized spectrum provides another important clue that chemical processes are involved [57, 67]. Signals from this element are weak or non-existent in other spectra (Fraunhofer, chromospheric, or coronal), leading proponents of the SSM to advocate depletion of Li in the Sun and the stars, despite its abundance in meteors [70]. Conversely, within the LMHSM, the paucity of detectable lithium has been linked to the ability of this element to stabilize metallic hydrogen, a proposal first advanced by Zurek et al. [75]. Coordination within the solar interior, not depletion, appears to be a more reasonable answer, especially given meteoric abundances [70]. This idea is also in keeping with the proposal that atoms, which are involved in condensation reactions, can be interface polarized in the excited state prior to emission. This helps to account for the presence of lithium in the Second Solar Spectrum. It also provides powerful evidence that interface polarization, not random processes and anisotropic radiation, is responsible for the production of the Second Solar Spectrum.

6 Conclusion

The study of solar and stellar polarimetry is one of the most fascinating aspects of astronomy, as the associated observations hold a treasure of clues, relative to the structure and functioning of the Sun, the stars, and the galaxies [76, 77]. At every turn, polarization studies also add tremendous support to the concept that the Sun is comprised of condensed matter [15]. In this regard, the LMHSM provides a strong platform to account for the polarization of the K-corona, enabling polarized self-emission from an anisotropic structure. At the same time, the model elegantly unifies the K-, F-, and T-coronas into a single entity, with variable emissivity based on cooling with elevation and increasingly radial anisotropy. The idea that the chromosphere and the corona act to recapture hydrogen and electrons which have escaped from the solar body has no equivalent in the SSM [23–27].

Given the evidence, it is more reasonable to postulate that the Second Solar Spectrum results from interface polarization and associated condensation reactions, rather than calling for anisotropic radiation, Hanle depolarization, and collisional depolarization.

Ample proof exists that the Second Solar Spectrum is inherently tied to chemistry, as the presence of Rare Earth elements, relevant ionization potentials, molecular lines, and phase sensitive lineshapes suggest. In the end, the Second Solar Spectrum is perhaps the most significant of all spectroscopic signals obtained from the Sun, as in its lines, the scientist can find compelling evidence for the presence of chemical reactions within the solar atmosphere.

Dedication

This work is dedicated to our friend, Larissa Borissova.

Submitted on: May 1, 2015 / Accepted on: May 11, 2015
First published online on: May 13, 2015

References

1. Kirchhoff G.R. Über das Verhältnis zwischen dem Emissionsvermögen und dem Absorptionsvermogen. der Körper fur Wärme und Licht. *Poggendorfs Annalen der Physik und Chemie*, 1860, v. 109, 275–301. (English translation by F. Guthrie: Kirchhoff G. On the relation between the radiating and the absorbing powers of different bodies for light and heat. *Phil. Mag.*, 1860, ser. 4, v. 20, 1–21; also found in Harper's Scientific Memoirs, edited by J. S. Ames: The Laws of Radiation and Absorption: Memoirs of Prévost, Stewart, Kirchhoff, and Kirchhoff and Bunsen, translated and edited by D. B. Brace, American Book Company, New York, 1901, 74–97, also available online).
2. Robitaille P.-M. and Crothers S.J. "The Theory of Heat Radiation" revisited: A commentary on the validity of Kirchhoff's law of thermal emission and Max Planck's claim of universality. *Progr. Phys.*, 2015, v. 11, no. 2, 120–132.
3. Robitaille P.-M. Blackbody radiation and the carbon particle. *Progr. Phys.*, 2008, v. 3, 36–55.
4. Robitaille P.-M. Kirchhoff's Law of thermal emission: 150 Years. *Progr. Phys.*, 2009, v. 4, 3–13.
5. Stewart B. An account of some experiments on radiant heat, involving an extension of Prévost's theory of exchanges. *Trans. Royal Soc.*

Edinburgh, 1858, v. 22, no. 1, 1–20 (also found in Harper's Scientific Memoirs, edited by J. S. Ames: The Laws of Radiation and Absorption: Memoirs of Prévost, Stewart, Kirchhoff, and Kirchhoff and Bunsen, translated and edited by D. B. Brace, American Book Company, New York, 1901, 21–50).

6. Wood R.W. Physical Optics (2nd Edition), The MacMillan Company, New York, N.Y., 1911.
7. Tait P.G. Sketch of Thermodynamics, Edmonston and Douglas, Edinburgh, 1868.
8. Feofilov P.P. The Physical Basis of Polarized Emission. Consultants Bureau, New York, N.Y., 1961.
9. Können G.P. Polarized Light in Nature (Translated by G.A. Beerling), Cambridge University Press, Cambridge, U.K., 1985.
10. Öhman Y. Polarized thermal emission from narrow tungsten filaments. *Nature*, 1961, v. 192, 254.
11. Bimonte G., Cappellin L., Carugno G., Ruoso G., Saadeh D. Polarized thermal emission by thin metal wires. *New J. Phys.*, 2009, v. 11, 033014.
12. Golyk V.A., Krüger M., Kardar M. Heat radiation from long cylindrical objects. *Phys. Rev. E*, 2012, v. 85, 046603.
13. Li P., Jiang K., Liu M., Li Q., Fan S. and Sun J. Polarized incandescent light emission from carbon nanotubes. *Appl. Phys. Lett.*, 2003, v. 82, 1763.
14. Singer S.B, Mecklenburg M., White E.R., and Regan B.C. Polarized light emission from individual incandescent carbon nanotubes. *Phys. Rev. B*, 2011, v. 83, 233404.
15. Robitaille P.-M. Forty lines of evidence for condensed matter – The Sun on trial: Liquid metallic hydrogen as a solar building block. *Progr. Phys.*, 2013, v. 4, 90–142.
16. Golub L. and Pasachoff J.M. The Solar Corona, Cambridge University Press, Cambridge, U.K., 1997.
17. Schuster A. On the polarization of the solar corona. *Mon. Not. Roy. Astron. Soc.*, 1879, v. 40, 35–56.
18. Young R.K. Polarization of the light in the solar corona. *Lick Observatory Bulletin*, 1910–1911, v. 6, no. 205, 166-181; summary in: *Publ. Astron. Soc. Pacific*, 1912, v. 24, no. 141, 123–125.
19. Lyot B. La couronne solaire étudiée en dehors des éclipses. *Comptes Rendus*, 1930, v. 191, 834–837.
20. Minnaert M. On the continuous spectrum of the corona and its polarisation. *Zeitschrift für Astrophysik*, 1930, v. 1, 209–236.
21. Dick S. Sky and Ocean Joined: The U.S. Naval Observatory 1830–2000. Cambridge University Press, Cambridge, 2003, p. 196–205.
22. Robitaille P.M. The Liquid Metallic Hydrogen Model of the Sun and the Solar Atmosphere II. Continuous Emission and Condensed Matter Within the Corona. *Progr. Phys.*, 2013, v. 3, L8–L10.
23. Robitaille P.M. The Liquid Metallic Hydrogen Model of the Sun and the Solar Atmosphere V. On the Nature of the Corona. *Progr. Phys.*, 2013, v. 3, L22–L25.
24. Robitaille P.M. The Liquid Metallic Hydrogen Model of the Sun and the Solar Atmosphere VII. Further Insights into the Chromosphere and Corona. *Progr. Phys.*, 2013, v. 3, L30–L36.
25. Robitaille P.M. The Liquid Metallic Hydrogen Model of the Sun and the Solar Atmosphere I. Continuous Emission and Condensed Matter Within the Chromosphere. *Progr. Phys.*, 2013, v. 3, L5–L7.
26. Robitaille P.M.The Liquid Metallic Hydrogen Model of the Sun and the Solar Atmosphere IV. On the Nature of the Chromosphere. *Progr. Phys.*, 2013, v. 3, L15–L21.
27. Robitaille P.M. The Liquid Metallic Hydrogen Model of the Sun and the Solar Atmosphere VI. Helium in the Chromosphere. *Progr. Phys.*, 2013, v. 3, L26–L29.
28. Hirsch J.E. Ferromagnetism in metallic hydrogen. *Phys. Letters A*, 1989, v. 141, 191–195.
29. Ichimaru S. Statistical Plasma Physics – Volume II: Condensed Plasmas, Addison-Westly, Redwood, CA, 1991 (reprinted by Westview Press, Boulder, CO, 2004).
30. Ichimaru S. and Kitamura H. Pycnonuclear reactions in dense astrophysical and fusion plasmas. *Phys. Plasmas*, 1999, v. 6, no. 7, 2649–2671.
31. Ichimaru S. Radiative proton-capture of high-Z nuclei in the sun and in liquid metallic hydrogen. *Phys. Letters A*, 2000, v. 266, 167–172.
32. van de Hulst H.C. The electron density of the solar corona. *Bull. Astron. Soc. Netherlands*, 1950, v. 11, no. 410, 135–149.
33. van de Hulst H.C. On the polar rays of the corona. *Bull. Astron. Soc. Netherlands*, 1950, v. 11, no. 410, 150–159.
34. Schmidt M. Brightness, polarization and electron density of streamers in the solar corona. *Bull. Astron. Soc. Netherlands*, 1953, v. 12, no. 447, 61–67.
35. Hayes A.P., Vorlidas A. and Howard R.A. Deriving the electron density of the solar corona from the inversion of total brightness measurements. *Astrophys. J.*, 2001, v. 548, 1081–1086.
36. Zirin H. The Solar Atmosphere. Blaisdell Publishing Company, Waltham, M.A., 1966.
37. Mukai T., Yamamoto T., Hasegawa H., Fujiwara A. and Koike C. On circumsolar grain materials. *Publ. Astron. Soc. Japan*, 1974, v. 26, 445–458.
38. Allen C.W. The spectrum of the corona at the eclipse of 1940 October1. *Mon. Not. Roy. Astron. Soc.*, 1946, v. 106, 137–150.
39. Phillips K.J.H, Feldman U. and Landi E. Ultraviolet and X-Ray Spectroscopy of the Solar Atmosphere. Cambridge University Press, Cambridge (U.K.), 2008.
40. Chandrasekhar S. Radiative Transfer. Dover Publications, Inc., New York, N.Y., 1960.
41. Chandrasekhar S. On the radiative equilibrium of a stellar atmosphere X. *Astrophys. J.*, 1946, v. 103, 351–370.
42. Sobolev V.V. A Treatise on Radiative Transfer (Translated by S.I. Gaposchkin), D. Van Nostrand Company, Inc., Princeton, N.J. 1963.
43. Dolginov A.Z., Gnedin Yu.N., and Silant'ev N.A. Propagation and Polarization of Radiation in Cosmic Media. Gordon and Breach Publishers, Basel, Switzerland, 1995.
44. Eddington A.S. The Internal Constitution of the Stars. Cambridge University Press, Cambridge, U.K., 1926.
45. Reddish V.C. The Physics of Stellar Interiors: An Introduction. Edinburgh University Press, Edinburgh, U.K., 1974.
46. Kippenhahn R. and Weigert A. Stellar Structure and Evolution. Springer-Verlag, Berlin, 1990.
47. Jenkins F.A. and White H.E. Fundamentals of Optics (4th Edition), McGraw-Hill, Inc, New York, 1976.
48. Planck M. The theory of heat radiation. P. Blakiston's Son & Co., Philadelphia, PA, 1914, http://gutenberg.org/ebooks/40030.
49. Fluri D.M. and Stenflo J.O. Continuum polarization in the solar spectrum. *Astron. Astrophys.*, 1999, v. 341, 902–911.
50. Stenflo J.O. Polarization of the Sun's continuous spectrum. *Astron. Astrophys.*, 2005, v. 429, 713–730.
51. van de Hulst H.C. Light Scattering by Small Particles, Dover Publications, New York, 1957.
52. Tenquist D.W., Whittle R.M., and Yarwood J. University Optics, Vol. II, Gordon and Breach Science Publishers, New York, 1970, p. 96–97.
53. Smith G.S. The polarization of skylight: An example from nature. *Am. J. Phys.*, 2007, v. 75, no. 1, 25–35.

54. Liu Y. and Voss K. Polarized radiance distribution measurement of skylight II. Experiment and data. *Applied Optics*, 1997, v. 36, no. 33, 8753–8764.
55. Bonin K.D. and Kresin V.V. Electric-Dipole Polarizabilities of Atoms, Molecules, and Clusters. World Scientific, Singapore, 1997.
56. Stenflo J.O. and Keller C.U. New window for spectroscopy. *Nature*, 1996, v. 382, 588.
57. Stenflo J.O. and Keller C.U. The Second Solar Spectrum: A new window for diagnostics of the Sun. *Astron. Astrophys.*, 1997, v. 321, 927–934.
58. Gandorfer A. A high resolution atlas of the Second Solar Spectrum.*APS Conference Series*, 2001, v. 236, 109–116.
59. Gandorfer A. The Second Solar Spectrum: A High Spectral Resolution Polarimetric Survey of Scattering Polarization at the Solar Limb in Graphical Representation, Vol. I: 4625Å to 6995Å, Hochschulverlag, AG an der ETH Zurich, 2000; Gandorfer A. The Second Solar Spectrum: A High Spectral Resolution Polarimetric Survey of Scattering Polarization at the Solar Limb in Graphical Representation, Vol. II: 3910Å to 4630Å, Hochschulverlag, AG an der ETH Zurich, 2002; Gandorfer A. The Second Solar Spectrum: A High Spectral Resolution Polarimetric Survey of Scattering Polarization at the Solar Limb in Graphical Representation, Vol. III: 3160Å to 3915Å, Hochschulverlag, AG an der ETH Zurich, 2005.
60. Nagendra K.N. and Stenflo J.O. Solar Polarization, Kluwer Academic Publishers, Dordrecht, Germany, 1999.
61. Belluzzi L. and Landi Degl'Innocenti E. A spectroscopic analysis of the most polarizing atomic lines in the Second Solar Spectrum. *Astron. Astrophys.*, 2009, v. 495, 577–586.
62. Fluri D.M. and Stenflo J.O. Depolarizing lines in the Sun's spectrum. *Astron. Astrophys.*, 2003, v. 398, 763–773.
63. Milić I. and Faurobert M. Modeling scattering polarization in molecular solar lines in spherical geometry. *Astron. Astrophys.*, 2012, v. 539, A10.
64. Landi Degl'Innocenti E. Polarization properties of resonance scattering in molecular bands.: The intermediate (a-b) coupling regime. *Astron. Astrophys.*, 2007, v. 461, 1–10.
65. Ramos A.A. and Bueno J.T. Evidence for collisional depolarization in MgH lines of the Second Solar Spectrum. *Astrophys. J.*, v. 635, L109–L112.
66. Manso Sainz R., Landi Degl'Innocenti E., and Bueno J.T. A qualitative interpretation of the Second Solar Spectrum of Ce II. *Astron. Astrophys.*, 2006, v. 447, 1125–1129.
67. Belluzzi L., Landi Degl'Innocenti E., and Bueno J.T. The physical origin and the diagnostic potential of the scattering polarization in the Li I resonance doublet at 6708Å. *Astrophys. J.*, 2009, v. 705, 218–225.
68. Maroulis G. Atoms, Molecules and Clusters in Electric Fields: Theoretical Approaches to the Calculation of Electric Polarizability. Imperial College Press, London, U.K., 2006.
69. CRC Handbook of Chemistry and Physics, 95th Edition (Internet Edition, W.M. Haynes, T.J. Bruno, D.R. Lide, Eds), Boca Raton, Fl, 2014–2015.
70. Robitaille P.M. Commentary on the Liquid Metallic Hydrogen Model of the Sun III. Insight into Solar Lithium Abundances. *Progr. Phys.*, 2013, v. 2, L12–L13.
71. Stenflo J.O. Limitations and Opportunities for diagnostics of solar and stellar magnetic fields in "Magnetic Fields across the Hertzsprung-Russell Diagram" (G. Mathys, S.K. Solanki, and D.T. Wickramasinghe, Eds.), APS Conference Series, 2001, v. 248, 639–650.
72. Derouich M., Sahal-Bréchot S. and Barklem P.S. Collisional depolarization and transfer rates of spectral lines by atomic hydrogen. IV. Application to ionized ions. *Astron. Astrophys.*, 2004, v. 426, 707–715.
73. Athay R.G. Radiation Transport in Spectral Lines. D. Reidel Publishing Company, Dordrocht, Hollarnd, 1972.
74. Barrett S.D. and Dhesi S.S. The Structure of Rare-Earth Metal Surfaces, Imperial College Press, London, 2001.
75. Zurek E., Hoffmann R., Ashcroft N.W., Oganov A.R., Lyakhov A.O. A little bit of lithium does a lot for hydrogen. *Proc. Nat. Acad. Sci. USA*, 2009, v. 106, no. 42, 17640–17643.
76. Clarke D. Stellar Polarimetry. Wiley-VCH Verlag GmbH & Co., Weinheim, Germany, 2010.
77. Dufay J. Galactic Nebulae and Interstellar Matter. Dover Publications, Inc., N.Y., N.Y., 1968.

LETTERS TO PROGRESS IN PHYSICS

Unmatter Plasma Discovered

Florentin Smarandache
University of New Mexico, Gallup, NM 87301, USA
E-mail: smarand@unm.edu

The electron-positron beam plasma was generated in the laboratory in the beginning of 2015. This experimental fact shows that unmatter, a new form of matter that is formed by matter and antimatter bind together (mathematically predicted a decade ago) really exists. That is the electron-positron plasma experiment of 2015 is the experimentum crucis verifying the mathematically predicted unmatter.

Unmmatter Plasma is a novel form of plasma, exclusively made of matter and its antimatter counterpart. It was first generated in the 2015 experiment [1, 2] based on the 2004 considerations [3].

There are four fundamental states of matter: solid, liquid, gas, and plasma. Plasma consists of positive ions and free electrons (negative particles), typically at low pressures, and it is overall almost neutral. Plasma is an ionized gas (as in fluorescent neon, in lightning, in stars, in nuclear reactors). An ion is a positive or negative charged particle. A positive ion is called cation, while a negative ion is called anion. If the ion is an atom, then it may contain less electrons than needed for being neutrally charged (hence one has a cation), or more electrons than needed for being neutrally charged (hence one has an anion). Similarly if the ion is a molecule or a group (of atoms or molecules). The process of forming ions is called ionization. The degree of ionization depends on the proportion of atoms that have lost or gained electrons. By applying a strong electromagnetic field to a gas, or by heating a gas, one obtains plasma.

Unmatter as theoretically predicted in the framework of the neutrosophic logic and statistics [4–6] is considered as a combination of matter and antimatter that bound together, or a long-range mixture of matter and antimatter forming a weakly-coupled phase. For example, the electron-positron pair is a type of unmatter. We coined the word *unmatter* that means neither matter nor antimatter, but something in between. Besides matter and antimatter there may exist unmatter (as a new form of matter) in accordance with the neutrosophy theory that between an entity and its opposite there exist intermediate entities.

The 2015 experiment [1, 2] on matter-antimatter plasma (*unmatter plasma*, in terms of the neutrosophic logic and statistics) was recently successful in the Astra Gemini laser facility of the Rutherford Appleton Laboratory in Oxford, United Kingdom. The 2015 experiment has produced electron-positron plasma. The positron is the antimatter of the electron, having an opposite charge of the electron, but the other properties are the same.

Also, the meson is a clear example of unmatter whose configuration includes a pair quark-antiquark. Unmatter is mostly expected to emerge in exotic states outside the boundaries of the Standard Model for particle physics (for example in the Dark Matter sector) and in the regime of high-energy astrophysical objects [7].

"It is definitely a jet of unmatter, because a plasma consisting of the electrons and the positrons is neither matter nor antimatter in the same time. This experiment is the truly verification of unmatter as the theoretical achievements of neutrosophic logic and statistics. This experiment is a milestone of both experimental physics and pure mathematics" [8].

Submitted on May 24, 2015 / Accepted on May 26, 2015

References

1. Sarri G., Poder K., Cole J., et al. Generation of neutral and high-density electron–positron pair plasmas in the laboratory. *Nature Communications*, 23 April 2015, 6:6747.
2. Feuerstein B. A matter-antimatter plasma. *Innovations Report*, 4 May 2015. Accessed from http://www.innovations-report.com/html/reports/physics-astronomy/a-matter-antimatter-plasma.html
3. Surko C.M. and Greaves R.G. Emerging science and technology of antimatter plasmas and trap-based beams. *Physics of Plasmas*, 2004, v.11, no. 5, 2333–2348.
4. Smarandache F. A new form of matter — unmatter, formed by particles and anti-particles. *Bull. of Pure and Appl. Sciences*, 2004, v. 23D, no. 2, 173–177.
5. Smarandache F. Matter, antimatter and unmatter. *Infinite Energy*, 2005, v.11, issue 62, 50–51.
6. Smarandache F. A new form of matter — unmatter, formed by particles and anti-particles. CERN CDS, EXT-2004-182, 2004.
7. Goldfain E. Private communication with the author. May, 2015.
8. Rabounski D. Private communication with the author. May, 2015.

Unexplained Oscillations in Deflection Angle Fluctuations of a Novel Type of Torsion Balance

Felix Scholkmann[1] and Alexander F. Pugach[2]

[1]Bellariarain 10, 8038 Zürich, Switzerland
[2]Main Astronomical Observatory of National Academy of Sciences, 27 Akademika Zabolotnoho St., 03680 Kiev, Ukraine
E-mails: felix.scholkmann@gmail.com, pugach@yandex.ru

For more than four years, fluctuations in the deflection angle $\theta(t)$ of novel type of torsion balance have been monitored at the Main Astronomical Observatory of National Academy of Sciences in Kiev, Ukraine. During this all-year recording, unpredictable spontaneous high-frequency oscillations were observed occasionally. The aim of the present paper was to investigate four of these high-frequency oscillatory events by performing a detailed time-frequency analysis. From the overall available $\theta(t)$ signal, we selected four 24-hour long segments containing a clearly visible oscillations observed on 20 and 21 November 2009 (data segments 1 and 2) and on 24 and 25 December 2012 (data segments 3 and 4). High-resolution time-frequency analysis was performed for each of the four data segments using the generalized S-transform with a hyperbolic window. The oscillation of $\theta(t)$ present in data segment 1 shows clearly an increase in frequency, starting at 0.0002205 Hz (period length $T = 75.59$ min) and ending at 0.0002325 Hz ($T = 71.68$ min). The oscillation of $\theta(t)$ present in data segment 2 has instead a stable frequency of $f = 0.000243$ Hz ($T = 68.59$ min). Both high frequency oscillations of $\theta(t)$ of data segment 3 and 4 show an increase in frequency, starting at 0.006179 Hz ($T = 161.84$ s) and ending at 0.006859 Hz ($T = 145.79$ s) for data segment 3, and starting at 0.005379 Hz ($T = 185.91$ s) and ending at 0.005939 Hz ($T = 168.38$ s) for data segment 4, respectively. In addition, the oscillation present in data segment 3 is periodically amplitude-modulated with a period length of $T = 57 \pm 4.2$ min. Regarding the origin of the observed high frequency oscillation we discuss possible technical or natural factors that could be related to these oscillations.

1 Introduction

At the Main Astronomical Observatory of National Academy of Sciences in Kiev, Ukraine, a high-sensitive torsion balance with a new design (termed "torsind", refering to the device's function as a *tors*ion *ind*icator) has been quasi-continuously measuring fluctuations of its angular deflection since 2009.

The specific design of the device (i.e. replacement of the linear light beam by a light disc of non-magnetic material and the free suspension of the disk with a specific type of monofilament) makes it insensitive to changes in the gravitational potential so that gravitational (tidal) influences from any directions are excluded in the measurements. In addition, since the device is sealed into a container, variations of temperature, pressure, humidity and environmental electric field strength do not influence the reading [1]. Also changes in the excitation of the ionosphere over the place of observation were shown not to influence the measured values of the device [1].

Based on the long-term measurement of the tosind's disc rotations, different types of non-random fluctuations in the time-dependent deflection angle $\theta(t)$ were observed.

The main oscillatory component in the variability is an (amplitude-modulated) diurnal oscillation (i.e. an increase in d/dt($\theta(t)$) at sunrise, a decrease at sunset and a maximum deflection at noon) [1, 2], having a period length of 1440.24 ± 2.60 min [2], indicating that it is related to solar and not sidereal time (length of sidereal day: 1436 min, solar day: 1440 min). Such a diurnal oscillation was also observed in other experiments where torsion or vertical pendulums were used [3–6].

The fluctuations of $\theta(t)$ measured by the torsind seem also to be related to cosmophysical processes and events since significant changes in $\theta(t)$ were observed during solar and lunar eclipses [1, 7–9], the transit of Venus across the Sun's disk [1], and even specific astronomical configurations [10]. Remarkably, it was observed that the torsind responds to a solar eclipse occurring on the opposite side of the globe [7, 10] or when the measurement is performed underground at a depth of 40 meters [8].

During the all-long recording as a whole, unpredictable spontaneous high-frequency (period length: $T < 24$ h) oscillations were observed occasionally.

The aim of the present paper was to investigate four of these high-frequency oscillatory events by performing a detailed time-frequency analysis.

The motivation to perform this kind of analysis was based on the first author's (FS) previous work on the analysis of unexplained oscillations in electrochemical reactions [11] and diffusion processes [12, 13].

2 Materials and Methods

2.1 Measurement Setup

As described in detail in [1], the torsind device resembles a classical torsion balance but has a very light aluminium disc (diameter: 120 mm, weight: approx. 100 mg) instead of a linear beam. The disc is suspended by a monofilament (diameter: 20 μm) made from natural silk, which has the advantage of not having a reverse torque when twisted. The disc rotation is monitored by a webcam and the image live-stream is processed automatically by custom-made software that determines the angular deflection θ every minute with a standard error of each measurement of $\pm$ 0.157° (determined under stable space weather conditions on 13 February 2013) [2].

The device is housed in a quartz glass cylinder (having a high of 240 mm and a wall thickness of 2 mm) with two round glass plates covering the top and bottom. Various efforts were made to isolate the torsind device from environmental changes [1]. To reduce electrostatic influences, the inner wall and the bottom of the glass cylinder are surrounded by a grounded aluminium foil. To ensure that environmental changes in humidity and pressure are not influencing the device, the edges of the quartz-glass housing are sealed with a silicon joint sealant material. The sealing also improves the thermal stabilization.

Measurements were made with the torsind in isolated, shaded room with tightly closed doors and windows at the Main Astronomical Observatory of National Academy of Sciences in Kiev. The place of measurement was selected to ensure that no technical electrical or mechanical processes were happening within a radius of 50 m that could influence the measurement (i.e. no electrical devices, no electromagnetic wireless data-transfer devices, no devices that cause mechanical vibrations).

Concerning the sensitivity of the torsind to detect (extremely) weak forces, the torque (M) of the minimal acceleration value that could be recorded by the device was estimated to be $M \approx 6.5 \times 10^{-12}$ Nm) [1].

2.2 Data

For the analysis presented in this paper, we selected four 24-hour-long signal segments from the overall available signal that contain a clearly visible oscillation. Two of the data segments show a long-lasting fast oscillation with multiple maxima during the 24-hour interval (recording dates: 20 November 2009 [data segment 1], 21 November 2009 [data segment 2]). The other two segments contain a brief, very fast oscillation (recording dates: 24 December 2012 [data segment 3], 25 December 2012 [data segment 4]). Thus, the two distinct oscillatory phenomena investigated in the present study occurred in November 2009 and December 2012. All signals were recorded with respect to Universal Time (UT1) which is the same everywhere on Earth due to its proportionality to the Earth's rotation angle with respect to the International Celestial Reference Frame.

2.3 Time-Frequency Analysis

High-resolution time-frequency analysis was performed for each of the four data segments, applying a specific type of Stockwell (S)-transform, the generalized S-transform (GST) with a hyperbolic window according to the approach developed by Pinnegar and Mansinha [14].

3 Results

3.1 Data Segments 1 and 2

Data segments 1 and 2 contain both a clearly visible oscillation of $\theta(t)$ (see subfigures a1–3 of Fig. 1).

The oscillation of $\theta(t)$ present in data segment 1 clearly shows a frequency increase, starting at 0.0002205 Hz (T = 75.59 min) and ending at 0.0002325 Hz (T = 71.68 min) (see subfigures b1 and c1 of Fig. 1). This is not the case for the oscillation of $\theta(t)$ present in data segment 2 which exhibits a stable frequency of f = 0.000243 Hz (T = 68.59 min) (see subfigures b2 and c2 of Fig. 1).

Subfigures b3 and c3 of Fig. 1 show the time-frequency spectrum of the combined signal (data segment 1 + data segment 2) with the increasing frequency on day one (20 November 2009) and the stable frequency on day two (21 November 2009).

3.2 Data Segments 3 and 4

A very high frequency oscillation is present in data segments 3 and 4.

The high frequency oscillation in data segment 3 started at 746 min and ended at 969 min (total duration: 223 min), whereas the start of the high frequency oscillation of data segment 4 started at 347 min and ended at 549 min (total duration: 202 min) (see subfigures a1 and b1, as well as a2 and b2 of Fig. 2). Thus, both periods of high-frequency activity are of similar duration.

Both high frequency oscillations of $\theta(t)$ of data segment 3 and 4 show an increase in frequency, starting at 0.006179 Hz (T = 161.84 s) and ending at 0.006859 Hz (T = 145.79 s) for data segment 3, and starting at 0.005379 Hz (T = 185.91 s) and ending at 0.005939 Hz (T = 168.38 s) for data segment 4. What distinguishes these two oscillatory events is that the oscillation present in data segment 3 is periodically amplitude-modulated (see subfigure c1 of Fig. 2) whereas such a periodic modulation is not obvious in the oscillation of data segment 4. Three peaks in the variability of the power can be distinguished that correspond to an amplitude-modulation with a period length of $T = 57 \pm 4.2$ min.

Besides the high frequency oscillations, both data segments contain strong shifts of $\theta(t)$. For data segment 3, two significant shifts can be identified within the time frame 318-376 min ($\theta(t)_{start} = 232.5°$, $\theta(t)_{end} = 774.7°$, resulting in $\Delta\theta(t)$

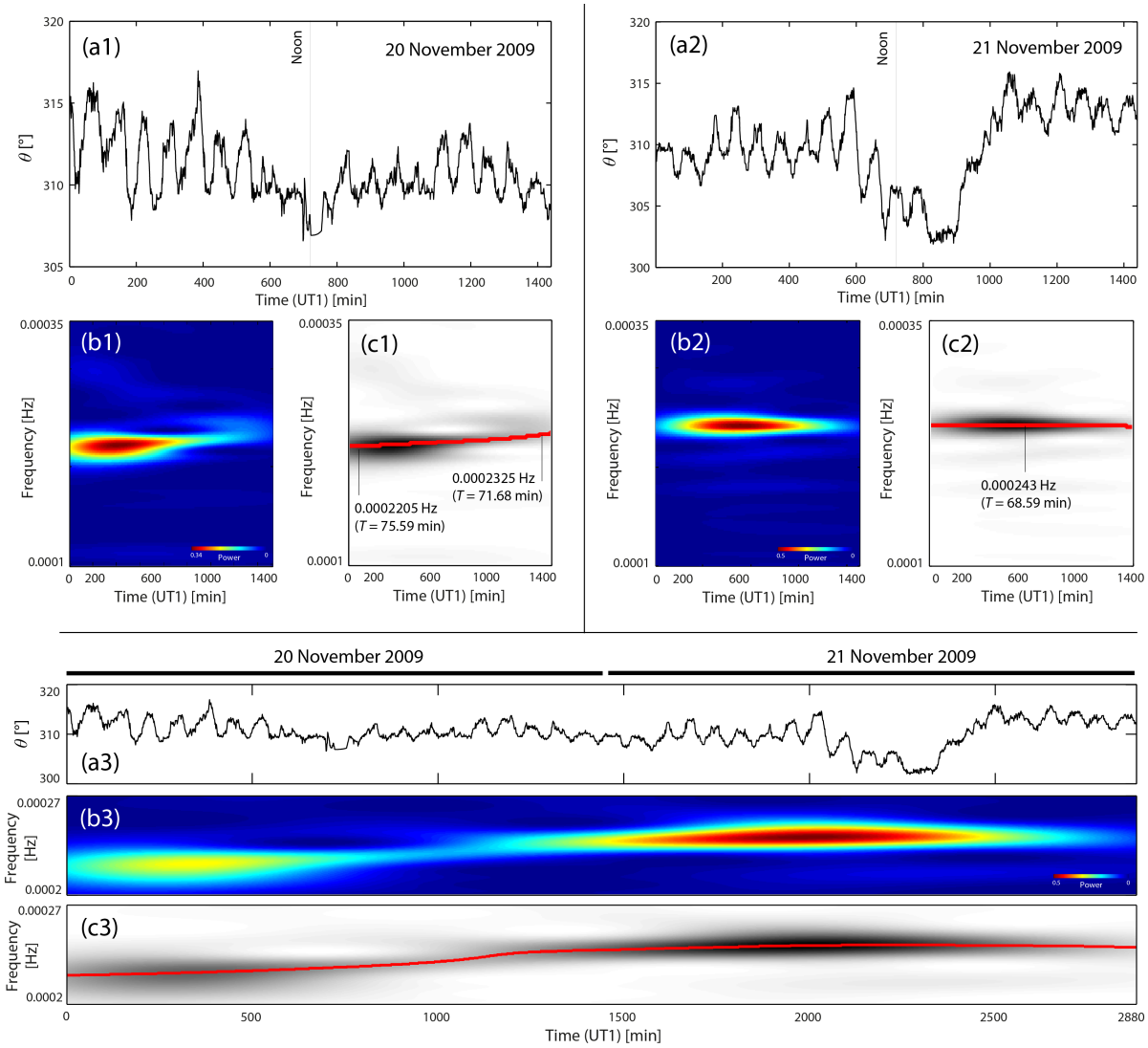

Fig. 1: (a1-a3) Time series of $\theta(t)$ recorded on 20 and 21 November 2009, as well as the stitched time series covering both dates. (b1-b3) Spectrogram showing the time-frequency changes of the oscillation. The power is color-coded. (c1-c3) Spectrogram with red line indicating the maximum power depending on frequency and time.

= 542.2°), and the time frame 1396–1402 min ($\theta(t)_{start}$ = 703.4°, $\theta(t)_{end}$ = 566.9°, resulting in $\Delta\theta(t)$ = 136.5°). In data segment 4, one strong shift is present, occurring in the time frame 1250–1273 min ($\theta(t)_{start}$ = 550.5°, $\theta(t)_{end}$ = 192.3°, $\Delta\theta(t)$ = 358.2°). These kind of shifts (also termed "spikes" [2]) correspond to moments when a strong rotational momentum is acting on the torsind.

4 Discussion and Conclusion

The analysis performed revealed that the fast variations observed in the four days of data segments exhibit oscillations with clearly defined frequencies. The fast oscillations starting at 20 and ending at 21 November 2009 are characterized by an increase in frequency. This characteristic of frequency increase is also observed in the very fast oscillations present in the data from 24 and 25 December 2012.

In the following we will briefly discuss the possibility that these oscillations could be artefacts caused by technical or natural processes, or effects from well-known factors associated with geophysical processes.

Artefacts caused by technical or natural processes. Torsion balance measurements can be generally influenced by changes in the local environmental parameters like temperature, humidity, pressure or electromagnetic fields. The influence of these factors was actively minimized during the measurement with the torsind by applying proper shielding and the effectiveness of the shielding was evaluated experimentally. For this reason, we conclude that it is unlikely that the observed oscillations are simply artifacts due to technical or

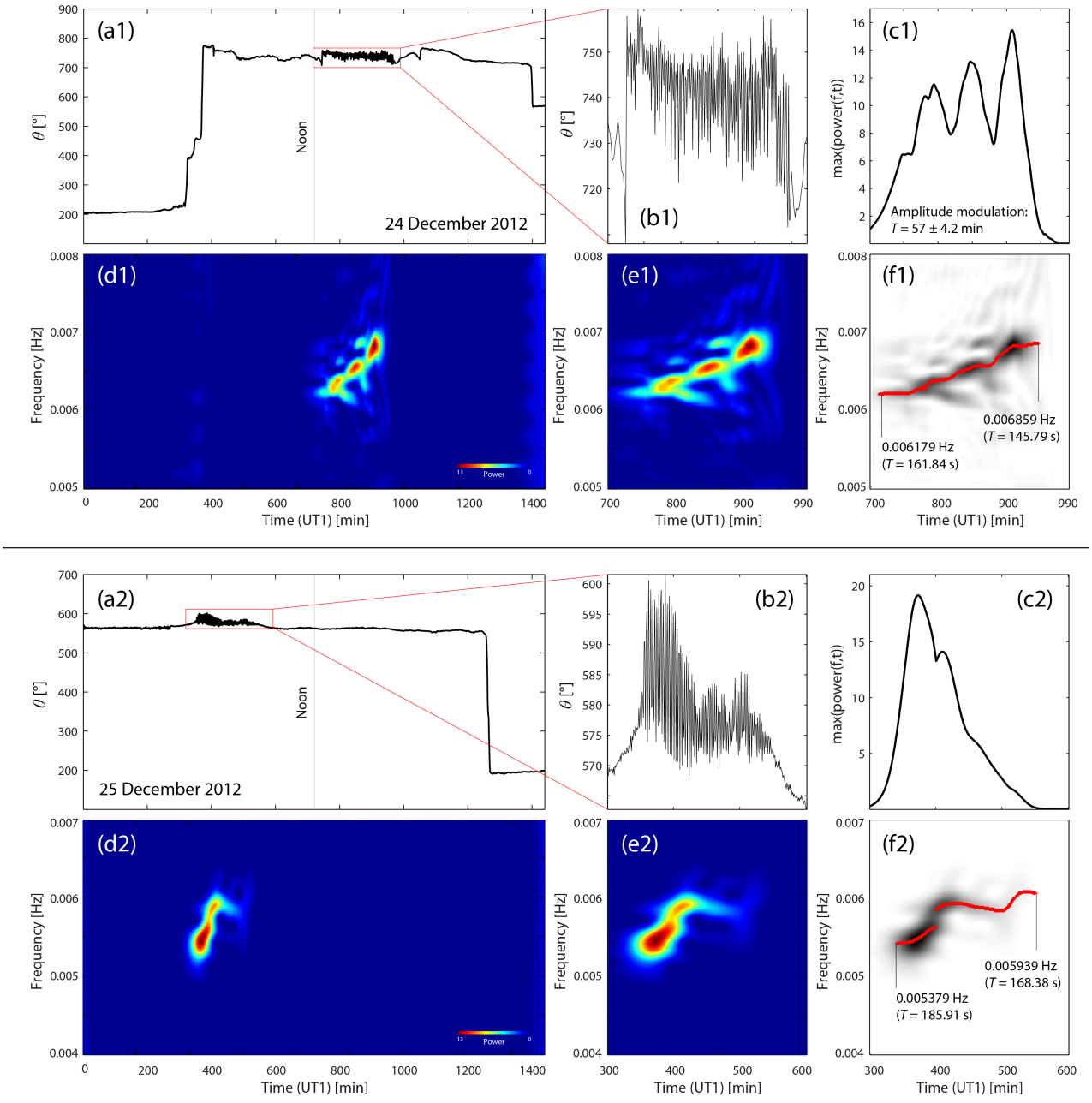

Fig. 2: (a1, a2) Time series of $\theta(t)$ recorded on 24 and 25 December 2012. (b1, b2) Zoom into the intervals with fast oscillations. (c1, c2) Time series of the maximum power depending on the frequency, showing a periodic (c1) and a unimodal (c2) amplitude modulation. (d1, d2) Spectrograms of the entire time series. The power is color-coded. (e1, e2) Spectrograms of the zoomed-in parts of the time series. (f1, f2) Spectrograms with red lines indicating the maximum power depending on frequency and time.

natural processes happening in the local environment of the measurement.

Effects from geophysical processes. What geophysical or astrophysical phenomena exhibit a frequency of approx. 0.002 Hz (as observed in data segments 1 and 2) or approx. 0.006–0.007 Hz (as observed in data segments 3 and 4)? It is known that the geomagnetic field can exhibit periodic fluctuations, termed "geomagnetic pulsations" [15, 16].

Those geomagnetic pulsations in the frequency range of 0.002–0.006 Hz ($T = 166.67 - 500$s), termed "Pc5 pulsations", overlap with the oscillation in $\theta(t)$ found in the present study. Geomagnetic pulsations are the result of solar wind disturbances (caused by increased solar activity) perturbing the magnetosphere and causing disturbances/modulations of the geomagnetic field. We checked whether there were any significant disturbances in the geomagnetic field on the dates of the data segments investigated (20–21 November 2009 and 24–25 December 2012) by analysing the hourly Dcx index (http://dcx.oulu.fi), i.e. the corrected Dst index [17, 18]. Geomagnetic disturbances are seen as negative deflections of the Dcx (and Dst) index, associated with an enhanced westward directed electric current during the geomagnetic storm. During the two periods (20–21 November 2009 and 24–25 December 2012) no geomagnetic storms or significant disturbances occurred. The observed oscillations in $\theta(t)$ can therefore to be regarded as most likely not caused by Pc5 geomagnetic pulsations.

Another principal possibility is low-frequency microseismic oscillations or "long-period seismic noise" [19]. However, it is known that in the range of 0.002–0.02 Hz microseismic activity is the lowest compared to the frequency ranges off approx. < 0.002 Hz and > 0.02 Hz [20, 21]. Also, these kinds of microseismic fluctuations in general do not exhibit the clear frequency stability and do not occur for such a long time span as observed in the $\theta(t)$ oscillations analysed in the present paper. Therefore, we believe microseismicity is unlikely to be responsible for the fast $\theta(t)$ oscillations.

Future experimental work involving measurements with the torsind and data analysis is needed to identify the mechanism causing the non-random fluctuations in $\theta(t)$ measured by the torsind device. Further data analysis is ongoing and will be reported in the near future.

Submitted on May 13, 2015 / Accepted on May 27, 2015

References

1. Pugach A. F. The torsind — A device based on a new principle for non-conventional astronomical observations. *International Journal of Astronomy and Astrophysics*, 2013, v. 3, 33–38.
2. Pugach A. F. Diurnal variations and spikes by the torsind registered and their impact on the accuracy of G measurement. *International Journal of Astronomy and Astrophysics*, v. 5 (1), 28–37.
3. Saxl E. J., Allen M. 1970 solar eclipse as "seen" by a torsion pendulum. *Physical Review D*, v. 3 (4), 823–825.
4. Neumann L., Kalenda P. Static vertical pendulum-apparatus for in-situ relative stress measurement. In F. Xie (Ed.), *Rock Stress and Earthquakes* (pp. 255–261). London: Taylor and Francis Group.
5. Bagley C. H., Luther G. G. Preliminary results of a determination of the Newtonian constant of gravitation: a test of the Kuroda hypothesis. *Physical Review Letters*, 1997, v. 78 (16), 3047–3050.
6. Stoyko N. Sur la variation jouralière de la mache des pendules et de la deviation de la verticale [On the diurnal variation of pendulum motion and of plumb line deflection]. *Comptes Rendus de l'Académie des Sciences*, 1947, v. 224 (20), 1440–1441.
7. Pugach A. F. Observations of the astronomical phenomena by torsion balance. *Physics of Consciousness and Life, Cosmology and Astrophysics*, v. 9 (2), 30–51.
8. Olenici D., Pugach A. F. Precise underground observations of the partial solar eclipse of 1 June 2011 using a Foucault pendulum and a very light torsion balance. *International Journal of Astronomy and Astrophysics*, 2012, v. 2 (4), 204–209.
9. Pugach A. F., Olenici D. Observations of correlated behavior of two light torsion balances and a paraconical pendulum in separate locations during the solar eclipse of January 26th, 2009. *Advances in Astronomy*, 2012, Article ID 263818.
10. Olenici D., Pugach A. F., Cosovanu I., Lesanu C., Deloly J.-B., Vorobyov D., Delets A., Olenici-Craciunescu S.-B. (2014). Syzygy effects studies performed simultaneously with Foucault pendulums and torsinds during the solar eclipses of 13 November 2012 and 10 May 2013. *International Journal of Astronomy and Astrophysics*, v. 4 (1), 39–53.
11. Scholkmann F., Muzuno T., Nagel D. J. Statistical analysis of unexpected daily variations in an electrochemical transmutation experiment. *Journal of Condensed Matter Nuclear Science*, 2012, v. 8 (3), 37–48.
12. Scholkmann F. Indications for a diurnal and annual variation in the anisotropy of diffusion patterns — A reanalysis of data presented by J. Dai (2014, Nat. Sci.). Progress in Physics, 2014, v. 10 (4), 232–235.
13. Scholkmann F. Solar-Time or sidereal-time dependent? The diurnal variation in the anisotropy of diffusion patterns observed by J. Dai (2014, Nat. Sci.). *Progress in Physics*, 2015, v. 11 (2), 137–138.
14. Pinnegar C. R., Mansinha L. The S-transform with windows of arbitrary and varying shape. *Geophysics*, v. 68 (1), 381–385.
15. Schott J. J., Kleimenova N. G., Bitterly J., Kozyreva O. V. The strong Pc5 geomagnetic pulsations in the initial phase of the great magnetic storm of March 24, 1991. *Earth, Planets and Space*, v. 50 (2), 101–106.
16. Saito T. Geomagnetic pulsations. *Sapce Science Reviews*, 1969, v. 10 (3), 319–412.
17. Marsular K., Karinen A. Explaining and correcting the excessive semiannual variation in the Dst index. *Geophysical Research Letters*, 2005, v. 32v. (14), L14107.
18. Karinen A., Marsula K. Correcting the Dst index: Consequences for absolute level and correlations. *Journal of Geophysical Research: Space Physics*, 2006, v. 111 (A8), A08207.
19. Tanimoto, T. Excitation of normal modes by atmospheric turbulence: source of long-period seismic noise. *Geophysical Journal International*, v. 136 (2), 395–402.
20. Nishida K., Kobayashi N., Fukao Y. Origin of Earth's ground noise from 2 to 20 mHz. *Geophysical Research Letters*, 2002, v. 29 (10), 51–54.
21. Agnew D. C., Berger J. Vertical seismic noise at very low frequencies. *Journal of Geophysical Research: Solid Earth*, 1978, v. 83 (B11), 5420–5424.

Analytical Study of the Van der Pol Equation in the Autonomous Regime

Hafeez Y. Hafeez [1], Chifu E. Ndikilar [2] and Sabo Isyaku [3]

Physics Department, Federal University Dutse, P.M.B. 7156, Jigawa State, Nigeria.
[1] Email: hafeezyusufhafeez@gmail.com
[2] Email: ebenechifu@yahoo.com
[3] Email: saboisyaku@gmail.com

The Van der Pol differential equation was constructed for an autonomous regime using link's law. The Van der Pol equation was studied analytically to determine fixed points, stability criteria, existence of limit cycles and solved numerically. The graphs of the equation are drawn for different values of damping coefficient μ.

1 Introduction

Balthazar Van der Pol (1899-1959) was a Dutch electrical engineer who initiated experimental dynamics in the laboratory during the 1920's and 1930's. He first introduced his (now famous) equation in order to describe triode oscillations in electric circuits, in 1927.

Van der Pol found stable oscillations, now known as limit cycles, in electrical circuits employing vacuum tubes. When these circuits are driven near the limit cycle they become entrained, i.e. the driving signal pulls the current along with it. The mathematical model for the system is a well known second order ordinary differential equation with cubic non linearity: the Van der Pol equation. The Van der Pol equation has a long history of being used in both the physical and biological sciences. For instance, Fitzhugh [1] and Nagumo [2] used the equation in a planer field as a model for action potential of neurons. The equation has also been utilized in seismology to model the plates in a geological fault [3].

During the first half of the twentieth century, Balthazar Van der Pol pioneered the field of radio telecommunication [4–9]. The Van der pol equation with large value of nonlinearity parameter has been studied by Cartwright and Littlewood in 1945 [10]; they showed that the singular solution exists. Also analytically, Lavinson [11] in 1949, analyzed the Van der Pol equation by substituting the cubic non linearity for piecewise linear version and showed that the equation has singular solution also. Also, the Van der Pol Equation for Nonlinear Plasma Oscillations has been studied by Hafeez and Chifu in 2014 [12]; they showed that the Van der pol equation depends on the damping co-efficient μ which has varying behaviour. In this article, the analytical study of the Van der Pol equation in the autonomous regime is studied.

2 Description of the Van der Pol oscillator

The Van der Pol oscillator is a self-maintained electrical circuit made up of an Inductor (L), a capacitor initially charged with a capacitance (C) and a non-linear resistance (R); all of them connected in series as indicated in Fig. 1 below. This oscillator was invented by Van der Pol while he was trying to find out a new way to model the oscillations of a self-maintained electrical circuit. The characteristic intensity-tension U_R of the nonlinear resistance (R) is given as:

$$U_R = -R_0\, i_0 \left[\frac{i}{i_0} - \frac{1}{3}\left(\frac{i}{i_0}\right)^3\right] \tag{1}$$

where i_0 and R_0 are the current and the resistance of the normalization respectively. This non linear resistance can be obtained by using the operational amplifier (op-amp). By applying the link's law to Fig. 1 below,

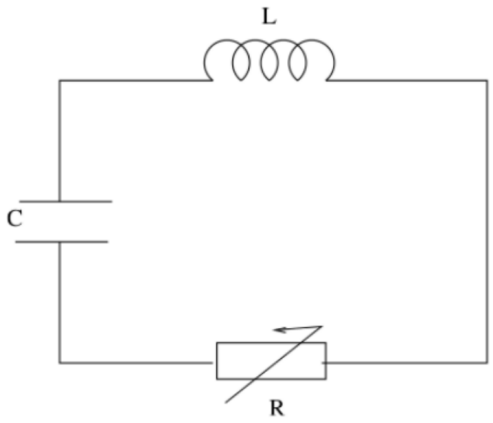

Fig. 1: Electric circuit modelizing the Van der Pol oscillator in an autonomous regime.

we have:

$$U_L + U_R + U_C = 0 \tag{2}$$

where U_L and U_C are the tension to the limits of the inductor and capacitor respectively and are defined as

$$U_L = L\frac{di}{d\tau} \tag{3}$$

$$U_C = \frac{1}{C}\int i d\tau. \tag{4}$$

Substituting (1), (3) and (4) in (2), we have:

$$L\frac{di}{d\tau} - R_0\, i_0 \left[\frac{i}{i_0} - \frac{1}{3}\left(\frac{i}{i_0}\right)^3\right] + \frac{1}{C}\int i d\tau = 0. \tag{5}$$

Differentiating (5) with respect to τ, we have

$$L\frac{d^2i}{d\tau^2} - R_0\left[1 - \frac{i^2}{i_0^2}\right]\frac{di}{d\tau} + \frac{i}{C} = 0. \tag{6}$$

Setting

$$x = \frac{i}{i_0} \tag{7}$$

and

$$t = \omega_e\tau \tag{8}$$

where $\omega_e = \frac{1}{\sqrt{LC}}$ is an electric pulsation, we have:

$$\frac{d}{d\tau} = \omega_e\frac{d}{dt} \tag{9}$$

$$\frac{d^2}{d\tau^2} = \omega_e^2\frac{d^2}{dt^2}. \tag{10}$$

Substituting (9) and (10) in (6), yields

$$\frac{d^2x}{dt^2} - R_0\sqrt{\frac{C}{L}}\left(1 - x^2\right)\frac{dx}{dt} + x = 0. \tag{11}$$

By setting $\mu = R_0\sqrt{\frac{C}{L}}$ Eq. (11) takes dimensional form as follows

$$\ddot{x} - \mu\left(1 - x^2\right)\dot{x} + x = 0 \tag{12}$$

where μ is the scalar parameter indicating the strength of the nonlinear damping, and (12) is called the Van der Pol equation in the autonomous regime.

3 Analytical study

3.1 Fixed points and stability

Transforming the higher order ODE (12) into a system of simultaneous ODE's i.e. let $x_1 = x$ and $x_2 = \dot{x}$

$$\begin{bmatrix} \dot{x_1} \\ \dot{x_2} \end{bmatrix} = \begin{bmatrix} x_2 \\ -x_1 + \mu\left(1 - x_1^2\right)x_2 \end{bmatrix}. \tag{13}$$

Introducing the standard transformation

$$y = x \tag{14}$$

$$z = \dot{x} - \mu\left(x - \frac{x^3}{3}\right) \tag{15}$$

and letting

$$F(x) = \mu\left(\frac{x^3}{3} - x\right), \tag{16}$$

now

$$\dot{y} = \dot{x}. \tag{17}$$

Using (15) we have,

$$\dot{y} = z + \mu\left(y - \frac{y^3}{3}\right) \tag{18}$$

and

$$\dot{z} = \ddot{x} - \mu\dot{x}\left(1 - x^2\right)$$

$$\dot{z} = -\mu\left(y^2 - 1\right)\dot{x} - x - \mu\left(1 - y^2\right)\dot{x} = -x = -y. \tag{19}$$

This transformation puts the equation into the form:

$$\begin{bmatrix} \dot{y} \\ \dot{z} \end{bmatrix} = \begin{bmatrix} z - \mu\left(\frac{y^3}{3} - y\right) \\ -y \end{bmatrix}. \tag{20}$$

Eq. (20) is the particular case of Lienard's Equation

$$\begin{bmatrix} \dot{y} \\ \dot{z} \end{bmatrix} = \begin{bmatrix} z - f(y) \\ -y \end{bmatrix} \tag{21}$$

where $f(y) = \mu\left(\frac{y^3}{3} - y\right)$. Linearizing (20) around the origin i.e. fixed point (0,0), we have

$$\begin{bmatrix} \dot{y} \\ \dot{z} \end{bmatrix} = \begin{bmatrix} \mu & 1 \\ -1 & 0 \end{bmatrix}\begin{bmatrix} y \\ z \end{bmatrix}. \tag{22}$$

The characteristic equation of (22) is given as

$$\lambda^2 - \mu\lambda + 1 = 0 \tag{23}$$

with eigenvalues of

$$\lambda_\pm = \frac{\mu \pm \sqrt{\mu^2 - 4}}{2} \tag{24}$$

and eigenvectors of

$$\vec{e}_+ = \begin{bmatrix} \frac{-2}{\mu - \sqrt{(\mu^2-4)}} \\ 1 \end{bmatrix}, \quad \vec{e}_- = \begin{bmatrix} \frac{-2}{\mu + \sqrt{(\mu^2-4)}} \\ 1 \end{bmatrix}. \tag{25}$$

The stability of this fixed point depends on the signs of the eigenvalues of the Jacobian matrix (22).

3.2 Existence of the limit cycles

Let us now analytically study the amplitude of the limit cycle by using the average method [13]. Considering the following transformations

$$x(t) = A(t)\cos\left(t + \varphi(t)\right) = A\cos\psi \tag{26}$$

$$\dot{x}(t) = -A(t)\sin\left(t + \varphi(t)\right) = -A\sin\psi \tag{27}$$

where $A(t)$ is the amplitude, $\varphi(t)$ being the phase and with $\psi(t) = \varphi(t) + t$. Supposing the amplitude and phase feebly vary during a period $T = 2\pi$, we have the fundamental equations of the average method as follows:

$$\dot{A}(t) = -\frac{\mu}{2\pi}\int_0^{2\pi} f(A\cos\psi, -A\sin\psi)\sin\psi\,\mathrm{d}\psi \tag{28}$$

$$\dot{\varphi}(t) = -\frac{\mu}{2\pi}\int_0^{2\pi} f(A\cos\psi, -A\sin\psi)\sin\psi\,\mathrm{d}\psi \tag{29}$$

Eqs. (28) and (29) help to determine the amplitude $A(t)$ and phase $\varphi(t)$ of the oscillator. Applying this method to (12) for which

$$f(x, \dot{x}, t) = (1 - x^2)\,\dot{x}$$

then, we have

$$f(A, \psi) = -A \sin\psi + A^3 \sin\psi \cos^2\psi. \tag{30}$$

Substituting (30) into (28) and (29), we get

$$\dot{A}(t) = -\frac{\mu}{2\pi}\int_0^{2\pi}\left(-A\sin^2\psi + A^3\sin^2\psi\cos^2\psi\right)\mathrm{d}\psi \tag{31}$$

$$\dot{\varphi}(t) = -\frac{\mu}{2\pi}\int_0^{2\pi}\left(-A\sin\psi\cos\psi + A^3\sin\psi\cos^3\psi\right)\mathrm{d}\psi. \tag{32}$$

Integration of (31) and (32) gives the evolution equation of the amplitude $A(t)$ and the phase $\varphi(t)$:

$$\dot{A}(t) = -\frac{\mu A(t)}{2}\left(1 - \frac{A^2(t)}{4}\right) \tag{33}$$

$$\dot{\varphi}(t) = 0. \tag{34}$$

The average method states that the amplitude and the phase feebly vary during a period. Therefore $\dot{A}(t) = 0$, and the amplitude is eventually $A(t) = 2$.

4 Numerical solution

The numerical solution to the Van der Pol equation for various values of μ are presented in Figs. 2 to 4.

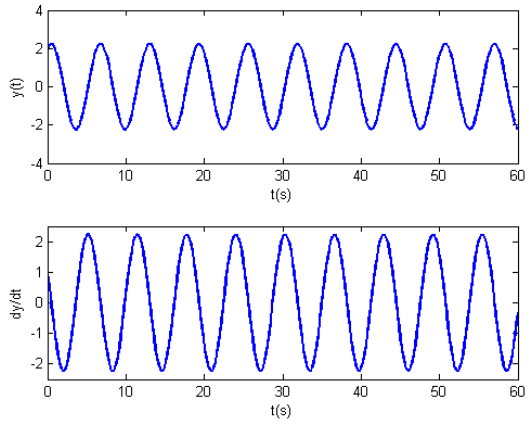

Fig. 2: Plot of $y(t)$ and dy/dt against $t(s)$ for $\mu = 0$.

5 Discussion

The classical Van der Pol equation (12) depends on the damping coefficient μ and the following varying behaviors were obtained. When $\mu < 0$, the system will be damped and the limit $\lim_{t\to\infty} \to 0$. From Fig. 2, where $\mu = 0$, there is no damping and we have a simple harmonic oscillator. From Figs. 3 and 4, where $\mu \geq 0$, the system will enter a limit cycle, with continuous energy to be conserved. The wave generated by this oscillator is periodic with sinusoidal form for $\mu \ll 1$ and relaxation for large value of μ [14] with fix amplitude equal to 2. Also when $-\infty < \mu \leq 0$ and $\lambda_\pm$ is $\mathrm{Re}(\lambda_\pm) < 0$, the point is stable; if $\mu = 0$ and $\lambda_\pm = \pm i$, the point is marginally stable and unstable; if $0 \leq \mu < \infty$ and $\lambda_\pm$ is $\mathrm{Re}(\lambda_\pm) > 0$, the origin is unstable. If $0 \leq \mu \leq 2$ and $\lambda_\pm$ is $\mathrm{Im}(\lambda_\pm) \neq 0$, then the fixed point (0,0) is an unstable center. If $2 < \mu < \infty$ and $\lambda_\pm$ is $\mathrm{Im}(\lambda_\pm) = 0$, then the fixed point (0,0) is still unstable.

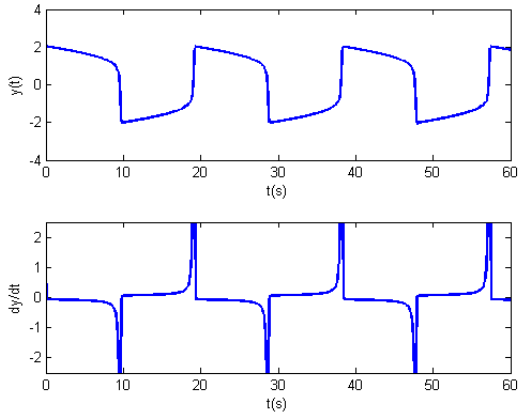

Fig. 3: Plot of $y(t)$ and dy/dt against $t(s)$ for $\mu = 10$.

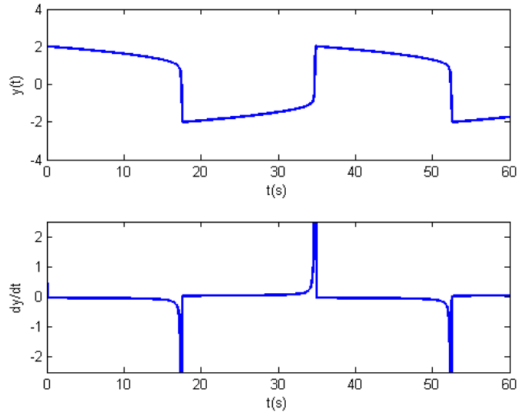

Fig. 4: Plot of $y(t)$ and dy/dt against $t(s)$ for $\mu = 20$.

6 Conclusion

In the above analysis, a class of analytical study of the Van der Pol equation in the autonomous regime is presented. Analytically, we conclude that the fixed point (0,0) is unstable whatever the value of the damping coefficient μ and the system enters a limit cycle with amplitude $A(t)$ of the Van der Pol oscillator limit cycle equal to 2. We showed that there exists a unique limit cycle.

Acknowledgement

The authors wish to thank Prof. J. Chabi Orou of African University of Science and Technology, Abuja for his time, useful discussions and help in the analytical study of this problem.

Submitted on April 19, 2015 / Accepted on May 11, 2015

References

1. Fitzhugh R. Impulse and physiological state in theoretical models of nerve membranes. *Biophys. J.*, 1961, v. 1, 444–466.
2. Nagumo J., Arimoto, S., and Yoshizawa S. An active pulse transmission line simulating nerve axons. *Proc. IRL*, 1960, v. 50, 2061–2070.
3. Cartwright J., Eguiluz V., Hernendez-Garcia E. and Piro O. Dynamic of elastic excitable media. *Internat. J. Bifur. Chaos Appl. Sci. Eng.*, 1999, v. 9, 2197–2202.
4. Cartwright M. L. Balthazar Van der Pol. *J. London Math. Soc.*, 1960, v. 35, 367–376.
5. Cartwright M. Van der Pol equation for relaxation oscillation. In Contribution to the theory of nonlinear oscillation II. Princeton Ann., Math. Stud. 2, Princeton University Press, Princeton, NJ, 1952, pp. 3–18.
6. Van der Pol B. A Theory of amplitude of force and force triode vibration. *Radio Review*, 1920, v. 1, 701–710, 754–762.
7. Van der Pol B. Relaxation Oscillations I. *Phil. Mag.*, 1926, v. 2, 978–992.
8. Van der Pol B. The nonlinear theory of electric oscillations. *Proc. IRE*, 1934, v. 22, 1051–1086.
9. Van der Pol B. and Van der Mark J. Frequency of demultiplication. *Nature*, 1927, v. 120, 363–364.
10. Cartwright M. L. and Littlewood J. E. *J. London Math. Soc.*, 1945, v. 20, 180.
11. Levinson N. A second order differential equation with singular solutions. *The Annals of Mathematics,* 2^{nd} *ser.*, 1949, v. 50 (1), 127–153.
12. Hafeez H. Y. and Chifu, E. N. Van der Pol Equation for Nonlinear Plasma Oscillations. *J. Adv. Phys.*, 2014, v. 3 (4), 278–281.
13. Nayfeh Ali Hassan. Introduction to perturbation techniques. Wiley-Vch, 2004, pp. 164–166.
14. Van der Pol B. *Phil. Mag.*, 1927, v. 3, 64

Shape Transition in the Even-Even Cerium Isotopes

Benyoucef Mohammed-Azizi[1], Abderrachid Helmaoui[2], and Djamal-Eddine Medjadi[3]

[1]University of Bechar, Bechar, Algeria. E-mail: aziziyoucef@voila.fr
[2]University of Bechar, Bechar, Algeria. E-mail: helmaouiabderrachid@yahoo.fr
[3]École Normale Supérieure, Vieux Kouba, Algiers, Algeria. E-mail: medjadide@voila.fr

The deformation energy of the even-even nuclei of the Cerium isotopic chain is investigated by means of the Macroscopic-Microscopic method with a semiclassical shell correction. We consider axially symmetric shapes. Binding energy and two neutron separation energy are also evaluated. For the sake of clarity several important details of the calculations are also given. It turns out that all these nuclei have prolate equilibrium shape. The regions of maximum deformation are obtained around $N = 64$ and $N = 102$. There is no critical-point of quantum phase transition in this isotopic chain.

1 Introduction

Nowadays it is well established that the majority of nuclei possess a nonzero intrinsic electric quadrupole moment (IE QM). This feature means that the charge distribution inside the nucleus deviates from the spherical symmetry. In other words, apart from very few nuclei, the surface of the nucleus is generally not spherical in its ground state. The intrinsic quadrupole electric moments (or equivalently the nuclear deformation) can be deduced from two types of measurements:

- The reduced electric quadrupole transition probability, $B(E2)$ [1];
- The static electric quadrupole moments of ground and excited states, Q [2].

It turns out that in a number of cases, the two methods of measurement do not systematically lead to the same values. Important discrepancies occur for several nuclei. This is essentially due to the fact that not only different experimental techniques are used but above all, because different models can be implemented to deduce the nuclear deformation for the both cases.

In [3] it is stated that deformations deduced from $B(E2)$ have a "more general character". In other words, "$B(E2)$-type" data reflect not only static nuclear deformation (permanent deviation of the nuclear shape from sphericity), but also dynamic deformation. Furthermore, $B(E2)$ measurements are model independent and thus are generally more reliable. This is corroborated by the fact that the only systematic compilation in which the deformation of the ground state is given explicitly is based on $B(E2; 0^+ \rightarrow 2^+)$ and has been published in [1]. In the present work, experimental values refer to these ones.

Theoretical approaches to the deformation energy can be divided into two categories; Dynamic calculations to find the shape of the ground state (or even of excited states) and static calculations by determining the absolute minimum (ground state) or multiple minima (shape isomers) in the potential energy surface (PES) for a given nucleus.

Thus, on the one hand, we have the so-called collective models, which themselves are subdivided into two groups: The "Geometric Collective Model" also called the "Collective Bohr Hamiltonian" (CBH and its variants) and the "Algebraic Model", well known under the name of the "Interacting Boson Model" (IBM and its variants) [4]. On the other hand, "particle models" consider the nucleus as a collection of interacting nucleons (fermions).

In practice, the classical N-body problem can be approximately solved by the usual approximation of the mean field with eventually residual interactions. In this respect, the "best" mean field is deduced after applying a variational principle in the Hartree-Fock-Bogoliubov method (HFB). In this model, the determination of the potential energy surface (PE S) of the nucleus amounts to perform constrained Hartree-Fock-Bogoliubov (CHFB) calculations [5]. We will not address very complicated methods "beyond the mean field" such as the Quasiparticle Random Phase Approximation (QRP A) or the Generator-Coordinate-Method (GCM) methods which are unsuitable in practice for large scale calculations.

Because of CHFB calculations are time consumers, especially in large studies, Microscopic-Macroscopic method (Mic-Mac) constitutes a good alternative which, is up to now, implemented [6]. In the present work, we use an improved variant of this method. The word "improved" means that we use semi-classical method to avoid the well-known drawbacks (spurious dependence on two mathematical parameters) of the standard Strutinsky shell correction (see text below).

The present study is devoted to the deformation energy, equilibrium nuclear shapes and binding energy of the ground state of the even-even cerium isotopes. There are many reasons to this choice. One of them is to re-test our previous calculations. In effect, similar calculations have been already performed by us in the xenon, barium, and cerium region [7]. However because the phenomenological mean potential varies smoothly with N and Z, we have made, in the past, a rough approximation by choosing the same set of parameters for the phenomenological mean potential, for the all treated

nuclei. Originally, this approximation was done only for simplifying the calculations.

Here, contrarily to that study, each nucleus has its "own" mean potential with a specific set of parameters. In this way it is possible to evaluate in a rigorous way the uncertainty introduced in the previous calculations. Apart from this remark, there are several main other reasons which could justify this choice: (i) First, it should be interesting to see how the deformation energy and binding energy vary with the neutron number (N) for this isotopic chain. (ii) Second, the present study extends the previous calculations to all cerium isotopes up to the drip lines (34 versus 13 nuclei). (iii) Third, we also will attempt to deduce, from potential energy surface (PES) curves, the shape transition from spherical to axially deformed nuclei, looking for the so-called $X(5)$ critical-point between U(5) and SU(3) symmetry limits of the IBM [8, 9].

It is worth to recall briefly some information deduced from the literature for the cerium isotopes. In the past, a number of experimental as well as theoretical studies have been done for the cerium isotopes. Among the numerous studies, we only cite some of them.

In 2005 Smith et al [10] have studied excited states of ^{122}Ce up to spin $14\hbar$ deducing a probable quadrupole deformation of about $\beta \approx 0.35$. The deformed nucleus ^{130}Ce has been studied in 1985, using the techniques of in-beam gamma -ray spectroscopy [11]. The corresponding data have been interpreted in terms of the cranking model by assuming a prolate deformation with $\varepsilon_2 \approx 0.25$ ($\beta \approx 0.27$).

High-spin states in ^{132}Ce have been also studied by A.J. Kirwan et al [12]. They found a superdeformed band with deformation $\beta \approx 0.4$ much more larger that the ground state deformation ($\beta \approx 0.2$). E. Michelakakis et al [13] by evaluating $\gamma-$ray transitions in ^{142}Ce and ^{144}Ce conclude that in cerium isotopes (near the beta-stable line) the onset of nuclear deformation occur between $N = 86$ and $N = 88$. "Pure" theoretical calculations have been performed in [14] and [15] with projected shell model (PSM) and Hartree-Bogoliubov ansatz in the valence space respectively for ^{122}Ce and $^{124-132}$Ce for low lying yrast spectra. Good values of energy levels and reduced transition probabilities $B(E2, 0^+ \rightarrow 2^+)$ have been obtained respectively in these two papers.

Other approaches for the rich-neutron cerium isotopes have been made in [16]. A study of the shape transition from spherical to axially deformed nuclei in the even Ce isotopes has been done in [17] using the nucleon-pair approximation of the shell model. The result of a such study is that the transition has been found too rapid. Relativistic Hartree-Fock-Bogoliubov theory has been used to predict ordinary halo for ^{186}Ce,^{188} Ce,^{190} Ce, and giant halo for ^{192}Ce,^{194} Ce,^{196} Ce, and ^{198}Ce near the neutron drip line.

Systematic studies about nuclear deformations and masses of the ground state can be found in [18–21] with respectively, the Finite-Range Droplet-Model (FRDM), Hartree-Fock-Bogoliubov (HFB), HFB+5-dimensional collective quadrupole Hamiltonian and Relativistic Mean Field (RMF) models.

2 The Macroscopic–Microscopic method

2.1 Liquid drop model and microscopic corrections

This method combines the so-called semi-empirical mass formula (or liquid drop model) with shell and pairing corrections deduced from microscopic model. Thus the binding energy is given as a function of nucleon numbers and deformation parameter (referred to as β) by mean of the usual symbols:

$$B(A, Z, \beta) = E_{LDM}(\beta) - \delta B_{micro}(\beta). \tag{1}$$

δB_{micro} contains the shell and pairing correction (see text below). The minus sign before δB_{micro} is consistent with the convention that the binding energy is defined as positive here.

For the liquid drop model we take the old version of Myers and Swiatecki [28] (because of its simplicity compared to more recent formulae). Here, there is no need to look for very high accuracy in binding energy, because this is not the purpose of the present work.

$$\begin{aligned} E_{LDM}(\beta) = C_V A - C_S A^{2/3} B_S(\beta) - C_C Z^2 A^{-1/3} B_C(\beta) + \\ + \varepsilon a_{pair} A^{-1/2} + C_d Z^2 A^{-1}. \end{aligned} \tag{2}$$

In (2), we have the usual contributions of volume, surface and coulomb energies.

The different constants of Myers and Swiatecki are given in Appendix A. The shape dependence (β) of the surface and coulomb energies are contained in $B_S(\beta)$ and $B_C(\beta)$. They are normalized to the unity for a spherical nuclear surface. The latter is symbolized by $\beta = 0$. The two last terms in (2) are respectively due to the smooth part of the pairing energy and the correction of the Coulomb energy to account for the diffuseness of the nucleus surface. The different constants will be fixed later.

The potential energy surface (PES without zero point energy correction) is defined as follows:

$$\begin{aligned} E_{PES}(\beta) &= E_{LDM}(0) - B(A, Z, \beta) \\ &= \Delta E_{LDM}(\beta) + \delta B_{micro}(\beta) \end{aligned} \tag{3}$$

in which

$$\begin{aligned} \Delta E_{LDM}(\beta) &= E_{LDM}(0) - E_{LDM}(\beta) \\ &= C_S A^{2/3} \left[B_S(\beta) - B_S(0) \right] + \\ &+ C_C Z^2 A^{-1/3} \left[B_C(\beta) - B_C(0) \right]. \end{aligned} \tag{4}$$

Constants C_V and C_S are expressed by means of three other constants a_V, a_S, and κ. For spherical shape, as said before, the normalization is expressed by: $B_S(0) = B_C(0) = 1$. As it can be easily seen, the potential energy surface is related only to two macroscopic constants C_S (which depends actually on

a_S and κ) and C_C. To calculate microscopic shell an pairing corrections contained in δB_{micro}, we have to proceed in two steps. The first consists in solving the Schrödinger equation and the second in deducing the shell and pairing corrections in an appropriate way, as explained in the following.

2.2 Microscopic model

We briefly present the microscopic model which is based on the Schrödinger equation of the deformed independent particle model:

$$\hat{H}(\beta) \mid \Psi_i(\beta)\rangle = \varepsilon_i(\beta) \mid \Psi_i(\beta)\rangle \tag{5}$$

where $|\Psi_i\rangle$ and ε_i are respectively the eigenfunctions and the associated eigenvalues of nucleons. Hamiltonian $\hat{H}$ contains four contributions which are: (i) kinetic energy, (ii) central deformed mean field, (iii) spin-orbit and (iv) Coulomb interactions.

We perform analogous calculations as in Nilsson model but our deformed mean potential is of Woods-Saxon type and therefore is "more realistic". Although calculations are not self consistent, they are microscopic. It is to be noted that our Schrödinger equation has a form which is very close to the one of the Skyrme-Hartree-Fock method. Eq. (5) is solved by our FORTRAN program described in details in [22] and improved in two successive versions [23] and [24].

2.3 Microscopic corrections

Microscopic corrections are defined as the sum of shell and pairing corrections which themselves are calculated separately for each kind of nucleons:

$$\begin{aligned}\delta B_{micro}(\beta) = \delta E_{shell}(N,\beta) + \delta E_{shell}(Z,\beta) + \\ + \delta P_{pairing}(N,\beta) + \delta P_{pairing}(Z,\beta).\end{aligned} \tag{6}$$

In this formula the shell correction is defined by the usual Strutinsky prescription, i.e. as the difference between the sum of the single particle energies (which contains the shell effects) and an averaged (or smoothed) sum (which is free from shell effects)

$$\delta E_{shell}(N \text{ or } Z) = \sum_{i=1}^{N\text{or}Z} \varepsilon_i(\beta) - \overline{\sum_{i=1} \varepsilon_i(\beta)}. \tag{7}$$

Energies $\varepsilon_i(\beta)$ are deduced from (5). In our procedure, the second sum is found by means of a semi-classical way instead a Strutinsky smoothing procedure, see [27]. This avoids the well-known weakness of the standard shell correction method, namely, the dependence on two unphysical parameters which are the "smoothing" parameter and the order of the curvature correction.

Moreover, it has been clearly shown that Strutinsky level density method is only an approximation of that of the semi-classical theory [26]. The "pure" pairing correlation energy is defined by:

$$P(\beta) = \sum_{i=1}^{\infty} 2\varepsilon_i(\beta)\upsilon_i^2 - \sum_{i=1}^{N/2\text{or}Z/2} 2\varepsilon_i(\beta) - \frac{\Delta^2}{G} \tag{8}$$

where υ_i^2, Δ and λ are the usual occupation probabilities, gap and Fermi energy of the BCS approximation (the factor "2" is simply due to the Kramers degeneracy). Since the smooth part of pairing correlations is already contained in the liquid drop model, we have to add only the one due to the shell oscillations of the level density. This contribution is defined by means of a formula similar to (7)

$$\delta P_{pairing}(N \text{ or } Z,\ \beta) = P(\beta) - \overline{P(\beta)} \tag{9}$$

where the averaged pairing is defined as

$$\overline{P(\beta)} = \frac{1}{2}\, g_{semicl.}(\lambda)\, \overline{\Delta}^2.$$

We use a simple BCS method to account for pairing correlations. To calculate (7) and (9) we follow the method detailed in [27] with its FORTRAN code. The treatment of the pairing has also been explained in [7] and references quoted therein.

2.4 Numerical constants and prescriptions

2.4.1 Constants of the microscopic model

For each kind of particles the mean central and the mean spin-orbit field are written as [22]:

$$\begin{aligned}V(\beta) &= \frac{V_0}{1 + \exp(R_V L_V(\beta)/a_0)} \\ V_{SO}(\beta) &= \lambda\left(\frac{\hbar}{2Mc}\right)\frac{V_0}{1 + \exp(R_{SO} L_{SO}(\beta)/a_0)}\end{aligned} \tag{10}$$

where $L_V(\beta)$ and $L_{SO}(\beta)$ contain the information on the deformation. In fact, these functions contain 9 constants: V_{0neut}, V_{0prot}, R_{Vneut}, R_{Vprot}, $R_{SO-neut}$, $R_{SO-prot}$, a_0, λ_{neut}, λ_{prot}. These quantities are taken from the "universal" parameters [29] (see Appendix B) which is an optimized set. The Coulomb mean field is approximated by a uniform charge distribution inside a deformed surface. The volume conservation is therefore $Vol = (4/3)\pi R_{ch}^3$ with the simple assumption $R_{ch} = R_{Vprot}$.

2.4.2 Constants of the liquid drop model

As already stated, we have chosen the parameters of Myers and Swiatecki (see Table 1) because this set contains a reduced number of parameters with respect to more modern formulae. All the constants are needed in the binding energy whereas only a_S, C_C, κ play a role in the potential energy surface.

	a_V	a_S	C_C	κ	C_d	a_{pair}
Myers and Swiatecki	15.67 MeV	18.56 MeV	0.72 MeV	1.79	1.21 MeV	11 MeV

Table 1: Parameters of the liquid drop model in the Myers and Swiatecki version [28].

2.4.3 Nuclear mass excesses

Nuclear masses are deduced as mass excesses:

$$M_{excess}(A,Z) = ZM_H + (A-Z)M_n - B(A,Z)$$

where $M_H = 7.289034$ MeV is the hydrogen mass excess and $M_n = 8.071431$ MeV the neutron mass excess. This makes comparisons with experimental values easiest.

3 Results

In our previous paper [7] calculations for isotopes $^{116-130}$Ce showed that the equilibrium deformations ($\beta \approx 0.25 - 0.30$) have always been obtained for symmetric prolate shapes ($\gamma = 0°$). Results obtained in [32] with a similar approach for the nuclei $^{116-130}Ce$, corroborate this fact. For these reasons, we think that it is needless to account for the axial asymmetry in a "pure" static study of the equilibrium deformation. However, we have to consider prolate ($\gamma = 0°$) as well as oblate ($\gamma = 60°$) nuclear shapes. In this regard, it is worth remembering that oblate shape given by ($\beta > 0, \gamma = 60°$) is equivalent to the set ($\beta < 0, \gamma = 0°$).

3.1 Comparison between the different contributions entering in the potential energy surface

It could be useful to compare the importance of the different terms entering in the right hand side of (6). In this respect, we have drawn in Fig.1 for axially prolate shape, the four microscopic contributions

$$\delta E_{shell}(N,\beta), \delta E_{shell}(Z,\beta), \delta P_{pairing}(N,\beta), \delta P_{pairing}(Z,\beta)$$

for the case of ^{160}Ce as functions of β. Following the cited order, we can say that the difference between the highest and lowest values in the interval $\beta \in [0.0, 0.7]$ are respectively about 11.0 MeV, 10.5 MeV, 5.7 MeV, 3.5 MeV for the four corrections.

Thus, these variations show that the shell corrections

$$\delta E_{shell}(N,\beta), \delta E_{shell}(Z,\beta)$$

are more important than

$$\delta P_{pairing}(N,\beta), \delta P_{pairing}(Z,\beta)$$

and have a clear minimum at respectively $\beta = 0.35$ and $\beta = 0.30$. It is well known that for each kind of nucleon the shell correction is in opposite phase with respect to the pairing correction (this means for that when $\delta E_{shell}(N,\beta)$ increases with β, $\delta P_{pairing}(N,\beta)$ decreases and vice versa).

Contrarily to these curves, the liquid drop model is strictly increasing with β, and its minimum occurs always at the beginning $\beta = 0.0$ (spherical shape). When all the contributions are added, the minimum of the potential energy surface of the nucleus is reached at about $\beta = 0.3$ and is mainly due to the shell corrections. When β becomes more and more, larger the contribution of the liquid drop energy becomes preponderant so that the equilibrium deformation occurs generally between $\beta = 0$ and $\beta = 0.4$. Because of the convention of the sign stated before, δB_{micro} defined in (1) must be negative in order to increase the binding energy of the nucleus. Since the shell corrections (for protons and neutrons) play a major role in δB_{micro}, it is naturally expected that negative (but absolute large) values of shell correction contribute to increase the binding energy of the nucleus.

In this respect, it is well known that the shell correction is essentially determined by the distribution of single-particle levels in the vicinity of the sharp Fermi level (defined here as midway between the last occupied level and the first empty level). Following [31], we can state that "the nuclear ground state, as well as any other relatively stable state, should correspond to the lowest possible degeneracy, or, in other words, the lowest density of state near the Fermi level". This is illustrated in Fig. 2 where the single-particle levels are drawn as function of the deformation β (γ being fixed at $\gamma = 0°$). To this end we have used the FORTRAN code of [22] and [24]. The area where the single-particle level density is low near the Fermi level (black stars) is indicated by a circle. Thus, it is not so surprising that, it is in this region where the neutron shell correction becomes the most important, involving a minimum in the PES of the nucleus.

3.2 Equilibrium deformations

Equilibrium deformations are given in Table (2) for prolate as well as oblate shapes (see table legend for details). The minima of PES for the corresponding wells are denoted *minpro* and *minobl*. The deformation energy is defined as the difference $E_{def} = E_{PES}(0) - E^{\min}_{PES}(\beta)$, i.e. the difference between the potential energy surface for a spherical shape and the one corresponding to the absolute minimum of PES. Permanent deformations will be in principle characterized by large values of E_{def} and are responsible of rotational spectra.

From this table, some remarks may be drawn:
(i) Two regions of prolate deformation are found. They occur around $N = 64$ and $N = 102$ with maximum deformation about $\beta \approx 0.30$. The deformation energy (between spherical and deformed shape) is about 6.70 MeV for $N = 64$ and

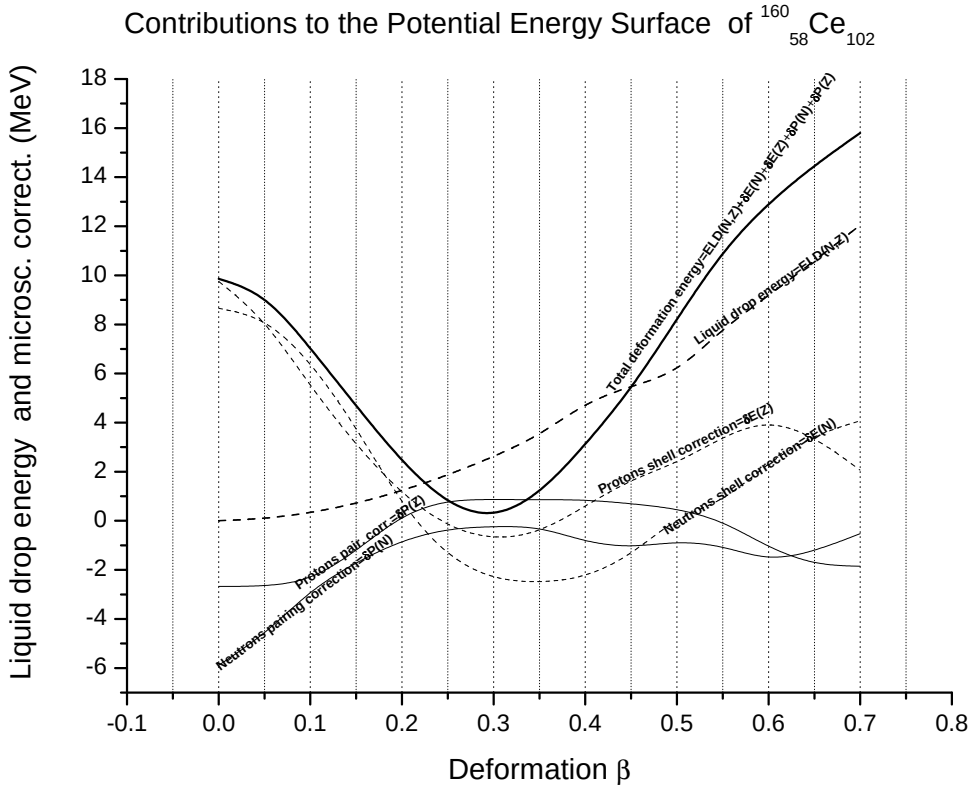

Fig. 1: Contributions of the shell and pairing corrections for the two kind of nucleons and the one of the liquid drop model to the total potential energy surface of the nucleus ^{160}Ce.

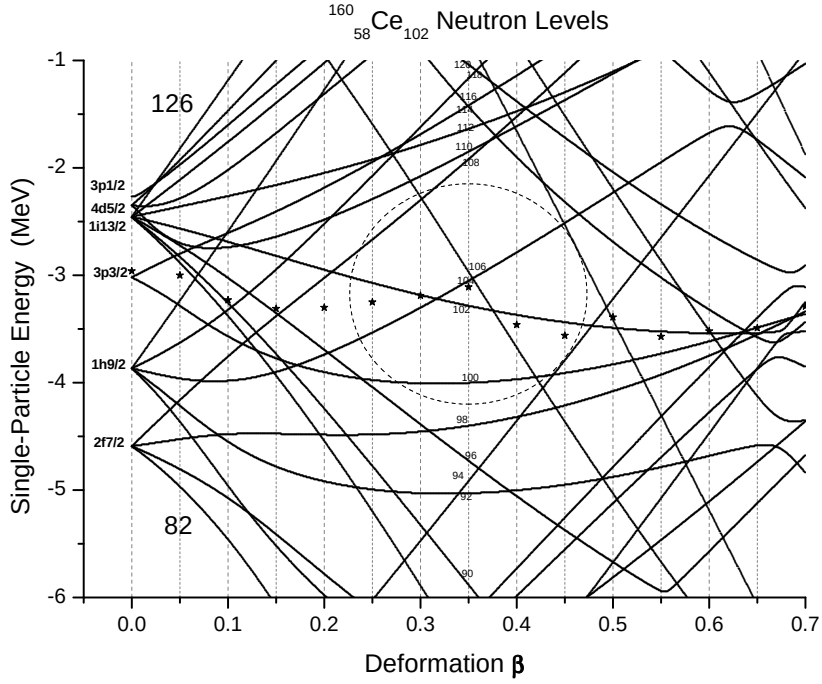

Fig. 2: Single-particle energies of the microscopic model as function of deformation for prolate shapes ($\beta > 0$) for the nucleus ^{160}Ce. Spherical spectroscopic notation is given for spherical deformation ($\beta = 0$) .The circle in dotted line indicates the area of lowest level density.

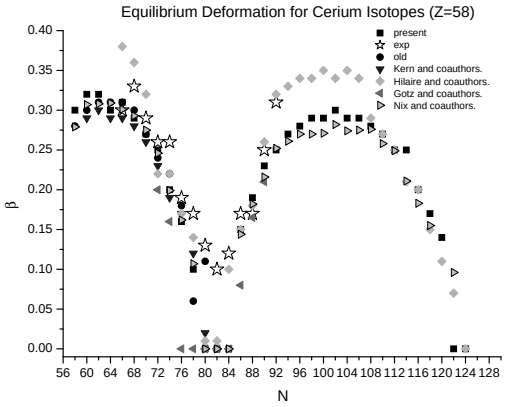

Fig. 3: Theoretical equilibrium deformations for even-even cerium isotopes evaluated by different or similar approaches.

9.30 MeV for $N = 102$ and decreases from either side from these two nuclei.
(ii) Spherical deformation occur at and near the (magic) numbers $N = 82$ and $N = 128$ (not shown).
(iii) The deformation energy decreases from $N = 64$ (maximum) to $N = 82$ (minimum) and reincreases again to $N = 102$ (maximum). We have found graphically that the first inflexion point occurs between $N = 72$ and $N = 74$ and a second inflexion point is found between $N = 90$ and $N = 92$. One can consider (somewhat arbitrarily) that spherical shapes occur approximately between these two limits.
(iv) The minima of prolate equilibrium deformations are, by far, always deeper compared to the ones of the oblate minima ($minpro \ll minobl$). In other words cerium isotopes prefer, by far, prolate shapes. In other words, the deformation energy increases in average with the asymmetry γ. This justifies a posteriori that, in a static study of the equilibrium deformation, it is needless to account for axial asymmetry. It is worth to remember that most of nuclei of the chart have prolate shape (see [25]).
(v) Even though the experimental deformations are known only in absolute value from $B(E2)$, a good agreement is obtained if one excepts the three "nearly magic" nuclei $^{138-142}$Ce

In Fig. (3) are displayed the present equilibrium deformations, experimental values [1] , our "old" calculations [7] and other studies performed by different authors which are: Kern et al. [32], Hilaire and Girod [34], Gotz et al. [33] and Nix et al. [18]. All calculations are based on Macro-Micro method (with different mean fields or different parameters). Except the one of [34] which uses Hartree-Fock-Bogoliubov model with Gogny force.
(i) Near magic number ($N = 82$) all calculations give spherical equilibrium deformation whereas experimental results are always slightly deformed (even for $N = 82$). It seems difficult to overcome this defect with a pure static approach which neglects the role of the mass parameters.
(ii) The overall tendency of these calculations is the same except the fact that HFB calculations differ significantly from the others with higher values in some regions.
(iii) Apart from HFB calculations, theoretical values are generally quite close from each others.
(iv) Our old and new calculations give very close results (see Table 3). Thus, even if it is better to choose a proper set of mean-field parameters for each nucleus, we do not commit a significant error by taking the same set of parameters for nuclei that do not differ strongly by the number of neutrons (N).

3.3 Mass excesses

We list from a FORTRAN file (see Fig. 4) the results of our theoretical calculations of the binding energies and mass excesses (m-excess) for the even-even cerium isotopic chain. For the sake of completeness, experimental mass excesses and the ones of the FRDM model (see [18]) are also given. We must keep in mind that only 6 parameters are used in the liquid drop model whereas 16 parameters are necessary in the FRDM model. This explains the "better quality" of the FRDM model. However, we have checked that the variations of binding energy or mass excesses from one isotope to the nearest is practically the same in our model and the one of FRDM (the deviations are about ±0.35 MeV). For this reason, the calculation of the two neutron separation energies (see the following subsection 3.4) will almost be probably the same for the two approaches even though our model is not so accurate.

3.4 Transitional regions in cerium isotopes

In Fig. 5 is shown the gradual transition in the potential energy surface from spherical vibrator to the axially deformed rotor when the number of neutrons (N) increases from 76 to 92. One signature of $X(5)$ symmetry which is a critical-point of phase/shape transitions (quantum phase transition between spherical and axial symmetries) should be a long flatness of the potential energy surface with eventually a weak barrier from prolate to oblate shapes. In this figure, for $N > 82$, the width of the flatness increases as one moves away from $N = 82$ but at the same time the difference between oblate and prolate minima and barrier between oblate and prolate shapes also increase. For example the differences between oblate and prolate energy minima and barriers for isotopes with $N = 88, 90, 92$ are respectively about 1.5 MeV, 2.5 MeV and 3.3 MeV with energy barrier about 2 MeV, 4 MeV and 5.5 MeV respectively. The wideness of the bottom of the well must be relativized with the height of the barrier. Thus for the case of $N = 92$ the width is important, i.e. about $\Delta\beta \approx \beta_{pro} - \beta_{obl} \approx 0.26 - (-0.20) \approx 0.46$ but the barrier is about 5.5 MeV and therefore seems too high. The case $N = 90$ gives a width of $\Delta\beta \approx 0.3$ with a barrier of about 4 MeV. For $N < 82$, the case $N = 76$ seems to be rela-

N	A	β_{pro}	$minpro$ (MeV)	β_{obl}	$minobl$ (MeV)	E_{def} (MeV)	$\lvert\beta_{\exp}\rvert$	N	A	β_{pro}	$minpro$ (MeV)	β_{obl}	$minobl$ (MeV)	E_{def} (MeV)	$\lvert\beta_{\exp}\rvert$
58	116	0.30	0.90	−0.21	3.62	4.80		92	150	0.25	1.23	−0.17	4.45	5.12	0.31
60	118	0.32	0.88	−0.23	4.07	5.87		94	152	0.27	1.21	−0.19	5.05	6.40	
62	120	0.32	1.03	−0.23	4.33	6.19		96	154	0.28	0.64	−0.21	4.94	7.47	
64	122	0.31	1.16	−0.23	4.23	6.68		98	156	0.29	0.66	−0.22	5.13	8.44	
66	124	0.30	1.47	−0.21	4.15	6.17	0.30	100	158	0.29	0.71	−0.22	5.14	9.08	
68	126	0.29	1.75	−0.21	3.87	5.43	0.33	102	160	0.30	0.32	−0.22	4.52	9.27	
70	128	0.27	1.82	−0.21	3.48	4.67	0.29	104	162	0.29	0.71	−0.22	4.42	9.08	
72	130	0.25	2.02	−0.2	3.27	3.34	0.26	106	164	0.29	1.00	−0.23	4.23	8.44	
74	132	0.20	1.90	−0.17	2.60	1.97	0.26	108	166	0.28	1.16	−0.23	3.92	7.57	
76	134	0.16	1.28	−0.14	1.63	0.93	0.19	110	168	0.27	1.46	−0.21	3.84	6.39	
78	136	0.10	0.04	−0.07	0.18	0.19	0.17	112	170	0.25	1.68	−0.20	3.55	5.33	
80	138	0.00	−1.93	0.00	−1.93	0.00	0.13	114	172	0.25	1.97	−0.19	3.20	4.19	
82	140	0.00	−3.96	0.00	−3.96	0.00	0.10	116	174	0.2	1.93	−0.17	2.79	2.95	
84	142	0.00	−2.07	0.00	−2.07	0.00	0.12	118	176	0.17	1.71	−0.16	2.17	1.68	
86	144	0.15	0.02	−0.06	0.53	0.50	0.17	120	178	0.14	1.39	−0.14	1.60	0.55	
88	146	0.19	0.73	−0.11	2.43	1.99	0.17	122	180	0.0	0.3	0.00	0.30	−0.15	
90	148	0.23	1.15	−0.14	3.76	3.15	0.25	124	182	0.0	−1.08	0.00	−1.08	−0.08	

Table 2: Equilibrium deformations as well as deformation energies for the cerium isotopic chain. The columns give successively the number of neutrons (N), the mass number (A), the prolate equilibrium deformation (β_{pro}), the minimum of the prolate well ($minpro$), the oblate equilibrium deformation (β_{obl}), the minimum of the oblate well ($minobl$), the deformation energy (E_{def},see text), the experimental equilibrium deformation ($\beta_{\exp}$). Note: The deformation energy is always given for the prolate equilibrium shape because no absolute minimum is obtained for oblate shape.

Cerium ($Z = 58$)	$N = 58$	60	62	64	66	68	70	72	74	76	78	80	82
Present β	+0.30	+0.32	+0.32	+0.31	+0.30	+0.29	+0.27	+0.25	+0.20	+0.16	+0.10	+0.00	+0.00
Old β	+0.28	+0.30	+0.31	+0.31	+0.31	+0.30	+0.27	+0.24	+0.22	+0.18	+0.06	+0.11	+0.00
Present $E_{def}(MeV)$	4.80	5.87	6.19	6.68	6.17	5.43	4.67	3.34	1.97	0.93	0.19	0.00	0.00
Old $E_{def}(MeV)$	4.82	5.77	6.03	6.31	7.08	5.36	4.41	3.35	2.13	0.77	0.00	0.24	0.00

Table 3: New equilibrium deformations and deformations energies vs old [7].

tively equivalent to $N = 90$ with a slightly smaller width and a lower height barrier. Thus it is difficult to determine clearly the existence of a $X(5)$ critical-point. Thus, everything seems to indicate a continuous transition.

In Fig. 6 is displayed the two-neutron separation energy (TSN) as function of the neutron number N. A clear jump is seen from $N = 82$ to $N = 84$, i.e. from one major shell to the following. Just before $N = 82$ and just after $N = 84$ the TSN varies more slowly. Far for the "jump" the curve becomes quasi-linear. Once again, no special behavior is noted around $N = 90$ which from [35] and [36] should constitute with $Z \approx 62$ the first order shape transition ($X(5)$ critical-point) in the rare earth region. In [37], it has been pointed out that "Empirical evidence of transitional symmetry at the $X(5)$ critical-point has been observed in ^{150}Nd, ^{152}Sm, ^{154}Gd, and ^{156}Dy". One of the most important signatures of the phase transition is given by a sudden jump in the value of the energy ratio $R_{4/2} = 4_1^+/2_1^+$ from one nucleus to the next. We found it useful to compare the experimental values of this ratio (see Fig. 7) in the cases of the isotopic chains of Ce and Sm (The experimental values of the considered levels have been deduced from the adopted level of $ENSDF$ site [38]). The figure shows clearly two facts. First, the important variation of $R_{4/2}$ near of the magic number $N = 82$ for both isotopic chains and then, the important difference between the behavior the two isotopic chain from $N = 88$ to $N = 90$. In effect

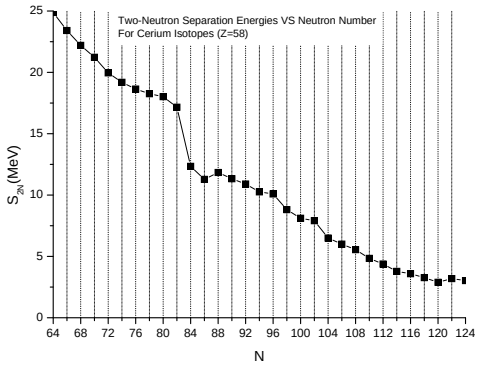

Fig. 6: Two-neutron separation energies (S_{2N}) along the cerium isotopic chain. This quantity is defined as $S_{2N}(A,Z,N) = Bind(A,Z,N) - Bind(A-2,Z,N-2)$ where the binding energy $Bind(A,Z,N)$ is given by (1). Note that in our approache the neutron drip line (where $S_{2N} \approx 0$) can be extrapolated around $N = 128$ for Cerium isotopes.

N	58	A	116.	Z	58	bind	914.85	m-excess	-23.94	exp	*********	frdm	-29.21
N	60	A	118.	Z	58	bind	942.64	m-excess	-35.59	exp	*********	frdm	-40.57
N	62	A	120.	Z	58	bind	968.86	m-excess	-45.66	exp	*********	frdm	-50.01
N	64	A	122.	Z	58	bind	993.74	m-excess	-54.40	exp	*********	frdm	-57.99
N	66	A	124.	Z	58	bind	1017.15	m-excess	-61.67	exp	*********	frdm	-64.93
N	68	A	126.	Z	58	bind	1039.35	m-excess	-67.73	exp	*********	frdm	-70.82
N	70	A	128.	Z	58	bind	1060.58	m-excess	-72.81	exp	*********	frdm	-75.54
N	72	A	130.	Z	58	bind	1080.54	m-excess	-76.63	exp	*********	frdm	-79.17
N	74	A	132.	Z	58	bind	1099.73	m-excess	-79.68	exp	*********	frdm	-81.89
N	76	A	134.	Z	58	bind	1118.37	m-excess	-82.18	exp	-84.750	frdm	-84.02
N	78	A	136.	Z	58	bind	1136.63	m-excess	-84.30	exp	-86.500	frdm	-85.67
N	80	A	138.	Z	58	bind	1154.66	m-excess	-86.18	exp	-87.570	frdm	-87.62
N	82	A	140.	Z	58	bind	1171.81	m-excess	-87.19	exp	-88.090	frdm	-88.68
N	84	A	142.	Z	58	bind	1184.16	m-excess	-83.39	exp	-84.540	frdm	-84.78
N	86	A	144.	Z	58	bind	1195.44	m-excess	-78.53	exp	-80.440	frdm	-80.23
N	88	A	146.	Z	58	bind	1207.28	m-excess	-74.23	exp	-75.720	frdm	-76.00
N	90	A	148.	Z	58	bind	1218.60	m-excess	-69.41	exp	-70.430	frdm	-70.83
N	92	A	150.	Z	58	bind	1229.50	m-excess	-64.17	exp	-64.990	frdm	-65.80
N	94	A	152.	Z	58	bind	1239.76	m-excess	-58.28	exp	*********	frdm	-59.78
N	96	A	154.	Z	58	bind	1249.85	m-excess	-52.23	exp	*********	frdm	-52.90
N	98	A	156.	Z	58	bind	1258.66	m-excess	-44.90	exp	*********	frdm	-45.40
N	100	A	158.	Z	58	bind	1266.78	m-excess	-36.87	exp	*********	frdm	-37.29
N	102	A	160.	Z	58	bind	1274.68	m-excess	-28.63	exp	*********	frdm	-28.70
N	104	A	162.	Z	58	bind	1281.19	m-excess	-19.00	exp	*********	frdm	-19.01
N	106	A	164.	Z	58	bind	1287.19	m-excess	-8.86	exp	*********	frdm	-8.62
N	108	A	166.	Z	58	bind	1292.74	m-excess	1.74	exp	*********	frdm	2.23
N	110	A	168.	Z	58	bind	1297.58	m-excess	13.04	exp	*********	frdm	13.43
N	112	A	170.	Z	58	bind	1301.96	m-excess	24.81	exp	*********	frdm	25.00
N	114	A	172.	Z	58	bind	1305.73	m-excess	37.17	exp	*********	frdm	36.82
N	116	A	174.	Z	58	bind	1309.33	m-excess	49.72	exp	*********	frdm	49.07
N	118	A	176.	Z	58	bind	1312.60	m-excess	62.59	exp	*********	frdm	61.53
N	120	A	178.	Z	58	bind	1315.49	m-excess	75.84	exp	*********	frdm	74.94
N	122	A	180.	Z	58	bind	1318.69	m-excess	88.79	exp	*********	frdm	87.48
N	124	A	182.	Z	58	bind	1321.72	m-excess	101.90	exp	*********	frdm	99.94

Fig. 4: Theoretical binding energies and mass excesses of the present approach compared to the experimental mass excesses and the ones given by the FRDM model of [18]. All energies are expressed in MeV. The experimental data as well as the frdm results have been entered manually in the code. Asterics mean that no experimental data is available for the corresponding nucleus.

in the case of Samarium, there is a sudden increase of this ratio whereas this is not the case for the Cerium isotopes. This has been attributed to the $X(5)$ critical-point symmetry of the nucleus ^{152}Sm. Thus the present study confirms that cerium isotopic chain is characterized by a continuous shape/phase transition.

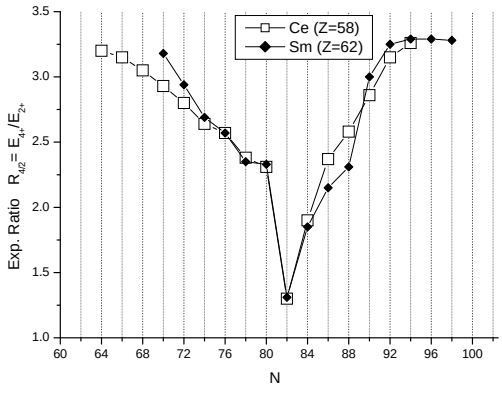

Fig. 7: $R_{4/2}$ energy ratio as function of neutron number for Cerium and Samarium isotopes. Sudden variations are associated with magic closure shells for the both chains (at $N = 82$) and with $X(5)$ critical point which occurs only for Sm (at $N = 90$).

4 Conclusion

Potential energy surfaces have been drawn for the cerium isotopic chain. All even-even nuclei between the two drip lines have been considered. To this end, we have used the microscopic–macroscopic method in which the quantum corrections have been evaluated by a semi-classical procedure. The microscopic model is based on a "realistic" Schrödinger equation including a mean field of a Woods-Saxon type. The macroscopic part of the energy is evaluated from the liquid drop model using the version of Myers and Swiatecki. The following points must be remembered:

(i) All equilibrium deformations have been found prolate with an important deformation energy compared to oblate shapes.

(ii) The maximum deformations are of order $\beta \approx 0.3$ and are located around $N = 64$ and $N = 102$ with deformation energy about 6 MeV and 9 MeV respectively. The equilibrium deformations decrease as one moves away from these two nuclei.

(iii) Spherical shapes are found in the neighborhood of $N = 82$.

(iv) Good agreement is obtained between theoretical and experimental values if one excepts the area of the shell closure $N = 82$ where the latter are slightly larger.

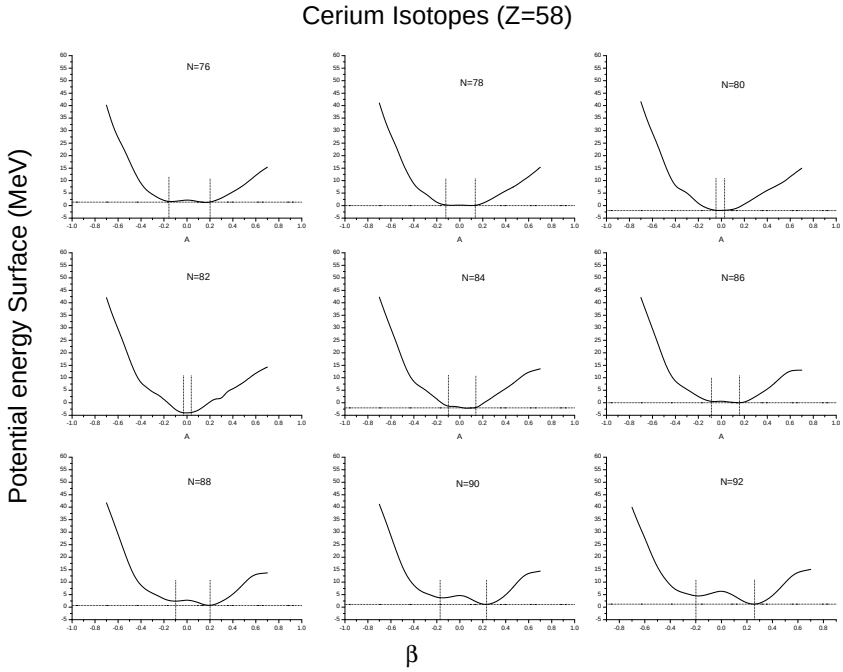

Fig. 5: Shape evolution for cerium isotopes from $N = 78$ to $N = 92$.

(v) This isotopic chain possesses a continuous shape/phase transition from spherical shapes toward the axially symmetric ones.

Submitted on May 2, 2015 / Accepted on May 22, 2015

References

1. Raman S., Nestor C. W. Jr. and Tikkanen P. *At. Data Nucl. Data Tables*, 2001, v. 78, 1.
2. Stone N. J., *At.Data Nucl.Data Tables*, 2005, v. 90, 75.
3. Boboshin I., Ishkhanov B., Komarov S., Orlin V., Peskov N., and Varlamov V. ND 2007 – International Conference on Nuclear Data for Science and Technology. Nice, France, April 22–27 2007.
4. Iachello F. and Arima, A. The Interacting Boson Model. Cambridge University Press, Cambridge, 1987.
5. Bayram T. *Rom. Journ. Phys.*, 2013, v. 58 (7–8), 931–938.
6. Bhagwat A., Viñas X., Centelles M., Schuck P., and Wyss R. *Phys. Rev. C*, 2010, v. 81, 044321.
7. Mohammed-Azizi B. and Medjadi D. E. *J. Phys. G : Nucl. Part. Phys.*, 2008, v. 35, 035101.
8. Cejna P., Jolie J., Casten R. F. *Rev. Mod. Phy.*, 2010, v. 82, 2155–2212.
9. Khalaf A. M., Gaballah N., Elgabry M. F. and Ghanim H. A. *Progress in Physics*, 2015, v. 11(2), 141–145.
10. Smith J. F. et al. *Phys. Lett.*, 2005, v. B625, 203.
11. Todd D. M. et al. *J. Phys. G. Nucl. Phys.*, 1984, v. 10, 1407.
12. Kirwan A. J., Ball G. C., Bishop E. J., Godfrey M. J., Nolan P. J., Thornley D. J., Love D. J. G. and Nelson A. H. *Phys. Rev. Lett.*, 1987, v. 58, 467.
13. Michelakakis E. et al. 4.International Conference on Nuclei Far From Stability, Helsingør, Denmark, 7–13 Jun 1981. In European Organization for Nuclear Research, Geneva, Switzerland, (20 Jul 1981), pp. 581–588.
14. Devi R., Sehgal B. D. and Khosa S. K. *Pramana Journal of Physics*, 2006, v. 67 (3), 467–475.
15. Bhat R. K., Devi R., and Khosa S. K. *Brazilian Journal of Physics*, 2003, v. 33 (2), 340–345.
16. Long Wen Hui, Ring Peter, Meng Jie, Giai Nguyen Van, and Bertulani Carlos A. *Phys. Rev. C*, 2010, v. 81, 031302.
17. Pittel S., Lei Y., Fu G. J. and Zhao Y. M. *Journal of Physics: Conference Series*, 2013, v. 445, 012031.
18. Moller P., Nix J. R., Myers W. D. and Swiatecki W. J. *At. Data Nucl. Data Tables*, 1995, v. 59, 185.
19. Goriely S., Samyn M., Bender M. and Pearson J. M. *Phys. Rev. C*, 2003, v. 68, 054325.
20. Delaroche J.-P., Girod M., Libert J., Goutte H., Hilaire S., Péru S., Pillet N., and Bertsch G. F. *Phys. Rev. C*,2010, v. 81, 014303.
21. Geng L., Toki H. and Meng J. *Progress of Theoretical Physics*, 2005, v. 113 (4), 785–800.
22. Mohammed-Azizi B. and Medjadi D. E. *Comput. Phys. Commun.*, 2004, v. 156, 241–282.
23. Mohammed-Azizi B. and Medjadi D. E. *Comput. Phys. Commun.*, 2007, v. 176, 634–635.
24. Mohammed-Azizi B. and Medjadi D. E. *Comput. Phys. Commun.*, 2014, v. 185, 3067–3068.
25. Stránský P., Frank A. and Bijker R. *Journal of Physics: Conference Series*, 2011, v. 322, 012018.
26. Mohammed-Azizi B. and Medjadi D. E. *Phys. Rev. C*, 2006, v. 74, 054302.
27. Mohammed-Azizi B. *Intern. Journal of Modern Physics C*, 2010, v. 21 (5), 681–694.
28. Myers W. D. and Swiatecki W. J. *Nucl. Phys. A*, 1966, v. 81, 1.
29. Cwiok S., Dudek J., Nazarewicz W. and Werner T. *Comput. Phys. Commun.*, 1987, v. 46, 379.
30. Pauli H. C. *Phys. Lett. C*, 1973, v. 7, 35.

31. Brack M., Damgaard L., Jensen A. S., Pauli H. C., Strutinsky V. M. and Wong C. Y. *Rev. Mod. Phys.*, 1972, v. 44, 320–405.
32. Kern B. D. et al. *Phys. Rev. C*, 1987, v. 36, 1514.
33. Gotz U., Pauli H. C., and Adler K. *Nucl. Phys. A*, 1971, v. 175, 481.
34. Hilaire S., Girod M. http://www-phynu.cea.fr/science_en_ligne/carte_potentiels_microscopiques/carte_potentiel_nucleaire.htm, Jan. 2015.
35. Casten R. F., Cakirli R. B. *Acta Physica Polonica B*, 2009, v. 40 (3), 493–502.
36. Anghel S., Danil G. C., Zamfir N. V., *Romanian Journ. Phys.*, 2009, v. 54 (3–4), 301–319.
37. Sarriguren P., Rodrıguez-Guzman R. R., Robledo L. M. *Journal of Physics: Conference Series*, 2010, v. 205, 012024.
38. http://www.nndc.bnl.gov/ensdf/, January 2015.

A Constants of the binding energy of the liquid drop model

The constants of (1) are defined as follows:

$$C_V = a_V \left[1 - \kappa I^2\right] \text{ (in the volume term)}$$

$$C_S = a_S \left[1 - \kappa I^2\right] \text{ (in the surface term)}$$

$$I = \frac{N - Z}{N + Z} \text{ (relative neutron excess)}$$

$$\varepsilon = +1 \text{ (even} - \text{even) (in the pairing term),}$$
$$0 \text{ (odd),}$$
$$-1 \text{ (odd} - \text{odd)}$$

$$C_C = \frac{3}{5}\frac{e^2}{r_0} \text{ (in the Coulomb term)}$$

$$C_d = \frac{\pi^2}{2}\left(\frac{a_0}{r_0}\right)^2 \frac{e^2}{r_0} \text{ (diffuseness correction)}$$

The last correction to the Coulomb energy takes into account that the liquid drop has not a sharp but a diffuse surface of the Woods-Saxon type. The diffuseness parameter is a_0 and the charge radius "contains" r_0 ($R_{ch} = r_0 A^{1/3}$).

B Constants of the Woods-Saxon mean potential

"Universal parameters" of the Woods-Saxon central and Spin-orbit potentials entering in (10).

Neutrons	
V_{0neut}=49.6(1-0.86I)	depth of cmf (MeV)
R_{Vneut}=1.347$A^{1/3}$	radius of cmf (fm)
λ=35.0 (dimensionless)	spin-orb. coupling strength
$R_{SO-neut}$=1.310$A^{1/3}$	Radius of somf (fm)
a_0=0.70	diffuseness of cmf (fm)
a_0=0.70	diffuseness of somf (fm)
Protons	
V_{0prot}=49.6(1+0.86I)	depth of cmf (MeV)
R_{Vprot}=1.275$A^{1/3}$	radius of cmf (fm)
λ=36.0 (dimensionless)	spin-orb. coupling strength
$R_{SO-nprot}$=1.200$A^{1/3}$	radius of somf (fm)
a_0=0.70	diffuseness of cmf (fm)
a_0=0.70	diffuseness of somf (fm)

cmf = central mean field
somf = spin-orbit mean field

Other Earths: Search for Life and the Constant Curvature

Megan M. Khoshyaran

Economics Traffic Clinic-ETC, 34 Avenue des champs Elyses, 75008 Paris, France
E-mail: megan.khoshyaran@wanadoo.fr

The objective of this paper is to propose a search methodology for finding other exactly similar earth like planets (or sister earths). The theory is based on space consisting of Riemann curves or highways. A mathematical model based on constant curvature, a moving frame bundle, and gravitational dynamics is introduced.

1 Introduction

The objective of this paper is to propose a search methodology that could show the way to finding other exactly similar earth like planets (or sister earths). The main idea in this paper lies behind the theory that space contains of what is called highways. The term highway refers to a path with no obstructions. Examples of obstructions are black holes and stars or any celestial objects with significant masses and gravitational forces. Paths are non-linear graphs.

Space is composed of these highways, on which there is at least one sister earth. Topologically highways are made up of constant Riemann curvatures, [1]. It is posited that sister earths are located at the points of constant curvature; more accurately, these are the points where two oppositely directed highways (or paths) with identical constant curvatures share a moving tangent frame where the coordinate frame is the derivative of their gravitational tensors with respect to the (x) coordinate.

A sister earth comes with its satellite (or a moon) just as earth has its satellite, the moon. A satellite is found at the point of intersection of two oppositely directed highways. The earth's moon provides a parallel highway to the earth's highway. So far the methods of detecting earth like exoplanets consist of observation through Hubble space telescope of extrasolar giant planets and their gravitational influence on parent stars, [2,3,4]. Transit method, [5], orbital brightness modulations, [6], timing variations, [7], gravitational microlensing, [8], direct imaging, [9], and polarimetry, [10], are among methods currently used for the detection of earth like exoplanets. In all these methods the main element of study is observation of light and gravitational changes as it distorts light around planets.

The advantage of the current theory proposed in this paper is that it provides an analytical approach based on Riemannian curvature, and the dynamics of gravitation mathematically represented by differential gravity calculations around the points of constant curvature. The important first step is to find pathways (or space highways) with constant curvatures. One Riemann path or space highway with constant curvature is known, and that is the Riemann path of the earth. The Riemann path of the moon is another known pathway or space highway that is parallel to the earth's Riemann path. Other Riemann paths can be traced out parallel to the earth's and the moon's Riemann paths or space highways. A path to a sister earth can be traced out assuming that it has the same curvature with different gravitational tensor described in the following section.

2 Space highways

Space highways are paths that extend to infinity. The word infinity is used to imply very long distances. These paths can be considered as Riemannian curves with constant curvatures. Riemann paths with constant curvatures contain no obstacles. Here, obstructions are mainly black holes, and massive stars, or any significant electrostatic system, moving with a certain velocity (v) corresponding to an electromagnetic momentum, (H).

In other words, any significant mass with inertia, momentum, and thus velocity that produces gravitational and electromagnetic forces. Vector $(\mathbf{H})$ represents the electromagnetic direction and magnitude. The electromagnetic momentum can be expressed as the multiplication of the vector $(\mathbf{H})$ by the velocity $(\mathbf{v})$, as $(\mathbf{H} \cdot \mathbf{v})$. The assumption of Riemann paths in dark regions of space is fundamental to the structure of the model to be introduced.

The earth's Riemann path with constant curvature can be constructed given the coordinates of the sun and the earth. Let's assume that the earth is in a stationary system $(\mathbf{K})$, where $[\mathbf{x}_\tau = (x, y, z, t) \in \mathbf{K}]$ denotes the coordinates and the system $(\mathbf{K})$ holds a homogeneous gravitational field, and gravitational acceleration equal to $[\gamma = (\gamma_x, \gamma_y, \gamma_z)]$. In system $(\mathbf{K})$, Newtonian laws hold in their most basic form, the same basic laws equally hold with respect to any other coordinate system moving in uniform translation with respect to $(\mathbf{K})$.

Let system $(\mathbf{K})$ represent the sun system. It is assumed that the coordinates of the sun are $(0, 0, 0, 0)$, meaning that the sun is considered to be the first solar system of its kind. Let's assume that earth is located in a second coordinate system $(\mathbf{K}')$, where $[\mathbf{x}_\sigma = (x', y', z', t') \in \mathbf{K}']$ signifies the coordinates in this system. It is also assumed that for any other coordinate system outside of the two systems $(\mathbf{K})$ and $(\mathbf{K}')$, the laws of general relativity hold with respect to the two coordinate systems.

By this it is meant that the velocity of light (c) in vacuum

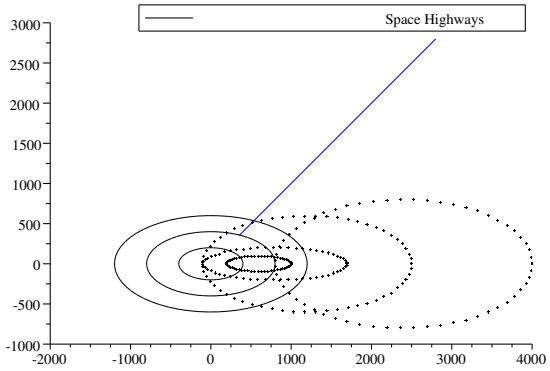

Fig. 1: A graphical representation of Riemann Paths.

is constant, [11], and in combination with the principles of relativity, follows the relativity of simultaneity, the Lorentz transformation rules, and the related laws indicating the behaviour of bodies in motion. The laws of geometry are taken directly as laws relating to relative positions of mass at rest. The laws of kinematics are to be taken as laws which describe the relation of a solid body with respect to another in terms of their distance from each other in definite length independent of the location and the orientation of the two bodies in time. An example of space highways is given in Fig. 1.

Let's consider the earth as an event point in system ($\mathbf{K}'$) in a uniform constant rotation in a finite space with respect to system ($\mathbf{K}$). The curvature from the event point to the stationary system ($\mathbf{K}$) is given by (1):

$$ds^2 = \sum_{\sigma\tau} G_{\sigma\tau} dx_\sigma dx_\tau. \tag{1}$$

(dx_σ) corresponds to differentials in system ($\mathbf{K}'$), (σ) represents the (x', y', z', t') coordinate system in ($\mathbf{K}'$), and (dx_τ) corresponds to differentials in system ($\mathbf{K}$), where τ represents the (x, y, z, t) coordinate system. ($G_{\sigma\tau}$) is the gravitation tensor, signifying the gravitational forces exerted mutually between systems ($\mathbf{K}$) and ($\mathbf{K}'$) multiplied by the differential of the electromagnetic force ($d\mathbf{H}$).

The gravitation tensor ($G_{\sigma\tau}$) is a matrix obtained by multiplying matrix ($g_{\sigma\tau}$), the matrix of the differentials of the gravitational force, given as:

$$g_{\sigma\tau} = \begin{pmatrix} \frac{\partial x'}{\partial x} & \frac{\partial x'}{\partial y} & \frac{\partial x'}{\partial z} & \frac{\partial x'}{\partial t} \\ \frac{\partial y'}{\partial x} & \frac{\partial y'}{\partial y} & \frac{\partial y'}{\partial z} & \frac{\partial y'}{\partial t} \\ \frac{\partial z'}{\partial x} & \frac{\partial z'}{\partial y} & \frac{\partial z'}{\partial z} & \frac{\partial z'}{\partial t} \\ \frac{\partial t'}{\partial x} & \frac{\partial t'}{\partial y} & \frac{\partial t'}{\partial z} & \frac{\partial t'}{\partial t} \end{pmatrix}$$

with matrix ($d\mathbf{H}$), the matrix of the differentials of the electromagnetic force or the matrix of the curl of ($\mathbf{H}$) given by (2):

$$G_{\sigma\tau} = g_{\sigma\tau} \times d\mathbf{H}. \tag{2}$$

The matrix of the curl of ($\mathbf{H}$), the electromagnetic force is given as:

$$d\mathbf{H} = \begin{pmatrix} \left(\frac{\partial H_{x'}}{\partial z} - \frac{\partial H_{z'}}{\partial x}\right) & 0 & 0 & 0 \\ 0 & \left(\frac{\partial H_{y'}}{\partial x} - \frac{\partial H_{x'}}{\partial y}\right) & 0 & 0 \\ 0 & 0 & \left(\frac{\partial H_{z'}}{\partial y} - \frac{\partial H_{y'}}{\partial z}\right) & 0 \\ 0 & 0 & 0 & 1 \end{pmatrix}.$$

In the presence of significant mass, and the electromagnetic momentum ($\mathbf{H} \cdot \mathbf{v}$), the diagonal entries of the curl of ($\mathbf{H}$) are given in (3)–(5) as:

$$\left(\frac{\partial H_{x'}}{\partial z} - \frac{\partial H_{z'}}{\partial x}\right) = \frac{1}{c} \times \rho \times v_{x'} \tag{3}$$

$$\left(\frac{\partial H_{y'}}{\partial x} - \frac{\partial H_{x'}}{\partial y}\right) = \frac{1}{c} \times \rho \times v_{y'} \tag{4}$$

$$\left(\frac{\partial H_{z'}}{\partial y} - \frac{\partial H_{y'}}{\partial z}\right) = \frac{1}{c} \times \rho \times v_{z'}. \tag{5}$$

In (3)–(5), (c) is the velocity of light, (ρ) is the volume-density charge of a mass, and the vector ($\mathbf{v}$) is the velocity of the electromagnetic momentum where $\mathbf{v} = (\mathbf{v_{x'}}, \mathbf{v_{y'}}, \mathbf{v_{z'}})$.

The curvature of the system ($\mathbf{K}$)-($\mathbf{K}'$) in a finite region between an event-point in system ($\mathbf{K}'$), and a stationary point in system ($\mathbf{K}$) such as the earth and the sun is well-known to be an ellipsoid in the form expressed by (6) as:

$$S = G_{\sigma\tau} \times \left(\frac{(\mathbf{x}_\sigma - \mathbf{x}_\tau)^2}{\mathbf{a^2}}\right). \tag{6}$$

($\mathbf{x}_\sigma$) is the vector of coordinates in the ($\mathbf{K}'$) system, where $\mathbf{x}_\sigma = (\mathbf{x}', \mathbf{y}', \mathbf{z}', \mathbf{t}')$, and ($\mathbf{x}_\tau$) is the vector of coordinates in the ($\mathbf{K}$) system, where $\mathbf{x}_\sigma = (\mathbf{x}, \mathbf{y}, \mathbf{z}, \mathbf{t})$. Equation (6) can be rewritten with respect to the coordinates given in (7):

$$\begin{aligned} S = A_1 \times \left(\frac{(x - x')^2}{{a_1}^2}\right) + A_2 \times \left(\frac{(y - y')^2}{{a_2}^2}\right) + \\ + A_3 \times \left(\frac{(z - z')^2}{{a_3}^2}\right) + A_4 \times \left(\frac{(t - t')^2}{{a_4}^2}\right). \end{aligned} \tag{7}$$

The coefficients ($\mathbf{A}$) are the columns of ($G_{\sigma\tau}$), the gravitation tensor. The denominators in (7), (a_1, a_2, a_3, a_4) are constants less than 1, and the coefficients ($\mathbf{A} = (\mathbf{A_1}, \mathbf{A_2}, \mathbf{A_3}, \mathbf{A_4})$) are given at the top of the next page.

The time (t) in the ($\mathbf{K}$) system is formulated in a relativistic sense as in (8):

$$t = \frac{\left(1 - \frac{v}{c}\right) \times t'}{\sqrt{1 - \frac{v^2}{c^2}}}. \tag{8}$$

$$\mathbf{A} = \begin{pmatrix} \frac{\partial x'}{\partial x} \times \left(\frac{\partial H_{x'}}{\partial z} - \frac{\partial H_{z'}}{\partial x}\right) & 0 & 0 & 0 \\ 0 & \frac{\partial y'}{\partial y} \times \left(\frac{\partial H_{y'}}{\partial x} - \frac{\partial H_{x'}}{\partial y}\right) & 0 & 0 \\ 0 & 0 & \frac{\partial z'}{\partial z} \times \left(\frac{\partial H_{z'}}{\partial y} - \frac{\partial H_{y'}}{\partial z}\right) & 0 \\ 0 & 0 & 0 & \frac{\partial t'}{\partial t} \times 1 \end{pmatrix}$$

The elements of the coefficient matrix (**A**) are:

$$A_{11} = \frac{\partial x'}{\partial x} \times \left(\frac{\partial H_{x'}}{\partial z} - \frac{\partial H_{z'}}{\partial x}\right) = \frac{1}{c} \times \rho \times \gamma_{x'} \tag{9}$$

$$A_{22} = \frac{\partial y'}{\partial y} \times \left(\frac{\partial H_{y'}}{\partial x} - \frac{\partial H_{x'}}{\partial y}\right) = \frac{1}{c} \times \rho \times \gamma_{y'} \tag{10}$$

$$A_{33} = \frac{\partial z'}{\partial z} \times \left(\frac{\partial H_{z'}}{\partial y} - \frac{\partial H_{y'}}{\partial z}\right) = \frac{1}{c} \times \rho \times \gamma_{z'} \tag{11}$$

and

$$A_{44} = \frac{\partial t'}{\partial t} = \frac{\left(\sqrt{1 - \frac{v_{x'}{}^2}{c^2}}\right)}{\left(1 - \frac{v_{x'}}{c}\right)} \times (t' - t)\,. \tag{12}$$

In (9–11), the vector (γ) is the vector of acceleration of the electromagnetic momentum ($\mathbf{H} \cdot \mathbf{v}$), where $\gamma = (\gamma_{\mathbf{x}'}, \gamma_{\mathbf{y}'}, \gamma_{\mathbf{z}'})$. The assumption is that the curvatures of Riemann paths or space highways should be formulated in exactly the same manner as the curvature formulated for the system (**K**)-(**K**′). This assumption can be justified since any event point (earth like planet) on a Riemann curve of constant curvature should exhibit the same characteristics as the event-point earth.

An important element to consider, is how to find the coordinates of an event point (earth like planet) with respect to the coordinate system (**K**). These coordinates are arbitrary since the only point of reference is the system (**K**). All the same, let's assign coordinates to an event point (earth like planet) as ($\mathbf{x}_\nu$) where [$\mathbf{x}_\nu = (\mathbf{x}'', \mathbf{y}'', \mathbf{z}'', \mathbf{t}'') \in \mathbf{K}''$] denotes the coordinate system in (**K**′′). The coordinates of the event point (earth like planet) can be determined given that the event point is in the finite region from the sun. The event point (earth like planet) in the dark region is chosen assuming that it is on an ellipsoid parallel to the ellipsoid that contains the coordinate system (**K**), with coordinates $\mathbf{x}_\tau = (\mathbf{x}, \mathbf{y}, \mathbf{z}, \mathbf{t})$, in other words the sun.

The curvature can be formulated in (9) as:

$$ds'^2 = \sum_{\nu\sigma} g^{\nu\sigma} \times G_{\sigma\tau} \times (dx_\sigma dx_\tau)\, dx_\nu. \tag{13}$$

The tensor ($g^{\nu\sigma}$) represents the gravitational force exerted between the two coordinate systems (**K**) and (**K**′′). Given that the coordinate system (**K**′′) is in a finite region with respect to the coordinate system (**K**), the tensor ($g^{\nu\sigma}$) takes on values equal to the Lorentz factor as is given in the first matrix at the top of the next page.

The Lorentz factor gives length contraction and time dilation. As the function of velocity (v), the Lorentz factor starts at value (1) at ($v = 0$), and approaches infinity as ($v \to c$), the velocity of a particle approaches the speed of light (c). The solution to differential equation (9) is an ellipsoid similar to the one given in (6), and its extended form similar to (7) is given in (10) as:

$$S' = \mathbf{B} \times \left(\frac{(\mathbf{x}_\nu - \mathbf{x}_\tau)^2}{\mathbf{b}^2}\right) \tag{14}$$

$$\begin{aligned} S = B_1 \times \left(\frac{(x'' - x)^2}{{b_1}^2}\right) + B_2 \times \left(\frac{(y'' - y)^2}{{b_2}^2}\right) + \\ + B_3 \times \left(\frac{(z'' - z)^2}{{b_3}^2}\right) + B_4 \times \left(\frac{(t'' - t)^2}{{b_4}^2}\right) = 1. \end{aligned} \tag{15}$$

The denominators in (11), (b_1, b_2, b_3, b_4) are constants less than 1, and the coefficients $\mathbf{B} = (\mathbf{B_1}, \mathbf{B_2}, \mathbf{B_3}, \mathbf{B_4})$ are given in the second matrix at the top of the next page.

The elements of the coefficient matrix (**B**) are:

$$\begin{aligned} B_{11} &= -\left(\frac{\partial x''}{\partial x} \times \frac{1}{\sqrt{1 - \frac{v^2_{x''}}{c^2}}}\right) \\ &= -\left(\frac{1}{\sqrt{1 - \frac{v^2_{x''}}{c^2}}}\right) \times |\, x'' - x\,| \end{aligned} \tag{16}$$

$$\begin{aligned} B_{22} &= -\left(\frac{\partial x''}{\partial x} \times \frac{1}{\sqrt{1 - \frac{v^2_{x''}}{c^2}}}\right) \\ &= -\left(\frac{1}{\sqrt{1 - \frac{v^2_{x''}}{c^2}}}\right) \times |\, y'' - y\,| \end{aligned} \tag{17}$$

$$\begin{aligned} B_{33} &= -\left(\frac{\partial x''}{\partial x} \times \frac{1}{\sqrt{1 - \frac{v^2_{x''}}{c^2}}}\right) \\ &= -\left(\frac{1}{\sqrt{1 - \frac{v^2_{x''}}{c^2}}}\right) \times |\, z'' - z\,| \end{aligned} \tag{18}$$

$$g^{\nu\sigma} = \begin{pmatrix} -\frac{1}{\sqrt{1-\frac{v^2_{x''}}{c^2}}} & 0 & 0 & 0 \\ 0 & -\frac{1}{\sqrt{1-\frac{v^2_{y''}}{c^2}}} & 0 & 0 \\ 0 & 0 & -\frac{1}{\sqrt{1-\frac{v^2_{z''}}{c^2}}} & 0 \\ 0 & 0 & 0 & \frac{\partial t''}{\partial t} \times \frac{1}{\sqrt{1-\frac{v^2_{x''}}{c^2}}} \end{pmatrix}$$

$$\mathbf{B} = \begin{pmatrix} -\frac{\partial x''}{\partial x} \times \frac{1}{\sqrt{1-\frac{v^2_{x''}}{c^2}}} & 0 & 0 & 0 \\ 0 & -\frac{\partial y''}{\partial y} \times \frac{1}{\sqrt{1-\frac{v^2_{y''}}{c^2}}} & 0 & 0 \\ 0 & 0 & -\frac{\partial z''}{\partial z} \times \frac{1}{\sqrt{1-\frac{v^2_{z''}}{c^2}}} & 0 \\ 0 & 0 & 0 & -\frac{\partial t''}{\partial t} \times \frac{1}{\sqrt{1-\frac{v^2_{x''}}{c^2}}} \end{pmatrix}$$

and

$$B_{44} = \frac{\partial t''}{\partial t} \times \left(\frac{1}{\sqrt{1-\frac{v^2_{x''}}{c^2}}} \right) = \left(\frac{1}{1-\frac{v_{x''}}{c}} \right) \times (t'' - t) \tag{19}$$

where $(\mid x'' - x \mid)$ is the absolute distance.

Any event point in the dark regions of space that does not violate the Lorentz factor impact of the gravitational force between the two coordinate systems (**K**) and (**K**″) can be considered to be on the constant curvature. The event point earth like planet should be found on such a constant curvature. Any other significant mass such as a black hole or a star would create discontinuity and thus disrupts the Riemann path.

Fig. 2 provides a graphical representation of an ellipsoidal curve with an event point (earth). Fig. 2 depicts the rotation of the earth around the sun scaled down to (100^{-3}) of the actual size. Fig. 3 demonstrates a Riemann path with respect to the sun system. Fig. 4 demonstrates Riemann paths with respect to the sun system.

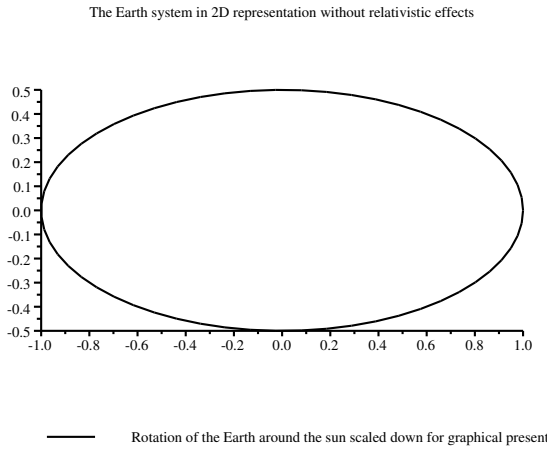

Fig. 2: A graphical representation of the rotation of the earth around the sun (the earth system).

3 Other earths

An event point (earth), is located at the point of constant curvature of two opposing Riemann paths or space highways, where the two curves share common points. Let (S') be the Riemann path of constant curvature of an ellipsoidal form given in (13). Let (S_{c_2}) be a Riemann path with a singular event point earth. The event point on (S_{c_2}) has a mass (M), and a density (ρ), and a velocity (v), equal to that of the earth. The values of mass, density, and velocity of the event point earth of the space highway (S_{c_2}) is independent of it's coordinates. Assuming that this condition holds, then the Riemann path (S_{c_2}) is in such a region of space where (S_{c_2}) is of constant curvature, and thus assumes an ellipsoidal form of type given in (13). The event point earth conserves its momentum and energy. The curvature (s_{c_2}) can be written as in (12).

The coordinates of this solar system are the same as the earth's solar system with the exception that the new sun's coordinates are that of our sun added the distance between the

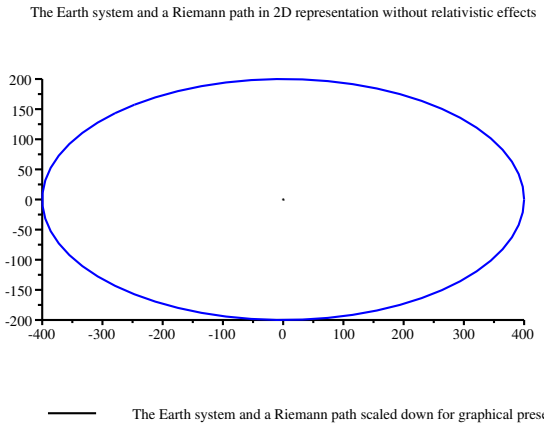

Fig. 3: A graphical representation of a Riemann path with respect to the sun system.

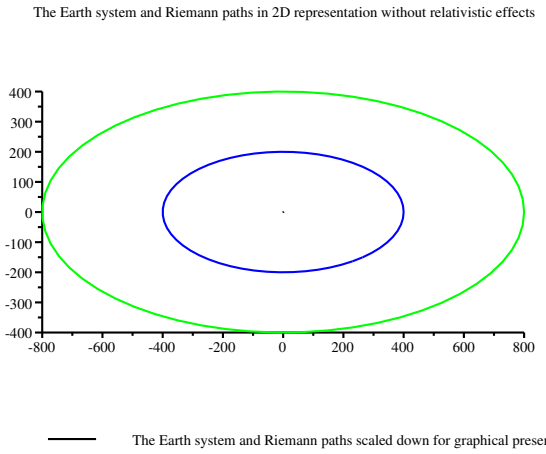

Fig. 4: A graphical representation of Riemann paths with respect to the sun system.

two stars. The coordinates of the new sun are

$$\mathbf{x}_{\tau'} = [(\mathbf{x}_{\tau'} + \Xi), \mathbf{y}_{\tau'}, \mathbf{z}_{\tau'}, \mathbf{t}_{\tau'}]$$

where (Ξ) is the distance between the two stars. The coordinates of the event point earth are

$$(\mathbf{x}_{\mathbf{c}_2}\eta) = [(\mathbf{x}_{\mathbf{c}_2} + \mathbf{\Gamma}), \mathbf{y}_{\mathbf{c}_2}, \mathbf{z}_{\mathbf{c}_2}, \mathbf{t}_{\mathbf{c}_2}]$$

where (Γ) is the distance from the sun to the point of constant curvature where the two Riemann paths meet.

The ellipsoidal form of the Riemann path (S_{c_2}) is given in (13) as:

$$ds^2_{c_2} = \sum_{\tau'\eta} G^{\tau'\eta}_{c_2} dx_{\tau'} dx^{\eta}_{c_2} \tag{20}$$

$$S_{c_2} = -\mathbf{G}^{\tau'\eta}_{\mathbf{c}_2} \times \frac{\left(\mathbf{x}_{\tau'} - \mathbf{x}^{\eta}_{\mathbf{c}_2}\right)^2}{\mathbf{b}^2_{\mathbf{c}_2}}. \tag{21}$$

The denominators in (13),

$$\left(\mathbf{b}_{\mathbf{c}_2} = \mathbf{b}^{\mathbf{c}_2}_{\mathbf{1}}, \mathbf{b}^{\mathbf{c}_2}_{\mathbf{2}}, \mathbf{b}^{\mathbf{c}_2}_{\mathbf{3}}, \mathbf{b}^{\mathbf{c}_2}_{\mathbf{4}}\right)$$

are constants less than 1, and the coefficients

$$-\mathbf{G}^{\tau'\eta}_{\mathbf{c}_2} = (-A^{c_2}_1, -A^{c_2}_2, -A^{c_2}_3, A^{c_2}_4)$$

are given at the top of the next page.

The elements of the coefficient matrix $(-\mathbf{G}^{\tau'\eta}_{\mathbf{c}_2})$ are:

$$-A^{c_2}_{11} = -\frac{\partial x^{\eta}_{c_2}}{\partial x_{\tau'}} \times \left(\frac{\partial H_{x^{\eta}_{c_2}}}{\partial z_{\tau'}} - \frac{\partial H_{z^{\eta}_{c_2}}}{\partial x_{\tau'}}\right) = \frac{1}{c} \times \rho \times -\gamma_{x^{\eta}_{c_2}} \tag{22}$$

$$-A^{c_2}_{22} = -\frac{\partial y^{\eta}_{c_2}}{\partial y_{\tau'}} \times \left(\frac{\partial H_{y^{\eta}_{c_2}}}{\partial x_{\tau'}} - \frac{\partial H_{x^{\eta}_{c_2}}}{\partial y_{\tau'}}\right) = \frac{1}{c} \times \rho \times -\gamma_{y^{\eta}_{c_2}} \tag{23}$$

$$-A^{c_2}_{33} = -\frac{\partial z^{\eta}_{c_2}}{\partial z_{\tau'}} \times \left(\frac{\partial H_{z^{\eta}_{c_2}}}{\partial y_{\tau'}} - \frac{\partial H_{y^{\eta}_{c_2}}}{\partial z_{\tau'}}\right) = \frac{1}{c} \times \rho \times -\gamma_{z^{\eta}_{c_2}} \tag{24}$$

and

$$A_{44} = \frac{\partial t''}{\partial t} = \frac{\sqrt{1 - \frac{\left(v_{x^{\eta}_{c_2}}\right)^2}{c^2}}}{\left(1 - \frac{v_{x^{\eta}_{c_2}}}{c}\right)} \times (t'' - t). \tag{25}$$

$(-\gamma_{x^{\eta}_{c_2}})$ states that the acceleration on the Riemann path (S_{c_2}) should be opposite of the acceleration on the (S') curve. In the above matrix the (x_{c_2}) coordinate should be taken equal to $(x_{c_2} + \Gamma)$.

The event point earth is located where

$$\frac{-\partial \mathbf{G}^{\nu\eta}_{\mathbf{c}_2}}{\partial x^{\eta}_{c_2}} = \frac{\partial \mathbf{B}_{\mathbf{x}_\nu}}{\partial x_\nu}$$

the derivative of the gravitational tensor $(-\mathbf{G}^{\tau'\eta}_{\mathbf{c}_2})$ belonging to the (c_2) Riemann path with respect to the coordinates of the (c_2) solar system, is equal to the derivative of the gravitational tensor of the (S') Riemann path with respect to its coordinate system. In Fig. 5, the event point earth can be found where the green ellipse Riemann path (S') and the Riemann path (c_2) (the red ellipse) meet. Fig. 6 depicts the tangent vector at the event point earth.

It should be stated that the magnitude of the electromagnetic force of the event point earth $(\mathbf{H}_{\mathbf{x}^{\eta}_{\mathbf{c}_2}})$ is equal to the magnitude of the electromagnetic force of the solar system's earth, $(\mathbf{H})$,

$$|\, \mathbf{H}_{\mathbf{x}^{\eta}_{\mathbf{c}_2}} \,| = |\, \mathbf{H} \,|\, .$$

Consequently, the curl of $(\mathbf{H}_{\mathbf{x}^{\eta}_{\mathbf{c}_2}})$, and the curl of $(\mathbf{H})$ should be equal. Thus the density, the volume-density charge of the mass, and the velocity of the event point earth are equal to that of the solar system's earth.

Let (T) be the set of all frames at all points of Riemann path (c_2). Let $[(U_\alpha, X^\alpha)_{\alpha\in c_2}]$, represent all pairs where (U_α)

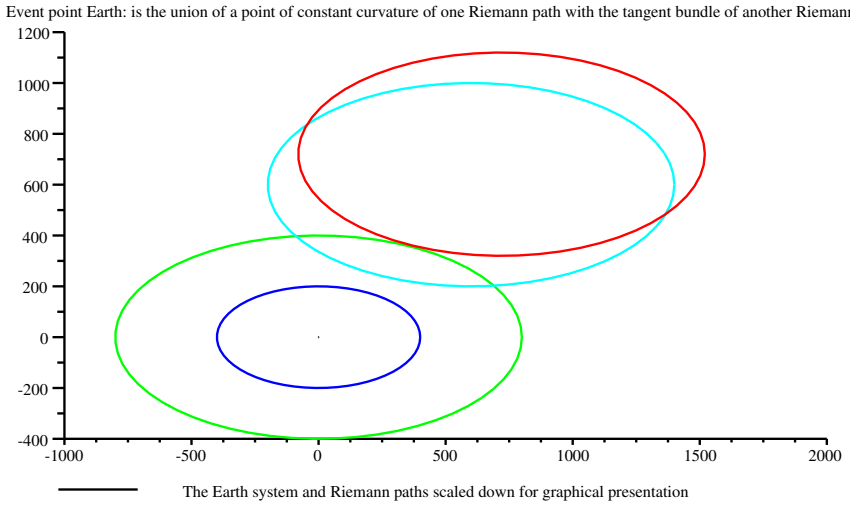

Fig. 5: A graphical representation of the event point earth.

$$-\mathbf{G}_{\mathbf{c_2}}^{\tau'\eta} = \begin{pmatrix} -\frac{\partial x_{c_2}^{\eta}}{\partial x_{\tau'}} \times \left(\frac{\partial H_{x_{c_2}^{\eta}}}{\partial z_{\tau'}} - \frac{\partial H_{z_{c_2}^{\eta}}}{\partial x_{\tau'}} \right) & 0 & 0 & 0 \\ 0 & -\frac{\partial y_{c_2}^{\eta}}{\partial y_{\tau'}} \times \left(\frac{\partial H_{y_{c_2}^{\eta}}}{\partial x_{\tau'}} - \frac{\partial H_{x_{c_2}^{\eta}}}{\partial y_{\tau'}} \right) & 0 & 0 \\ 0 & 0 & -\frac{\partial z_{c_2}^{\eta}}{\partial z_{\tau'}} \times \left(\frac{\partial H_{z_{c_2}^{\eta}}}{\partial y_{\tau'}} - \frac{\partial H_{y_{c_2}^{\eta}}}{\partial z_{\tau'}} \right) & 0 \\ 0 & 0 & 0 & \frac{\partial t_{c_2}^{\eta}}{\partial t_{\tau'}} \times 1 \end{pmatrix}$$

is an open subset of (T), and $(X^{\alpha} = (X_1^{\alpha}, ..., X_n^{\alpha}))$ is a moving frame on (U_{α}), then

$$\left(U, \frac{-\partial \mathbf{G}_{\mathbf{c_2}}^{\nu\eta}}{\partial X^{\alpha}} = \frac{\partial \mathbf{B}_{\mathbf{x}_{\nu}}}{\partial X^{\beta}} \right) \in (U_{\alpha}, X^{\alpha})_{\alpha \in c_2},$$

where $(X^{\beta} = (X_1^{\beta}, ..., X_n^{\beta}))$ is a moving frame on (S'). This gives the following set of differential equations for each $(\alpha \in c_2)$, and $(\beta \in S')$:

$$\begin{aligned} &\frac{\partial}{\partial X^{\alpha}} \left(\frac{\partial X^{\alpha}}{\partial x_{\tau'}} \times \left(\frac{\partial H_{X^{\alpha}}}{\partial z'_{\tau}} - \frac{\partial H_{X^{\alpha}}}{\partial x'_{\tau}} \right) \right) \\ &= -\frac{\partial}{\partial X^{\beta}} \left(\frac{\partial X^{\beta}}{\partial x''} \times \frac{1}{\sqrt{1 - \frac{v_{x''}^2}{c^2}}} \right) \end{aligned} \tag{26}$$

and

$$\frac{\partial}{\partial X^{\alpha}} \left(\frac{\partial t_{c_2}^{\eta}}{\partial t_{\nu}} \times 1 \right) = -\frac{\partial}{\partial X^{\beta}} \left(\frac{\partial t'}{\partial t} \times \frac{1}{\sqrt{1 - \frac{v_{x''}^2}{c^2}}} \right). \tag{27}$$

The equalities in (26) and (27) mean that the moving frame contains an open set of points $(X^{\alpha} = X^{\beta})$ where accelerations on the two Riemann paths (c_2) and (S') are equal. For (26) and (27) to hold a condition is imposed. The condition is that (26) and (27) must respect the linear translation $(L_{n\times n}, \Re)$, where (n) is the dimension of a matrix. If (M) was a (2×2) matrix , then the Jacobian of (M) would be equal to 1, $([M] = 1)$. This implies that the tangent bundle forms an isomorphic group to $(\Re^1)$. Matrix (M) is given at the top of the next page. $[M]$ is given by (28) below:

$$\begin{aligned} [M] = &\frac{\partial}{\partial X^{\alpha}} \left(\frac{\partial X^{\alpha}}{\partial x_{\tau'}} \times \left(\frac{\partial H_{X^{\alpha}}}{\partial z'_{\tau}} - \frac{\partial H_{X^{\alpha}}}{\partial x'_{\tau}} \right) \right) \times \\ &\times \left(-\frac{\partial}{\partial X^{\beta}} \left(\frac{\partial t'}{\partial t} \times \frac{1}{\sqrt{1 - \frac{v_{x''}^2}{c^2}}} \right) \right) \\ &- \frac{\partial}{\partial X^{\alpha}} \left(\frac{\partial t_{c_2}^{\eta}}{\partial t_{\nu}} \times 1 \right) \times \left(-\frac{\partial}{\partial X^{\beta}} \left(\frac{\partial X^{\beta}}{\partial x''} \times \frac{1}{\sqrt{1 - \frac{v_{x''}^2}{c^2}}} \right) \right) \\ &= 1. \end{aligned} \tag{28}$$

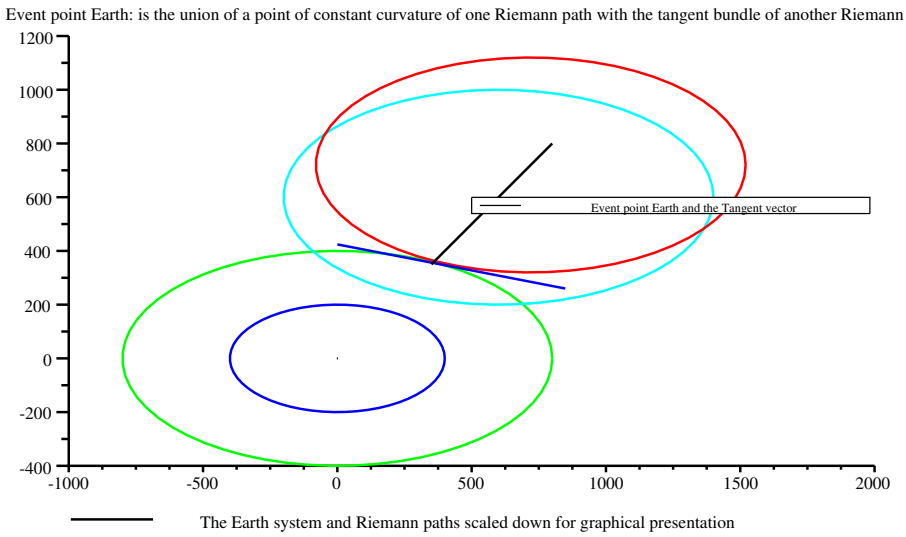

Fig. 6: Tangent vector at the event point earth.

$$M = \begin{pmatrix} \frac{\partial}{\partial X^\alpha}\left(\frac{\partial X^\alpha}{\partial x_{\tau'}} \times \left(\frac{\partial H_{X^\alpha}}{\partial z'_\tau} - \frac{\partial H_{X^\alpha}}{\partial x'_\tau}\right)\right) & \frac{\partial}{\partial X^\alpha}\left(\frac{\partial t^\eta_{c_2}}{\partial t_\nu} \times 1\right) \\ -\frac{\partial}{\partial X^\beta}\left(\frac{\partial X^\beta}{\partial x''} \times \frac{1}{\sqrt{1-\frac{v^2_{x''}}{c^2}}}\right) & -\frac{\partial}{\partial X^\beta}\left(\frac{\partial t'}{\partial t} \times \frac{1}{\sqrt{1-\frac{v^2_{x''}}{c^2}}}\right) \end{pmatrix}$$

(M) is the representation of $(\Re^1)$ in the (2×2) matrix form, thus is an invertible linear transformation of the tangent bundle. Given that the Riemann path is of constant curvature, then the implication is that the tangent bundle is invariant with respect to space-time. This condition would give the point on the (S_{c_2}) path that touches the (S') Riemann path. Therefore, it traces out the movement of the event point earth.

4 Conclusion

In this paper a new methodology is introduced that gives a mathematical approach to finding other exactly similar earth like planets. The mathematical model is based on finding what is called "space highways" or "Riemann paths". The characteristic of these highways is that they are found in the dark regions or non-deformed by gravitational forces regions of space, where there are no stars, or black holes, or planets. Riemann paths are considered as paths of constant curvature. Space highways are modelled as ellipsoidal forms with coefficients as columns of a gravitational tensor.

It is assumed that the coordinates of the sun are $(0, 0, 0, 0)$, meaning that the sun is considered to be the first solar system of its kind. This assumption is justified, since there is no evidence to the contrary to this day.

Space highways or Riemann paths are parallel to each other if they are in the same direction. The location of the event point earth (or exactly similar earth type planet) is where a Riemann path or space highway intersects at points of constant curvature with another space highway coming from an opposite direction. The movement of the event point earth is traced out where the two Riemann paths share the same tangent bundle. It is hoped that the search methodology introduced in this paper opens up a new possibility of finding planets that harbor life as we know it.

Acknowledgements

This research has made use of the Exoplanet Orbit Database and the Exoplanet Data Explorer at exoplanets.org.

Submitted on May 27, 2015 / Accepted on May 28, 2015

References

1. Wolfe J. A. Spaces of Constant Curvature. AMS Chelsea Publishing, Providence, 2000.
2. Eunkyu H., Wang S. X., Wright J. T., Feng Y. K., Zhao M., Fakhouri O., Brown J. I., Hancock C. Exoplanet Orbit Database. II. Updates to Exoplanets.org. *Publications of the Astronomical Society of the Pacific*, 2014, v. 126 (943), 827–837. California Planet Survey. http://exoplanets.org/, 14 October 2014.

3. Extrasolar Planet Search Programme at Haute-Provence Observatory. http://obswww.unige.ch/ udry/planet/elodie.html, 14 October 2014.
4. The Extrasolar Planets Encyclopaedia. http://exoplanet.eu, 14 October 2014.
5. Deming D., Seager S., Richardson J. Infrared radiation from an extrasolar planet. *Nature*, 2005, v. 434, 740–743.
6. Jenkin J. M., Doyle L. R. Detecting reflected light from close-in giant planets using space-based photometers. *Astrophysical Journal*, 2003, v. 595, 429–445.
7. Beaulieu J. P. Discovery of a cool planet of 5.5 Earth masses through gravitational microlensing. *Nature*, 2005, v. 439, 437–440.
8. Janson M., Brandener W., Henning T., Zinnecker H. Early come on + adaptive optics observations of GQ Lupi and its sub stellar companion. *Astronomy and Astrophysics*, 2006, v. 453 (2), 609–614.
9. Einstein A. On the Influence of Gravitation on the Propagation of Light. *Annalen der Physik*, 1911, v. 35, 898–908.

On the Possible Mechanism of Interaction of High-Energy Particles with Nuclei

Mirzajan A. Asimov and Takhir R. Akhmedov

333 S. Webster Ave., Suite 4, Norman, OK 73069, USA. E-mail: TakhirAkhmedov@yandex.ru

Based on an analysis of classical views stating that a charged particle creates certain magnetic field around its trajectory, we draw a conclusion about possible polarization of target nuclei within the magnetic field of approaching charged particle.

1 Introduction

While studying of scattering of electrons and neutrons by nuclei Mott [1] and J. Schwinger [2] suggested the mechanism of interaction of the scattering particle's magnetic moment with Coulomb field of a nucleus. Such scattering has been known as Mott-Schwinger interaction. Polarization of scattered particles is considered within the framework of this interaction [3].

In the present study, the interaction of the magnetic field of the scattering charged particles with the magnetic moment of nuclei is investigated.

It was demonstrated earlier that within the framework of this interaction the nucleus is also polarized. Spin of the nucleus interacting with the fast-moving (primary) charged particle orient itself in the plane perpendicular to the direction of the primary particle's momentum.

2 Magnetic field of the charged particle

The charged particle moving with the velocity v induces magnetic field H wrapped around its path. H depends on the distance from the charged particle as follows [4]:

$$H = \frac{e\,v\sin\theta}{r^2}\,, \tag{1}$$

where e is the charge of the scattered particle, r is the distance from the particle, and θ is the angle between the direction of the particle's velocity and r. Using this expression, one can calculate the intensity of the magnetic field H as a function of r and the speed of the particle with $\beta \sim 1$. It is assumed that laws of electromagnetism apply for small distances down to 10^{-13} cm. The calculations are presented in Table 1.

The numbers in the Table 1 indicate that pretty strong fields still not achieved by any experimental instrument. As it is known the magnetic field of a single charged particle has rotational characteristics.

3 Interaction of the magnetic field of the charged particle with the magnetic field of the nucleus

Magnetic charge of the scattering particle functions as an external magnetic field in respect to the nucleus. However, specific characteristic of the rotational magnetic field must be accounted for. Magnetic intensity lines are in the plane that is perpendicular to the direction of the particle's velocity. At the same time the vector of the magnetic field H at any arbitrary point on that plane at the distance r from the path of the particle is tangential to the circle of the radius r, and the direction of H is determined by the right-hand screw rule.

Let's consider that the nucleus is not exactly in the center of such a circle, but instead at some distance r from it. One can estimate the energy of interaction of the magnetic moment of the nucleus, μ, and the field H at distance r:

$$U = \mu H\,. \tag{2}$$

One has to take into consideration that magnetic moment acts like a top, and, in non-relativistic case, precession of the nucleus is simple Larmor precession. Relativistic case was described by Bargman et al [5].

Following Bargman, one can consider the case when the angle between the spin of the nucleus and magnetic field H is close to $\frac{\pi}{2}$. The spin will start precessing around the magnetic field H with the frequency

$$\Omega = \omega L\left(\frac{g}{2} - 1\right), \tag{3}$$

where $\omega L = \frac{e}{m\gamma} H$ is the frequency of Larmor precession, g is gyromagnetic ratio, and $\gamma = (1–\beta^2)–2$. It follows that

$$\Omega = \frac{eH}{m\gamma}\left(\frac{g}{2} - 1\right). \tag{4}$$

As Ω can be expressed as $\Omega = \frac{2\pi}{t}$ and for those nuclei whose spin satisfies the condition of $\frac{g}{2} \neq 1$ the spin of the target nucleus will precess in the magnetic field of the incoming particle. Forced polarization appears while turning the direction of the spin by $\frac{\pi}{2}$.

Time necessary for the turn is determined by

$$t = \frac{m\pi\gamma}{eH}\,(g-2)\,, \tag{5}$$

where m is the mass of the nucleus. For $\gamma = 10$, $m = 50$ a.m.u., we have $(g-2) \sim 1$, and $\mu = 1$ (nuclear magneton). Other examples in Table 2 demonstrate some interesting faces of the interaction.

Figures in Table 2 demonstrate that during the interaction of a fast moving charged particle with a nucleus (at $r \sim 10^{-12}$ cm) the orientation of the spin of the target nucleus takes as little time as $\sim 10^{-26}$ seconds. During this time interval the fast moving charged particle covers only 3×10^{-16} cm. This allows drawing a conclusion that right at the beginning of the interaction the nucleus target has time to orient its spin and further interaction takes place with the already polarized nucleus.

r, cm	10^{-13}	10^{-12}	10^{-11}	10^{-10}	10^{-9}	10^{-8}
H, Ersted	4.8×10^{16}	4.8×10^{14}	4.8×10^{12}	4.8×10^{10}	4.8×10^{8}	4.8×10^{6}

Table 1: The magnetic field intensity H as a function of r and the speed of the particle with $\beta \sim 1$.

r, cm	10^{-13}	10^{-12}	10^{-11}	10^{-10}	10^{-9}	10^{-8}
T, sec	10^{-28}	10^{-26}	10^{-24}	10^{-22}	10^{-20}	10^{-18}
$l = ts$, cm	3×10^{-18}	3×10^{-16}	3×10^{-14}	3×10^{-12}	3×10^{-10}	3×10^{-8}
$U = \mu H$, eV	1.5×10^{5}	1.5×10^{3}	15	0.15	1.5×10^{-3}	1.5×10^{-5}

Table 2: During the interaction of a fast moving charged particle with a nucleus (at $r \sim 10^{-12}$ cm), the orientation of the spin of the target nucleus takes as little time as $\sim 10^{-26}$ seconds.

4 Evaluation of energy required to change orientation of the nuclear spin within the external magnetic field

In known experiments of Dr. Wu et al [6], Co-60 nuclei were polarized at $T \sim 0.003$ K and the parity conservation was tested. Low temperatures were achieved by adiabatic demagnetization of Cerous Magnesium Nitrate. The energy of the effect can be estimated to be < 2.5 eV. Energy of the interaction of Co-60 nucleus magnetic moment with the outside magnetic field of a few hundred oersteds is negligible.

Therefore, the condition $\mu H \gg \kappa T$ is satisfied entirely (see Table 2): $\mu H \sim 10^3$, $\kappa T \sim 10^{-2}$.

Submitted on May 26, 2015 / Accepted on May 28, 2015

References

1. Mott N.F., Massey H.S.W. The Theory of Atomic Collisions. Oxford University Press, Oxford, 1965.
2. Schwinger J. On the polarization of fast neutrons. *Phys. Rev.*, 1948, v. 73, 407.
3. Tolhoek H.A. Electron polarization, theory and experiment. *Rev. Mod. Phys.*, 1956, v. 28, 277.
4. Landau L.D., Lifshitz E.M. The Classical Theory of Fields. 3rd edition, Butterworth-Heinemann, 2002.
5. Bargmann V., Michel L., and Telegdi V.L. Precession of the polarization of particles moving in a homogeneous electromagnetic field. *Phys. Rev. Lett.*, 1959, v. 2, 435.
6. Wu C.S., Ambler E., Hayward R.W., Hoppes D.D., and Hudson R.P. Experimental test of parity conservation in beta decay. *Phys. Rev.*, 1957, v. 105, 1413.

A Review on Natural Reality with Physical Equations

Linfan Mao
Chinese Academy of Mathematics and System Science, Beijing 100190, P. R. China
E-mail: maolinfan@163.com

A natural behavior is used to characterize by differential equation established on human observations, which is assumed to be on one particle or one field complied with reproducibility. However, the multilateral property of a particle P and the mathematical consistence determine that such an understanding is only local, not the whole reality on P, which leads to a central thesis for knowing the nature, i.e. *how to establish a physical equation with a proper interpretation on a thing*. As it is well-known, a thing consists of parts. Reviewing on observations, we classify them into two categories, i.e. *out-observation* and *in-observation* for discussion. The former is such an observation that the observer is out of the particle or the field P, which is in fact a macroscopic observation and its dynamic equation characterizes the coherent behavior of all parts in P, but the later is asked into the particle or the field by arranging observers simultaneously on different subparticles or subfields in P and respectively establishing physical equations, which are contradictory and given up in classical because there are not applicable conclusions on contradictory systems in mathematics. However, the existence naturally implies the necessity of the nature. Applying a combinatorial notion, i.e. G^L-solutions on non-solvable equations, a new notion for holding on the reality of nature is suggested in this paper, which makes it clear that the knowing on the nature by solvable equations is macro, only holding on these coherent behaviors of particles, but the non-coherent naturally induces non-solvable equations, which implies that the knowing by G^L-solution of equations is the effective, includes the classical characterizing as a special case by solvable equations, i.e. mathematical combinatorics.

1 Introduction

An observation on a physical phenomenon, or characters of a thing in the nature is the received information via hearing, sight, smell, taste or touch, i.e. sensory organs of the observer himself, little by little for human beings fulfilled with the reproducibility. However, it is difficult to hold the true face of a thing for human beings because he is analogous to a blind man in "*the blind men with an elephant*", a famous fable for knowing the nature. For example, let $\mu_1, \mu_2, \cdots, \mu_n$ be all observed and $\nu_i, i \geq 1$ unobserved characters on a particle P at time t. Then, P should be understood by

$$P = \left(\bigcup_{i=1}^{n}\{\mu_i\}\right)\bigcup\left(\bigcup_{k\geq 1}\{\nu_k\}\right) \tag{1.1}$$

in logic with an approximation $P^\circ = \bigcup_{i=1}^{n}\{\mu_i\}$ for P at time t. All of them are nothing else but Smarandache multispaces ([17]). Thus, $P \approx P^\circ$ is only an approximation for its true face of P, and it will never be ended in this way for knowing P as Lao Zi claimed "*Name named is not the eternal Name*" in the first chapter of his *TAO TEH KING* ([3]), a famous Chinese book.

A physical phenomenon of particle P is usually characterized by differential equation

$$\mathscr{F}\left(t, x_1, x_2, x_3, \psi_t, \psi_{x_1}, \psi_{x_2}, \cdots, \psi_{x_1x_2}, \cdots\right) = 0 \tag{1.2}$$

in physics established on observed characters of $\mu_1, \mu_2, \cdots, \mu_n$ for its state function $\psi(t, x)$ in $\mathbb{R}^4$. Usually, these physical phenomenons of a thing is complex, and hybrid with other things. *Is the reality of particle P all solutions of* (1.2) *in general?* Certainly not because (1.2) only characterizes the behavior of P on some characters of $\mu_1, \mu_2, \cdots, \mu_n$ at time t abstractly, not the whole in philosophy. For example, the behavior of a particle is characterized by the Schrödinger equation

$$i\hbar\frac{\partial\psi}{\partial t} = -\frac{\hbar^2}{2m}\nabla^2\psi + U\psi \tag{1.3}$$

in quantum mechanics but observation shows it in two or more possible states of being, i.e. superposition. We can not even say which solution of the Schrödinger equation (1.3) is the particle because each solution is only for one determined state. Even so, the understanding of all things is inexhaustible by (1.1).

Furthermore, *can we conclude* (1.2) *is absolutely right for a particle P?* Certainly not also because the dynamic equation (1.2) is always established with an additional assumption, i.e. the geometry on a particle P is a point in classical mechanics or a field in quantum mechanics and dependent on the observer is out or in the particle. For example, a water molecule H_2O consists of 2 Hydrogen atoms and 1 Oxygen atom such as those shown in Fig. 1. If an observer receives information on the behaviors of Hydrogen or Oxygen atom but stands out of the water molecule H_2O by viewing it a geometrical point, then such an observation is an out-observation because it only receives such coherent information on atoms H and O with the water molecule H_2O.

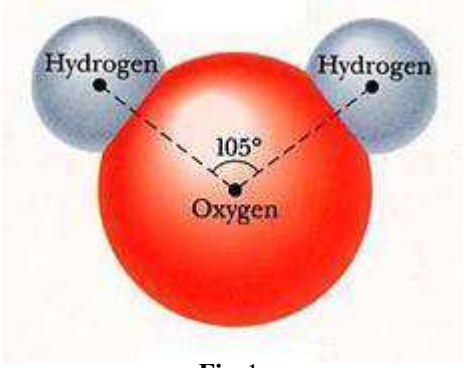

Fig. 1

If an observer is out the water molecule H_2O, his all observations on the Hydrogen atom H and Oxygen atom O are the same, but if he enters the interior of the molecule, he will view a different sceneries for atom H and atom O, which are respectively called *out-observation* and *in-observation*, and establishes 1 or 3 dynamic equations on the water molecule H_2O.

The main purpose of this paper is to clarify the natural reality of a particle with that of differential equations, and conclude that a solvable one characterizes only the reality of elementary particles but non-solvable system of differential equations essentially describe particles, such as those of baryons or mesons in the nature.

For terminologies and notations not mentioned here, we follow references [1] for mechanics, [5] for combinatorial geometry, [15] for elementary particles, and [17] for Smarandache systems and multispaces, and all phenomenons discussed in this paper are assumed to be true in the nature.

2 Out-observations

An *out-observation* observes on the external, i.e. these macro but not the internal behaviors of a particle P by human senses or via instrumental, includes the size, magnitudes or eigenvalues of states, ..., etc.

Certainly, the out-observation is the fundamental for quantitative research on matters of human beings. Usually, a dynamic equation (1.2) on a particle P is established by the principle of stationary action $\delta S = 0$ with

$$S = \int_{t_1}^{t_2} dt\, L(q(t), \dot{q}(t)) \tag{2.1}$$

in classical mechanics, where $q(t), \dot{q}(t)$ are respectively the generalized coordinates, the velocities and $L(q(t), \dot{q}(t))$ the *Lagrange function* on the particle, and

$$S = \int_{\tau_2}^{\tau_1} d^4x \mathcal{L}(\phi, \partial_\mu \psi) \tag{2.2}$$

in field theory, where ψ is the state function and $\mathcal{L}$ the *Lagrangian density* with τ_1, τ_2 the limiting surfaces of integration by viewed P an independent system of dynamics or a field. The principle of stationary action $\delta S = 0$ respectively induced the *Euler-Lagrange equations*

$$\frac{\partial L}{\partial q} - \frac{d}{dt}\frac{\partial L}{\partial \dot{q}} = 0 \quad \text{and} \quad \frac{\partial \mathcal{L}}{\partial \psi} - \partial_\mu \frac{\partial \mathcal{L}}{\partial(\partial_\mu \psi)} = 0 \tag{2.3}$$

in classical mechanics and field theory, which enables one to find the dynamic equations of particles by proper choice of L or $\mathcal{L}$. For examples, let

$$\mathcal{L}_S = \frac{i\hbar}{2}\left(\frac{\partial \psi}{\partial t}\overline{\psi} - \frac{\partial \overline{\psi}}{\partial t}\psi\right) - \frac{1}{2}\left(\frac{\hbar^2}{2m}|\nabla\psi|^2 + V|\psi|^2\right),$$
$$\mathcal{L}_D = \overline{\psi}\left(i\gamma^\mu \partial_\mu - \frac{mc}{\hbar}\right)\psi,$$
$$\mathcal{L}_{KG} = \frac{1}{2}\left(\partial_\mu \psi \partial^\mu \psi - \left(\frac{mc}{\hbar}\right)^2 \psi^2\right).$$

Then we respectively get the Schrödinger equation (1.3) or the Dirac equation

$$\left(i\gamma^\mu \partial_\mu - \frac{mc}{\hbar}\right)\psi(t, x) = 0 \tag{2.4}$$

for a free fermion $\psi(t, x)$ and the Klein-Gordon equation

$$\left(\frac{1}{c^2}\frac{\partial^2}{\partial t^2} - \nabla^2\right)\psi(x, t) + \left(\frac{mc}{\hbar}\right)^2 \psi(x, t) = 0 \tag{2.5}$$

for a free boson $\psi(t, x)$ hold in relativistic forms by (2.3), where $\hbar = 6.582 \times 10^{-22}$MeV s is the Planck constant, c is the speed of light,

$$\nabla = \left(\frac{\partial}{\partial x}, \frac{\partial}{\partial y}, \frac{\partial}{\partial z}\right), \qquad \nabla^2 = \frac{\partial^2}{\partial x^2} + \frac{\partial^2}{\partial y^2} + \frac{\partial^2}{\partial z^2},$$
$$\partial_\mu = \left(\frac{1}{c}\frac{\partial}{\partial t}, \frac{\partial}{\partial x_1}, \frac{\partial}{\partial x_2}, \frac{\partial}{\partial x_3}\right),$$
$$\partial^\mu = \left(\frac{1}{c}\frac{\partial}{\partial t}, -\frac{\partial}{\partial x_1}, -\frac{\partial}{\partial x_2}, -\frac{\partial}{\partial x_3}\right)$$

and $\gamma^\mu = \left(\gamma^0, \gamma^1, \gamma^2, \gamma^3\right)$ with

$$\gamma^0 = \begin{pmatrix} I_{2\times 2} & 0 \\ 0 & -I_{2\times 2} \end{pmatrix}, \quad \gamma^i = \begin{pmatrix} 0 & \sigma_i \\ -\sigma_i & 0 \end{pmatrix}$$

with the usual Pauli matrices

$$\sigma_1 = \begin{pmatrix} 0 & 1 \\ 1 & 0 \end{pmatrix}, \ \sigma_2 = \begin{pmatrix} 0 & -i \\ i & 0 \end{pmatrix}, \ \sigma_3 = \begin{pmatrix} 1 & 0 \\ 0 & -1 \end{pmatrix}.$$

Furthermore, let $\mathcal{L} = \sqrt{-g}R$, where $R = g^{\mu\nu}R_{\mu\nu}$, the Ricci scalar curvature on the gravitational field. The equation (2.3) then induces the vacuum Einstein gravitational field equation

$$R_{\mu\nu} - \frac{1}{2}g_{\mu\nu}R = 0. \tag{2.6}$$

Usually, the equation established on the out-observations only characterizes those of coherent behaviors of all parts in a particle P. For example, a water molecule H_2O obeys the Schrödinger equation (1.3), we assume its Hydrogen atom H and oxygen atom O also obey the Schrödinger equation (1.3) as a matter of course. However, the divisibility of matter initiates human beings to search elementary constituting cells of matter, i.e. elementary particles such as those of quarks, leptons with interaction quanta including photons and other particles of mediated interactions, also with those of their antiparticles at present ([14]), and unmatters between a matter and its antimatter which is partially consisted of matter but others antimatter ([8-19]). For example, a baryon is predominantly formed from three quarks, and a meson is mainly composed of a quark and an antiquark in the models of Sakata, or Gell-Mann and Ne'eman on hadron and meson, such as those shown in Fig. 2, where, $q_i \in \{\mathbf{u}, \mathbf{d}, \mathbf{c}, \mathbf{s}, \mathbf{t}, \mathbf{b}\}$ denotes a quark for $i = 1, 2, 3$ and $\overline{q}_2 \in \left\{\overline{\mathbf{u}}, \overline{\mathbf{d}}, \overline{\mathbf{c}}, \overline{\mathbf{s}}, \overline{\mathbf{t}}, \overline{\mathbf{b}}\right\}$, an antiquark. But a free quark was never found in experiments. We can not even conclude the Schrödinger equation (1.3) is the right equation (1.2) for quarks because it is established on an independent particle, can not be divided again in mathematics.

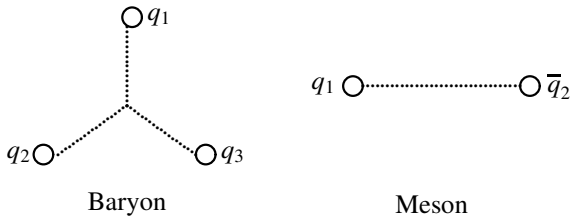

Fig. 2

Then, *why is it believed without a shadow of doubt that the dynamical equations of elementary particles such as those of quarks, leptons with interaction quanta are (*1.3*) in physics?* It is because that all our observations come from a macro viewpoint, the human beings, not the particle itself, which rationally leads to H. Everett's multiverse interpretation on the superposition by letting parallel equations for the wave functions $\psi(t, x)$ on positions of a particle in 1957 ([2]). We only hold coherent behaviors of elementary particles, such as those of quarks, leptons with interaction quanta and their antiparticles by (1.3), not the individual, and it is only an equation on those of particles viewed abstractly to be a geometrical point or an independent field from a macroscopic point, which leads physicists to assume the internal structures mechanically for hold the behaviors of particles such as those shown in Fig. 2 on hadrons. However, such an assumption is a little ambiguous in logic, i.e. we can not even conclude which is the point or the independent field, the hadron or its subparticle, the quark.

In fact, a point is non-divisible in geometry. Even so, the assumption on the internal structure of particles by physicists was mathematically verified by extending Banach spaces to extended Banach spaces on topological graphs $\overrightarrow{G}$ in [12]:

Let $(\mathscr{V}; +, \cdot)$ be a Banach space over a field $\mathscr{F}$ and $\overrightarrow{G}$ a strong-connected topological graph with vertex set V and arc set X. A vector labeling $\overrightarrow{G}^L$ on $\overrightarrow{G}$ is a $1-1$ mapping $L: \overrightarrow{G} \to \mathscr{V}$ such that $L: (u, v) \to L(u, v) \in \mathscr{V}$ for $\forall (u, v) \in X\left(\overrightarrow{G}\right)$ and it is a $\overrightarrow{G}$-flow if it holds with

$$L(u, v) = -L(v, u) \quad \text{and} \quad \sum_{u \in N_G(v)} L(v^u) = \mathbf{0}$$

for $\forall (u, v) \in X\left(\overrightarrow{G}\right)$, $\forall v \in V(\overrightarrow{G})$, where $\mathbf{0}$ is the zero-vector in $\mathscr{V}$.

For $\overrightarrow{G}$-flows $\overrightarrow{G}^L$, $\overrightarrow{G}^{L_1}$, $\overrightarrow{G}^{L_2}$ on a topological graph $\overrightarrow{G}$ and $\xi \in \mathscr{F}$ a scalar, it is clear that $\overrightarrow{G}^{L_1} + \overrightarrow{G}^{L_2}$ and $\xi \cdot \overrightarrow{G}^L$ are also $\overrightarrow{G}$-flows, which implies that all $\overrightarrow{G}$-flows on $\overrightarrow{G}$ form a linear space over $\mathscr{F}$ with unit $\mathbf{O}$ under operations + and $\cdot$, denoted by $\overrightarrow{G}^{\mathscr{V}}$, where $\mathbf{O}$ is such a $\overrightarrow{G}$-flow with vector $\mathbf{0}$ on (u, v) for $\forall (u, v) \in X\left(\overrightarrow{G}\right)$. Then, it was shown that $\overrightarrow{G}^{\mathscr{V}}$ is a Banach space, and furthermore a Hilbert space if introduce

$$\begin{aligned} \left\|\overrightarrow{G}^L\right\| &= \sum_{(u,v) \in X\left(\overrightarrow{G}\right)} \|L(u, v)\|, \\ \left\langle \overrightarrow{G}^{L_1}, \overrightarrow{G}^{L_2} \right\rangle &= \sum_{(u,v) \in X\left(\overrightarrow{G}\right)} \langle L_1(u, v), L_2(u, v) \rangle \end{aligned}$$

for $\forall \overrightarrow{G}^L, \overrightarrow{G}^{L_1}, \overrightarrow{G}^{L_2} \in \overrightarrow{G}^{\mathscr{V}}$, where $\|L(u, v)\|$ is the norm of $L(u, v)$ and $\langle \cdot, \cdot \rangle$ the inner product in $\mathscr{V}$ if it is an inner space. The following result generalizes the representation theorem of Fréchet and Riesz on linear continuous functionals on $\overrightarrow{G}$-flow space $\overrightarrow{G}^{\mathscr{V}}$, which enables us to find $\overrightarrow{G}$-flow solutions on linear equations (1.2).

Theorem 2.1([12]) *Let* $\mathbf{T}: \overrightarrow{G}^{\mathscr{V}} \to \mathbb{C}$ *be a linear continuous functional. Then there is a unique* $\overrightarrow{G}^{\widehat{L}} \in \overrightarrow{G}^{\mathscr{V}}$ *such that*

$$\mathbf{T}\left(\overrightarrow{G}^L\right) = \left\langle \overrightarrow{G}^L, \overrightarrow{G}^{\widehat{L}} \right\rangle$$

for $\forall \overrightarrow{G}^L \in \overrightarrow{G}^{\mathscr{V}}$.

For non-linear equations (1.2), we can also get $\overrightarrow{G}$-flow solutions on them if $\overrightarrow{G}$ can be decomposed into circuits.

Theorem 2.2([12]) *If the topological graph* $\overrightarrow{G}$ *is strong-connected with circuit decomposition*

$$\overrightarrow{G} = \bigcup_{i=1}^{l} \overrightarrow{C}_i$$

such that $L(u^v) = L_i(\mathbf{x})$ *for* $\forall (u,v) \in X\left(\overrightarrow{C}_i\right)$, $1 \le i \le l$ *and the Cauchy problem*

$$\begin{cases} \mathscr{F}_i(\mathbf{x}, u, u_{x_1}, \cdots, u_{x_n}, u_{x_1x_2}, \cdots) = 0 \\ u|_{\mathbf{x}_0} = L_i(\mathbf{x}) \end{cases}$$

is solvable in a Hilbert space $\mathscr{V}$ *on domain* $\Delta \subset \mathbb{R}^n$ *for integers* $1 \le i \le l$, *then the Cauchy problem*

$$\begin{cases} \mathscr{F}_i(\mathbf{x}, X, X_{x_1}, \cdots, X_{x_n}, X_{x_1x_2}, \cdots) = 0 \\ X|_{\mathbf{x}_0} = \overrightarrow{G}^L \end{cases}$$

such that $L(u^v) = L_i(\mathbf{x})$ *for* $\forall (u,v) \in X\left(\overrightarrow{C}_i\right)$ *is solvable for* $X \in \overrightarrow{G}^{\mathscr{V}}$.

Theorems 2.1 – 2.2 conclude the existence of $\overrightarrow{G}$-flow solution on linear or non-linear differential equations for a topological graph $\overrightarrow{G}$, such as those of the Schrödinger equation (1.3), Dirac equation (2.4) and the Klein-Gordon equation (2.5), which all implies the rightness of physicists assuming the internal structures for hold the behaviors of particles because there are infinite many such graphs $\overrightarrow{G}$ satisfying conditions of Theorem 2.1 – 2.2, particularly, the bouquet $\overrightarrow{B}_N^{L_\psi}$, the dipoles $\overrightarrow{D^{\perp}}_{0,2N,0}^{L_\psi}$ for elementary particles in [13].

3 In-observations

An *in-observation* observes on the internal behaviors of a particle, particularly, a composed particle P. Let P be composed by particles $P_1, P_2, \cdots, P_m$. Different from out-observation from a macro viewing, in-observation requires the observer holding the respective behaviors of particles $P_1, P_2, \cdots, P_m$ in P, for instance an observer enters a water molecule H_2O receiving information on the Hydrogen or Oxygen atoms H, O.

For such an observation, there are 2 observing ways:

(1) there is an apparatus such that an observer can simultaneously observe behaviors of particles $P_1, P_2, \cdots, P_m$, i.e. $P_1, P_2, \cdots, P_m$ can be observed independently as particles at the same time for the observer;

(2) there are m observers $O_1, O_2, \cdots, O_m$ simultaneously observe particles $P_1, P_2, \cdots, P_m$, i.e. the observer O_i only observes the behavior of particle P_i for $1 \le i \le m$, called *parallel observing*, such as those shown in Fig. 3 for the water molecule H_2O with $m = 3$.

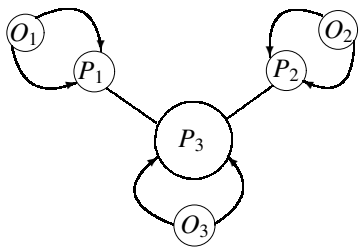

Fig. 3

Certainly, each of these observing views a particle in P to be an independent particle, which enables us to establish the dynamic equation (1.2) by Euler-Lagrange equation (2.3) for P_i, $1 \le i \le m$, respectively, and then we can apply the system of differential equations

$$\begin{cases} \dfrac{\partial L_1}{\partial \mathbf{q}} - \dfrac{d}{dt}\dfrac{\partial L_1}{\partial \dot{\mathbf{q}}} = 0 \\ \dfrac{\partial L_2}{\partial \mathbf{q}} - \dfrac{d}{dt}\dfrac{\partial L_2}{\partial \dot{\mathbf{q}}} = 0 \\ \cdots \\ \dfrac{\partial L_m}{\partial \mathbf{q}} - \dfrac{d}{dt}\dfrac{\partial L_m}{\partial \dot{\mathbf{q}}} = 0 \\ \mathbf{q}(t_0) = \mathbf{q}_0, \dot{\mathbf{q}}(t_0) = \dot{\mathbf{q}}_0 \end{cases} \tag{3.1}$$

for characterizing particle P in classical mechanics, or

$$\begin{cases} \dfrac{\partial \mathcal{L}_1}{\partial \psi} - \partial_\mu \dfrac{\partial \mathcal{L}_1}{\partial(\partial_\mu \psi)} = 0 \\ \dfrac{\partial \mathcal{L}_2}{\partial \psi} - \partial_\mu \dfrac{\partial \mathcal{L}_2}{\partial(\partial_\mu \psi)} = 0 \\ \cdots \\ \dfrac{\partial \mathcal{L}_m}{\partial \psi} - \partial_\mu \dfrac{\partial \mathcal{L}_m}{\partial(\partial_\mu \psi)} = 0 \\ \psi(t_0) = \psi_0 \end{cases} \tag{3.2}$$

for characterizing particle P in field theory, where the i^{th} equation is the dynamic equation of particle P_i with initial data $\mathbf{q}_0, \dot{\mathbf{q}}_0$ or ψ_0.

We discuss the solvability of systems (3.1) and (3.2). Let

$$S_{\mathbf{q}_i} = \left\{ (x_i, y_i, z_i)(\mathbf{q}_i, t) \in \mathbb{R}^3 \,\middle|\, \frac{\partial L_1}{\partial \mathbf{q}_i} - \frac{d}{dt}\frac{\partial L_1}{\partial \dot{\mathbf{q}}_i} = 0, \ \mathbf{q}_i(t_0) = \mathbf{q}_0, \dot{\mathbf{q}}_i(t_0) = \dot{\mathbf{q}}_0 \right\}$$

for integers $1 \le i \le m$. Then, the system (3.1) of equations is solvable if and only if

$$\mathscr{D}(\mathbf{q}) = \bigcap_{i=1}^{m} S_{\mathbf{q}_i} \neq \emptyset. \tag{3.3}$$

Otherwise, the system (3.1) is non-solvable. For example, let particles P_1, P_2 of masses M, m be hanged on a fixed pulley, such as those shown in Fig. 4.

Then, the dynamic equations on P_1 and P_2 are respectively

$$P_1 : \ \ddot{x} = g, \ x(t_0) = x_0 \text{ and } P_2 : ddotx = -g, \ x(t_0) = x_0$$

but the system

$$\begin{cases} \ddot{x} = g \\ \ddot{x} = -g, \ x(t_0) = x_0 \end{cases}$$

is contradictory, i.e. non-solvable.

Similarly, let $\psi_i(x,t)$ be the state function of particle P_i, i.e. the solution of

$$\begin{cases} \dfrac{\partial \mathcal{L}_i}{\partial \psi_i} - \partial_\mu \dfrac{\partial \mathcal{L}_i}{\partial(\partial_\mu \psi_i)} = 0 \\ \psi(t_0) = \psi_0. \end{cases}$$

Then, the system (3.2) is solvable if and only if there is a state function $\psi(x,t)$ on P hold with each equation of system (3.2), i.e.

$$\psi(x,t) = \psi_1(x,t) = \cdots = \psi_m(x,t), \quad x \in \mathbb{R}^3,$$

which is impossible because if all state functions $\psi_i(x,t)$, $1 \le i \le m$ are the same, the particles $P_1, P_2, \cdots, P_m$ are nothing else but just one particle. Whence, the system (3.2) is non-solvable if $m \ge 2$, which implies we can not characterize the behavior of particle P by classical solutions of differential equations.

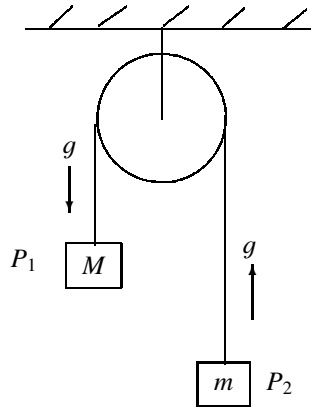

Fig. 4

For example, if the state function $\psi_O(x,t) = \psi_{H_1}(x,t) = \psi_{H_2}(x,t)$ in the water molecule H_2O for $x \in \mathbb{R}^3$ hold with

$$\begin{cases} -i\hbar \dfrac{\partial \psi_O}{\partial t} = \dfrac{\hbar^2}{2m_O}\nabla^2\psi_O - V(x)\psi_O \\ -i\hbar \dfrac{\partial \psi_{H_1}}{\partial t} = \dfrac{\hbar^2}{2m_{H_1}}\nabla^2\psi_{H_1} - V(x)\psi_{H_1} \\ -i\hbar \dfrac{\partial \psi_{H_2}}{\partial t} = \dfrac{\hbar^2}{2m_{H_2}}\nabla^2\psi_{H_2} - V(x)\psi_{H_2} \end{cases}$$

Then $\psi_O(x,t) = \psi_{H_1}(x,t) = \psi_{H_2}(x,t)$ concludes that

$$A_O e^{-\frac{i}{\hbar}(E_O t - \mathbf{p}_O x)} = A_{H_1} e^{-\frac{i}{\hbar}(E_{H_1} t - \mathbf{p}_{H_1} x)} = A_{H_2} e^{-\frac{i}{\hbar}(E_{H_2} t - \mathbf{p}_{H_2} x)}$$

for $\forall x \in \mathbb{R}^3$ and $t \in \mathbb{R}$, which implies that

$$A_O = A_{H_1} = A_{H_2},\ E_O = E_{H_1} = E_{H_2} \text{ and } \mathbf{p}_O = \mathbf{p}_{H_1} = \mathbf{p}_{H_2},$$

a contradiction.

Notice that each equation in systems (3.1) and (3.2) is solvable but the system itself is non-solvable in general, and they are real in the nature. Even if the system (3.1) holds with condition (3.3), i.e. it is solvable, we can not apply the solution of (3.1) to characterize the behavior of particle P because such a solution only describes the coherent behavior of particles $P_1, P_2, \cdots, P_m$. Thus, we can not characterize the behavior of particle P by the solvability of systems (3.1) or (3.2). We should search new method to characterize systems (3.1) or (3.2).

Philosophically, the formula (1.1) is the understanding of particle P and all of these particles $P_1, P_2, \cdots, P_m$ are inherently related, not isolated, which implies that P naturally inherits a topological structure $G^L[P]$ in space of the nature, which is a vertex-edge labeled topological graph determined by:

$$V\left(G^L[P]\right) = \{P_1, P_2, \cdots, P_m\},$$
$$E\left(G^L[P]\right) = \{(P_i, P_j) | P_i \bigcap P_j \neq \emptyset,\ 1 \le i \neq j \le m\}$$

with labeling

$$L:\ P_i \to L(P_i) = P_i \quad \text{and}$$
$$L:\ (P_i, P_j) \to L(P_i, P_j) = P_i \bigcap P_j$$

for integers $1 \le i \neq j \le m$. For example, the topological graphs $G^L[P]$ of water molecule H_2O, meson and baryon in the quark model of Gell-Mann and Ne'eman are respectively shown in Fig. 5,

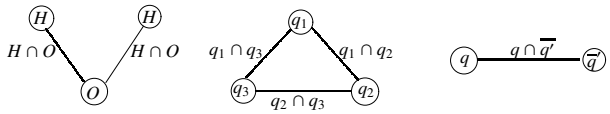

H_2O Baryon Meson

Fig. 5

where $O, H, q, \overline{q'}$ and $q_i, 1 \le i \le 3$ obey the Dirac equation but $O \cap H, q \cap \overline{q'}, q_k \cap q_l, 1 \le k, l \le 3$ comply with the Klein-Gordon equation.

Such a vertex-edge labeled topological graph $G^L[P]$ is called G^L-*solution* of systems (3.1)–(3.2). Clearly, the global behaviors of particle P are determined by particles $P_1, P_2, \cdots, P_m$. We can hold them on G^L-solution of systems (3.1) or (3.2). For example, let $u^{[v]}$ be the solution of equation at vertex $v \in V\left(G^L[P]\right)$ with initial value $u_0^{[v]}$ and $G^{L_0}[P]$ the initial G^L-solution, i.e. labeled with $u_0^{[v]}$ at vertex v. Then, a G^L-solution of systems (3.1) or (3.2) is *sum-stable* if for any number $\varepsilon > 0$ there exists $\delta_v > 0$, $v \in V(G^{L_0}[P])$ such that each $G^{L'}$-solution with

$$\left|u'^{[v]}_0 - u^{[v]}_0\right| < \delta_v, \qquad \forall v \in V(G^{L_0}[P])$$

exists for all $t \ge 0$ and with the inequality

$$\left| \sum_{v \in V(G^{L'}[P])} u'^{[v]} - \sum_{v \in V(G^L[P])} u^{[v]} \right| < \varepsilon$$

holds, denoted by $G^L[P] \overset{\Sigma}{\sim} G^{L_0}[P]$. Furthermore, if there exists a number $\beta_v > 0$ for $\forall v \in V(G^{L_0}[P])$ such that every $G^{L'}[P]$-solution with

$$\left|u'^{[v]}_0 - u^{[v]}_0\right| < \beta_v, \qquad \forall v \in V(G^{L_0}[P])$$

satisfies

$$\lim_{t\to\infty}\left|\sum_{v\in V(G^{L'}[P])} u'^{[v]} - \sum_{v\in V(G^{L}[P])} u^{[v]}\right| = 0,$$

then the $G^L[P]$-solution is called asymptotically stable, denoted by $G^L[P] \overset{\Sigma}{\to} G^{L_0}[P]$. Similarly, the energy integral of G^L-solution is determined by

$$E(G^L[P]) = \sum_{G\le G^{L_0}[P]} (-1)^{|G|+1} \int_{\mathscr{O}_G} \left(\frac{\partial u^G}{\partial t}\right)^2 dx_1 dx_2 \cdots dx_{n-1},$$

where u^G is the $\mathbb{C}^2$ solution of system

$$\left.\begin{array}{l} \dfrac{\partial u}{\partial t} = H_v(t, x_1, \cdots, x_{n-1}, p_1, \cdots, p_{n-1}) \\ u|_{t=t_0} = u^{[v]}_0(x_1, x_2, \cdots, x_{n-1}) \end{array}\right\} v \in V(G)$$

and $\mathscr{O}_G = \bigcap\limits_{v\in V(G)} \mathscr{O}_v$ with $\mathscr{O}_v \subset \mathbb{R}^n$ determined by the vth equation

$$\left\{\begin{array}{l} \dfrac{\partial u}{\partial t} = H_v(t, x_1, \cdots, x_{n-1}, p_1, \cdots, p_{n-1}) \\ u|_{t=t_0} = u^{[v]}_0(x_1, x_2, \cdots, x_{n-1}). \end{array}\right.$$

All of these global properties were extensively discussed in [7–11], which provides us to hold behaviors of a composed particle P by its constitutions $P_1, P_2, \cdots, P_m$.

4 Reality

Generally, the reality is the state characters (1.1) of existed, existing or will exist things whether or not they are observable or comprehensible by human beings, and the observing objective is on the state of particles, which then enables us to find the reality of a particle. However, an observation is dependent on the perception of the observer by his organs or through by instruments at the observing time, which concludes that to hold the reality of a particle P can be only little by little, and determines local reality of P from a macro observation at a time t, no matter what P is, a macro or micro thing. Why is this happening because we always observe by one observer on one particle assumed to be a point in space, and then establish a solvable equation (1.2) on coherent, not individual behaviors of P. Otherwise, we get non-solvable equations on P contradicts to the law of contradiction, the foundation of classical mathematics which results in discussions following:

4.1 States of particles are multiverse

A particle P understood by formula (1.1) is in fact a multiverse consisting of known characters $\mu_1, \mu_2, \cdots, \mu_n$ and unknown characters $\nu_k, k \ge 1$, i.e. different characters characterize different states of particle P. This fact also implies that the multiverse exist everywhere if we understand a particle P with in-observation, not only those levels of $I - IV$ of Max Tegmark in [24]. In fact, the infinite divisibility of a matter M in philosophy alludes nothing else but a multiverse observed on M by its individual submatters. Thus, the nature of a particle P is multiple in front of human beings, with unity character appeared only in specified situations.

4.2 Reality only characterized by non-compatible system

Although the dynamical equations (1.2) established on unilateral characters are individually compatible but they must be globally contradictory with these individual features unless all characters are the same one. It can not be avoided by the nature of a particle P. Whence, the non-compatible system, particularly, non-solvable systems consisting of solvable differential equations are suitable tools for holding the reality of particles P in the world, which also partially explains a complaint of Einstein on mathematics, i.e. *as far as the laws of mathematics refer to reality, they are not certain; and as far as they are certain, they do not refer to reality* because the multiple nature of all things.

4.3 Reality really needs mathematics on graph

As we know, there always exists a universal connection between things in a family in philosophy. Thus, a family $\mathscr{F}$ of things naturally inherits a topological graph $G^L[\mathscr{F}]$ in space and we therefore conclude that

$$\mathscr{F} = G^L[\mathscr{F}] \tag{4.1}$$

in that space. Particularly, if all things in $\mathscr{F}$ are nothing else but manifolds $M_T(x_1, x_2, x_3; t)$ of particles P determined by equation

$$f_T(x_1, x_2, x_3; t) = 0, \qquad T \in \mathscr{F} \tag{4.2}$$

in $\mathbb{R}^3 \times \mathbb{R}$, we get a geometrical figure $\bigcup\limits_{T\in\mathscr{F}} M_T(x_1, x_2, x_3; t)$, a combinatorial field ([6]) for $\mathscr{F}$. Clearly, the graph $G^L[\mathscr{F}]$ characterizes the behavior of $\mathscr{F}$ no matter whether the system (4.2) is solvable or not. Calculation shows that the system (4.2) of equations is non-solvable or not dependent on

$$\bigcap_{T\in\mathscr{F}} M_T(x_1, x_2, x_3; t) = \emptyset \ \text{ or not.}$$

Particularly, if $\bigcap\limits_{T\in\mathscr{F}} M_T(x_1, x_2, x_3; t) = \emptyset$, the system (4.2) is non-solvable and we can not just characterize the behavior of $\mathscr{F}$ by the solvability of system (4.2). We must turn the contradictory system (4.2) to a compatible one, such as those

shown in [10] and have to extend mathematical systems on graph $G^L[\mathscr{F}]$ ([12]) for holding the reality of $\mathscr{F}$.

Notice that there is a conjecture for developing mathematics in [4] called *CC conjecture* which claims that *any mathematical science can be reconstructed from or turned into combinatorization*. Such a conjecture is in fact a combinatorial notion for developing mathematics on topological graphs, i.e. finds the combinatorial structure to reconstruct or generalize classical mathematics, or combines different mathematical sciences and establishes a new enveloping theory on topological graphs for hold the reality of things $\mathscr{F}$.

5 Conclusion

Reality of a thing is hold on observation with level dependent on the observer standing out or in that thing, particularly, a particle classified to out- or in-observation, or parallel observing from a macro or micro view and characterized by solvable or non-solvable differential equations, consistent with the universality principle of contradiction in philosophy. For holding on the reality of things, the out-observation is basic but the in-observation is cardinal. Correspondingly, the solvable equation is individual but the non-solvable equations are universal. Accompanying with the establishment of compatible systems, we are also needed to characterize those of contradictory systems, particularly, non-solvable differential equations on particles and establish mathematics on topological graphs, i.e. *mathematical combinatorics*, and only which is the appropriate way for understanding the nature because all things are in contradiction.

Submitted on June 18, 2015 / Accepted on June 20, 2015

References

1. Abraham R. and Marsden J. E. Foundation of Mechanics, 2nd ed. Addison-Wesley, Reading, MA, 1978.
2. Everett H. Relative state formulation of quantum mechanics. *Rev.Mod.Phys.*, 1957, v. 29, 454–462.
3. Lu J. C. Fangfo Analyzing LAO ZHI – Explaining TAO TEH KING by TAI JI (in Chinese). Tuan Jie Publisher, Beijing, 2004.
4. Linfan Mao. Combinatorial speculation and combinatorial conjecture for mathematics. *International J.Math. Combin.*, 2007, v. 1 (1), 1–19.
5. Linfan Mao. Combinatorial Geometry with Applications to Field Theory. The Education Publisher Inc., USA, 2011.
6. Linfan Mao. Combinatorial fields – an introduction. *International J. Math.Combin.*, 2009, v. 3, 1–22.
7. Linfan Mao. Global stability of non-solvable ordinary differential equations with applications. *International J.Math. Combin.*, 2013, v. 1, 1–37.
8. Linfan Mao. Non-solvable equation systems with graphs embedded in $\mathbf{R}^n$. in Proceedings of the First International Conference on Smarandache Multispace and Multistructure, The Education Publisher Inc., July 2013.
9. Linfan Mao. Geometry on G^L-systems of homogenous polynomials. *International J.Contemp. Math. Sciences*, 2014, v. 9 (6), 287–308.
10. Linfan Mao. Mathematics on non-mathematics – A combinatorial contribution. *International J.Math. Combin.*, 2014, v. 3, 1–34.
11. Linfan Mao. Cauchy problem on non-solvable system of first order partial differential equations with applications. *Methods and Applications of Analysis*, 2015, v. 22 (2), 171–200.
12. Linfan Mao. Extended Banach $\vec{G}$-flow spaces on differential equations with applications. *Electronic J.Mathematical Analysis and Applications*, 2015, v. 3 (2), 59–91.
13. Linfan Mao. A new understanding of particles by $\vec{G}$-flow interpretation of differential equation, *Progress in Physics*, 2015, v. 11, 39–50.
14. Nambu Y. Quarks: Frontiers in Elementary Particle Physics. World Scientific Publishing, 1985.
15. Quang Ho-Kim and Pham Xuan Yem. Elementary Particles and Their Interactions. Springer-Verlag, Berlin Heidelberg, 1998.
16. Reid T. An inquiry into the human mind on the principles of common sense. in Brookes D., ed., Edinburgh University Press, 1997.
17. Smarandache F. Paradoxist Geometry. State Archives from Valcea, Rm. Valcea, Romania, 1969, and in Paradoxist Mathematics. Collected Papers (Vol. II). Kishinev University Press, Kishinev, 1997, pp. 5–28.
18. Smarandache F. A new form of matter – unmatter, composed of particles and anti-particles. *Progress in Physics*, 2005, v 1, 9–11.
19. Smarandache F. and Rabounski D. Unmatter entities inside nuclei, predicted by the Brightsen nucleon cluster model. *Progress in Physics*, 2006, v. 2, 14–18.
20. Tegmark M. Parallel universes. in Barrow J. D., Davies P. C. W. and Harper C. L., eds. Science and Ultimate Reality: From Quantum to Cosmos. Cambridge University Press, 2003.

LETTERS TO PROGRESS IN PHYSICS

Abraham I. Fet (1924–2007). In Memory of the 90th Anniversary

Abraham I. Fet (1924–2007) belonged to a particular "species of human" that is becoming extinct today: he could be rather a man of Renaissance in late Medieval Italy or Enlightenment in France in the 18th century, or a bright representative of intelligentsia in Russia of the 19th century.

A. Fet got his basic university education in mathematics and submitted a brilliant candidate (PhD) thesis at Moscow University being barely 24 years old. The mathematical results of his doctoral (DSc) thesis, presented later at the same University, still remain unsurpassed. He mainly published papers in mathematics, but he was also enrolled to research in physics that he started in collaboration with Yuriy B. Rumer, the famous Russian theoretical physicist. The results of their joint work were published in two co-authored books *Theory of Unitary Symmetry* (1970) and *Group Theory and Quantum Fields* (1977). Then there followed *Symmetry Group of Chemical Elements*, a book written by Fet alone, which presented a new physical perspective of the System of Chemical Elements and has become classics.

His research interests, however, were not limited to mathematics and physics. He remarkably explored many sciences and humanities, among which biology, economics, history, philosophy, sociology, psychology, and even literature, music, and arts. Moreover, being an encyclopedic scientist, he was not just an "erudite": with his powerful intellect, he built up a solid worldview from seemingly dispersed lines of knowledge.

First and utmost, Abraham Fet was a thinker, and his thinking was a blend of intellect, passion and concern. His major concern was about the fate of Mankind; he felt himself an active and responsible protagonist rather than being an observer "heeding to good and evil with equanimity, knowing neither pity nor ire".

A. Fet thought a lot on the human society, on the biological and cultural nature of man, on religious beliefs and ideals, and on the social mission of the intelligentsia, which he saw primarily in enlightening. He summarized his ideas in numerous essays and several books: *Pythagoras and the Ape* (1987), *Letters from Russia* (1989–1991), *Delusions of Capitalism, or the Fatal Conceit of Professor Hayek* (1996), and finally *Instinct and Social Behavior* (2005). The latter became his main work, where he investigated the history of culture in terms of ethology, with the aim to "reveal the impact of the social instinct on the human society, to describe the conditions frustrating its manifestations and to explain the effects of various attempts to suppress this invincible instinct". That

Abraham Ilych Fet

was his discovery and first study of a social instinct unique to humans, which he called "the instinct of intraspecific solidarity". With comprehensive historic examples, he has convincingly demonstrated how the morals and love for our neighbors originated from tribal solidarity within a minor kindred group and how the mark of kinship spread progressively to ever larger communities, as far as the entire mankind.

Two previously published books, together with a wealth of unpublished manuscripts, are now coming to the public with his *Collected Works* in seven volumes*.

With his excellent command of seven European languages, Abraham Fet not only had an extremely broad range of reading but also chose some important books and translated them for his friends and broad public. It was especially valuable in the conditions of harsh censorship in the Soviet times, when many books, for instance on psychology, were forbidden. Thus he translated Eric Berne, Erich Fromm, Karen Horney, Gregory Bateson, and many others. Being himself fascinated with the works of Konrad Lorenz, Fet was the first to introduce Lorenz's main books to the Russian readers. Namely,

*The publicaiton is just in Russian; an English volunteer translator is wanted. Ask Ludmila Petrova aifet@academ.org, for detail.

he translated *Das sogennannte Böse* ("The So-Called Evil"), *Die acht Todsünden der zivilisierten Menschheit* ("Civilized Man's Eight Deadly Sins"), *Die Rückseite des Spiegels* ("Behind the Mirror"), which were then published twice in post-Soviet Russia.

Abraham Fet was an ardent opponent to tyranny. Although being more a thinker than an active public person, he signed the "*Letter of 46*" in spring 1968 in defense of imprisoned dissidents. That lost him his job, both at the research institute and the university, and left him unemployed for years, to survive from occasional earns. Another reason of his dismissal, though, besides the very fact of signing the letter, was rather his spirit of independence and straight speaking. He called things the way he saw them, were they professional or personal characteristics of his fellows, or intrigues of functionaries or the privileges in science. A moral maximalist, Abraham Fet despised those who "lived as the others do" and called this lifestyle "the life of insects".

Beginning with the mid-1970s, Fet closely followed the events which took place in Poland. He perceived the revolt of 1980–1981 as the start of collapse of the so-called socialist camp. His book *The Polish Revolution* written in the wake of the events was anonymously published in 1985 in Munich and London. He not only provided deep review of the Polish events but also disclosed their historic prerequisites, demonstrated the outstanding role of the Polish intellectuals and foretold the further historic paths of the country.

Making retrospective of Fet's life and works, we can definitely put his name along with the most outstanding scientists and thinkers of the 20th century. He was among those who rarely get recognition during their lifetime. Rather than being in line with the "spirit of epoch", his ideas were against the mainstream. However, these are the ideas that are worth the most as they blaze truly trails to the science of the future and appeal to the future Mankind. Let his memory live for ever!

A. V. Gladky, L. P. Petrova, R. G. Khlebopros

Progress in Physics is an American scientific journal on advanced studies in physics, registered with the Library of Congress (DC, USA): ISSN 1555-5534 (print version) and ISSN 1555-5615 (online version). The journal is peer reviewed and listed in the abstracting and indexing coverage of: Mathematical Reviews of the AMS (USA), DOAJ of Lund University (Sweden), Zentralblatt MATH (Germany), Scientific Commons of the University of St.Gallen (Switzerland), Open-J-Gate (India), Referential Journal of VINITI (Russia), etc. Progress in Physics is an open-access journal published and distributed in accordance with the Budapest Open Initiative: this means that the electronic copies of both full-size version of the journal and the individual papers published therein will always be acessed for reading, download, and copying for any user free of charge. The journal is issued quarterly (four volumes per year).

Electronic version of this journal: http://www.ptep-online.com

Advisory Board of Founders:
Dmitri Rabounski, Editor-in-Chief
Florentin Smarandache, Assoc. Editor
Larissa Borissova, Assoc. Editor

Editorial Board:
Pierre Millette
Andreas Ries
Gunn Quznetsov
Felix Scholkmann
Ebenezer Chifu

Postal address:
Department of Mathematics and Science, University of New Mexico,
705 Gurley Avenue, Gallup, NM 87301, USA